Constraints on the Fourth-Generation Quark Mixing Matrix from Precision Flavour Observables

D I S S E R T A T I O N

zur Erlangung des akademischen Grades

Dr. rer. Nat.
im Fach Physik (Spezialisierung Experimentalphysik)

eingereicht an der
Mathematisch-Naturwissenschaftlichen Fakultät
Humboldt-Universität zu Berlin

von
Dipl.-Phys. Andreas Menzel

Präsident der Humboldt-Universität zu Berlin:
Prof. Dr. Jan-Hendrik Olbertz

Dekan der Mathematisch-Naturwissenschaftlichen Fakultät:
Prof. Dr. Elmar Kulke

Gutachter:
1. Prof. Dr. Heiko Lacker
2. Prof. Dr. Peter Uwer
3. Prof. Dr. Thorsten Feldmann

eingereicht am: 10. März 2016
Tag der mündlichen Prüfung: 18. Oktober 2016

Abstract

The present PhD thesis is the last result of a joint project which succeeded at excluding the existence of an additional sequential generation of Dirac fermions (SM4) at the 5.3 σ level in 2012. This exclusion was achieved in a combined fit of the SM4 to Electroweak Precision Observables and the production cross sections and branching fractions of the newly-discovered Higgs boson. The Flavour sector had not been included. Thus, there was still the possibility that the significance of the exclusion of the SM4 might at least be reduced if it described Flavour physics better than the SM3.

Consequently, this thesis presents a combined fit of the SM4 to a typical set of Flavour physics observables and the results of the previously performed Electroweak Precision fit. Where necessary, quantities extracted in an SM3 framework are reinterpreted in SM4 terms and the adapted theoretical expressions are given. The fits were performed with the CKMfitter software. The resultant constraints on the SM4's CKM matrix, its potentially CP-violating phases and the mass of the new up-type quark t' are given. Where necessary, the interplay of individual constraints and parameters is discussed and plotted.

To compare the relative performance of the SM4 and the SM3, this work uses the χ^2 values achieved in the fit. The values $\chi^2_{min,\mathrm{SM3}} = 15.35$ and $\chi^2_{min,\mathrm{SM4}} = 9.56$ are almost perfectly consistent with both models describing the experimental data equally well with the SM3 having six degrees of freedom more. The dimuon charge asymmetry A_{SL} was not used as a fit input because the interpretation of its measurement was subject to debate at the time when the fits were produced, but its prediction in the fit was used as an additional test of the SM4. The SM3's prediction differs from the experimental values by about 2 σ, and the SM4's prediction by $\approx$3 σ.

In summary, these results do not suggest that any significant reduction of the 5.3 σ exclusion could be achieved by combining the Electroweak Precision Observables and Higgs inputs with Flavour physics data. However, the exact effect of the Flavour physics input on the significance of the SM4's exclusion cannot be given at this point because the CKMfitter software is currently not able to perform a statistically stringent likelihood comparison of non-*nested* models.

Zusammenfassung

Die vorliegende Dissertation ist das letzte Ergebnis einer Gemeinschaftsarbeit, die 2012 die Existenz einer zusätzlichen sequentiellen Fermiongeneration mit einer Signifikanz von 5.3 σ ausschließen konnte. Dies wurde durch einen kombinierten Fit des Standardmodells mit vier Fermiongenerationen (SM4) an Elektroschwache Präzisionsobservable sowie Produktionsquerschnitte und Verzweigungsverhältnisse des gerade neu entdeckten Higgs-Bosons erreicht. Der Flavoursektor wurde nicht mit einbezogen. Deshalb bestand noch die Möglichkeit, dass die Signifikanz des Ausschlusses des SM4 zumindest reduziert werden konnte, falls das SM4 die Flavourphysik besser beschrieb als das SM3.

Folglich beschreibt diese Dissertation einen Fit des SM4 an eine Kombination eines typischen Satzes von Flavour-Observablen mit den Ergebnissen des zuvor durchgeführten Elektroschwachen Präzisionsfits. Wo notwendig, werden in einem SM3-Kontext extrahierte Größen gemäß ihrer Bedeutung im SM4 reinterpretiert und die angepassten theoretischen Ausdrücke angegeben. Die Fits wurden mit dem Computerprogramm CKMfitter durchgeführt. Die resultierenden Einschränkungen der CKM-Matrix des SM4, ihrer potentiell CP-verletzenden Phasen sowie der Masse des neuen up-type-Quarks t' werden angegeben. Wo es nötig erscheint, wird die gegenseitige Beeinflussung der einzelnen Einschränkungen bzw. Parameter diskutiert und ihr Zusammenhang grafisch dargestellt.

Zum Vergleich des SM4 mit dem SM3 werden die erreichten χ^2-Werte genutzt. Die Werte $\chi^2_{min,\mathrm{SM3}} = 15.35$ und $\chi^2_{min,\mathrm{SM4}} = 9.56$ passen fast vollkommen zu einer gleich guten Beschreibung der Experimente durch beide Modelle, wobei das SM3 aber sechs Freiheitsgrade mehr besitzt. Da die Interpretation der Messung der Dimyon-Ladungsasymmetrie A_{SL} zum Zeitpunkt der Berechnungen gerade Gegenstand von Diskussionen war, wurden diese Messwerte in den Fits nicht benutzt. Es wurden nur die SM3- bzw. SM4-Vorhersagen der Fits als zusätzliches Vergleichskriterium genutzt. Die Vorhersage des SM3 ist ca. 2 σ vom experimentellen Wert entfernt, die des SM4 ca. 3 σ.

Zusammengefasst deuten diese Ergebnisse nicht darauf hin, dass die Signifikanz des 2012 erreichten Ausschlusses des SM4 durch die Hinzunahme von Flavour-Observablen zu den damals verwendeten elektroschwachen Präzisionsobservablen und Higgs-Querschnitten bedeutend verringert würde.

Derzeit kann jedoch keine genaue quantitative Aussage über die Auswirkungen der Flavourobservablen auf diese Signifikanz getroffen werden, weil das Programm CKMfitter derzeit likelihood-ratio-Berechnung nur durchführen kann, wenn sich eines der untersuchten Modelle durch Fixierung von Parametern aus dem anderen ergibt, was hier nicht der Fall ist.

Inhaltsverzeichnis

1. Introduction **1**

2. Theoretical background **5**
2.1. The Standard Model of Particle Physics . . . 5
2.1.1. Interactions and particle content of the Standard Model . . . 5
2.1.2. Gauge Theories and Perturbation Theory . . . 6
2.1.3. Electroweak coupling of fermions . . . 9
2.1.4. Fermion Mass Generation in the Standard Model . . . 10
2.2. Origin of fermion mixing . . . 11
2.2.1. More Than One Fermion Family . . . 11
2.2.2. Charged Current Interactions . . . 12
2.2.3. The CKM and PMNS Matrices . . . 13
2.2.4. The Effects of Neutrino Mixing in the SM4 in a Nutshell . . . 13
2.2.5. Parametrization of the Quark Mixing Matrix . . . 15
2.3. Weak Interactions at Low Energies . . . 16
2.3.1. Operator Product Expansion (OPE) . . . 17
2.3.2. Hadronic Matrix Elements and Bag Parameters . . . 19
2.4. Discrete Symmetries in Nature and Their Violation . . . 19
2.4.1. Parity Transformation **P** . . . 20
2.4.2. Charge Conjugation **C** . . . 20
2.4.3. Time Reversal **T** . . . 21
2.4.4. **CP** - Keeping Scientists Busy Since 1964 . . . 21
2.4.5. **CPT** . . . 21
2.4.6. The Unitarity Triangle - Visualising CP Violation . . . 22
2.5. CP Violation in Meson Oscillation . . . 23
2.5.1. General formalism . . . 23
2.5.2. Mass and Lifetime Differences Δm and $\Delta\Gamma$ . . . 26
2.6. Types of CP Violation . . . 27
2.6.1. Meson Oscillation in the SM3 and SM4 . . . 29
2.7. The Electroweak Precision Fit . . . 32

3. The CKMfitter package **35**
3.1. Statistical framework of CKMfitter - Rfit . . . 35
3.1.1. Metrology . . . 37
3.2. The CKMfitter package . . . 38
3.2.1. Mathematica . . . 38

3.2.2. Components of the CKMfitter package . . . 39
3.2.3. The Process of Minimum Search in CKMfitter . . . 41
3.2.4. Further Speedup: Multithreading with OpenMP . . . 42
3.3. Theory Packages written or changed for this work . . . 44

4. Constraining the CKM matrix in SM4 **47**
4.1. Tree Level observables . . . 47
4.1.1. $|V_{ud}|$ From Superallowed Nuclear β Decays . . . 47
4.1.2. $|V_{us}|$ From Semileptonic K-Meson Decays . . . 48
4.1.3. $|V_{ub}|$ From Semileptonic B-Meson Decays . . . 48
4.1.4. $|V_{ub}|$ from $\mathcal{B}(B \to \tau\nu)$ . . . 49
4.1.5. $|V_{cd}|$ from Deep Inelastic Neutrino-Nucleon Scattering . . . 49
4.1.6. $|V_{cs}|$ from Semileptonic D Meson Decays . . . 50
4.1.7. $|V_{cb}|$ from Semileptonic B Meson Decays . . . 50
4.1.8. $|V_{tb}|$ . . . 51
4.1.9. Leptonic W boson decays . . . 54
4.1.10. The UT angle γ . . . 55
4.2. Loop Observables Respecting CP Symmetry . . . 65
4.2.1. Results of the Electroweak Precision Fit . . . 65
4.2.2. $\mathbf{\Delta m_d}$ . . . 65
4.2.3. $\mathbf{\Delta m_s}$ . . . 67
4.2.4. $\Gamma(b \to s\gamma)/\Gamma(b \to ce\bar{\nu})$ . . . 67
4.2.5. $\mathcal{B}(\mathbf{B_d} \to \mu^+\mu^-)$ and $\mathcal{B}(\mathbf{B_s} \to \mu^+\mu^-)$ . . . 71
4.3. CP violating Loop observables . . . 72
4.3.1. $|\epsilon_{\mathbf{K}}|$ . . . 72
4.3.2. $\sin(\mathbf{2}\beta)$ and $\sin(\mathbf{2}\beta - \mathbf{2}\theta_{\mathbf{d}})$ . . . 75
4.3.3. Semileptonic Charge Asymmetry a^s_{SL} . . . 79
4.3.4. Semileptonic Charge Asymmetry a^d_{SL} . . . 81
4.4. A Few Words on the Choice of Inputs . . . 84
4.4.1. Phase $\phi_{\mathbf{s}}$ between mixing and decay in the B^0_s system . . . 84
4.4.2. The UT angle α . . . 84
4.4.3. Mass Difference in the Neutral D Meson System . . . 85
4.4.4. Dimuon Charge Asymmetry A_{SL} . . . 86

5. SM4 Fits and their Results **93**
5.1. Tree Level Inputs only . . . 97
5.1.1. Interplay of Tree Level Inputs . . . 97
5.1.2. Results of the Global Fit With the Tree Level Input Set . . . 101
5.2. More Input: CP-*non*violating Loop Observables . . . 105
5.2.1. The Effects of the Electroweak Precision Fit . . . 105
5.2.2. Constraining More Phases . . . 105
5.2.3. Global Fit Results . . . 109
5.3. Adding CP Violating Loop Observables . . . 118
5.3.1. Fit results . . . 118

5.4. All In: Including Semileptonic Charge Asymmetries . . . 123
5.5. Overview Of Results . . . 126
5.5.1. CKM Matrix Elements . . . 126
5.5.2. CKM Matrix Parameters δ, ϕ_2 and ϕ_3 . . . 134
5.5.3. UT Angles and Related . . . 136
5.5.4. t' Quark Mass . . . 138
5.5.5. A_{SL} and Related . . . 139
5.5.6. Effects of Individual Inputs on the Fit . . . 141

6. SM4 vs. SM3 **145**
6.1. Statistical Caveats in Comparing SM3 and SM4 . . . 145
6.2. The Higgs Boson at LHC and the Fourth Generation . . . 146
6.2.1. Higgs Discovery and the SM4 . . . 147
6.3. Comparison of SM4 and SM3 fit results . . . 151
6.4. A_{SL} and $a_{SL}^{d,s}$ Predictions in the SM4 and the SM3 . . . 154

7. Conclusion **159**

A. Other Parametrisations of the CKM Matrix **163**
A.1. Standard SM3 parametrisation . . . 163
A.2. Wolfenstein Parametrisation . . . 163
A.3. Botella-Chau parametrization . . . 164

B. Convergence Problems with BC parametrization **167**
B.1. A Surprisingly Late Solution . . . 173

C. Loop Functions and Wilson Coefficients **175**
C.0.1. Meson Oscillation . . . 175
C.0.2. Di-Leptonic Meson Decay . . . 175
C.0.3. Effective Wilson Coefficients in $\Gamma(b \to s\gamma)/\Gamma(b \to ce\bar{\nu})$ . . . 175

1. Introduction

The idea of extending the Standard Model of elementary particle physics by additional generations of fermions has been around for a while in several incarnations. This is perhaps not surprising as the number of fermion generations is not trivial to predict. Also, the extension by another generation had proved fruitful before: When two generations were experimentally confirmed, the prediction of a third generation in combination with quark mixing had provided a means to implement CP violation in the Standard Model. The estimates for an upper limit on the number of generations ranged from three ([1], offering an explanation to CP violation, and [2], based on nucleosynthesis) to eight ([3], based on the condition that QCD remain asymptotically free. A number of more recent publications (e.g. [4, 5, 6]) find that more than four generations are clearly disfavoured by the Electroweak Precision fit.

The present work investigates what is probably the simplest among such extensions: One additional generation of fermions which differ from known particles only in their mass, just like i.e. the second generation differs from the third. This extension is known as a sequential fourth generation or family. The version of the Standard Model with this extension will be called the SM4 in this thesis. The Standard Model without it will be called the SM3. Occasionally, the notation SM3(4) will be used to make clear that a certain statement applies to both cases.

At the beginning of the 1990s, a fourth generation had been suggested to save the idea of flavour democracy [7, 8, 9]. In the following two decades, the SM4 was occasionally proposed both as a solution to profound unanswered questions concerning our understanding of the universe, and as an explanation for tensions between measurements and their theoretical prediction within the SM3. The first category includes, but is not limited to, the strong CP problem, gauge coupling unification (without supersymmetry), mechanisms of dynamical electroweak symmetry breaking, and a number of others. A fourth generation of fermions was also suggested to increase both the CP violation [10] and the strength of the phase transition [11, 12] required for baryogenesis of the universe (Sakharov conditions, [13]). Sufficiently stable heavy neutrinos were among the dark matter candidates. Of the second category, there is e.g. a number of observations on different B meson species. There were discrepancies between different extractions of $\sin(2\beta)$ (β being an angle of the Unitarity Triangle) and its prediction in the SM3 of over 3 σ [14, 15]. Belle measured the difference in direct CP violation between the decays $B^+ \to K^+\pi^0$ and $B^0 \to K^+\pi^-$ which were also several σ away from its predicted value [3, 16]. The CDF and D0 experiments reported [17, 18] possible hints at non-standard large CP violation in the $B_s^0 \to \psi\phi$ decay. There were tensions between results from *BABAR* [19] and Belle [20] and the SM prediction of the forward-backward asymmetry in $\bar{B} \to \bar{K}^*\mu^+\mu^-$. In 2010, D0 observed an anomalous like-sign dimuon charge asymmetry A_{SL}[21]. For a more exhaustive listing giving references on each of the topics, see e.g. [22, 3, 23, 4, 24, 25]. In each of these cases, the fourth generation was among the suggested solutions (see e.g. [15, 3, 26, 27] and references given therein). Many of these discrepancies were resolved by more recent measurements.

1. Introduction

With the availability of precision measurements in the electroweak sector from SLC and LEP on the one hand and precision flavour data from the B factory experiments *BABAR* and Belle the other hand, these results were also used to obtain constraints on the SM4. It was the Electroweak Precision Fit which lead to a number of slightly premature statements of the SM4 being excluded. Let a quote from a 2008 PDG review by Erler and Langacker [28] serve as an example on how much attention to detail is needed to perform such a study and to understand it correctly:

> "An extra generation of ordinary fermions is excluded at the 6 σ level on the basis of the S parameter alone, corresponding to $N_F = 2.71 \pm 0.22$ for the number of families. This result assumes that there are no new contributions to T or U and therefore that any new families are degenerate. This restriction can be relaxed by allowing T to vary as well, since $T > 0$ is expected from a non-degenerate extra family."

It seems that the second sentence of this quote was sometimes overlooked. Another main argument against a fourth family was that it was supposedly strongly disfavoured by the number of invisible light neutrino flavours at the Z^0 resonance counted at LEP.

In 2007, Kribs, Plehn, Spannowski and Tait published [4] conditions for masses and mass differences of fourth generation fermions and Higgs masses to be compatible with the experimental results of the day and especially the Electroweak Precision fits. Moreover, in agreement with other authors (e.g. [29, 5]) they showed that a sequential fourth generation could reconcile a heavy (up to around 500 GeV) Higgs boson with Electroweak Precision data in case this would be found. Also, the then-new LHC accelerator is able to probe previously unreachable mass regions, and numerous studies had explored how a fourth generation fulfilling certain sets of assumptions could be observed in a given experiment while avoiding conflict with previous results. Furthermore, there was a number of reasons to believe that the member particles of the fourth generation could indeed be produced at energies which the LHC can actually attain. The unitarity upper limit of around 500 to 1000 GeV [30] and the numerically similar and conceptually related triviality bound [31] were often cited - to name a few examples, see [32],[16], [33], [22], [15], [23], [25], [29]. However, these bounds give a mass scale at which contributions beyond the leading order have to be considered in calculations and *not* a limit on how heavy fermions are allowed to be [34]. Other estimates, such as one based on the requirement that heavy fermion corrections must not destabilize the SM vacuum, are again discussed in [24] and the references given there. Consequently, the SM4 was among those New Physics scenarios which were expected to be soon confirmed or excluded and activity in SM4 research was correspondingly high. It soon became clear (e.g. [29]) that, due to the non-trivial interplay between flavour physics and the electroweak sector as well as increased experimental precision, a consistent study had to combine both. Subsequently, a number of such publications (e.g. [25, 23, 22]) appeared.

In 2010, Otto Eberhardt, Heiko Lacker, Alexander Lenz, Ulrich Nierste, Martin Wiebusch and the author of the present thesis formed a collaboration as part of a larger DFG project, and started a joint effort to combine Electroweak Precision Observables and Precision Flavour results in one common fit in order exclude the 4th generation of fermions or at least constrain its parameters. The present thesis is the last part of the results of this effort. The exact physics scenario examined is further specified by a number of assumptions. Firstly, throughout this work and other results of the same project, neutrinos were assumed to be purely Dirac fermions. Effects of neutrinos having

at least a Majorana component should not have any overly dramatic effects, though (e.g. [4, 35]). Secondly, this work assumes that perturbation theory can be trusted up to a 4th generation quark mass of 1 TeV. This is in conflict with the limits usually assumed (about half as much) and may well mean that the theoretical expressions used in the fit do not give accurate predictions at what turns out to be the preferred value of the mass of the fourth generation's up-type quark. Finally, neutrino mixing parameters were not free in the fit. With the exception of a small shift and an increased uncertainty of the CKM matrix element $|V_{ud}|$ and the Fermi constant G_F, the effect of letting them float freely is negligible anyway.

Previous publications did indeed use similar combinations of observables to constrain the parameters of the SM4, see e.g. [36, 37, 25, 22, 23, 16, 15]. In most cases, however, their results were obtained by randomly generating a large number of points in the parameter space to be explored. A point was accepted or rejected depending on how well the corresponding values of the observables agreed with experimental results. The authors of [22] did obtain their constraints on the parameters examined by making use of an actual χ^2 value. However, is not quite made clear in the paper how this happened. Scattering plots, at least, do not contain any quantitative statistical information. They can comb the parameter space for points or areas compatible with experiment, but the probability of a parameter or observable to assume the value(s) corresponding to a given point cannot reliably be inferred. This is where the tool we use, i.e. the CKMfitter software, sets our project apart from the studies named above: Not only can the global χ^2 be minimized, but CKMfitter is in principle able to provide statistically meaningful confidence intervals of any quantity entering the fit. For more details on CKMfitter's statistics approach and some technical information, see Chapter 3.

However, the statistics engine of CKMfitter was not suited to the task of calculating the p-value of the exclusion of *non-nested* models. A new piece of software, Martin Wiebusch's *my*Fitter, was written to cope with the challenge. In 2012, slightly more than 4 months after the Higgs discovery had been announced by the ATLAS and CMS collaborations [38, 39], it enabled us to exclude the existence of a fourth generation at the 5 σ level [40]. The latter fit combined the mass of the Higgs resonance and the signal strengths of its decay with the Electroweak Precision Observables. Not only did the SM4 perform worse than the SM3 in the fit but differences between the Higgs branching fractions and their SM3 predictions tend to be opposite of what one would expect from the SM4. For technical reasons, Flavour observables were not considered at this point.

The present thesis completes the work of our collaboration on the SM4 by presenting the analysis of a sequential fourth generation in the Flavour sector. Due to the limitations of CKMfitter's statistics engine mentioned above, no stringent quantitative statement on the significance of the exclusion of the SM4 can be given. While such results can be obtained by using the *my*Fitter software, this would have required a re-coding of the entire set of flavour physics observables for *my*Fitter. This was not possible within the time frame allocated to the project.

Keeping the statistical caveats in mind, the salient result of the present thesis is that the SM4 turns out to be compatible with all observables from the Flavour sector and the Electroweak Precision Fit. While its performance in the fit is in some aspects even superior to the SM3, it seems unlikely that this is enough to challenge the exclusion of the SM4 by the Higgs measurements. Also, it does not alleviate the tension between the measured value of A_{SL} and its theoretical prediction.

This thesis is organized as follows: The following **Chapter 2** recalls the physical concepts needed in this work and attempts to provide the reader with references to more in-depth treatments of those. **Chapter 3** describes the CKMfitter software, i.e. its statistical approach and some technical aspects. It also lists the modifications to the CKMfitter software which were made in order to produce this thesis. **Chapter 4** describes the observables which will be used to constrain the SM4's parameter space. Where necessary, a description is given of the process in which the input value was obtained. Also, the (re)interpretation of this value or its measurement process in an SM4 framework is discussed. Where a reinterpretation is necessary, a theoretical expression is given. Where a value extracted in an SM3 framework is used "as is", this will be justified. The observables are classified into the categories Tree Level - Loop Observables without CP violation - Loop Observables violating CP symmetry. In **Chapter 5**, the fits performed for this thesis are described. For convenience, input observables and parameters are tabulated. Fit results are presented numerically and, if appropriate, graphically. **Chapter 6** contains a discussion of the findings of Chapter 5 in view of a comparison of the performance of the SM3 and the SM4 in the fits and also recalls how the measurements on the Higgs boson had to be used to finally exclude the SM4. **Chapter 7** is a conclusion of the findings of this study.

There is also an **Appendix**. Its **first section** contains some parametrisations of the CKM matrix which are mentioned or used in this thesis. The **second section** deals with one of the problems which delayed this work for so long, i.e. the effects of an unsuited parametrisation, how (not) to find the reason for convergence problems and how (not) to deal with them once found. The **third**, and last, **section** of the Appendix contains a few useful formulae used in the theoretical expressions in Chapter 4, as well as a few plots which were not found to be important enough to be shown elsewhere.

2. Theoretical background

This chapter provides a brief introduction to the most important concepts needed to explain the work presented here and the theoretical expressions describing them. Contents in this section are compiled from references [41], [42], [43], [44] and [45] where this background is provided and derived in more detail.

2.1. The Standard Model of Particle Physics

The most successful theory of elementary particle physics to date is the Standard Model (SM). It describes the fundamental components of matter and the interactions between them.

2.1.1. Interactions and particle content of the Standard Model

Matter is built of fermions with a spin of 1/2 and spin-1-particles called gauge bosons. The gauge bosons mediate the interactions between the fermions. The fermions carry charges to which the bosons couple and whose (non)presence and value in a particle allow for further classification, as listed in Table 2.1. Fermions are grouped in so-called families. Each family contains one up-type quark (u), one down-type quark (d), one charged lepton (ℓ) and one neutrino (ν). Only quarks carry color charges (called red, green and blue) which couple to the gauge bosons of the strong interaction called gluons (g). All fermions except neutrinos carry an electric charge which couples them to photons γ. Only left-handed fermions carry a weak isospin I which couples to the W bosons of the weak interaction. The coupling to the Z boson is more complicated and depends on electric charge, handedness and weak isospin of the fermions involved (see Sec. 2.1.3). Effectively, charged fermions couple to the Z with a strength depending on their handedness, while only left-handed neutrinos couple to the Z. Each fermion has an antifermion "partner" of the same mass and spin, but opposite electric charge and weak isospin component I_3. The opposite of a color charge is simply called its anti-color (e.g. red $r \leftrightarrow$ antired $\bar{r}$). The interactions of the SM together

	Flavour	Electric charge Q/e_0	Color	Weak Isospin (I, I_3) left-handed	Weak Isospin (I, I_3) right-handed
Quarks	up-type u_i	$+\frac{2}{3}$	i=r,g,b	(1/2, +1/2)	(0,0)
	down-type d_i	$-\frac{1}{3}$		(1/2, -1/2)	(0,0)
Leptons	neutrino ν	0	–	(1/2,+1/2)	–
	charged lepton ℓ^-	-1		(1/2,-1/2)	(0,0)

Table 2.1.: Fermion types in the SM. e_0 is the elementary charge.

with the bosons mediating them and the charge they couple to are listed in Table 2.2. If a type of gauge bosons themselves carry the charges they couple to, these bosons interact among each other. This is the case for the W bosons whose $I_3 = \pm 1$ and the gluons which carry a color and an anti-color each. The SM does not include gravity due to unsolved theoretical challenges in its quantum mechanical description. With regard to describing those particle experiments which can be performed with today's technology, gravity is not relevant due to its extreme weakness compared to the other interactions.

2.1.2. Gauge Theories and Perturbation Theory

Mathematically, the SM is a gauge field theory. That is, a Lagrange density $\mathcal{L}$[1] which depends on various space-time dependent fields is required to remain invariant under certain local (i.e. space-time dependent) unitary transformations. This is achieved by introducing so-called gauge fields whose quanta are the gauge bosons mentioned in the last section and which enter the Lagrangian in *covariant derivatives*. Eq. (2.4) in the next section is an example of this. The remaining type of object needed for the SM or any other gauge field theory is the coupling constant which describes how strongly one type of particle interacts with another, and which is usually denoted by a g with some subscript.

Provided that the coupling constant is small enough, it is possible to compute the cross section of interactions between particles perturbatively: The propagators which can be constructed in the theory are expanded in a power series in g. A Feynman graph is the graphical representation of a term from such an expansion. In order to *perfectly* describe a process occuring in nature, one would have to sum an infinite number of graphs/terms, up to $\mathcal{O}(g^\infty)$. For a given process (for example $e^+e^- \to \mu^+\mu^-$), the number of initial and final state particles is fixed. As every vertex in a Feynman graph corresponds to a factor of the square root of the coupling constant, a higher order graph is a graph with more vertices for the same number of initial and final state particles, leading to a graph with loops. The 4-momenta of particles in a loop are integrated over, usually from the physical mass of the respective particle to infinity.

As an infinite expansion series cannot be computed, calculations usually stop at a certain power of g. Hence the use of expressions like "two-loop order" which state the order of perturbation

[1] Not to be confused with $\mathcal{L}$ in section 3.1 which refers to a Likelihood function. The Lagrange density will only be mentioned in this chapter.

Interaction	couples to	Bosons	Mass(Boson)	J^P	Charge (boson)
Electomagnetic	q	photon γ	0	1^-	–
Weak	I_3	$W^\pm$	80.398 GeV [46]	1	$I_3 = \pm 1$, $q = \pm e$
Weak	I_3, q*	Z^0	91.1876 GeV [46]	1	–
Strong	c	8 gluons g	0	1^-	$c\bar{c}'$

Table 2.2.: Gauge bosons of the SM and their gauge charges. I is the weak isospin, I_3 its third component, J is the spin, P the parity eigenvalue, q the electric charge and c color charge.
* Charge, spin and I_3 together determine the coupling.

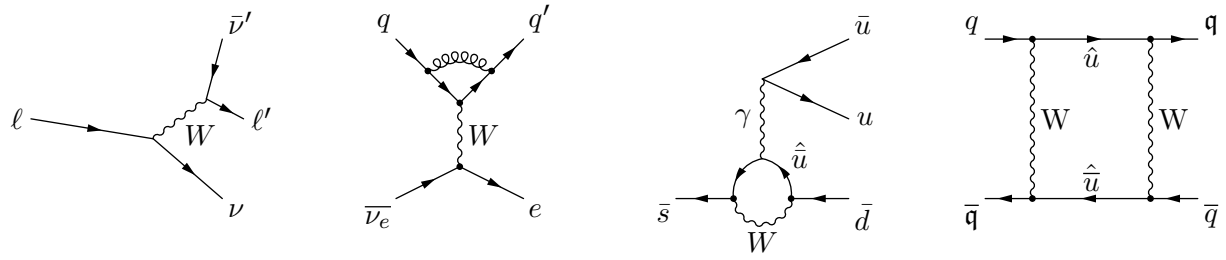

(a) Tree (level) graph

(b) A QCD correction to a tree graph

(c) (Electromagnetic) penguin graph.

(d) Box graph

Figure 2.1.: Examples of a number of Feynman graph types whose names will be used in this thesis. $\hat{u}$ denotes any up-type flavoured quark. The classification of penguin graphs depends on the boson which is attached to the loop - there are also gluonic and electroweak penguins. The term "magnetic" refers to the tensor structure of this vertex. Box graphs also occur with the fermion and W boson lines in the loop interchanged (cf. Fig. 2.5). Readers interested in the origin of the name "penguin graphs" might want to read [47].

that has been included in the calculation. Some processes do already occur at the lowest order of the perturbation series. As the corresponding graphs do not contain any loops, they are called tree level graphs. Like other graph types' names, this is due to their appearance - see Fig. 2.1.

The strong interaction is described by quantum chromodynamics (QCD), a gauge field theory based on the gauge group $SU(3)_C$, with the C denoting "color". At high momentum transfers Q^2, its coupling constant α_s is sufficiently small for pertubative calculations of strong interactions. At low momentum transfer, with Q^2 below roughly 0.5 GeV, α_s becomes so large that perturbative calculations are impossible. The former characteristic is referred to as *Asymptotic Freedom*. The latter leads to a phenomenon called *Confinement* which basically means that if two quarks are separated from each other, it is energetically favourable to create new quark-antiquark pairs from the gluon field between them instead of having the original two quarks interact strongly over an ever-larger distance. The gluon field between them effectively "breaks" where a new quark-antiquark pair is formed. This leads to the formation of bound quark states (hadrons) and is a consequence of the self-interaction of gluons. In agreement with this theory, no free quarks or gluons have been observed yet; they are always *confined* to the interior of hadrons or, in case of the top quark, decay too quickly to form bound states. In detectors, quark or gluon production therefore manifests itself as "jets" of many hadrons moving more or less in the direction of the original quark or gluon. The dependency of α_s on Q^2 at one-loop level is [48]

$$\alpha_s^{(1)}(Q^2) = \frac{4\pi}{(11 - (2/3)n_f)\ln(Q^2/\Lambda^2_{QCD})} \ , \tag{2.1}$$

where n_f is the number of quark flavours that are kinematically accessible at the given Q^2. Λ_{QCD} is a fundamental parameter of QCD which must be determined from experiment. Equation (2.1) features the behaviour described above. For $Q^2 \to \infty$, $\alpha_s \to 0$ and it diverges for $Q^2 \to$

Λ_{QCD}, prohibiting perturbative calculations in the low-energy regime. In this thesis, the strong interaction appears only in correction terms to electroweak processes and will therefore not be discussed in deeper detail.

Glashow, Salam and Weinberg showed that electromagnetic and weak interaction can be unified in the electroweak interaction. It is described by a $\mathrm{SU}(2)_L \otimes \mathrm{U}(1)_Y$ gauge field theory. The index L accounts for the experimental fact that the W bosons couple only to left-handed fermions which form weak isospin doublets. Purely right-handed fermions do not couple to charged-current electroweak interactions and are weak isospin singlets:

$$\begin{pmatrix} u \\ d \end{pmatrix}_L \qquad \begin{pmatrix} \nu_\ell \\ \ell \end{pmatrix}_L \qquad u_R,\, d_R \qquad \ell_R. \tag{2.2}$$

In charged-current weak interactions, a left-handed fermion is transformed into the other member of its doublet. Until now, no right-handed neutrinos have been observed. In the original standard model, neutrinos were assumed to be massless. In this thesis, neutrinos are assumed to be Dirac particles. A massless Dirac particle has a Lorentz frame independent helicity as it moves at the speed of light. A massless right-handed neutrino would be right-handed in all Lorentz frames and could therefore never interact. The resulting non-observability in interactions, equivalent to non-existence of right-handed neutrino states, would be consistent with the theory. However, the phenomenon of neutrino oscillations (see e.g. [49]) can only be explained if neutrinos are massive particles, and massive Dirac particles always have a right-handed component as they travel slower than the speed of light. Current upper limits of neutrino masses are remarkably small, ranging from lower than 2 eV for electron based neutrinos to below 18.2 MeV for τ based neutrinos ([50], 95% CL). As will be explained in sec. 2.2.4, a 4th neutrino would have to be at least half as heavy as the Z boson. Its right-handed component would therefore clearly not be negligible.

The $\mathrm{U}(1)_Y$ transformations are generated by the weak hypercharge operator

$$Y = 2(Q - I_3) \tag{2.3}$$

where Q is the operator of electric charge, with eigenvalue -1 for the electron.

If a gauge field theory is to be used to predict results of experiments, it has to be renormalizable. This means that divergences from integrating over the momenta of particles in loops of Feynman graphs cancel or disappear when observables are expressed in terms of other observables and not in terms of parameters of the theory. For massive Yang-Mills-theories, i.e. Lagrangians which are invariant under non-abelian local gauge transformations while containing massive gauge bosons, renormalizability was proved by T'Hooft [51]. The electroweak sector of the SM with its massive gauge bosons (not identical to the $W^\pm$ and Z^0 from Table 2.2, cf. section 2.1.3) arising from the non-abelian $SU(2)_L$ gauge group falls into that category. The QCD sector contains massless gauge bosons from its $SU(3)_C$ gauge symmetry. T'Hooft proved the renormalizability of such a theory in a previous publication [52]. The renormalizability of Abelian gauge field theories - relevant due to the $U(1)_Y$ part of the SM Lagrangian - had been known before [53, 54].

A consequence of this is the dependency of coupling constants on momentum transfer referred to as "running coupling". One example is the behaviour of $\alpha_s(Q^2)$ described above, but also the electromagnetic coupling constant α_{EM} depends on momentum transfer.

All of the above considered, the SM is a renormalizable $SU(3)_C \otimes SU(2)_L \otimes U(1)_Y$ gauge field theory.

2.1.3. Electroweak coupling of fermions

If one only considers the electroweak interaction, the requirement of local $SU(3)_C$ symmetry which generates the strong interaction can be dropped. What remains is the requirement for $\mathcal{L}$ to be invariant under a local $SU(2)_L \otimes U(1)_Y$ symmetry. To ensure this property, the space-time derivative $\partial_\mu \Phi$ of fields Φ entering the Lagrangian is replaced by the covariant derivative

$$D_\mu \Phi = \left[\partial_\mu + \mathrm{i}\frac{g_1}{2} B_\mu + \mathrm{i}\frac{g_2}{2} \mathbf{W}_\mu \right] \Phi, \tag{2.4}$$

where B_μ and $\mathbf{W}_\mu$ are the space-time dependent U(1) and SU(2) gauge fields, respectively. $\mathbf{W}$ is a three dimensional vector in isospin space, i.e.

$$\mathbf{W}_\mu(x) = \sum_{i=1}^{3} W_\mu^i(x) \cdot \tau^i \tag{2.5}$$

where the τ^i are the generators of the group SU(2). A common choice for the representation of the τ^i are the Pauli matrices. $g_{1,2}$ are the coupling constants of the gauge fields. At this point, they are free parameters of the theory. g_2 must have the same value for *all* fermions due to the group SU(2) being non-abelian. There is no such restriction for g_1, the coupling constant of the Abelian group $U(1)$.

The physical electromagnetic field A_μ and weak field Z^0 are not identical to B_μ or any of the three components of $\mathbf{W}_\mu$, but "mixed" between W_μ^3 and B_μ:

$$Z_\mu = W_\mu^3 \cos\theta_W - B_\mu \sin\theta_W, \tag{2.6}$$

$$A_\mu = W_\mu^3 \sin\theta_W + B_\mu \cos\theta_W \tag{2.7}$$

where θ_W is the weak mixing angle or Weinberg angle, defined by

$$\cos\theta_W = \frac{g_2}{\sqrt{g_1^2 + g_2^2}} \qquad \text{and} \qquad \sin\theta_W = \frac{g_1}{\sqrt{g_1^2 + g_2^2}}. \tag{2.8}$$

Analysing the various interaction terms arising from the electroweak Lagrangian will yield, among all other electroweak interactions, the couplings between fermion fields of quarks, leptons and neutrinos and the gauge boson fields $W^\pm = (W_\mu^1 \mp W_\mu^2)/\sqrt{2}$ to the photon field A_μ. This corresponds to the particles described by these fields having an electric charge. By selecting values for g_1 and g_2, their coupling to the electromagnetic field can be tuned in such way that the theory correctly describes the observations made in experiments, i.e. giving them the "correct" charge. One finds the values

$$g_1 = \frac{e}{\sin\theta_W}, \qquad g_2 = \frac{e}{\cos\theta_W} \tag{2.9}$$

for all fermions, i.e. quarks, neutrinos and leptons.

2.1.4. Fermion Mass Generation in the Standard Model

In order to incorporate masses without spoiling local gauge symmetries, the Standard Model uses the Higgs mechanism of spontaneous symmetry breaking. Since this mechanism is explained in most of the references of this section, it will not be described in detail here, but certain important steps and choices will be revisited here, if only to define the notation.

In the SM, an additional two-component complex field,

$$\Phi = \begin{pmatrix} \Phi_A \\ \Phi_B \end{pmatrix} = \begin{pmatrix} \phi_1 + \mathrm{i}\phi_2 \\ \phi_3 + \mathrm{i}\phi_4 \end{pmatrix}, \tag{2.10}$$

is introduced. A Lagrangian with the required $SU(2)_L \otimes U(1)_Y$ symmetry is

$$\mathcal{L}_\Phi = (D_\mu \Phi)^\dagger D^\mu \Phi - V(\Phi^\dagger \Phi) = (D_\mu \Phi)^\dagger D^\mu \Phi - \frac{m^2}{2\phi_0^2}\left[(\Phi^\dagger \Phi) - \phi_0^2\right]^2. \tag{2.11}$$

Every Φ with a norm of ϕ_0 minimizes $\mathcal{L}$. Therefore, the ground state is infinitely degenerate. The SU(2) symmetry is spontaneously broken by selecting a particular ground state. A choice usually taken in the literature is

$$\Phi_{\text{ground}} = \begin{pmatrix} 0 \\ \phi_0 \end{pmatrix}, \tag{2.12}$$

with excited states

$$\Phi = \begin{pmatrix} 0 \\ \phi_0 + h(x)/\sqrt{2} \end{pmatrix}. \tag{2.13}$$

h is the real scalar Higgs field and its mass turns out to be m. Particles now gain their masses by means of interaction terms which couple them to the Φ field. If there was only one family of fermions, the mass generating terms in the Lagrangian would be

$$\mathcal{L}'_{m(u)} = -\left[c_u(\mathbf{L_q}^\dagger \varepsilon \Phi^*) u_R - c_u^* u_R^\dagger (\Phi^{\mathrm{T}} \varepsilon \mathbf{L_q})\right], \tag{2.14}$$

$$\mathcal{L}'_{m(d)} = -\left[c_d(\mathbf{L_q}^\dagger \Phi) d_R + c_d^* d_R^\dagger (\Phi^\dagger \mathbf{L_q})\right], \tag{2.15}$$

$$\mathcal{L}'_{m(\nu)} = -\left[c_\nu(\mathbf{L}_\ell^\dagger \varepsilon \Phi^*) \nu_R - c_\nu^* \nu_R^\dagger (\Phi^{\mathrm{T}} \varepsilon \mathbf{L}_\ell)\right] \quad \text{and} \tag{2.16}$$

$$\mathcal{L}'_{m(\ell)} = -\left[c_\ell(\mathbf{L}_\ell^\dagger \Phi) \ell_R + c_\ell^* \ell_R^\dagger (\Phi^\dagger \mathbf{L}_\ell)\right]. \tag{2.17}$$

$\mathbf{L}_q$ and $\mathbf{L}_\ell$ are the left-hand doublets of quarks and leptons, respectively. The various c's are coupling constants. $\varepsilon = \begin{pmatrix} 0 & 1 \\ -1 & 0 \end{pmatrix}$ enables the upper component of each $\mathbf{L}$ to couple to the lower component of Φ which is not zero. Upon breaking of the SU(2) symmetry, the resulting mass

terms are

$$\mathcal{L}'_{m(u)} = -\phi_0 \left[c_u u_L^\dagger u_R + c_u^* u_R^\dagger u_L \right], \tag{2.18}$$

$$\mathcal{L}'_{m(d)} = -\phi_0 \left[c_d d_L^\dagger d_R + c_d^* d_R^\dagger d_L \right], \tag{2.19}$$

$$\mathcal{L}'_{m(\nu)} = -\phi_0 \left[c_\nu \nu_L^\dagger \nu_R + c_\nu^* \nu_R^\dagger \nu_L \right], \tag{2.20}$$

$$\mathcal{L}'_{m(\ell)} = -\phi_0 \left[c_\ell \ell_L^\dagger \ell_R + c_\ell^* \ell_R^\dagger \ell_L \right]. \tag{2.21}$$

2.2. Origin of fermion mixing

2.2.1. More Than One Fermion Family

Until now, the existence of several families of fermions has been glossed over in the description of the theory. As this thesis explores constraints on the mixing between several - i.e. three and four, respectively - quark families, it seems useful to describe the effects of the existence and mixing of several fermion families in the Standard Model with four families (SM4) from the beginning. If not stated otherwise, the SM3 case follows by just omitting any terms involving a fourth family.

If the quark sector is extended by another family, the same must happen to the lepton sector. The reason is that the Adler-Bell-Jackiw- or axial anomaly which is theoretically described in [55] and whose implications for the SM are explained in textbooks like Refs. [41, 42, 43, 45] must cancel if the theory is to be renormalizable. It only does so if there are the same number each of up-type quarks, down-type quarks, charged leptons and neutrinos. The universality of the electroweak coupling constants g_2 and g_1 extends not only to the particles of one family, but it is well established experimentally that they are the same for all fermion families. In case of g_2, this is also dictated by the non-abelian gauge group $SU(2)_L$.

If there are four fermion families, it is possible to write the quark mass generating terms of (2.18) as

$$\mathcal{L}_{m(u)} = -\phi_0 \sum_{i,j=1}^{4} \left[G_{ij}^u u_{Li}^\dagger u_{Ri} + G_{ij}^{u*} u_{Ri}^\dagger u_{Li} \right] \quad \text{and} \tag{2.22}$$

$$\mathcal{L}_{m(d)} = -\phi_0 \sum_{i,j=1}^{4} \left[G_{ij}^d d_{Li}^\dagger d_{Ri} + G_{ij}^{d*} d_{Ri}^\dagger d_{Li} \right], \tag{2.23}$$

$$\tag{2.24}$$

where the G_{ij} are complex 4×4 (3×3 in the SM3, obviously) matrices and the summation indices run over the four (three) families. The matrices $\mathbf{G}$ are called mass matrices. They are not diagonal in the basis of the SU(2) weak eigenstates, but they can be transformed into a real diagonal form by

$$\phi_0 \mathbf{G^d} = \mathbf{D_L^\dagger m^d D_R}, \tag{2.25}$$

$$\phi_0 \mathbf{G^u} = \mathbf{U_L^\dagger m^u U_R} \tag{2.26}$$

where $\mathbf{D_L}$, $\mathbf{D_R}$, $\mathbf{U_L}$ and $\mathbf{U_R}$ are unitary matrices. They are unique up to complex phase transformations like

$$\begin{pmatrix} e^{i\phi_1} & 0 & 0 & 0 \\ 0 & e^{i\phi_2} & 0 & 0 \\ 0 & 0 & e^{i\phi_3} & 0 \\ 0 & 0 & 0 & e^{i\phi_4} \end{pmatrix} \tag{2.27}$$

by which both **D**s and **U**s can be multiplied from the same side. The phases $\phi_1, \phi_2, \phi_3, \phi_4$ of the **U** matrices are not necessarily the same as those of the **D** matrices, referred to as $\varphi_1, \varphi_2, \varphi_3, \varphi_4$.

This means that the weak eigenstates are linear combinations of the mass eigenstates:

$$d_{Li}^{\text{mass}} = D_{Lij} d_{Lj}, \qquad d_{Ri}^{\text{mass}} = D_{Rij} d_{Rj}, \tag{2.28}$$

$$u_{Li}^{\text{mass}} = U_{Lij} u_{Lj}, \qquad u_{Ri}^{\text{mass}} = U_{Rij} u_{Rj}, \tag{2.29}$$

where indices i and j denote the family and j is summed over.

2.2.2. Charged Current Interactions

Among the interaction terms which arise from the electroweak Lagrangian is the charged current interaction between W bosons and fermions. The corresponding term of the Lagrangian is of the form

$$\mathcal{L}_{CC} = -\frac{e}{\sqrt{2}} \left(J^{\mu\dagger} W_\mu^+ + J^\mu W_\mu^- \right) \tag{2.30}$$

The currents are made up of several flavour components, i.e. the lepton contributions

$$J_\ell^\mu = e_L^\dagger \tilde{\sigma}^\mu \nu_{eL} + \mu_L^\dagger \tilde{\sigma}^\mu \nu_{\mu L} + \tau_L^\dagger \tilde{\sigma}^\mu \nu_{\tau L} \tag{2.31}$$

and those from quarks:

$$J_q^\mu = \sum_{i=1}^{4} u_{Li}^\dagger \tilde{\sigma}^\mu d_{Li} \quad + \text{Hermitian conjugate} \tag{2.32}$$

with $\tilde{\sigma}^\mu = (\sigma^0, \sigma^1, \sigma^2, \sigma^3)$ where σ^0 is the 2-dimensional identity matrix and the $\sigma^{1,2,3}$ are the Pauli matrices. Going from the basis of weak eigenstates to the mass basis, J_q^μ is changed to

$$J_q^{\text{mass},\mu} = \sum_{i=1}^{4} u_{Li}^{\text{mass}\dagger} (\mathbf{U_L D_L^\dagger}) \tilde{\sigma}^\mu d_{Li}^{\text{mass}} \quad + \text{Hermitian conjugate.} \tag{2.33}$$

The matrix $\mathbf{U_L D_L}^\dagger \equiv V_{CKM}$ from (2.33) is the CKM matrix (named after Cabibbo [56], Kobayashi and Maskawa, [1]) which implements quark mixing in the theory. In principle a similar matrix arises in the lepton sector. See the next section for more details.

2.2.3. The CKM and PMNS Matrices

The quark mixing matrix has an equivalent in the lepton sector which is usually denoted by U_{PMNS}. It is called the PMNS matrix after Pontecorvo, Maki, Nakagawa and Sakata. The mixing matrices imply that quark and lepton states participating in charged current weak interactions are not mass eigenstates, but linear combinations of those. The unitary matrices which diagonalize the mass matrices in eq. (2.25) are not measurable. Only the mixing matrices and the eigenvalues of the mass matrices are [57]. The quark mixing matrix describes the relative orientation of the bases in which the mass matrices $\mathbf{G^d}$ and $\mathbf{G^u}$ are diagonal (cf. eg. (2.25)). The neutrino mixing matrix describes the relative orientation between the bases in which the neutrino and charged lepton mass matrices are diagonal. This means it is possible to define them in such way that e.g. the up-type quark states and the charged lepton states participating in the weak interaction coincide with their mass eigenstates. With this choice, only the down-type quarks and the neutrinos mix. It is important to distinguish between their respective mass eigenstates and the weak states coupling to the W boson in the weak interaction. In the literature, the weak basis states are usually denoted by a prime. For example, the down-quark weak state is d'. This could be a source of confusion in the SM4 because the fourth family quarks are usually called t' and b' in the mass basis. Therefore, the weak states coupling to W bosons will hereafter be marked by use of different fonts if necessary. The designation $^{\text{mass}}$ used before is dropped.

$$\begin{pmatrix} \mathfrak{d} \\ \mathfrak{s} \\ \mathfrak{b} \\ \mathfrak{b}' \end{pmatrix} = \begin{pmatrix} V_{ud} & V_{us} & V_{ub} & V_{ub'} \\ V_{cd} & V_{cs} & V_{cb} & V_{cb'} \\ V_{td} & V_{ts} & V_{tb} & V_{tb'} \\ V_{t'd} & V_{t's} & V_{t'b} & V_{t'b'} \end{pmatrix} \cdot \begin{pmatrix} d \\ s \\ b \\ b' \end{pmatrix} \tag{2.34}$$

$$\begin{pmatrix} \nu_e \\ \nu_\mu \\ \nu_\tau \\ \nu_E \end{pmatrix} = \begin{pmatrix} U^*_{e1} & U^*_{e2} & U^*_{e3} & U^*_{e4} \\ U^*_{\mu 1} & U^*_{\mu 2} & U^*_{\mu 3} & U^*_{\mu 4} \\ U^*_{\tau 1} & U^*_{\tau 2} & U^*_{\tau 3} & U^*_{\tau 4} \\ U^*_{E1} & U^*_{E2} & U^*_{E3} & U^*_{E4} \end{pmatrix} \cdot \begin{pmatrix} \nu_1 \\ \nu_2 \\ \nu_3 \\ \nu_4 \end{pmatrix} \tag{2.35}$$

Since both mixing matrices are products of unitary matrices, the mixing matrices themselves are unitary matrices. A unitary matrix in n dimensions is described by n^2 real parameters, yielding 16 for each mixing matrix in the case of four fermion generations and 9 in the SM3. However, only phase differences $\phi_i - \varphi_j$ between phases ϕ_i from the $\mathbf{U_{L,R}}$ matrices and phases φ_j from the matrices $\mathbf{D_{L,R}}$ appear in a mixing matrix. As a consequence, only seven of the 16 possible differences in the SM4 and five of nine in the SM3 are independent from each other. After using this freedom, effectively by absorbing (unphysical) phases into the fermion fields, nine parameters remain for each fermion mixing matrix in the SM4 and four in the SM3. They are not predicted by the Standard Model and have to be measured in experiments.

2.2.4. The Effects of Neutrino Mixing in the SM4 in a Nutshell

Many of the inputs used in the fits of this thesis are based on the assumption that either there are only three lepton generations or that the fourth generation neutrino ν_E does not mix with the other three, i.e. that the 3×3 submatrix $U_{3\times3}$ of the four-dimensional PMNS matrix U is

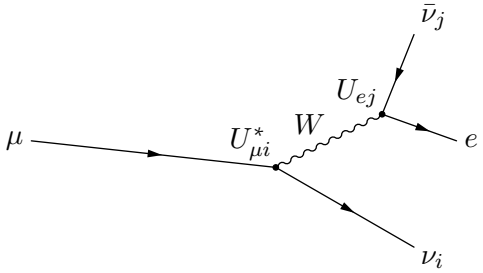

Figure 2.2.: Lowest order graph in the decay $\mu \to e\nu_i\bar{\nu}_j$, i,j=1,2,3.

unitary by itself. Then, a decay with final state leptons such as the decay of the muon - whose lifetime is measured to extract the Fermi constant G_F (see section 2.3) to an extraordinarily high precision (e.g. [58]) - can be described by an expression such as

$$\Gamma\left(\mu^- \to e^-\bar{\nu}_e\nu_\mu(\gamma)\right) = \frac{G_F^2 m_\mu^5}{192\pi^3} R_\mu F_{\mu,e} \tag{2.36}$$

where R_μ describes electroweak radiative corrections and $F_{\mu,e}$ is a phase space factor. As the lowest-order Feynman graph of this decay - see Fig. 2.2 - implies, the expression in eq. (2.36) is actually a sum over six different graphs, each of them with a different combination of neutrinos due to mixing, and weighted with the modulus of the appropriate PMNS matrix element. The processes are not distinguished because neutrinos are not detected in the experiment. As the Feynman graph shows, expression (2.36) therefore actually picks up an additional factor of

$$\sum_{i,j=1}^{3} |U_{\mu i}|^2 \, |U_{ej}|^2 \tag{2.37}$$

which is missing in eq. (2.36) because the unitarity of the SM3 PMNS matrix forces it to be exactly 1. In the SM4, the submatrix $U_{3\times3}$ which describes the mixing between ν_e, ν_μ and ν_τ cannot be assumed to be unitary. Also, the 4th generation neutrino ν_4 cannot be produced in the decay of a muon because it is too heavy. In order for the SM4 to be compatible with the number of invisible neutrino flavours observed at Z^0 resonance at the LEP, the ν_4 must be at least half as heavy as the Z^0, i.e. $m_{\nu_4} > m_Z/2$[24]. The sum expression in eq. (2.37) does not change with the addition of a fourth fermion family, but it does no longer add up to 1. An SM4 extraction of G_F can therefore not rely on measurements of muon decays alone but becomes more involved and less precise [59]. An updated value obtained by the method described in [59] is

$$G_F^{\mathrm{SM4}} = 1.1685^{+0.00013}_{-0.00014} \cdot 10^{-5}\,\mathrm{GeV}^{-2}. \tag{2.38}$$

Comparing this with the value quoted in [50] as obtained by the MuLan experiment [60], $G_F = (1.1663787 \pm 0.0000006) \cdot 10^{-5}\,\mathrm{GeV}^{-2}$, this is an upwards shift by 1.8 permille and a relative error 225 times as large.

The above argument is valid for any other measurement in (semi)leptonic decays. Also, wherever G_F was used as an input in the extraction of an observable or parameter within the SM3 framework, e.g. the modulus of a CKM matrix element, the change of G_F has to be accounted for

in a truly consistent SM4 analysis. However, in case of most inputs used in this thesis, the other contributions to their published uncertainty dominate over the contribution from using eq. (2.38) instead of the MuLan result in their extraction. For this reasion, the published SM3 result and uncertainty will be used as they are if there are no other effects to consider. The only exception from this is the modulus of the CKM matrix element V_{ud} (cf. sec. 4.1.1) due to the high precision of the extraction.

2.2.5. Parametrization of the Quark Mixing Matrix

It is customary to express as many of the free parameters mentioned in section 2.2.3 as possible as rotation angles and the rest as phases. In the SM3, three rotation angles are available and usually called θ_{12}, θ_{13} and θ_{23}. The fourth parameter is then expressed as a potentially CP violating phase δ in a complex exponential factor $e^{-i\delta}$. In the PDG's "Standard" parametrization of the CKM matrix proposed by Chau and Keung [61] they appear as follows:

$$V_{CKM3} = \begin{pmatrix} V_{ud} & V_{us} & V_{ub} \\ V_{cd} & V_{cs} & V_{cb} \\ V_{td} & V_{ts} & V_{tb} \end{pmatrix} \tag{2.39}$$

$$= \begin{pmatrix} 1 & 0 & 0 \\ 0 & c_{23} & s_{23} \\ 0 & -s_{23} & c_{23} \end{pmatrix} \cdot \begin{pmatrix} c_{13} & 0 & s_{13}e^{-i\delta} \\ 0 & 1 & 0 \\ -s_{13}e^{i\delta} & 0 & c_{13} \end{pmatrix} \cdot \begin{pmatrix} c_{12} & s_{12} & 0 \\ -s_{12} & c_{12} & 0 \\ 0 & 0 & 1 \end{pmatrix} \tag{2.40}$$

$$= \begin{pmatrix} c_{12}c_{13} & s_{12}c_{13} & s_{13}e^{-i\delta} \\ -s_{12}c_{23} - c_{12}s_{23}s_{13}e^{i\delta} & c_{12}c_{23} - s_{12}s_{23}s_{13}e^{i\delta} & s_{23}c_{13} \\ s_{12}s_{23} - c_{12}c_{23}s_{13}e^{i\delta} & -c_{12}s_{23} - s_{12}c_{23}s_{13}e^{i\delta} & c_{23}c_{13} \end{pmatrix} \tag{2.41}$$

Here, s_{ij} and c_{ij} are shorthand notations for $\sin\theta_{ij}$ and $\cos\theta_{ij}$. In case of the SM4, there are six rotation angles available, so three phases appear. Any CP violation in the quark sector is, in the present context, to be described in terms of those. In this thesis, the additional rotation angles are denoted by θ_u, θ_v and θ_w while the new phases are called ϕ_2 and ϕ_3. This nomenclature was used by Botella and Chau [62] who proposed the parametrization (A.8) of the SM4 CKM matrix used in CKMfitter at the beginning of the work on this thesis. As it proved unsuitable numerically - see Appendix B - another parametrization proposed by Hou and Soni in [63] was tried with more success. The difference between this parametrization and the Botella/Chau parametrization is the order in which the matrices in the product in eq. (2.42) are multiplied to

obtain V_{CKM4}:

$$V_{CKM4} = \begin{pmatrix} & V_{CKM3} & & 0 \\ & & & 0 \\ & & & 0 \\ 0 & 0 & 0 & 1 \end{pmatrix} \cdot \begin{pmatrix} 1 & 0 & 0 & 0 \\ 0 & 1 & 0 & 0 \\ 0 & 0 & c_u & s_u \\ 0 & 0 & -s_u & c_u \end{pmatrix} \cdot \begin{pmatrix} 1 & 0 & 0 & 0 \\ 0 & c_v & 0 & s_v e^{-i\phi_2} \\ 0 & 0 & 1 & 0 \\ 0 & -s_v e^{i\phi_2} & 0 & c_v \end{pmatrix} \cdot \begin{pmatrix} c_w & 0 & 0 & s_w e^{-i\phi_3} \\ 0 & 1 & 0 & 0 \\ 0 & 0 & 1 & 0 \\ -s_w e^{i\phi_3} & 0 & 0 & c_w \end{pmatrix} \tag{2.42}$$

The resulting matrix contains particularly simple expressions for the 4th row and 3rd column, simplifying terms involving interactions of t' quarks on the one hand and b quarks on the other hand:

$$\left(\begin{array}{c|c|c|c} c_{12}c_{13}c_w & s_{12}c_{13}c_v & s_{13}c_u e^{-i\delta} & c_{12}c_{13}s_w e^{-i\phi_3} \\ -s_{12}c_{13}s_v s_w e^{i(\phi_3-\phi_2)} & -s_{13}s_u s_v e^{i(-\delta+\phi_2)} & & +s_{12}c_{13}s_v c_w e^{-i\phi_2} \\ -s_{13}s_u c_v s_w e^{i(\phi_3-\delta)} & & & +s_{13}s_u c_v c_w e^{-i\delta} \\ \hline -s_{12}c_{23}c_w & c_{12}c_{23}c_v & s_{23}c_{13}c_u & c_{12}c_{23}s_v c_w e^{-i\phi_2} \\ -c_{12}s_{13}s_{23}c_w e^{i\delta} & -s_{12}s_{13}s_{23}c_v e^{i\delta} & & +c_{13}s_{23}s_u c_v c_w \\ -c_{12}c_{23}s_v s_w e^{i(\phi_3-\phi_2)} & -c_{13}s_{23}s_u s_v e^{i\phi_2} & & -s_{12}c_{23}s_w e^{-i\phi_3} \\ -c_{13}s_{23}s_u c_v s_w e^{i\phi_3} & & & -c_{12}s_{13}s_{23}s_w e^{i(\delta-\phi_3)} \\ +s_{12}s_{13}s_{23}s_v s_w e^{i(\delta-\phi_2+\phi_3)} & & & -s_{12}s_{13}s_{23}s_v c_w e^{i(\delta-\phi_2)} \\ \hline -c_{12}c_{23}s_{13}c_w e^{i\delta} & -c_{12}s_{23}c_v & c_{13}c_{23}c_u & c_{13}c_{23}s_u c_v c_w \\ +s_{12}s_{23}c_w & -s_{12}c_{23}s_{13}c_v e^{i\delta} & & -c_{12}s_{23}s_v c_w e^{-i\phi_2} \\ -c_{13}c_{23}s_u c_v s_w e^{i\phi_3} & -c_{13}c_{23}s_u s_v e^{i\phi_2} & & c_{12}c_{23}s_{13}s_w e^{i(\delta-\phi_3)} \\ c_{12}s_{23}s_v s_w e^{-i(\phi_2-\phi_3)} & & & +s_{12}c_{23}s_{13}s_v c_w e^{-(\delta-\phi_2)} \\ +s_{12}c_{23}s_{13}s_v s_w e^{i(\delta-\phi_2+\phi_3)} & & & +s_{12}s_{23}s_w e^{-i\phi_3} \\ \hline -c_u c_v s_w e^{i\phi_3} & -c_u s_v e^{i\phi_2} & -s_u & c_u c_v c_w \end{array}\right). \tag{2.43}$$

All rotation angles can be chosen to lie in the interval $[0, \pi/2]$. Phases δ and $\phi_{2,3}$ lie within the interval $[0, 2\pi]$ [64]. There is another frequently used naming convention for the rotation angles which is in accordance with the PDG's, i.e. their indices indicate between which axes the rotation takes place:

$$\theta_u = \theta_{34}, \qquad \theta_v = \theta_{24} \qquad \text{and} \qquad \theta_w = \theta_{14} \tag{2.44}$$

2.3. Weak Interactions at Low Energies

Many of the inputs used in the fits of Chapter 5 were obtained in measurements of processes at low energies. "Low" means that the four-momentum transfers Q^2 are small compared to the mass of the W boson mass. In Chapter 4, the SM3 values of these inputs will be checked for consistency with the assumption of the existence of a fourth fermion generation. Their theoretical expressions are based on a number of techniques to calculate cross sections of low-energy processes. Therefore, some familiarity with these techniques and their terminology on part of the reader is required.

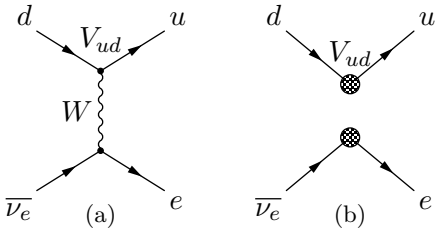

Figure 2.3.: β decay drawn at first order in the underlying Electroweak theory (a) and in effective theory (b).

As an in-depth description is clearly far beyond the scope of this thesis, the present section was written to recall a number of basic concepts and to refer readers to a number of works where the methods in question are explained in more detail.

Calculations using the complete electroweak theory with W bosons as dynamical entities are only necessary for processes taking place at energies of at least $\mathcal{O}(M_W)$. The charged current processes generally considered in this thesis, however, happen at much lower energies of $\mathcal{O}(m_B)$ and below. At these energies, it is possible to perform computations using an effective theory which can be considered as a generalisation of the Fermi theory for β decays (see e.g. [65]). If M_W dominates all other mass/energy scales present in a physics scenario, the W bosons' contribution to the electroweak Lagrangian density can be approximated by

$$\mathcal{L}_W \approx -\frac{g_2^2}{2M_W^2} J_\mu^\dagger J_\mu \tag{2.45}$$

from which one obtains the Fermi theory

$$\hat{H}_{eff}^{\text{tree}} = \frac{G_F}{\sqrt{2}} J_\mu^+ J^{-\mu} \tag{2.46}$$

if one defines the Fermi constant

$$G_F = \frac{g_2^2}{4\sqrt{2}M_W^2} = \frac{e^2}{4\sqrt{2}M_W^2 \sin^2\theta_W}. \tag{2.47}$$

In this regime, heavy particles such as W bosons and top quarks only appear as virtual particles whose effects are limited to changing the absolute value of a given amplitude. The effect usually depends on the momentum transfer Q^2.

2.3.1. Operator Product Expansion (OPE)

Processes beyond tree level can be described by a series of effective vertices known as operator product expansion (OPE) [66]:

$$\mathcal{H}_{eff} = \frac{G_F}{\sqrt{2}} \sum_l V_{CKM}^{(l)} C_i(\mu) \hat{Q}_i(\mu). \tag{2.48}$$

The lectures in [67] provide a thorough introduction of this method but certain aspects central to its use in the context of this work are also given in [68].

$V_{CKM}^{(l)}$ in eq. (2.48) is not just one CKM matrix element, but in general a product of several, depending on which quark lines meet in the effective vertex of the corresponding summand.

The local operator $\hat{Q}_i$ is represented by this effective vertex. The construction of such a local operator has to take into account all sorts of properties of the attached fermions such as color, flavour and tensor structure [67].

$C_i(\mu)$ is called a Wilson coefficient and could be described as an effective coupling constant for the vertex which represents $\hat{Q}_i$. It depends on a scale μ which serves as a divider between short distance effects of high four-momentum transfer Q^2 included in the Wilson coefficients, and long distance effects of low Q^2. The latter are put into the matrix elements of the $\hat{Q}_i$. The former can be calculated in perturbative QCD due to asymptotic freedom. They contain the effects of heavy particles which were eliminated as dynamical fields in this effective theory but which still appear as virtual particles in loops. The quantum corrections thus caused must be expected to be sizeable [68].

The matrix elements of $\hat{Q}_i$, such as $\langle \hat{Q}_i \rangle = \langle f | \hat{Q}_i | M \rangle$ in the case of a meson M decaying into a final state f, must also depend on μ because, as said before, μ only serves as a separation criterion between what goes into the $C_i(\mu)$ and what is put into the local operators $\hat{Q}_i$. A frequent choice is $\mu \approx \mathcal{O}(\text{mass of decaying hadron})$, but it can in principle be chosen arbitrarily. Also, a notable exception from the statement just made is the decay of B hadrons since its mass far exceeds the characteristic scales of the strong interactions involved [68]. A good choice is highly non-trivial to make and requires some considerations. However, this freedom means that the μ dependence of the C_i must cancel the μ dependence of the associated $\langle f | \hat{Q}_i | m \rangle$ in a given process. The cancellation generally involves terms belonging to different orders of the expansion in eq. (2.48).

The Wilson coefficients and therefore also the local operators' matrix elements depend not only on μ but also on the renormalization scheme used. Since the individual matrix elements of $\hat{H}_{eff}$ are each scaled by their assigned Wilson coefficient, this *non-multiplicative renormalization* can cause e.g. operators with new chirality, color or flavour structures to emerge (see [68] and its references [69] and[70]).

Not surprisingly, effective vertices come with their effective Feynman rules which have to be used in the calculation of amplitudes. They result from applying the fundamental Feynman rules of the Standard Model to the internal particles of effective vertices. In the context of this thesis, the coupling strength is the of those effective vertices. It depends on CKM matrix elements occuring in the respective effective vertex and on the mass of the internal fermions of the contributing diagrams of each effective vertex. The latter dependency obeys a number of basic functions called Inami-Lim functions after the authors who calculated them in [71]. Those Inami-Lim functions which are used in this thesis are explicitely printed in Appendix C. Mesons oscillations on which some of the inputs of this thesis were measured are described by box graphs as in Fig. 2.5 whose description in the effective theory uses the Inami-Lim function $S_0(x_i, x_j)$ (cf. eq. (C.1)), where $x_i = \frac{m_{q_i}^2}{m_W^2}$ and i denotes the flavour of the quark involved. The subscript 0 indicates that QCD corrections are not included. The derivation of equation $S_0(x_i, x_j)$ assumes the unitarity of the CKM matrix but is valid independent of the number of families. If both

virtual quarks in the box graph are of the same flavour, the Inami-Lim function simplifies to $S_0(x) = \lim_{x_j \to x} S(x, x_j)$ as given in (C.2).

2.3.2. Hadronic Matrix Elements and Bag Parameters

Calculations of the matrix elements of the operators $\hat{Q}_i$ in eq. (2.48) by definition involve long-distance (low Q^2) corrections. They must therefore use non-perturbative methods and are considered challenging. Despite considerable advances and enhancements during the last decade, they are still the main source of theoretical uncertainty. Several methods with different (dis)advantages are available and occasionally, it is possible to use e.g. a combination of measurements in which the resulting uncertainties cancel.

In case of non-leptonic decays of hadrons, non-perturbative effects are parametrized by means of a scale-dependent "bag parameter" B_M in combination with a meson decay constant f_M. In this thesis, such bag parameters will be encountered in the expressions of quantities extracted from meson oscillation, i.e. $\left\langle \bar{M}^0 \middle| \hat{O}_i \middle| M^0 \right\rangle$. The ansatz is to exploit [72, 68] that a complete set $\{\psi_i\}$ of quantum mechanical states can be used to express the identity operator as $\mathbf{1} = \sum_i |\psi_i\rangle \langle\psi_i|$. Such an identity is inserted between the currents of which $\hat{O}_i$ consists. In case of B_d^0 oscillation, for example

$$\left\langle \bar{B}_d^0 \middle| \hat{O}_i \middle| B_d^0 \right\rangle = \left\langle \bar{B}_d^0 \middle| \bar{b}\gamma^\mu\gamma^5 d \bar{b}\gamma_\mu\gamma^5 d \middle| B_d^0 \right\rangle = \sum i \left\langle \bar{B}_d^0 \middle| \bar{b}\gamma^\mu\gamma^5 d |\psi_i\rangle \langle\psi_i| \bar{b}\gamma_\mu\gamma^5 d \middle| B_d^0 \right\rangle . \tag{2.49}$$

Assuming that the vacuum state $|0\rangle$ dominates the sum, one approximates

$$\left\langle \bar{B}_d^0 \middle| \hat{O}_i \middle| B_d^0 \right\rangle \approx \left\langle \bar{B}_d^0 \middle| \bar{b}\gamma^\mu\gamma^5 d |0\rangle \langle 0| \bar{b}\gamma_\mu\gamma^5 d \middle| B_d^0 \right\rangle = \tag{2.50}$$

$$= \frac{2}{3} m_{B_d}^2 f_{B_d}^2 B_{B_d}(\mu). \tag{2.51}$$

B_d is the previously-mentioned bag factor. Its deviation from 1 parametrizes the error introduced by the above ansatz which is called "vacuum insertion" or "vacuum saturation approximation". QCD bag parameters generally depend both on the renormalization scheme and the renormalization scale μ. This μ dependence of the matrix element has to be cancelled by a corresponding μ dependence of the Wilson coefficient. The latter is caused by radiative QCD corrections which can be comprised in correction factors $\hat{\eta}_M$. The requirement that physical predictions be independent from scale and renormalization scheme can then be formulated by requiring the product $\hat{\eta}_M \cdot B$ must be scale and scheme independent. This can also be achieved by defining a scale independent bag parameter $\hat{B} = b(\mu) \cdot B(\mu)$ and a scale dependent QCD correction factor $\eta(\mu)_M = \hat{\eta}_M(\mu)/b(\mu)$. This is the convention which is used in the present work and in which the numerical values of the bag factors $\hat{B}_K$, $\hat{B}_{B_d}$ and $\hat{B}_{B_s}$ will be given later.

2.4. Discrete Symmetries in Nature and Their Violation

The symmetries briefly mentioned in section 2.1 on which the Standard Model's interactions are built are continuous symmetries described by Lie groups. This means, roughly speaking, that the parameters defining a transformation which belongs to these symmetry groups - i.e. the

components of the W_μ^i of the vector $\mathbf{W}_\mu$ of the SU(2) transformation in eq. 2.5 - can take on continuous values. Another example is the U(1) phase which likewise is a real number. By contrast, there are *discrete* transformations whose effects on physical processes can be studied and must be reflected in the mathematical description of such processes.

In the context of particle physics, the three basic symmetries of this kind are space inversion/-parity P, charge conjugation C, time reversal T and the combinations CP and CPT.

Before the advent of particle physics or, more precisely, relativistic quantum mechanics, all known physics and, hence, its description, was symmetric under both P and T ([68], chapters 1-3). The concept of antiparticles which is needed to give charge conjugation a meaning in the first place was not known yet. Time reversal invariance was theoretically allowed by classical mechanics and electrodynamics, which at the time meant: All known dynamics. In practise, though, it was obscured by macroscopic phenomena like friction and statistical effects such as the 2nd law of thermodynamics. In non-relativistic quantum mechanics, there are final states of the original process which are impossible to prepare as initial state of the time reversed process. As early as 1928, a little-known experiment by Cox, McIlwraith and Kurrelmeyer [73] actually observed parity violation, but this was not understood at the time [74]. Only in 1956, the discovery by Lee and Yang [75] that there was no evidence for P symmetry in weak interactions motivated the Wu experiment [76] which found that parity is indeed violated 100% in β decays. In the SM, this is reflected in the restriction of weak interaction to left-handed fermions as in eq. 2.2. Seven years later, Christenson, Cronin, Fitch and Turlay [77] discovered CP violation, providing scientists with another big surprise.

In this section, these three symmetries will be very briefly recalled. Slightly longer paragraphs will introduce the combinations CPT and especially CP which is closely connected to the constraints on an SM4 CKM matrix as described in sections 2.5, 4.1.10 and 4.2. For the implementation of the symmetry transformations as operators in quantum mechanics, see e.g. the discussion in [68].

2.4.1. Parity Transformation P

As mentioned above, this was the first symmetry which proved to be broken in weak interactions. Under this symmetry transformation, vectors in space change their sign, i.e.

$$\vec{x} \xrightarrow{\mathbf{P}} -\vec{x}. \tag{2.52}$$

In other words, **P** performs a point reflection at the origin. Objects such as angular momenta ($\vec{l} = \vec{x} \times \vec{p}$), where $\vec{p}$ is a momentum and $\vec{x}$ is a position, do not change their sign. They are therefore classified as axial vectors. By multiplying an axial vector with a vector, one obtains a pseudoscalar, i.e. a scalar which changes its sign under parity.

2.4.2. Charge Conjugation C

Unlike **P** and **T**, the charge conjugation **C** is not a space time transformation. It reverses the signs of all charges of a particle f, turning it into its anti-particle with the same spin (indicated

by the vertical arrow subscript):

$$|f_\uparrow\rangle \xrightarrow{\mathbf{C}} \left|\bar{f}_\uparrow\right\rangle \tag{2.53}$$

2.4.3. Time Reversal T

This operation mirrors the time axis, i.e. it maps $t \mapsto -t$. As one would expect from "moving back the time", momenta and angular momenta are reversed:

$$|f_\uparrow(\vec{x}, t, \vec{p})\rangle \xrightarrow{\mathbf{T}} |f_\downarrow(\vec{x}, -t, -\vec{p})\rangle \tag{2.54}$$

Unlike charge conjugation and parity transformation which are performed by applying unitary operators to the Lagrangian, time reversal in quantum mechanics is implemented by an antiunitary operator.

2.4.4. CP - Keeping Scientists Busy Since 1964

The above symmetry transformations can be combined. One such combination is **CP**. In terms of the notation used above,

$$|f_\uparrow(\vec{x}, t, \vec{p})\rangle \xrightarrow{\mathbf{CP}} \left|\bar{f}_\downarrow(-\vec{x}, t, -\vec{p})\right\rangle . \tag{2.55}$$

CP violation means that observing a process happening with particles will yield a different result from what is obtained when observing the process happening with anti-particles in a spatial setup reflected at the origin, i.e. a different reaction rate. The historical discovery of 1964 was the observation of the decay $K_L \to \pi\pi$. CP violation can currently only be described (by means of the mixing matrices, for example) phenomenologically but is not yet actually understood [68]. The CP violation which occurs in the phenomena serving as inputs for the fits presented in this work is described by means of the CKM matrix.

In Quantum Chromodynamics, CP violation puzzles scientists with its *absence*. It can be shown in several ways [68] that the general QCD Lagrange density $\mathcal{L}_{QCD}$ contains terms which violate time reversal and parity invariance. If this is not to manifest itself in experiment - e.g. in an non-zero electric dipole moment of the neutron - then the parameters of $\mathcal{L}_{QCD}$ appear to be fine-tuned as there is no apparent reason why they should conspire to set CP violation in QCD to zero. Indeed, e.g. the result of measuring the neutron's electric dipole moment is compatible with zero [78]:

$$d_N < 2.9 \cdot 10^{-26} \text{e cm at } 90\% \text{ CL} \tag{2.56}$$

This so-called "strong CP problem" has not yet been solved. It will not be considered any further in the present thesis. For the present purpose, CP violation is assumed to be caused by the KM mechanism in electroweak interactions.

2.4.5. CPT

Before going into more detail concerning CP violation in the next sections, the combination of all three discrete symmetry operations will be mentioned. While CPT can be violated in modern string or d-brane theories [79], it was shown by Lüders [80] that a relativistic local quantum

field theory will always be invariant under this tranformation. As the SM with both three and four families falls under this category, CPT symmetry is assumed throughout this thesis and in the formalisms used. One consequence of CPT being a symmetry of a system and the theory describing it, respectively, is that CP violation always implies a time-reversal asymmetry.

2.4.6. The Unitarity Triangle - Visualising CP Violation

The unitarity of the CKM matrix $V_{\mathrm{CKM}}^{\dagger} V_{\mathrm{CKM}} = V_{\mathrm{CKM}} V_{\mathrm{CKM}}^{\dagger} = \mathbf{1}$ can also be expressed in terms of matrix elements, i.e.

$$\sum_{i=1}^{N_g} V_{il} V_{ki}^{*} = \sum_{i=1}^{N_g} V_{il}^{*} V_{ki} = \delta_{k,l} \tag{2.57}$$

where V is short for V_{CKM}, N_g is the number of fermion generations and $\delta_{k,l}$ is a Kronecker symbol. As the elements of the CKM matrix are generally complex, all products $V_{il} V_{ki}^{*}$ can be represented by vectors in the complex plane $\mathbb{C}$. If $k \neq l$, eq. (2.57) is zero and the "arrowhead" of the vector representing the last summand connects to the origin, i.e. the "tail" of the vector representing the first summand.

In case of three fermion generations, the picture one obtains is a triangle in the complex plane (Pointed out by Bjorken, [81], [82]). One can form six different triangles in this case. While they look quite different from each other, it can be shown that they all have the same area

$$A_{\triangle} = \frac{1}{2} J \tag{2.58}$$

where J is the Jarlskog [83], [57] determinant:

$$J = \pm \mathrm{Im}\left(V_{ij} V_{kl} V_{il}^{*} V_{kj}^{*} \right) \qquad i \neq k,\ j \neq l \tag{2.59}$$

J is phase convention independent and thus a physical observable which measures the amount of CP violation in the SM3. Different phase choices due to e.g. different parametrizations of the CKM matrix rotate the whole triangle in the complex plane without changing its shape.

Usually, and also in this thesis, the term "Unitarity Triangle" refers to the triangle which is measured in the B_d^0-$\overline{B}_d^0$ meson system and shown in Fig. 2.4. Its horizontal side length is equal to 1 due to the division of the sides by $V_{cd} V_{cb}^{*}$. In this thesis the angles of the Unitarity Triangle will be called α, β and γ as indicated in Fig. 2.4. Their definition is

$$\alpha = \arg\left(-\frac{V_{td} V_{tb}^{*}}{V_{ud} V_{ub}^{*}} \right), \qquad \beta = \arg\left(-\frac{V_{cd} V_{cb}^{*}}{V_{td} V_{tb}^{*}} \right), \qquad \gamma = \arg\left(-\frac{V_{ud} V_{ub}^{*}}{V_{cd} V_{cb}^{*}} \right). \tag{2.60}$$

Unitarity Polygon in the SM4

The last equations make it clear that in the SM4 there are four vectors in the complex plane to be arranged head-to-tail instead of three. They now form a quadrangle. While this makes the definition of an SM4 equivalent of the Jarlskog determinant rather complicated (see e.g. [85], [86]

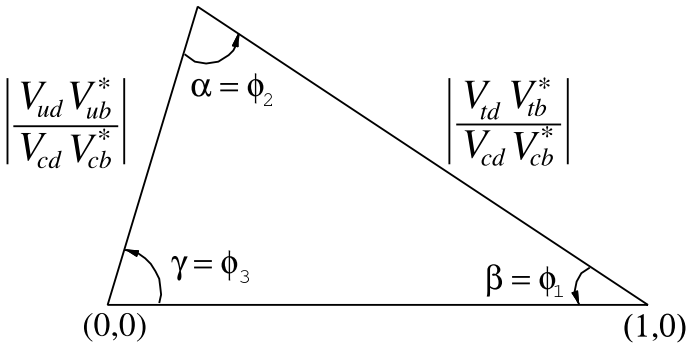

Figure 2.4.: The Unitarity Triangle of the B_d^0 system in the SM3. ϕ_1, ϕ_2 and ϕ_3 are just the angles in eq. (2.60), in a different naming convention which will not be used in the present work. They are not to be confused with the parameters in the parametrisation of the CKM matrix eq. (2.43). All sides are normalized to $\left|V_{cd}V_{cb}^*\right|$. Reproduced from [84].

and references therein, and [10]), for this thesis it is mostly of interest because it points to one of the questions which have to be asked before any input measured in the SM3 framework is used in SM4 related fits: Do the experiments really measure the same quantity in the SM4 as in the SM3? If they do not, are any SM4-specific contributions negligible so that the interpretation of the measurement can remain SM3-like or must the theoretical expressions be adapted? For each input used in the fits presented in sec. 5, a discussion is provided in sec. 4.

2.5. CP Violation in Meson Oscillation

2.5.1. General formalism

Meson oscillation is the name of the process when an electrically neutral meson M^0 spontaneously turns into its antiparticle $\overline{M}^0$. Such events are observed in K^0, B_d^0, B_s^0 and D^0 mesons. There is a priori no reason for these processes to be CP conserving. Meson oscillation is to be understood in quantum mechanical terms, i.e. if one prepares a pure M^0 initial state and identifies it at a later time - by detecting its decay products, for instance - it is possible that what one finds is an $\overline{M}^0$. This occurs in vacuum and thus without any interactions of the meson with any other matter or radiation. The general formalism presented in this section describes meson oscillation and is discussed in greater detail e.g. in [68] and other publications. It is assumed that M^0 and $\overline{M}^0$ are distinguished by an internal quantum number F and that no interactions violate electric charge conservation. In the context of the present work, these internal quantum numbers are the flavour quantum numbers Strangeness (S), Charm (C) and Beauty (B), or the respective weak isospin component I_3 (cf. Tab. 2.1). Within the GSW theory of electroweak interaction (i.e.: the Standard Model), these quantum numbers can only be changed by the weak interaction. An oscillation $M^0 \to \overline{M}^0$ is a $\Delta F = 2$ transition. It can thus be brought about by one application of a Hamilton Operator $H_{\Delta F=2}$ to the initial state $\left|M^0\right\rangle$ or by applying another Hamiltonian $H_{\Delta F=1}$

twice. A weak Hamiltonian could be written as

$$\mathcal{H} = H_{\Delta F=0} + H_{\Delta F=1} + H_{\Delta F=2}. \tag{2.61}$$

$H_{\Delta F=2}$ is not needed in an SM-like context as it allows (hypothetical) so-called super-weak forces which have not been discovered and are not part of the SM. The Hamiltonian thus becomes

$$\mathcal{H} = H_{\Delta F=0} + H_{\Delta F=1}. \tag{2.62}$$

In order to be able to do at least some calculations, this general situation is then simplified by a number of assumptions:

- The initial state is a superposition of M^0 and $\overline{M}^0$ only: $|\Psi(t=0)\rangle = a(t)\left|M^0\right\rangle + b(t)\left|\overline{M}^0\right\rangle$.
- Only $a(t)$ and $b(t)$ are of interest (not any coefficients of final states to which M^0 or its antiparticle can decay).
- The time scale considered is much larger than typical time scales of the strong interaction (Weisskopf-Wigner approximation, [87], [88]). This allows one to treat the weak interaction as independent from the strong interaction.

The system's state $|\Psi\rangle$ is thus constrained to the subspace spanned by M^0 and $\overline{M}^0$ and its Schrödinger equation can be written as

$$\mathrm{i}\hbar\frac{\partial}{\partial t}|\Psi(t)\rangle = \mathcal{H}|\Psi(t)\rangle \tag{2.63}$$

where

$$\Psi(t) = \begin{pmatrix} a(t) \\ b(t) \end{pmatrix} \qquad \text{and} \qquad \mathcal{H} = \mathbf{M} - \frac{\mathrm{i}}{2}\mathbf{\Gamma} = \begin{pmatrix} M_{11} - \frac{\mathrm{i}}{2}\Gamma_{11} & M_{12} - \frac{\mathrm{i}}{2}\Gamma_{12} \\ M_{21} - \frac{\mathrm{i}}{2}\Gamma_{21} & M_{22} - \frac{\mathrm{i}}{2}\Gamma_{22} \end{pmatrix}. \tag{2.64}$$

Any transitions $\left|M^0\right\rangle \leftrightarrow \left|\overline{M}^0\right\rangle$ are governed by the off-diagonal elements of $\mathcal{H}$. While $\mathbf{M}$ and $\mathbf{\Gamma}$ are hermitian, $\mathcal{H}$ is not [89] as it describes the decay of a particle by its "vanishing" [79]. Still, this is enough to simplify the Hamiltonian a bit:

$$\mathcal{H} = \begin{pmatrix} M_{11} - \frac{\mathrm{i}}{2}\Gamma_{11} & M_{12} - \frac{\mathrm{i}}{2}\Gamma_{12} \\ M_{12}^* - \frac{\mathrm{i}}{2}\Gamma_{21}^* & M_{22} - \frac{\mathrm{i}}{2}\Gamma_{22} \end{pmatrix}$$

The matrix elements can be constrained by symmetry requirements. With the definitions

$$\hat{C}\left|M^0\right\rangle = -\left|\overline{M}^0\right\rangle, \qquad \hat{P}\left|M^0\right\rangle = -\left|\overline{M}\right\rangle \qquad \text{and} \qquad \hat{T}\left|M^0\right\rangle = -\left|M^0\right\rangle, \tag{2.65}$$

these are

$$\textbf{CPT} \text{ or } \textbf{CP} \text{ invariance} \implies M_{11} = M_{22}, \quad \Gamma_{11} = \Gamma_{22} \tag{2.66}$$

$$\textbf{CP} \text{ or } \textbf{T} \text{ invariance} \implies \operatorname{Im} M_{12} = 0 = \operatorname{Im}\Gamma_{12}, \tag{2.67}$$

$$M_{12} = M_{21}, \quad \Gamma_{12} = \Gamma_{21}. \tag{2.68}$$

Of course, of these symmetries only CPT is conserved in the phenomena of this chapter. The resulting form of $\mathcal{H}$ is then

$$\mathcal{H} = \begin{pmatrix} M_{11} - \frac{\mathrm{i}}{2}\Gamma_{11} & M_{12} - \frac{\mathrm{i}}{2}\Gamma_{12} \\ M_{12}^* - \frac{\mathrm{i}}{2}\Gamma_{21}^* & M_{11} - \frac{\mathrm{i}}{2}\Gamma_{11} \end{pmatrix}. \tag{2.69}$$

In order to find the mass eigenstates of $\mathcal{H}$, it is diagonalized in a way that simultaneously does so for $\mathbf{M}$ and $\mathbf{\Gamma}$. The method which was developed in [90] and [91] and is described in [68] makes use of the representation of $\mathcal{H}$ as a linear combination of the Pauli matrices σ_i:

$$\mathcal{H} = \mathbf{M} - \frac{\mathrm{i}}{2}\mathbf{\Gamma} = E_1\sigma_1 + E_2\sigma_2 + E_3\sigma_3 - \mathrm{i}D\mathbf{1} \tag{2.70}$$

Comparing both sides of eq. (2.70) one finds in the most general case *without* invoking any symmetry requirements yet:

$$E_1 = \mathrm{Re}\,(M_{12}) - \frac{\mathrm{i}}{2}\mathrm{Re}\,(\Gamma_{12}) \tag{2.71}$$

$$E_2 = -\,\mathrm{Im}\,(M_{12}) + \frac{\mathrm{i}}{2}\mathrm{Im}\,(\Gamma_{12}) \tag{2.72}$$

$$E_3 = \frac{1}{2}(M_{11} - M_{22}) - \frac{\mathrm{i}}{4}(\Gamma_{11} - \Gamma_{22}) \tag{2.73}$$

$$D = \frac{\mathrm{i}}{2}(M_{11} + M_{22}) + \frac{1}{4}(\Gamma_{11} + \Gamma_{22}) \tag{2.74}$$

Writing the vector $\vec{E} = (E_1, E_2, E_3)$ in spherical coordinates

$$\vec{E} = \left|\vec{E}\right| \cdot \begin{pmatrix} \sin\theta\cos\varphi \\ \sin\theta\sin\varphi \\ \cos\theta \end{pmatrix} \tag{2.75}$$

and keeping in mind that oscillations require the off-diagonal elements of $\mathcal{H}$ to be non-zero reveals a general condition for $M^0 \leftrightarrow \overline{M}^0$ oscillations:

$$\left|\vec{E}\right| \neq 0 \qquad \sin\,\theta \neq 0. \tag{2.76}$$

The contraints which various symmetries place on the matrix elements of both $\mathbf{M}$ and $\mathbf{\Gamma}$ (Eqs. (2.66) and(2.67)) can now be translated into constraints on θ and ϕ:

$$\textbf{CPT} \text{ or } \textbf{CP} \text{ invariance} \quad \Longrightarrow \quad \cos\theta = 0 \tag{2.77}$$

$$\textbf{CP} \text{ or } \textbf{T} \text{ invariance} \quad \Longrightarrow \quad \cos\varphi = 0 \tag{2.78}$$

Oscillations are therefore a necessary consequence of both CPT and CP invariance. The converse is not true: There are phase conventions in which CP is violated but $\cos\,\theta = 0$ or $\varphi = 0$.

The resulting mass eigenstates are

$$|m_1\rangle = p_1 \left|M^0\right\rangle + q_1 \left|\overline{M^0}\right\rangle \text{ and} \tag{2.79}$$
$$|m_2\rangle = p_2 \left|M^0\right\rangle - q_2 \left|\overline{M^0}\right\rangle \text{ and}$$

If CPT symmetry holds, $p_1 = p_2 = p$, $q_1 = q_2 = q$. The mass eigenvalues are then

$$m_1 - \frac{\mathrm{i}}{2}\Gamma_1 = -\mathrm{i}D + E = M_{11} - \frac{\mathrm{i}}{2}\Gamma_{11} + \frac{q}{p}\left(M_{12} - \frac{\mathrm{i}}{2}\Gamma_{12}\right) \tag{2.80}$$
$$m_2 - \frac{\mathrm{i}}{2}\Gamma_2 = -\mathrm{i}D - E = M_{11} - \frac{\mathrm{i}}{2}\Gamma_{11} - \frac{q}{p}\left(M_{12} - \frac{\mathrm{i}}{2}\Gamma_{12}\right) \tag{2.81}$$

where $m_{1,2}$ and $\Gamma_{1,2}$ are real and

$$\frac{q}{p} = \pm\sqrt{\frac{M_{12}^* - \frac{\mathrm{i}}{2}\Gamma_{12}^*}{M_{12} - \frac{\mathrm{i}}{2}\Gamma_{12}}}. \tag{2.82}$$

Choosing the negative instead of the positive sign here is equivalent to interchanging the subscripts of the eigenstates in eqs. (2.80) and (2.81) as these are only distinguished by this particular sign. It is noteworthy that $|M_1\rangle$ and $|M_2\rangle$ are not necessarily orthogonal if CP is violated. This is in agreement with $\mathcal{H}$ not being hermitian.

2.5.2. Mass and Lifetime Differences Δm and $\Delta\Gamma$

With eqs. (2.80) and (2.81) the mass and decay rate differences between the eigenstates of $\mathcal{H}$ are

$$\Delta m = m_2 - m_1 = -2\mathrm{Re}\left(\frac{q}{p}\left(M_{12} - \frac{\mathrm{i}}{2}\Gamma_{12}\right)\right) \qquad \text{and} \tag{2.83}$$
$$\Delta\Gamma = \Gamma_1 - \Gamma_2 = -4\mathrm{Im}\left(\frac{q}{p}\left(M_{12} - \frac{\mathrm{i}}{2}\Gamma_{12}\right)\right),$$

respectively. Δm is defined to be positive for kaons. In this work, only Δm_d and Δm_s of $B_{d,s}$ mesons are used as inputs, however. As absolute phases are not physically relevant, it is possible to change them by suitable transformations. One such transformation of the Hamiltonian is

$$M_{12} - \frac{\mathrm{i}}{2}\Gamma_{12} \longrightarrow e^{\mathrm{i}\xi}\left(M_{12} - \frac{\mathrm{i}}{2}\Gamma_{12}\right). \tag{2.84}$$

A relative phase ζ between M_{12} and Γ_{12} as in the following equation, however, is *not* irrelevant and is indeed observable in indirect CP violation (cf. sec. 2.6):

$$\frac{\Gamma_{12}}{M_{12}} = \frac{|\Gamma_{12}|}{|M_{12}|}e^{\mathrm{i}\zeta}. \tag{2.85}$$

For B_d and B_s mesons, it is measured [92] that $|\Gamma_{12}| \ll |M_{12}|$. Therefore, a phase transformation as in (2.84) can be used to simplify the first line in (2.83) to

$$\Delta m \simeq -2\,|M_{12}|\,. \tag{2.86}$$

This implies that CP is *not* appreciably violated in the oscillation, as can be inferred from eqs. (2.67). The simplification given in (2.86) is the formulation used for constraining SM(4) parameters with measurements of Δm of neutral B and B_s mesons.

Such measurements use the fact that the mass eigenstates in (2.79) undergo an exponential time evolution:

$$|m_{1,2}(t)\rangle = e^{-i(m_{1,2}-\mathrm{i}/2\Gamma_{1,2})t}\,|m_{1,2}(t=0)\rangle \tag{2.87}$$

Expressed in flavour eigenstates (describing, for example, an initially pure $\left|K^0\right\rangle$ beam), this is

$$\begin{aligned}\left|M^0(t)\right\rangle &= f_+\left|M^0\right\rangle + f_-\frac{q}{p}\left|\overline{M}^0\right\rangle \\ \left|\overline{M}^0(t)\right\rangle &= f_+\left|\overline{M^0}\right\rangle + f_-\frac{q}{p}\left|M^0\right\rangle\end{aligned} \tag{2.88}$$

with

$$f_\pm = \frac{1}{2}e^{-(\mathrm{i}m_1-\frac{1}{2}\Gamma_1)t}\left(1 \pm e^{-(\mathrm{i}\Delta m-\frac{1}{2}\Delta\Gamma)t}\right). \tag{2.89}$$

2.6. Types of CP Violation

CP violating phenomena are often classified into three complementary groups. As later Chapters of the present work will occasionally make use of the corresponding nomenclature, this classification is repeated here. For more detail, see e.g. [68], [72] and [93].

CP Violation in Decay

Let A_f be the amplitude $\langle f\,|\,\mathcal{H}\,|\,M\rangle$ of the decay $M \to f$. The charge conjugated process is then denoted by $\bar{A}_{\bar{f}} = \left\langle \bar{f}\,\middle|\,\mathcal{H}\,\middle|\,\bar{M}\right\rangle$. Assuming that several processes contribute to these amplitudes, the total amplitudes can be written as the sums

$$A_f = \sum_i A_{f,i} \quad \text{and} \quad \bar{A}_{\bar{f}} = \sum_i \bar{A}_{\bar{f},i}, \tag{2.90}$$

respectively. In general, each amplitude comes with a "weak phase" ϕ_W which changes sign under charge conjugation and another phase ϕ_s which does not. The latter is called "strong phase" because its dominant contribution is from strong interaction of intermediate states of the respective decay [72]. One can therefore write

$$A_{f,i} = \left|A_{f,i}\right| e^{\mathrm{i}(\phi_{s,i}+\phi_{W,i})} \quad \text{and} \quad \bar{A}_{f,i} = \left|A_{f,i}\right| e^{\mathrm{i}(\phi_{s,i}-\phi_{W,i})}. \tag{2.91}$$

Then,

$$\left|\frac{\bar{A}_{\bar{f}}}{A_f}\right| = \left|\frac{\sum_i A_{f,i} e^{\mathrm{i}(\phi_{s,i}-\phi_{W,i})}}{\sum_i A_{f,i} e^{\mathrm{i}(\phi_{s,i}+\phi_{W,i})}}\right|. \tag{2.92}$$

For CP violation to occur, i.e.

$$\left|A_f\right|^2 - \left|\bar{A}_{\bar{f}}\right|^2 = -2\sum_{i,j} A_{f,i}A_{f,j}\sin(\phi_{W,i}-\phi_{W,j})\sin(\phi_{s,i}-\phi_{s,j}) \neq 0 \quad \Leftrightarrow \quad \left|\frac{\bar{A}_{\bar{f}}}{A_f}\right| \neq 1, \tag{2.93}$$

there must at least be two contributing amplitudes $A_{f,i}$ which differ from each other both in their weak and their strong phases. No other phenomena such as oscillation are required for this type of CP violation to arise, leading to the term *CP violation in decay*. Perhaps less clear is the other frequently encountered appellation *direct CP violation*. Unfortunately, the latter is sometimes also used for another case (see below).

If no oscillation occurs, i.e. $\Delta M = \Delta\Gamma = 0$ and, of course, in the case of charged mesons, this is the only way to generate CP violation.

CP Violation in Mixing - Flavour-Specific Decays

In cases where $\left|A_f\right| = \left|\bar{A}_{\bar{f}}\right|$ and $\left|A_{\bar{f}}\right| = \left|\bar{A}_f\right| = 0$, i.e.

$$M^0 \to f \not\leftarrow \bar{M}^0 \quad \text{and} \quad M^0 \not\to \bar{f} \leftarrow \bar{M}^0, \tag{2.94}$$

CP violation can occur due to mixing

$$M^0 \to \bar{M}^0 \to \bar{f} \quad \text{and} \quad \bar{M}^0 \to M^0 \to f \tag{2.95}$$

and manifest itself in "wrong-sign" final states as in the semileptonic asymmetries described in Sec. 4.3. The requirement here is $\left|A(M^0 \to \bar{M}^0)\right| \neq \left|A(\bar{M}^0 \to M^0)\right|$, leading to the name *CP violation in mixing*. In terms of the formalism presented previously, this is implemented by

$$\left|\frac{q}{p}\right| \neq 1, \tag{2.96}$$

i.e. there is a relative phase between $\mathbf{M_{12}}$ and $\mathbf{\Gamma_{12}}$ (cf. eq. (2.82)). In some sources, this type of CP violation is referred to as *indirect CP violation*.

Interference in Flavour-*non*specific Final States

Even if the conditions for the above two types of CP violations, eqs. (2.93) and (2.96), are not met, CP violation can still occur if

$$\frac{q}{p}\cdot\frac{\bar{A}_{\bar{f}}}{A_f} \neq \pm 1. \tag{2.97}$$

The "full name" of this phenomenon is "CP violation in interference between decays with and without mixing", i.e. a final state is fed by decays of both M^0 and $\bar{M}^0$:

$$M^0 \to f \leftarrow \bar{M}^0 \leftarrow M^0 \quad \text{and} \quad \bar{M}^0 \to f \leftarrow M^0 \leftarrow \bar{M}^0 \tag{2.98}$$

This is sometimes called "interference between mixing and decay" and, probably to confuse the uninitiated, there exists a special case of this type which is called "direct CP violation" [72]. This term will *not* be used in this sense in the present work.

The three types of CP violation are *not* mutually exclusive - there is a priori no reason why they should occur only one at at time.

2.6.1. Meson Oscillation in the SM3 and SM4

After presenting a formalism with the necessary features to describe and calculate CP violation in meson oscillations in sec. 2.5.1, the various quantities introduced here will be connected to the SM3(4) by writing them in terms of the effective Hamiltonians describing weak interactions at low energies. In the SM3 (and therefore also in the SM4, which contains no new interactions), meson oscillations receive contributions from such Feynman graphs as shown in Fig. 2.5. These are the lowest order contribution to the non-diagonal elements of an effective Hamiltonian, i.e. [68]

$$\left\langle B^0 \left| \mathcal{H}^\dagger \right| \overline{B}^0 \right\rangle_{(\mu)} = M_{12} - \frac{\mathrm{i}}{2}\Gamma_{12} \tag{2.99}$$

where μ denotes the energy scale at which QCD corrections are evaluated. The corresponding QCD corrected expression for M_{12} from the effective theory in the SM4 is - see e.g. [25] -

$$M_{12} = \frac{G_F^2 m_M \hat{B} f_M^2 m_W^2}{12\pi^2} \cdot \sum_{i,j} \left(\eta_{ij}(\mu) S_0(x_i, x_j) \lambda_i^M \lambda_j^M \right). \tag{2.100}$$

Here, i and j denote the up-type quark flavours which can occur in the box graph while the superscript M of the λ indicates the type of meson and hence the down type quark flavours it is made up of. m_M and f_M are the mass and the decay constant of the oscillating meson. $\hat{B}$ is a bag factor, and m_W ist the W boson mass. The λ is a product of CKM matrix elements of the form $V_{\hat{u}_i q} V^*_{\hat{u}_j \mathfrak{q}}$ and the S_0 are the Inami-Lim functions given in Appendix C.0.1. For $i = j$, S_0 simplifies to eq. (C.2). The η_{ij} are the QCD corrections.

Equation (2.100) gives the general expression for the meson oscillations relevant in this work, i.e. those of kaons, B^0 and B_s^0. In chapter 4, the observables used to constrain the CKM matrix are discussed and suitable versions of eq. (2.100) will be given. They follow from (2.100) by specifying the meson type M and thus its constituent quarks and omitting those contributions which are numerically irrelevant. These are from box graphs whose amplitudes are very small due to the small $\lambda^M_{\hat{u}_i q}$ and/or the low mass of the virtual up-type quarks $\hat{u}_{i,j}$ and the resulting small value of the S_0.

Γ_{12} arises from decays of both the meson and its antimeson to common final states. The decay is calculated by combining two $\Delta B = 1$ operators of the effective theory as in the leading order graphs shown in Fig. 2.6. The up-type quark states drawn as intermediate states $\hat{u}$ in Fig. 2.5 are

u and c quarks whose mass is considerably lower than the b mass. They are *physical* intermediate states in the calculation, but final states of the decay. The matrix element of the decay can in this way be calculated by means of a loop integral instead of a complicated phase-space problem [237]. The expression for Γ_{12} used in this thesis, i.e. the one needed for $B^0_{(s)}$ mesons, is given in [94]:

$$\Gamma_{12} = -\left(\lambda_c^{(M)\,2}\Gamma_{12}^{cc} + \lambda_u^{(M)\,2}\Gamma_{12}^{uu} + 2\lambda_c^{(M)}\lambda_u^{(M)}\Gamma_{12}^{uc}\right) \tag{2.101}$$

The λ are defined like those in eq. (2.100). The coefficients Γ_{12}^{ab} determine the magnitude of the contribution with the corresponding CKM structure. They are computed by means of a Heavy Quark Expansion (HQE), i.e. the decay width difference is expanded in powers of Λ_{QCD}/m_b and each of the terms in the series is then multiplied by a series of radiative correction in $\alpha_S(m_b)$ [96]. The theoretical expressions for Γ_{12}^{ab} used in this thesis are given in [95] where a new operator basis was introduced. It considerably reduces the theoretical uncertainties compared to previous publications on the subject. These expressions read

$$\Gamma_{12}^{ab} = \frac{G_F^2 m_b^2}{24\pi} m_{B_q} f_{B_q}^2 \left[\left(G^{ab}(z) + \frac{\alpha_2}{2}G_S^{ab}(z)\right)\frac{8}{3}B + G_S^{ab}(z)\frac{\alpha_1}{3}\widetilde{B}'_S\right] + \widetilde{\Gamma}^{ab}_{12,1/m_b}. \tag{2.102}$$

Here,

$$G^{ab}_{(S)} = (-)\left(F^{ab}_{(S)}(z) + P^{ab}_{(S)}(z)\right) \tag{2.103}$$

where the $F^{ab}_{(S)}$ are contributions from current-current operators Q_1 and Q_2 while the smaller coefficients $P^{ab}_{(S)}$ come from penguin operators $Q_{3\ldots6,8}$ of the corresponding OPE. The quantities with a subscript $_S$ are coefficients of the operator Q_S which arises in the calculation [97] and refers to this operator's **s**calar tensor strucure. $\widetilde{\Gamma}^{ab}_{12,1/m_b}$ comprises effects suppressed by $\bar{\Lambda}/m_b$. B and $\tilde{B}'_S$ are bag factors.
α_1 and α_2 contain NLO corrections and are specific to the $\overline{\text{MS}}$ scheme used in [95] and also in this work:

$$\begin{aligned}\alpha_1 &= 1 + \frac{\alpha_S(\mu_2)}{4\pi}\frac{4}{3}\left(12\ln\frac{\mu_2}{m_b} + 6\right)\\ \alpha_2 &= 1 + \frac{\alpha_S(\mu_2)}{4\pi}\frac{4}{3}\left(6\ln\frac{\mu_2}{m_b} + \frac{13}{2}\right)\end{aligned} \tag{2.104}$$

$4/3$ is a colour factor and μ_2 is the scale at which the operators Q and $\widetilde{Q}_S$ are defined. A full listing of the expressions $F^{ab}_{(S)}$ and $P^{ab}_{(S)}$ would be beyond the purpose of this discussion and can be found in [94].

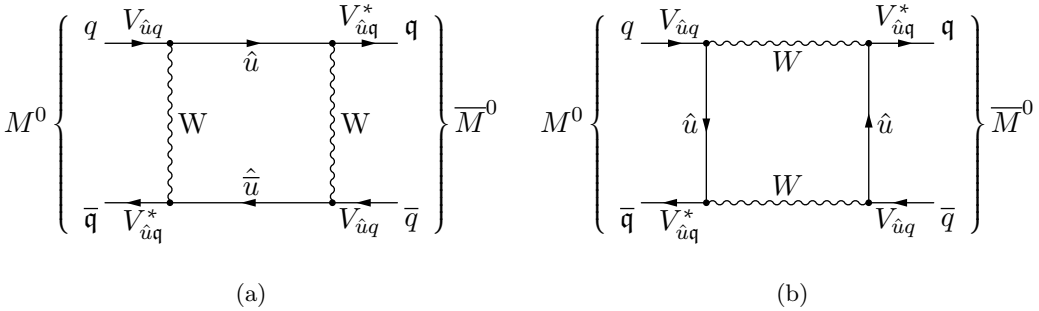

Figure 2.5.: Lowest order SM(4) weak interaction processes contributing to meson oscillation. $\hat{u}$ can be either u, c, t or t$'$. The meaning of $\mathfrak{q}$ and q depends on the M^0 under consideration. For $M^0 = K^0$, $\mathfrak{q} = s$ and $q = d$. For both B^0 and B^0_s, $\mathfrak{q} = b$ while $q = d$ and s, respectively. The CKM matrix elements must be chosen accordingly.

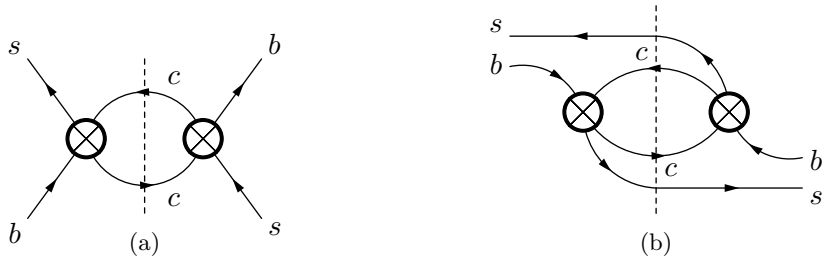

Figure 2.6.: Examples of quark level graphs contributing to Γ^{cc}_{12} at leading order in a B^0_s decay. For Γ^{uc}_{12} or Γ^{uu}_{12}, replace one and two c quarks by an u, respectively. For B^0 decay, replace s by d. The dashed lines indicate the presence of a physical $c\bar{c}$ state. In case of a decay - and not an oscillation - takes place. The crosses denote any of the operators Q_{1-6} of the OPE (cf. [95]). For the relevant NLO QCD graphs, see [96].

.

2.7. The Electroweak Precision Fit

The experiments at the LEP and SLC electron/positron colliders allowed high-precision extractions of a number of observables, mostly measured at or around the Z boson resonance. They can be used to perform a global fit of the Standard Model's electroweak sector and evaluate its consistency. This also works for New Physics models such as the SM4. In order to fully exploit the high precision achieved by these experiments, one needs at least similarly precise theoretical calculations. This means that various loop contributions have to be considered. Such corrections can be classified [98] as being either "direct" corrections of vertices and box graphs which modify the form of the interaction, or "oblique" corrections. The latter are vacuum polarizations as in Fig. 2.7 which modify the propagators of the gauge bosons γ, W and Z. CKM matrix elements enter oblique corrections by means of graphs as d) in Fig. 2.7, with quarks as loop fermions f and $\bar{f}'$. In general, a modified fermion vertex affects only few particle species. A gauge boson, on the other hand, couples to any suitably charged particle so that more diagrams are affected at a given order. The oblique corrections thus can be expected to have a larger effect on precision measurements [99]. As a consequence, the non-oblique corrections were in the past frequently neglected while oblique corrections were often approximated by means of the so-called oblique parameters S, T and U as proposed by Peskin and Takeuchi [98]. This treatment has the additional advantage that any divergences cancel in the calculation of S, T and U. However, the validity of this parametrization depends on three requirements:

1. Before spontaneous symmetry breaking, the electroweak gauge symmetry must be $SU(2) \otimes U(1)$ as in the GSW model.
2. The mass of new particles must be well above the Z scale.
3. No vertex corrections from new particles arise.

In the SM4, a violation of the 2nd and 3rd condition cannot be excluded as vertex corrections can arise from mixing between 4th generation fermions and SM3 particles. Additionally, the mass of the 4th generation neutrino may be as low as $m_Z/2$. Therefore, the participants of our project decided to use the entire set of Electroweak Precision (pseudo)observables in the publications [100], [101] and [40].

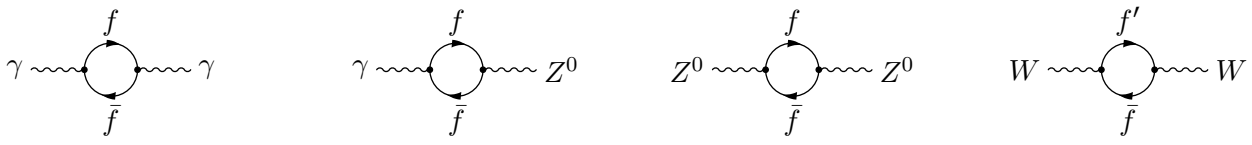

(a) (b) (c) (d)

Figure 2.7.: Lowest order vacuum polarisations which modify the self-energies of the gauge bosons γ, Z and W. The amplitude of d) is proportional to $\left|V_{\hat{u}\hat{d}}\right|^2$ if $f'\bar{f} = \hat{u}\bar{\hat{d}}$ or $\hat{d}\bar{\hat{u}}$, where the $\hat{}$ indicates that the quark can be *any* up-type or any down-type quark. In the language of the STU-parameters, this graph and hence the CKM matrix elements enter only the parameter T[50].

Figure 2.8.: Lowest order $Zb\bar{b}$ vertex corrections. The right graph's contribution depends on CKM matrix elements. Again, $\hat{u}$ can be any up-type flavour.

While non-oblique corrections affect only the $Zq\bar{q}$ vertex as e.g. in Fig. 2.8, it was shown in [102] that their effect can indeed reach the order of the experimental precision in case of the partial width of the decay $Z \to$ hadrons Γ_{had}. Indeed the dependence of the ratio R_b^0 of the partial widths of the decays $Z \to b\bar{b}$ to all hadronic Z decays on the CKM matrix parameter θ_u is dominated by non-oblique corrections. The non-oblique corrections thus provide another "lever" for a fourth generation to make its presence felt in a global fit of SM4 masses, CKM matrix elements and couplings. The virtual fermions in loops like those in Figs. 2.7 and 2.8 can be much more massive than particles which can be generated in the collider used by the experiment. Fitting the results of such calculations to the experimental results therefore allows probing physics at these high mass scales. Thus, constraints on New Physics models can be derived even if they include particles with masses beyond the capabilities of the collider. "Electroweak Precision Fits" were, for example, performed by means of the software packages Zfitter and later Gfitter. A recent overview of Zfitter's history is given in [103]. For a description of Gfitter, see e.g. [104]. A full listing of the expressions involved would be far beyond the scope of this work. The remainder of the present section is therefore only a short list of the inputs used in the Electroweak Precision Fit which in turn provided the input for the fits presented in chapter 5. A superscript ^{0} on a quantity indicates that the measured value was corrected for radiative effects, γ exchange and $\gamma - Z$ interference. Numerical values will be given in sec. 4.2.1, together with a description of how the aforementioned result was finally used. From this point on, the abbrevation EWP will be used in this work to denote any observable used in or constraint coming from the Electroweak Precision Fit.

- m_Z - The mass of the Z boson, assigned to the peak of the Z boson's resonance.
- $\Delta\alpha^{(5)}_{\text{had}}$: The electroweak fine structure constant $\alpha_{EM}(q^2 \to 0)$ is modified by photon self-energy contributions. Their magnitude depends on the energy at which the fine structure constant is measured. The difference between its value in the Thomson limit (low-energy, $q^2 \to 0$) and its value at m_Z is $\Delta\alpha(m_Z)$. It contains a contribution from light hadrons $\Delta\alpha^{(5)}_{\text{had}}$ which is uncalculable but can be extracted from measurements [99]. In the Electroweak Precision fit, this measured contribution has to be provided as an input.
- $\alpha_s(m_Z)$ - Strong coupling strength at the Z mass scale.
- σ^0_{had} - Total hadronic cross section of $e^+e^- \to X_{\text{had}}$ measured at the Z pole.

- $R_b^0 = \frac{\Gamma_Z^b}{\Gamma_Z^{\mathrm{had}}}$ - i.e. partial width of the decay $Z \to b\bar{b}$ normalized to the total hadronic Z decay width.
- $R_c^0 = \frac{\Gamma_Z^c}{\Gamma_Z^{\mathrm{had}}}$ - partial width of the decay $Z \to c\bar{c}$ normalized to the total hadronic Z width.
- $R_\ell^0 = \frac{\Gamma_Z^{\mathrm{had}}}{\Gamma_Z^\ell}$ - *inverse* ratio of the leptonic Z decay width to the total hadronic decay width. Lepton universality is assumed, i.e. $R_e^0 = R_\mu^0 = R_\tau^0$.
- Γ_Z - The total decay width of the Z boson, obtained by means of a beam energy ($\sqrt{s}$) scan around the Z peak.
- $A_{\mathrm{FB}}^{0,f}$ - Forward-backward asymmetry in $Z \to f\bar{f}$ at the Z pole:

$$A_{\mathrm{FB}}^{0,f} = \frac{\#(\text{forward-scattering events}) - \#(\text{backward-scattering events})}{\#(\text{forward-scattering events}) + \#(\text{backward-scattering events})} \tag{2.105}$$

  An event $e^+e^- \to f\bar{f}$ is counted as "forward" if the angle θ between the fermion's (as opposed to: anti-fermion's) track and the electron beam satisfies $\theta < \pi/2$. If $\theta > \pi/2$, it is counted as "backward". The Electroweak Precision fit providing inputs for this work uses the forward-backward asymmetries of b and c quarks and leptons $A_{FB}^{0,b}$, $A_{FB}^{0,c}$ and $A_{FB}^{0,\ell}$. Lepton universality is assumed.

- $\mathcal{A}_f$ - The above forward-backward asymmetries, together with left-right- asymmetries and left-right-forward-backward asymmetries can be condensed into asymmetry parameters $\mathcal{A}_f$ [105]. They depend only on the ratio of vector- and axial-vector couplings of the fermion species f to the Z boson:

$$\mathcal{A}_f = 2\frac{g_{Vf}/g_{Af}}{1 + (g_{Vf}/g_{Af})^2} \tag{2.106}$$

  The fits in chapter 5 are based on results in whose generation the asymmetry parameters $\mathcal{A}_b$, $\mathcal{A}_c$ and $\mathcal{A}_\ell$ were used.

- $\sin^2\theta_\ell^{\mathrm{eff}}$ - Effective weak mixing angle, extracted from hadronic forward-backward charge flow asymmetry at the Z peak.
- m_W - Mass of the W boson, measured at Tevatron.
- Γ_W - Decay width of the W boson, measured at Tevatron.
- m_t^{pole} - top quark pole mass.

This finishes the introduction to the physical concepts which went into the present work. As there was - naturally - no way to give an in-depth treatment, references to such works were given where appropriate.

The next Chapter contains a description of the tool used to obtain the results presented later, i.e. the CKMfitter software.

3. The CKMfitter package

The CKMfitter package is a piece of software developed and used by the CKMfitter group, a collaboration of experimental physicists associated to the experiments ATLAS, *BABAR*, Belle and LHCb, and theorists. The CKMfitter package was written to perform a global analysis of the CKM matrix to

- compare different realisations of the Standard Model (i.e. different combinations of parameters) with regard to their ability to describe experimental data, or find constraints on such parameters,
- particularly, constrain parameters of the CKM matrix and QCD (see sec. 6.1 for limitations),
- predict observables from global CKM fits within the Standard Model,
- in extended theoretical frameworks, constrain parameters of specific New Physics scenarios.

More information on the CKMfitter group and their publications is available on their website [106]. This chapter mostly deals with technical aspects which have not changed much and is paraphrased from [106, 107, 108]. Some statements, however, have been updated to reflect the current state of affairs or to describe technical details which are new to CKMfitter or which are needed to understand e.g. the convergence problems described in Appendix B.

3.1. Statistical framework of CKMfitter - Rfit

Originally, the Mathematica based version of CKMfitter offered a choice between several statistical approaches. Ref. [106] lists *R*fit, *ER*fit, the 95% CL Scan method and a Bayesian approach. Recently, different approaches were examined and tested (see e.g. [109]), but this started only after work on this project had begun in 2010. At the time, *R*fit was the default method. It was therefore used in the present thesis and is shortly described here. In [107, 110], it is explained in detail and also compared to the approaches mentioned above. These references are also the sources of most of the information provided below.

The analysis is performed on a set of N_{exp} measurements

$$x_{exp} = \{x_{exp}(1), ..., x_{exp}(N_{exp})\} \tag{3.1}$$

which are described by theoretical expressions

$$x_{theo} = \{x_{theo}(1), ..., x_{theo}(N_{exp})\}. \tag{3.2}$$

These N_{exp} theoretical expressions are functions of N_{mod} model parameters $y_{mod} = \{y_{mod}(1), ..., y_{mod}(N_{mod})\}$. N_{theo} of these parameters are fundamental and free parameters of the theory and denoted by $y_{theo} = \{y_{theo}(1), ..., y_{theo}(N_{theo})\}$. Other parameters in y_{mod} concern regimes where perturbative calculations do not apply - such as in the estimation of hadronic quantities like form factors, decay constants etc. They can be calculated e.g. by means of effective field theories or lattice QCD. Their uncertainty is dominated by non-statistical systematics which is why they are not considered to obey a probability distribution function. They are denoted by

$$y_{QCD} = \{y_{QCD}(1), ..., y_{QCD}(N_{QCD})\} \tag{3.3}$$

with $N_{QCD} = N_{mod} - N_{theo}$.

By definition,

$$\chi^2\left(x_{exp}, y_{mod}\right) \equiv -2\ln\mathcal{L}\left(x_{exp}, y_{mod}\right) \tag{3.4}$$

where $\mathcal{L}$ is the likelihood function

$$\begin{aligned}\mathcal{L}\left(x_{exp}, y_{mod}\right) &= \mathcal{L}_{exp}\left(x_{exp} - x_{theo}\left(y_{mod}\right)\right) \cdot \mathcal{L}_{theo}\left(y_{QCD}\right) \\ &= \prod_{i=1}^{N_{exp}} \mathcal{L}_{exp}(i) \cdot \prod_{j=1}^{N_{QCD}} \mathcal{L}_{theo}(j).\end{aligned} \tag{3.5}$$

If both $\mathcal{L}_{exp}(i)$ and $\mathcal{L}_{theo}(j)$ are built from purely Gaussian measurements, the number of degrees of freedom N_{dof} is given by

$$N_{dof} = N_{exp} - N_{mod}. \tag{3.6}$$

One can then calculate confidence levels (CLs) using

$$\mathrm{CL} = \mathrm{Prob}\left(\chi^2\left(y_{mod}\right), N_{dof}\right) \tag{3.7}$$

$$= \frac{1}{\sqrt{2^{N_{dof}}} \cdot \Gamma(N_{dof}/2)} \int_{\chi^2(y_{mod})}^{\infty} e^{t/2} t^{N_{dof}/2-1}\, \mathrm{d}t \tag{3.8}$$

in which Prob is the name of a CERN library [111] routine which implements eq. (3.8). However, there are in general some non-Gaussian components in both $\mathcal{L}_{exp}$ and $\mathcal{L}_{theo}$: $\mathcal{L}_{exp}$ must handle experimental systematics as well as inconsistent measurements. $\mathcal{L}_{theo}$ has to deal with quantities y_{QCD} whose uncertainty cannot a priori be assumed to follow a Gaussian distribution. The same is also true for some of the experimental systematics but since they are not usually the dominant part of experimental uncertainties, the problem is less relevant in that case [107].

The frequentist *R*fit scheme is an attempt to cope with both of these problems. In *R*fit, the likelihoods $\mathcal{L}_{theo}$ do not contribute to the fit's χ^2 and the parameters y_{QCD} only take values within predefined "allowed ranges" $[y_{QCD}]$. All values within $[y_{QCD}]$ are treated equally, although this is not to be confused with assuming them to follow an uniform probability density function [107]. If CKMfitter encounters such non-Gaussian inputs in a given fit, the user receives a warning:[1]

```
WARNING: Ndof is ill-defined because of theoretical uncertainties;
approximate Ndof is [...] and assuming a \\[Chi]2-distribution one gets the following
```

[1] It is advisable to check the log file if not running CKMfitter in the Mathematica GUI.

`pValue` [...] *R*fit results are to be considered as valid only if the true values of the y_{QCD} are contained in the allowed ranges assigned to them. Therefore, choosing them too small may well yield invalid results while choosing them too big will possibly obscure a discovery.

3.1.1. Metrology

In the metrological phase, one assumes that the theory as a whole is correct and examines how well the experimental data agree with various realizations of this theory, i.e. distinct sets of y_{mod} values.

Let $\chi^2_{min;y_{mod}}$ denote the absolute minimum value of χ^2 which can be obtained if all N_{mod} parameters in y_{mod} are allowed to vary freely. Since experimental and theoretical systematics are described by allowed ranges, this does in general not correspond to a unique point in y_{mod} space, but to a domain hereafter called y^{opt}_{mod} that usually is multi-dimensional. To determine this domain as precisely as possible is the goal of the metrological phase. The quantity to be minimized in this process is the offset-corrected χ^2,

$$\Delta\chi^2\left(y_{mod}\right) = \chi^2\left(y_{mod}\right) - \chi^2_{min;y_{mod}}. \tag{3.9}$$

Its minimum value is zero by construction and has the practical advantage that once $y_{mod} \in y^{opt}_{mod}$, CLs equal to unity are obtained which is consistent with the assumption that the theory used in the fit is correct.

One is not necessarily interested in CLs for all of the y_{mod}, as some parameters may be less relevant for the physics in question (like values of QCD parameters when one is interested in CP violation in the SM3, which can be summarized in the Jarlskog determinant J) or because a CKM fit cannot significantly constrain them. The set of the N_a parameters which still *are* interesting is hereafter denoted by a, the remaining N_μ parameters will be summarized as μ. In other words, quoting from [107]:

> "The goal is to set CLs in the a space, irrespective of the μ values"

To exclude as large parts of "a space" as possible, a CL_{cut} is defined. Then, for a fixed value of a, μ is varied and

$$\mathrm{CL}(a) = \mathrm{Max}_\mu\{\mathrm{CL}(a,\mu)\}. \tag{3.10}$$

The theoretical parameters in y_{QCD} are allowed to vary freely within their $[y_{QCD}]$ ranges. A given point in a will be excluded if $\mathrm{CL}(a,\mu) < \mathrm{CL}_{cut}\ \forall\mu$. The a space is discretely scanned in this fashion, determining contours of allowed areas. Similarly as in the above discussion,

$$\chi^2_{min;\mu}(a) = \mathrm{Min}_\mu\{\chi^2\left(y_{mod}\right)\}, \tag{3.11}$$

with $\chi^2\left(y_{mod}\right)$ as in 3.8. For metrological purposes, the offset-corrected

$$\Delta\chi^2(a) = \chi^2_{min;\mu}(a) - \chi^2_{min;y_{mod}} \tag{3.12}$$

is used. Like $\Delta\chi^2(y_{mod})$ in 3.9, $\Delta\chi^2(a)$ is equal to zero if $y_{mod} \in y^{opt}_{mod}$. In a Gaussian case, the

CL for a particular value of a can be calculated using Prob:

$$\mathcal{P}\left(y_{mod}\right) = \mathrm{Prob}\left(\Delta\chi^2\left(y_{mod}\right), N_{dof}\right)$$

Here, $N_{dof} = \mathrm{Min}\left(N_{exp} - N_{\mu}, N_a\right)$. N_a is 1 in an 1D scan and 2 in a 2D scan. This is also how the results of the 1D scans presented in Chapter 5 were obtained.

While these results can be considered reliable in the *R*fit sense (i.e. they are fine as long as the true value of the y are within the allowed ranges), there are a few more caveats to consider [110]. Firstly, in the case of different constraints affecting the same parameter having widely different precisions, a sensible choice of N_{dof} may be problematic to find even a purely Gaussian case. Secondly, some inputs may not be appropriately described by a central value and Gaussian errors. Thirdly, the calculation may also be affected by *physical* limits which certainly do not obey a Gaussian distribution - e.g. the upper limit of the sine of an angle close to $\pi/2$ is exactly one, no matter what the value of its Gaussian uncertainty is at this point. Thirdly, for a truly consistent treatment, $\Delta\chi^2(a)$ has to be considered as a test statistic and in order to compute the CL for a, one has to use a Monte Carlo simulation to determine its distribution. Finally, CKMfitter can at the time of writing only perform likelihood ratio tests comparing *nested* models. This means, applied to the case examined in this thesis, that the SM3 would have to be equivalent to an SM4 with certain parameters fixed to specific values. For the ramifications, see sec. 6.1.

3.2. The CKMfitter package

The CKMfitter package started out as a Fortran program to which some C++ augmentations were added later. As fit problems became more and more complex, computing time increased and Jérôme Charles initiated the development of a Mathematica based version in which symbolic calculations are used to simplify expressions in the fit. In the Mathematica based version, only the expressions needed for a given fit are then used to construct the χ^2 function which is exported to Fortran and compiled. These two features speed up the process by a factor of more than 100 [108] compared to the Fortran version in which the necessary theory predictions were queried anew in every step of the fit.

In 2012, Martin Wiebusch and Otto Eberhardt developed an interface which enables CKMfitter to call functions from other programs and use their output. Thus, if a well-tried software for the calculation of a given observable exists, it is possible to use this software instead of reimplementing the necessary terms in a CKMfitter theory package. Usually, this means that the analytical gradient (with respect to the theory's parameters, see 3.2.2) cannot be used because it is not provided by the external software. As of the writing of this thesis, this new feature had been used to call the `DIZET` routine of the Zfitter package [112] for the calculation of Electroweak Precision Observables within the SM3 and for HGrids, a program which uses high-dimensional lookup tables to calculate the Higgs signal strengths in Refs. [101, 35, 40].

3.2.1. Mathematica

Mathematica is a computer algebra system developed by Wolfram Research under a proprietary license. The version available at the time of writing is 9 [113]. CKMfitter was originally

written in version 5.2 but is being updated to version 8 which is the version used for the fits presented in this thesis. In CKMfitter, Mathematica is used to perform symbolic calculations like simplification of expressions. Mathematica consists of a kernel which interactively performs the calculation, and a GUI by means of which the user controls the kernel, enters expressions to be calculated etc. Alternatively, the kernel can be run from the command-line. Successions of commands for Mathematica are stored in so-called "notebooks" (`.nb`) or `.m` files. Due to a number of bugs (at least) in previous versions of Mathematica, it cannot be recommended to use the "notebooks" (`.nb`) files for CKMfitter. This is also why all Theory Packages which come with CKMfitter are now in the `.m` format: It is more robust since it is a simple text file containing only the technically relevant code. The "notebooks" contain all sorts of layout commands and, at least in v5.2, are prone to somewhat erratic behaviour.

3.2.2. Components of the CKMfitter package

The following list contains the components of CKMfitter which are important to reproduce the results in this thesis. Most of them are explained in more detail in [108]. They are located in a directory commonly named `fastfitter`.

- **Analysis datacards** are located in the subdirectory `analysis` of the `fastfitter` program folder and carry the file extension `.m`. They contain settings, flags and options for running a fit, e. g. which input files to consider. They also set the granularity of the scans explained in the last section, that is, into how many discrete steps the scanned range is divided. Technically, they are text files which contain a Mathematica replacement list.

- **Input datacards** - located in the subdirectory `inputs`, they contain numerical values for input quantities, e.g. $|V_{tb}|$. Technically, they are the same as analysis datacards, but their file extension is `.data`. However, not all inputs are sourced from these files. A number of quantities with negligible errors - considered as constants - are stored in `inputs/PDG.m`. Their values as used in this thesis are given in Table 3.1.

- `CKMfitter.m` - the user interface of CKMfitter. In order to perform CKMfits in the SM4 using the Hou/Soni parametrization of the CKM matrix, one needs to replace the line

  ```
  analysisTheory =
    loadTheory["CKMmatrix‘", theoryPackage /. framework];
  ```

  by

  ```
  analysisTheory = loadTheory["CKMmatrix4DHSpdg‘", theoryPackage
  /. framework];
  ```

  To perform a fit, the user runs this file after entering the file name of the analysis datacard in the first input line. For the fits shown in the present thesis, `CKMfitter.m` calls the following analysis steps:

  - reading inputs and settings from datacards
  - constructing the χ^2 function
  - translating the χ^2 function to Fortran

- calling the compiler to write the minimizer program containing the χ^2 function
- running the minimizer
- if specified in the analysis card (which is usually the case), performing a scan over one or two observables or parameters (corresponding to a in the metrology section 3.1.1)
- exporting output files

There is now also the possibility to include routines from third-party software. This requires a few more steps to be called by `CKMfitter.m`, but those features were not used to obtain the results presented here. They are therefore not described because the default settings are chosen in such a way that datacards written before their introduction still work, i.e. they can be disregarded if they are not needed.

To avoid cluttering the program directories with output files, it is recommended to create a working directory different from `fastfitter`, place a copy of `CKMfitter.m` there and use the copy to perform fits.

- **Theory Packages** contain the theoretical expressions for observables as functions of the N_{mod} parameters. They are stored in a binary format optimized for Mathematica, `.mx`, and generated by running a `.m` file in which the theoretical expressions $x_{theo}(y_{mod})$ are defined. The expressions for the x_{theo} and their derivatives with respect to each parameter present in the package $\frac{\partial x_{theo}}{|\partial y_{mod}|}$ are also included. The latter provide the analytical gradient of the expressions which is later used in the search for the global minimum of χ^2. It is possible to include several theoretical scenarios in one Theory Package. In this case, expressions referring to the same quantity in different scenarios are distinguished by version labels, e.g. `["SM4PMNS"]`. The Theory Packages changed or created in this thesis are listed in Sec. 3.3.

- **Lookup Tables** - If an input quantity cannot be expressed as central value with an error interval or if there is a complicated correlation between two variables, it is possible to use the experimental likelihood as an input after translating it to a χ^2 contour. These are provided as discrete lookup tables (LUTs) where values in-between the LUT entries are calculated by Cubic Spline Interpolation. Tools for generating 1-D and 2-D LUTs can be found in the subdirectory `tools`. LUTs are called from inside input datacards and stored in the subdirectory `inputs` with the extension `.dat`.

- **Output** - When CKMfitter is run via the Mathematica GUI, it generates `dat` files and `png` graphics. The latter ones are not produced if CKMfitter is run in console mode. The output text files contain a header with the settings from the analysis datacard and fit results in the column format `xbin (ybin) x (y) Chi2|CL 1-CL`. They can be used to produce graphical plots with ROOT. Corresponding ROOT macros were written by Vincent Tisserand. The `png` files contain a plot of the p-value (1-CL) as a function of the quantity which was scanned over. For quick plotting which is impossible with ROOT there is now also the GNUplot based shell script `ckmgnuplot` in the `tools` directory. The limits of the 1 σ, 2 σ and 3 σ ranges given in the output on the Mathematica GUI are those values of the scanned quantity where the p-value curve drops below the corresponding value, i.e. below 31.74%

Quantity	Value
Particle masses [GeV]	
m_e	$0.510998910 \cdot 10^{-3}$
m_μ	$105.6583668 \cdot 10^{-3}$
m_τ	1.77682
m_π	0.13957018
m_ρ	0.77549
m_ω	0.78265
$m_{\eta\prime}$	0.95778
m_ϕ	1.019455
m_{K^0}	0.493677
m_{K^*}	0.89166
$m_{J/\psi}$	3.096916
m_{B^0}	5.27917
m_{B^*}	5.3251
$m_{B_s^0}$	5.3663
m_{D^0}	1.86957
$m_{D_s^\pm}$	1.96845
m_W	80.399
m_Z	91.1876
mass difference of K^0 mass eigenstates [GeV]	
Δm_K	$3.48326 \cdot 10^{-15}$

Quantity	Value
decay constants [GeV]	
f_π	0.13039
f_{K^0}	0.15712
$f_{\eta\prime}$	0.137
f_ρ	0.210
f_ω	0.187
f_ϕ	0.215
$f_{J/\psi}$	0.384
Particle life times [ps]	
τ_{B^0}	1.519
$\tau_{B\prime}$	1.641
τ_{B_s}	1.472
$\tau_{D\prime}$	1.040
τ_{D_s}	0.500
τ_π	26033
$\tau_{K^\pm}$	12380.0
τ_τ	0.2906
$\hbar$ [MeV ns]	$6.58211899 \cdot 10^{-13}$
$\hbar c$ [GeV fm]	0.1973269631
α_{EM}	1/137.035999679
G_{F3} [GeV^{-2}]	$1.1663788 \cdot 10^{-5}$
$\sin^2\theta_W$	0.23116
Number of colors N_C	3

Table 3.1.: Quantities with negligible errors as provided in `inputs/PDG.nb` at the time of writing.

at the edges of the 1 σ interval, below 4.54% at the edges of the 2 σ interval and below 0.26% at the edges of the 3 σ interval.

3.2.3. The Process of Minimum Search in CKMfitter

For a long time, the progress on this work was brought to a halt by convergence problems which occurred in fits including any one of the inputs $|\epsilon_K|$, a_{SL}^d and a_{SL}^s. They are in some detail described in Appendix B. Their solution was to change the parametrization of the CKM matrix, with the Hou/Soni parametrization in eq. (2.43) being the one which worked. In order to better understand these problems, the process which is used both in the search for the global minimum and each step of a scan is shortly described in this section. As explained above, the mathematical expressions predicting an observable are defined in a Theory Package together with its gradient with respect to the parameters, $\frac{\partial x_{theo}}{\partial y_{mod}}$. In a CKMfitter run, the expressions relevant for the fit

are used to build the χ^2 function and the derivatives are used for its analytical gradient whose use is generally recommended. This χ^2 function is an actual Fortran `subroutine` written to the file `minimirChi2.f` in the working directory and then compiled into the minimizer binary whose file name is `minimir`. The user should define the `startRanges` flag in the analysis datacard. It assigns to each parameter an interval in which the user expects the global minimum to be located. In this region of the parameter space, the program generates a random point which is used as a starting point for a gradient search. Defining a `startRange` is not necessarily needed but can speed up the search by avoiding the usually huge regions of the parameter space where no good agreement with the measurements can be expected. The gradient search itself is performed by a code written by David M. Gay [114]. Once the minimum is found, its χ^2 value is stored and a new random initial point is generated for the next gradient search. This process is repeated as often as specified by the user-defined flag `globalMinSearches` in the analysis datacard. The parameter values with which the lowest χ^2 was obtained are then accepted as location of the global χ^2 minimum $\chi^2_{min;y_{mod}}$. This minimum is then used as starting point for the scans over an interval of a parameter or an observable (denoted by a in section 3.1.1. It is possible to run several similar gradient searches at each point of the scan, the number of which is set by the `nbOfFits` flag in the analysis datacard. Usually, a two-digit number is enough because if the χ^2 function is numerically stable and smooth enough, a small step along the axis of the quantity scanned over will not cause any huge shifts in a parameter. In case of the SM4 fits, it turned out that, even with the Hou/Soni parametrisation described in section 2.2.5, convergence was so bad occasionally that `nbOfFits` had to be increased to 200 or even 500. This corresponds to rather lengthy computing times because, provided that each call of the gradient search routine takes the same time in a given scan, the time required for an 1D scan scales linearly with the value both these flags and with `granularity`. In case of 2D scans, the duration follows the square of `granularity`.

When judging a scan result which has passed the first checks - i.e. the $\chi^2_{min;y_{mod}}$ found, a suitable scan range covering the 3 σ interval, etc., - care has to be taken to avoid mistaking "well-disguised" convergence problems for a nicely tight constraint on the quantity scanned over: Suppose that, because of a lowish `nbOfFits`, one scan step does not achieve *nearly* as low a χ^2 as its predecessor, and neither do the subsequent steps. Then, the p-value plot will contain a "step" which may lead to a narrowed 1-, 2-, or 3σ constraint, but what looks like a good constraint is actually an artefact. Depending on inputs, `scanRange` and `granularity`, such a step may actually be physical, but it should only be trusted after a number of checks. If, e.g., the "edges" of the step are rounded, chances are that it is actually a correct result. Also, reproducing the plot is another way, possibly "zooming" in on the step by means of `scanMin` and `scanMax` and `granularity`. Comparison with a 2D scan, one of whose axes is the quantity scanned over in the suspicious 1D scan, might help, but it typically takes a long time to produce. If used solely, none of these criteria is reliable enough for judging a CKMfitter result. One should always check several ones.

3.2.4. Further Speedup: Multithreading with OpenMP

Despite the speed advantage enjoyed by the Mathematica based version of CKMfitter, current computers are not fast enough to make long series of complex SM4 fits feasible with the Fortran

code which was available for the actual minimization when the work on this thesis started. Even after the convergence problems (cf. section B) were solved, an individual one-dimensional scan of a variable took easily several days - not to mention the requirement to do two-dimensional scans. While two-dimensional scans can be - and were at the time, occasionally - decomposed into an array of one-dimensional scans, the only feasible way to speed up the latter was by multithreading. An analysis of the Fortran code revealed that OpenMP suited the needs and the files `fortran/minimir.f` and `fortran/fit.f` were modified accordingly. As the CKMfitter code is not public, the changes made will be shortly described in prose.

The OpenMP API

OpenMP is an API[2] for shared memory multiprocessing, i.e. several threads of a program - typically, running on one processor each - can access and process data which is stored in one common memory area. It was first published in 1997 by its developer, the Open MP Architecture Review Board OMPARB. The current stable version 4.0 supports programming in C++, C and Fortran for most operating systems and processor architectures [115].

As usage of OpenMP is activated by compiler command line options and a number of compiler directives to be placed in the source code - typically around any loops to be parallelized - it turned out to be rather simple to produce a multi-threaded version of the CKMfitter minimizing routines. The main caveat is to avoid so-called racing conditions in which e.g. one thread relies on results provided by another thread which the latter might not yet have finished calculating, and any situations in which variables accessed by all threads are overwritten without proper coordination. An excellent introduction to OpenMP in Fortran codes is provided by [116].

Multithreading in CKMfitter

There were three parts of the code which were changed to run on multiple processors:

1. The number of global minimum searches as described in section 3.2.3 was split over multiple threads. The time needed for the global minimum searches is reduced as expected, i.e. by a factor of $\approx \frac{\text{runtime single thread}}{\text{number of threads}}$ (if one does not manually set the number of threads higher than the number of processors available).

2. For one-dimensional scans, the `nbOfFits` for each step in the scan is now distributed to the number of threads. The speedup is not quite as high here, because in case one of the threads converges slower than the others, the latter are idle until the "straggler" has finished.

3. Internally, two-dimensional scans are treated as a sequence of one-dimensional scans, with the two variables which are scanned over fixed according to each step. Therefore, the parallelisation of one-dimensional scans is at work here, as well.

Testing and Assessment

The multithreaded version of CKMfitter was tested to return the same results as the original version in two steps. For the global minimum search, a number of minimisations on different χ^2

[2] Application Programming Interface

Fortran functions - i.e. different sets of inputs - were performed with manually selected random seeds. The resulting minima were identical. In case of actual scans, the testing is less simple because a new random number is generated for each fit at each step in a scan. For testing, around 40 one-dimensional scans were performed several times each with the single threaded original software and the multi-threaded version. The results were then displayed in common plots and compared visually. Differences between the results produced by the multi-threaded version and those by the original software were not greater than those between the results of individual runs of the original software. Such differences do occur and, while normally negligible numerically, they point to a slightly low `nbOfFits`, a low `granularity` or simply bad convergence with the parametrization and set of inputs chosen.

After this testing, all plots were produced with the multi-threaded version. Without multi-threading, the repeated production of even one-dimensional scans would have caused major time problems. This would have dramatically reduced the ability of the author to verify any strange results or perform cross-checks. While the production of two-dimensional fits would not have become impossible, it would have been much more awkward as every one of them would have to be decomposed into a series of one-dimensional scans whose results would have had to be reassembled later.

3.3. Theory Packages written or changed for this work

Most of the packages written particularly for SM4 work or derived from packages originally intended for SM3 work have names like `[indicationOfPhysicalContent]4D.m`. In order to function, they need a theory package which provides the parametrization of the CKM matrix. At the beginning of the work on this thesis, the package `CKMmatrix4DBCpdg` containing the parametrization given in eq. (A.8) was used. When this parametrization was identified as the main source of the convergence problems described in Appendix B, it was replaced by the one given in eq. (2.43) which is implemented in the package `CKMmatrix4DHSpdg`. All SM4 related packages were then changed so that they can be easily adapted to any new parametrization. So, if there should ever be either renewed interest in the SM4 packages or any need to adapt them to a more advanced model with four fermion families, it should be easy to create a new parametrization package (equivalent of `CKMmatrix` and `CKMmatrix4D*`) and use the theory packages with a minimum of changes. In the following listing, a very short explanation of the packages' function is given. The expressions used for the quantities provided by the packages are given and explained in chapter 4.

`CKMmatrixHSpdg` Provides parametrizations of products of CKMmatrix elements of the form $V_{ij}V_{kl}^*$ as functions of the mixing and phase angles of the SM4. It also provides the expressions for quantities which only depend on these products, such as moduli of CKM matrix elements and angles of the Unitarity Triangle. The $V_{ij}V_{kl}^*$ are accessible from inside other theory packages so that they can be used to parametrize any expressions defined there.

`BBbarKKbarDDbarMixing4D` Provides expressions for K^0, D^0, B_d^0 and B_s^0 meson mixing related quantities. Those actually used in this thesis are Δm_d, Δm_s, ϵ_K, $\sin(2\beta)$, $\sin(2\beta - 2\theta_d)$ and the charge asymmetries a_{SL}^s, a_{SL}^d and A_{SL}.

`BtoXsGamma4D` Defines the expression for $R_{b\to s\gamma}$.

`DiLeptonicDecay4D` Expressions for $\mathcal{B}(B_d \to \mu^+\mu^-)$ and $\mathcal{B}(B_s \to \mu^+\mu^-)$.

`LeptonicDecay4D` Defines a whole number of observables concerning leptonic decays of mesons. Only $\mathcal{B}(B \to \tau\nu)$ is used in this thesis.

`BFWLeptonic` This SM3 package implements the branching fractions of leptonic W decays $\mathcal{B}(W \to \ell\nu)$.

`BtoXgamLO` The original SM3 theory package `BtoXgam` implementing the decay $b \to X_s\gamma$ contains higher-order corrections than used in the SM4 for the present study (cf. sec. 4.2.4). To guarantee comparability of the SM3 and SM4 fits, the package `BtoXsgamLO` was created with the same leading order expressions as in the SM4 package reduced to SM3.

Most of these packages rely on other packages which provide the expressions for running couplings such as `QCD` and `QED`. Others are needed to define quantities such as quark masses, coupling constants etc. globally so that CKMfitter recognizes that e.g. `LeptonicDecay4D`GFermi` and `BtoXsGamma4D`GFermi` are actually the same quantity, i.e. the Fermi constant G_F. The package `TheoryTools` defines a number of functions which are needed for the compilation of each theory package.

This chapter provided the necessary insights into the procedures in which the results of the present work were obtained. The next chapter will describe the experimental results which were "fed" to the CKMfitter software to obtain these results.

4. Constraining the CKM matrix in SM4

This chapter contains descriptions of the inputs used to place constraints on the SM4 in this thesis. It is divided into three sections. The first section describes so-called tree-level observables, i.e. observables measured in electroweak processes which are, at lowest order, described by tree-level Feynman graphs. The second section deals with processes which can only be calculated at higher order of the perturbation theory but which are not CP violating. The third is about CP violating observables which can also only be calculated at higher order.

If the extraction of an input value is either particularly involved, specific to numerical values obtained by the CKMfitter group or not necessary reliable or valid in an SM4 setting, it will be described in somewhat more detail. If the SM4 expression for a measured quantity differs from the SM3 expression, the SM4 expression will be motivated and given, usually with further references. In cases where the SM3 value is used, this will be justified by an argument why the SM4 influence is negligible.

The chapter ends with a list of some observables which were occasionally used to constrain SM4 parameters in the literature but which were not used in this work, and reasons why they were not used. If a value is used with separate statistical and systematic uncertainty, the statistical error will be given first as by common convention:

$$x_{\text{input}} = x \pm \Delta x_{\text{stat}} \pm \Delta x_{\text{syst}} \tag{4.1}$$

4.1. Tree Level observables

4.1.1. $|V_{ud}|$ From Superallowed Nuclear β Decays

The most precise values of $|V_{ud}|$ to date were extracted from superallowed $0^+ \to 0^+$ nuclear β decays. At quark level, these are $d \to u$ transitions. Compared to the other methods of measuring $|V_{ud}|$, namely its extraction from neutron and pion decays, the precise extraction from nuclear β decay is less challenging. Superallowed β decays are pure vector transitions and independent of the structures of both parent and daughter states [117] which makes them rather clean theoretically. Even so, the result by [118]

$$|V_{ud}| = 0.97418 \pm 0.00026. \tag{4.2}$$

was made possible by advances in theoretical understanding of the underlying physics. It is an average of measurements of superallowed nuclear β decays of many different nuclei. This is currently the most precisely measured modulus of an element of the CKM matrix. Indeed its precision is so much higher than the others' that it is the only one in which the non-unitarity of the PMNS submatrix $U_{3\times3}$ discussed in sec. 2.2.4 has to be taken into account in an SM4 context. The value used in the SM4 fits in this thesis is an update of the one given in [59] but obtained in

the same fashion:

$$|V_{ud}| = 0.97421^{+0.00034}_{-0.00029} \tag{4.3}$$

4.1.2. $|V_{us}|$ From Semileptonic K-Meson Decays

The input value used for $|V_{us}|$ was obtained in measurements of kaon decays $K_L \to \pi e\nu$, $K_L \to \pi\mu\nu$, $K_S \to \pi e\nu$, $K^\pm \to \pi e\nu$ and $K^\pm \to \pi\mu\nu$ performed by the experiments KLOE, KTeV, ISTRA+ and NA48 and analysed by FlaviaNet in [119]. Their result is $|V_{us}| \cdot f_+(0) = 0.21664 \pm 0.00048$. $f_+(0)$ is the $K \to \pi$ vector form factor at zero momentum transfer. The CKMfitter group averaged lattice QCD results from JLQCD12 [120], ETMC09 [121] and RBC-UKQCD10 [122] obtaining $f_+(0) = 0.9593 \pm 0.0026 \pm 0.0012$. Using this value yields the value used here,

$$|V_{us}| = 0.2558 \pm 0.0008 \pm 0.0012. \tag{4.4}$$

In the SM4, a perfectly precise analysis would consider the non-unitarity of the PMNS submatrix $U_{3\times3}$ and hence treat each of the kaon decay channels separately, depending on whether an electron or a muon occurs in the final state. However, this is not necessary here since the error caused by the omission is much smaller than the uncertainty of the measured input [59].

4.1.3. $|V_{ub}|$ From Semileptonic B-Meson Decays

This modulus[1] is extracted from measurements of branching fractions $\mathcal{B}(B \to X_u \ell\bar{\nu})$. At quark level, the process is $b \to u\ell\bar{\nu}$. In exclusive measurements, X_u is a light meson while in inclusive measurements, the sum is taken over all charmless hadronic final states. Both methods suffer from sizeable theoretical uncertainties. The most precise exclusive determination is performed on data from $B \to \pi\ell\nu$ decays. *BABAR* and Belle performed measurements in which one B meson of the meson-antimeson pair produced decays to a light meson while the other one is not reconstructed ("untagged"). The measured q^2-spectrum of these decays is then fitted using Lattice QCD predictions of the form factor $f_+(q^2)$ of the decay. The CKMfitter group's result is

$$|V_{ub}|_{\text{excl}} = (3.28 \pm 0.15 \pm 0.26) \cdot 10^{-3}. \tag{4.5}$$

In other determinations, the beauty quantum number (B = 1 or -1) of the decaying B or $\overline{B}$ meson was reconstructed ("tagged"). If these results are taken into account, the fit's p-value drops below 0.1 % because the measurements differ at low q^2 (<8 GeV). The resulting shift in the central value is covered by the error one obtains in the extraction described above.

In inclusive measurements, the charmed meson background is removed by phase-space cuts which, however, imply a sizable theoretical uncertainty in the prediction of the measured partial branching fraction. The CKMfitter group's result is

$$|V_{ub}|_{\text{incl}} = (4.36 \pm 0.18 \pm 0.44) \cdot 10^{-3}. \tag{4.6}$$

Although the 1-σ ranges of $|V_{ub}|_{\text{excl}}$ and $|V_{ub}|_{\text{incl}}$ do not overlap, their weighted average is calculated, taking into account only the statistical errors. The uncertainty of the average is accepted as

[1] References for this section: Heiko Lacker, private communication and CKMfitter internal notes.

statistical uncertainty, while the smaller theoretical error of $|V_{ub}|_{\text{excl}}$ is accepted as the theoretical error of the average. The result

$$|V_{ub}| = (3.70 \pm 0.12 \pm 0.26) \cdot 10^{-3} \tag{4.7}$$

of this procedure is then used as input in the fits presented here.

4.1.4. $|V_{ub}|$ from $\mathcal{B}(B \to \tau\nu)$

Of the purely leptonic processes $B \to \ell\nu$, only the rate with $\ell = \tau$ is measured since the other two are helicity suppressed and only upper limits are known. The rates are proportional to $f_B^2 |V_{ub}|$ where f_B is the B meson decay constant and only known from lattice computations. While the $|V_{ub}|$ extraction from $\mathcal{B}(B \to \tau\nu)$ does not yield as precise results as other methods, it provides a consistency check because f_B also appears in the mixing observable Δm_d. Factoring it out permits the a prediction of $\mathcal{B}(B \to \tau\nu)$ from other measurements. Up to ICHEP 2012, there was a significant tension between the measurement of $\mathcal{B}(B \to \tau\nu)$ and its prediction by fits performed by the CKMfitter group. This was to a certain degree alleviated by a new world average including results from both *BABAR* and Belle published with much of the above statements in [123]:

$$\mathcal{B}(B \to \tau\nu) = (1.15 \pm 0.23) \cdot 10^{-4} \tag{4.8}$$

4.1.5. $|V_{cd}|$ from Deep Inelastic Neutrino-Nucleon Scattering

The value of $|V_{cd}|$ is obtained by averaging the results of several experiments measuring deep-inelastic scattering of high-intensity muon neutrino beams off fixed targets. In the experiments CDHS and CHARM II at CERN and CCFR at Fermilab [84], these targets consist of iron and the neutrinos' partners in the reaction are down quarks in the iron's nucleons. The experiments determine the ratio of the cross sections of single muon and dimuon events $\sigma_{\mu^+\mu^-}/\sigma_\mu$. A dimuon event is accepted if two muons of opposite charge are identified in the detector, in addition to a number of other criteria (see e.g. [124], [84] and references therein). Such events are interpreted as the process $\nu_\mu + d \to \mu^- + c$ with the c quark decaying in $c \to X\mu^+\nu_\mu$, as depicted in Fig. 4.1. The cross section ratio then determines $\mathcal{B}(X_c \to \mu X) \cdot |V_{cd}|^2$, where $\mathcal{B}(X_c \to \mu X)$ is the branching fraction of the decay of X_c into a muon final state, averaged over all charmed hadrons X_c that can be produced in the reaction. In the extraction of $|V_{cd}|$, it has to be provided as a measured input. The same process is measured in the CHORUS experiment, also at CERN. Here, the target is not iron but a nuclear emulsion of AgBr in a gelatine layer [125]. Compared to the iron targets of CDHS, CHARM II and CCFR, CHORUS has lower background and better spatial resolution which enables the topological identification of charmed hadron decays [126]. The PDG average of results from all four of the above measurements is used as input in the fits of Chapter 5:

$$|V_{cd}| = 0.230 \pm 0.011 \tag{4.9}$$

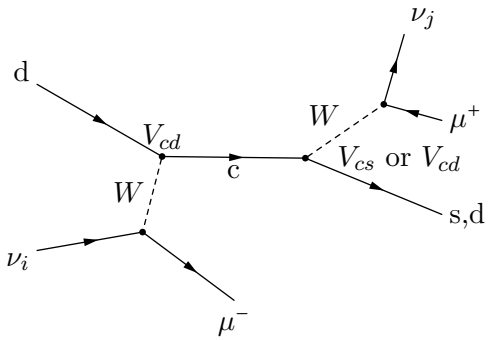

Figure 4.1.: Lowest order graph of the dimuon events used to measure $|V_{cd}|$.

4.1.6. $|V_{cs}|$ from Semileptonic D Meson Decays

$|V_{cs}|$ can be determined in several ways. At LEP2, DELPHI measured it in $W \to c\bar{s}$ decays. Belle, CLEO-c and *BABAR* extracted $|V_{cs}|$ each from leptonic $D_s^+ \to \ell\nu$ decays, semileptonic decays $D \to K\ell\nu$ and $D \to \pi\ell\nu$ and, finally, $D \to K\ell\nu$. The $D \to K\ell\nu$ results were averaged by the PDG [84]. Using the lattice QCD form factor calculation from [127], they obtained the input value used here:

$$|V_{cs}| = 0.98 \pm 0.01 \pm 0.10 \tag{4.10}$$

In a global fit of the CKM matrix, the lower limit on $|V_{cs}|$ can be severely pushed upwards if leptonic W decays are included in the fit as inputs. This will be discussed in section 4.1.9.

A newer value has become available in the 2014 edition [50] of the Particle Data Booklet. Its systematic uncertainty is reduced by a factor of 4 compared to eq. (4.10) thanks to new unquenced lattice results. Although it was not used in the recent work, this should not change the overall result too much because the $|V_{cs}|$ fit result lies within its 1σ interval.

4.1.7. $|V_{cb}|$ from Semileptonic B Meson Decays

Not unlike the previously discussed $|V_{ub}|$, the input value of $|V_{cb}|$ is an average of an inclusive and an exclusive determination. In this case, semileptonic B-meson decays to charmed final states X_c are observed. At quark level, the decay process is $b \to c\ell\nu$. In the exclusive extraction, X_c is required to be a D or D^* meson (the asterisk denotes an excited D meson state). In the inclusive measurement, the branching fractions of all charmed hadronic final states are summed over, i.e. one measures $\sum_{X_c} \mathcal{B}(B \to X_c\ell\nu)$.

The inclusive result to be used in the average below was calculated in [128] in a fit to the moments of semileptonic B decay distributions. In this publication, the $|V_{cb}|$ value obtained is given as $(42.42 \pm 0.86) \cdot 10^{-3}$. The uncertainty was split[2] into an error contribution from the fit and another from purely theoretical uncertainties. In the result,

$$|V_{cb}|_{\text{incl}} = (42.42 \pm 0.44 \pm 0.74) \cdot 10^{-3}, \tag{4.11}$$

the first uncertainty given is the fit's contribution adopted from [129]. The theory error was

[2] P. Urquiho, CKMfitter internal talk, CKMfitter Spring Meeting 2014

chosen so that both error intervals reproduce the $0.86 \cdot 10^{-3}$ uncertainty of [128] when standard Gaussian error propagation is applied.

Concerning exclusive determinations, the value

$$|V_{cb}|_{\text{excl}} = (38.99 \pm 0.49 \pm 1.17) \cdot 10^{-3}, \tag{4.12}$$

enters the input used in the fits. It is obtained as follows: The average calculated in [129] is rescaled to make use of the improved lattice QCD determination of the zero-recoil form factor $\mathcal{F}(1)$ published in [130]. However, unlike in the latter publication, the systematic uncertainties are added linearly[3]. The average and its uncertainties used in this work ,

$$|V_{cb}| = (41.00 \pm 0.33 \pm 0.74) \cdot 10^{-3}, \tag{4.13}$$

stem from Ref. [131]. They were obtained by the method described in the section on $|V_{ub}|$.

4.1.8. $|V_{tb}|$

Before single top production was observed at the Tevatron, $|V_{tb}|$ was estimated from the ratio

$$R = \frac{\Gamma(t \to Wb)}{\Gamma(t \to Wq)} = \frac{|V_{tb}|^2}{|V_{td}|^2 + |V_{ts}|^2 + |V_{tb}|^2} \tag{4.14}$$

measured in the decay of $t\bar{t}$ pairs. In the SM3, the denominator is equal to 1 due to the 3×3 unitarity of the CKM matrix and therefore, $R = |V_{tb}|^2$.

Single top quark production provides the opportunity to directly measure $|V_{tb}|$ at the Tevatron and the LHC where single top quarks are produced in one of the three processes depicted in Fig. 4.2. In all three cases, the single top production cross section is proportional to $|V_{tb}|^2$ which can therefore be extracted without the assumption of 3×3 unitarity of the CKM matrix. The

[3] ibid.

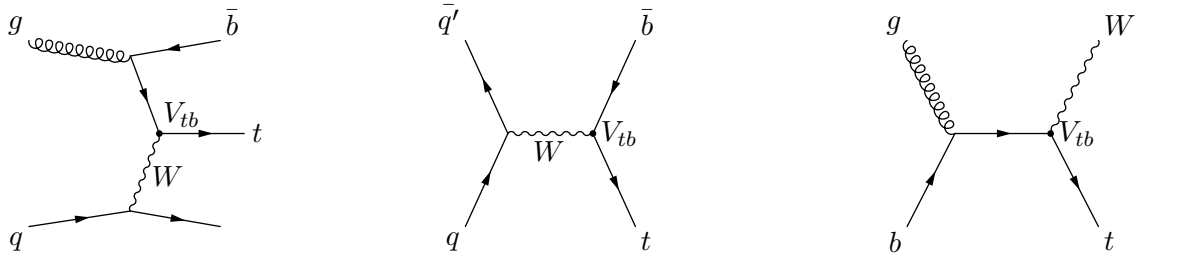

(a) Gluon splitting t channel production.

(b) Production in decay of time-like virtual W in s channel.

(c) Wt associated production.

Figure 4.2.: Single top production channels at Tevatron and LHC (lowest order). The graphs depict the common assumption that $|V_{tb}| = 1$. If the assumption is dropped as described in the text, the b quarks can be replaced by another down-type quark.

Collaboration	Channel	$\sqrt{s}$	Int. Lumi.	$\lvert V_{tb}\rvert$	Ref.
CMS	Wt	8 TeV	12.2 fb^{-1}	$1.03 \pm 0.12 \pm 0.03$	[132]
ATLAS	Wt	8 TeV	20.3 fb^{-1}	$1.10 \pm 0.12 \pm 0.03$	[133]
D0	s+t	1.96 TeV	9.7 fb^{-1}	$1.12^{+0.09}_{-0.08}$	[134]
CMS	t	7 and 8 TeV	see text	$0.998 \pm 0.038 \pm 0.016$	[135]
ATLAS	t	8 TeV	20.3 fb^{-1}	$0.97^{+0.09}_{-0.10}$	[136]
ATLAS	t	7 TeV	4.59 fb^{-1}	1.02 ± 0.07	[38]
CDF	s+t+Wt	1.96 TeV	7.5 fb^{-1}	$0.95 \pm 0.09 \pm 0.05$	[137]
Average				1.017 ± 0.028	

Table 4.1.: $|V_{tb}|$ extractions included in the average used in the fits. For more detail than given in the text, see original publications.

quantity measured in LHC experiments is the product

$$\sigma(pp \to)t \cdot \mathcal{B}(t \to b). \tag{4.15}$$

At the Tevatron, the initial state is $p\bar{p}$. Eq. (4.15) is proportional to $|V_{tb}|^2$ and independent of other CKM matrix elements under the following assumptions:

1. $|V_{tb}|$ dominates the third row of the SM3 CKM matrix, i.e. $\mathcal{B}(t \to b) \simeq 1$ and only initial state (sea) b quarks give relevant contributions to the production cross section
2. only SM processes contribute to the single top production rate
3. Wtb interaction conserves CP and is $V - A$

An average of several recent (cf. Table 4.1) single top results was calculated for the fits presented later in this thesis.

In [138], it was pointed out that a consistent analysis of $|V_{tb}|$ based on single top production measurements and R should not rely on $|V_{tb}|$ being much larger than $|V_{td}|$ and $|V_{ts}|$. This is supported by the D0 result $R = 0.90 \pm 0.04$ [139] and CDF's value $R = 0.87 \pm 0.07$ [140]: As was pointed out in [141],

$$H = \frac{\sqrt{|V_{td}|^2 + |V_{ts}|^2}}{|V_{tb}|} = \sqrt{\frac{1-R}{R}} \tag{4.16}$$

takes a value of $H \simeq 0.39$ and $H < 0.61$ (!) at 95% confidence level for the value of R published by D0. This clearly contradicts the above assumption. Also, sizeable $|V_{td}|$ and $|V_{ts}|$ mean that d and s quarks in the initial state of t-channel single top production (see Fig. 4.2) contribute to the production cross section. Obviously, a top quark can then also decay into a d or an s quark. We presented an improved extraction method based on these observations in [141]. Perhaps more important for the choice of inputs for the fits presented in chapter 5, the large values of $|V_{td}|$ and $|V_{ts}|$ demanded by the D0 and CDF results are in conflict with the unitarity of the CKM matrix: The large central values of $|V_{ud}|$ and $|V_{cs}|$ in connection with the well-measured $|V_{us}|$ and $|V_{cd}|$ do

not leave the required "space" for $|V_{td}|$ and $|V_{ts}|$ if $\sum_{i=1}^{4} \left|V_{id,s}\right|^2 = 1$ is to be satisfied - even if the elements in the fourth row of the CKM matrix are zero. Using the input values from the previous subsections and assigning all of $H = \sqrt{(1-R)/R}$ to *either* V_{td} *or* $|V_{ts}|$, e.g.:

$$|V_{ud}|^2 + |V_{cd}|^2 + |V_{td}|^2 = 1.17 \pm 0.02 \qquad \text{for } V_{ts} = 0 \tag{4.17}$$

$$|V_{ud}|^2 + |V_{cd}|^2 + |V_{td}|^2 = 1.17 \pm 0.2 \qquad \text{for } V_{td} = 0 \tag{4.18}$$

$$\tag{4.19}$$

In the second case, the error shrinks considerably once the branching fractions of leptonic W decays improve the lower limit of $|V_{cs}|$ (see next subsection.). Also, there is a tension between the small $|V_{tb}|$ demanded by R and the observed single top event yields [141] and, consequently, the $|V_{tb}|$ values extracted in single-top experiments.

Luckily, it turns out that no $|V_{tb}|$ input is actually needed in most of the fits performed for this thesis: In [101], the CKM matrix parameter θ_{34} was constrained to lie below 0.08 at 95 % CL by Electroweak Precision Data. Ref. [101] used the Botella-Chau given in eq. (A.8), and θ_{34} in [101] is θ_u in eq. (A.8). Noting that

$$V_{tb'} = \cos(\theta_v) \cdot \cos(\theta_w) \cdot \sin(\theta_u) \leq 1 \cdot 1 \cdot \theta_u, \tag{4.20}$$

this upper limit translates to a corresponding lower limit on $|V_{tb}|$. In order to compare this limit to the one given by the single top measurements average above, two global fits were performed to produce the p-value plots shown in Fig. 4.3. One fit was performed in what will be called the Tree Level input set in chapter 5: The observables included as inputs are $|V_{ud}|$, $|V_{us}|$, $|V_{ub}|$, $|V_{cd}|$, $|V_{cs}|$, $|V_{cb}|$ and $|V_{tb}|$, the branching fraction of the leptonic B meson decay $\mathcal{B}(B \to \tau\nu)$, those of the three leptonic W boson decays $\mathcal{B}(W \to \ell\nu)$ (with ℓ=e, μ and τ) and the angle γ of the Unitarity Triangle. For the input values used, see Table 5.1 in Chapter 5. The $|V_{tb}|$ input used in this fit is the average of the measurements in Table 4.1. The other fit did not use the $|V_{tb}|$ input, but instead the upper limit placed on $|V_{t'b}|$ by the EWP data. The resulting p-level plot in Fig. 4.3 clearly shows that the most stringent constraint on $|V_{tb}|$ does not come from any single-top production cross section measurement but from the effects of EWP observables. This, and the observation that the EWP limit is more compatible with the single top average than with the R measurements from D0 and CDF, lead to the following decision: In order to obtain consistent results, a constraint on $|V_{tb}|$ is needed in all fits including the fits with the Tree Level input set. The EWP measurements are by definition not part of the Tree Level input set but compatible with the average of the extractions from single top cross section measurements which reads

$$|V_{tb}| = 1.017 \pm 0.028. \tag{4.21}$$

This average was used as an input in *all* fits. In the Tree Level input set, it prevents $|V_{tb'}|$ and $|V_{t'b}|$ from growing to $\mathcal{O}(1)$. This would otherwise be allowed in this input set because the CKM matrix elements which are *not* provided as inputs are only constrained by unitarity. Also due to unitarity, this would imply a small $|V_{tb}|$ which is prevented by the EWP inputs in the other input sets. Whenever the EWP Lookup Table - cf. sec. 4.2.1 - is used as input, the $|V_{tb}|$ input eq. (4.21) loses its importance.

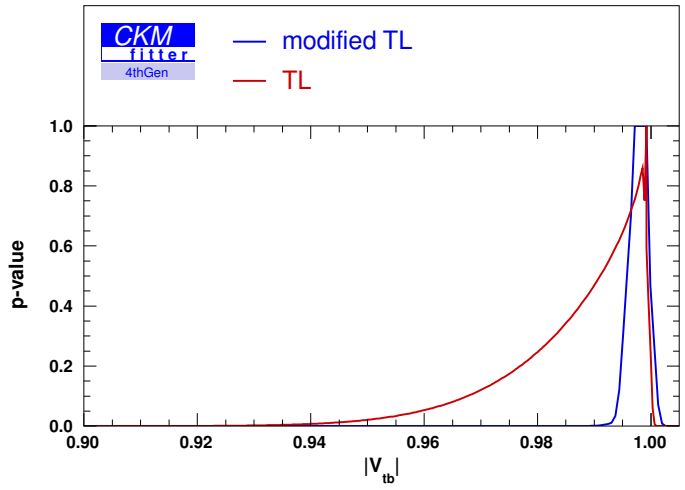

Figure 4.3.: Comparison of p-value contours/limits on $|V_{tb}|$ in the Tree Level set of inputs described in sec. 5 ("TL", red) and the modified set ("modified TL", blue) in which the $|V_{tb}|$ input from single top was replaced by the limit placed on $|V_{t'b}|$ by the Electroweak Precision Fit. The EWP constraint is much stricter, justifying the use of the single top input in the TreeLevel set of inputs.

As the above values for R conflict with all other inputs and even unitarity, R is not used in any fit.

4.1.9. Leptonic W boson decays

Roughly 30% of all W bosons decay into leptons, i.e. $\sum_\ell \mathcal{B}(W \to \ell\bar{\nu}) \approx 30\%$ with $\ell = e, \mu, \tau$. The SM3 prediction of each of these decays is (e.g. [142])

$$\mathcal{B}(W \to \ell\bar{\nu}_\ell)^{-1} = 3\left[1 + \sum_{i=u,c}\sum_{j=d,s,b}|V_{ij}|^2\left(1 + \frac{\alpha_s(m_W, \Lambda_{QCD})}{\pi}\right)\right] \tag{4.22}$$

if differences between the phase space factors of different leptonic final states are neglected. This can be done since all possible final state fermions - both leptons and quarks - have a much lower mass than the decaying W boson. $\alpha_S(m_W)$ is the strong coupling constant taken at the W boson mass scale. The value is, in our fits, calculated at two-loop level by the expression [48]

$$\alpha_s^{(2)}(Q^2, \Lambda_{QCD}) = \alpha_s^{(1)}(Q^2)\left(1 - \frac{102 - 10n_f - \frac{8}{3}n_f}{(11 - \frac{2}{3}n_f)^2} \cdot \frac{\ln(\ln(Q^2/\Lambda_{QCD}^2))}{\ln(Q^2/\Lambda_{QCD}^2)}\right). \tag{4.23}$$

$\alpha_s^{(1)}(Q^2)$ is the one-loop expression quoted in eq. (2.1) in section 2.1.1 where Λ_{QCD} is also explained. $n_f = 5$ is the number of kinematically accessible quark flavours.

In the SM4 case, the non-unitarity of the SM3 submatrix $U_{3\times3}$ of the PMNS matrix complicates the expression since sums such as $\sum_{i=1}^{3}|U_{\ell i}|^2$ are no longer equal to one as is assumed in eq. 4.22. However, updates of the fits performed in [59] show their values to be reasonably close to one so that using eq. 4.22 in SM4 fits does not noticably distort the fit results. The effect of the three inputs $\mathcal{B}(W \to \ell\bar{\nu})$ on an SM4 fit is to improve the lower constraint on $|V_{cs}|$. This is due to the dependence of eq. 4.22 on the squared moduli of the CKM matrix elements $|V_{ud}|$, $|V_{us}|$, $|V_{ub}|$, $|V_{cd}|$, $|V_{cs}|$ and $|V_{cb}|$. The larger such a modulus is, the more can its variation within its error interval change the result of eq. 4.22. All moduli except $|V_{cs}|$ are either smaller than $|V_{cs}|$ or have much smaller absolute uncertainties, so $|V_{cs}| \approx 1$ is the one which will be constrained by assigning an input to $\mathcal{B}(W \to \ell\bar{\nu})$. The values used here are

$$\begin{aligned}\mathcal{B}(\mathrm{W} \to \mathrm{e}\nu) &= (10.75 \pm 0.13)\% \\ \mathcal{B}(\mathrm{W} \to \mu\nu) &= (10.57 \pm 0.15)\% \\ \mathcal{B}(\mathrm{W} \to \tau\nu) &= (11.25 \pm 0.20)\%\end{aligned} \tag{4.24}$$

as given in the 2012 PDG average [46]. Their errors are correlated. Since a correlation table of those values was not available, a correlation table from [142] was used because both [46] and [142] use similar data in their averages. Both use the same results from the LEP experiments ALEPH, L3 and DELPHI. The difference lies in the contribution from OPAL. In [142] an OPAL result [143] extracted from 183 pb^{-1} of data taken at a center-of-mass energy of 189 GeV combined with results obtained at lower energies was used. The PDG average [46] uses a more recent result [144] including measurements at higher energies. The values obtained in the average based on the older data differ only very slightly from the ones quoted above, with $\mathcal{B}(W \to e\nu) = (10.69 \pm 0.17)$ %, $\mathcal{B}(W \to \mu\nu) = (10.57 \pm 0.16)$ % and $\mathcal{B}(W \to \tau\nu) = (11.39 \pm 0.23)$ %. With all this in mind, it seems justifiable in the context of the present work to use the correlation coefficients from [142] with the branching fractions from [46]. With the rows and columns arranged in the order $(\mathcal{B}(W \to e\nu), \quad \mathcal{B}(W \to \mu\nu), \quad \mathcal{B}(W \to \tau\nu))$, this correlation matrix reads

$$\begin{pmatrix} 1 & 0.110 & -0.195 \\ 0.110 & 1 & -0.132 \\ -0.195 & -0.132 & 1 \end{pmatrix}. \tag{4.25}$$

$\mathcal{B}(W \to \tau\bar{\nu})$ is actually larger than predicted either by the SM3 or the SM4 . Whenever these inputs are used, the total χ^2 of the fit therefore worsens by about 6 to 8.

4.1.10. The UT angle γ

In the context of the SM3 Unitarity Triangle and CP violation, the angle $\gamma = \arg\left(-\frac{V_{ud}V_{ub}^*}{V_{cd}V_{cb}^*}\right)$ (see sec. 2.4.6) is of particular interest for two reasons: Firstly, it is the only CP violating parameter that can be cleanly extracted from electroweak observables which can be described, at first order, already at Tree Level [145]. Secondly, it can be extracted in decays to which no penguin graphs contribute, keeping theoretical uncertainties at a low level. Also, it is unaffected by New Physics in mixing [146]. Its extraction is, however, challenging compared to the other two angles α and

β. The SM3 input value [131] used in this thesis, for example,

$$\gamma = 69.9^{+8.0\,\circ}_{-9.2} \mod 180^\circ, \tag{4.26}$$

has a significantly greater uncertainty than $\alpha = 85.4^{+4.0\,\circ}_{-3.9}$ and $\beta = 21.50^{+0.75\,\circ}_{-0.74}$ (both also from [131]).

Results from three different extraction methods (several more exist) were combined to obtain the above value of γ. Since it is not a priori clear that these results can be used in an SM4 context, they will be discussed here in some detail. Since they are all based on a common basic idea, this section starts with a short discussion along the lines of [147]. After this, the three extraction methods will be recalled, starting with the oldest. For the respective merits and drawbacks of each method, refer to the publications cited above and also [148].

All three methods measure the rates of hadronic decays of the type $B^\mp \to D^{0\,(*)} K^\mp$ and $B^\mp \to D^0 K^{\mp\,0}$ where the $^{(*)}$ indicates that it is possible to use excited states of neutral D or charged K mesons. The $D^{(*)}$ meson as produced in the decay of the B meson is an admixture

$$\tilde{D}^{(*)} = D^{0\,(*)} + r_B e^{\mathrm{i}(\delta_B^s - \delta_B^W)}\, \bar{D}^{0\,(*)}. \tag{4.27}$$

Here,

$$r_B = \frac{\left|A(B^- \to \bar{D}^{0\,(*)} K^-)\right|}{\left|A(B^- \to D^{0\,(*)} K^-)\right|} \qquad \text{and} \qquad \delta_B^s - \delta_B^W = \arg\left(\frac{A(B^- \to D^{0\,(*)} K^-)}{A(B^- \to \bar{D}^{0\,(*)} K^-)}\right). \tag{4.28}$$

Due to CKM suppression of the amplitude in the numerator, $r_B < 1$. The phase difference of the amplitudes is comprised of a strong phase difference δ_B^s and a weak phase difference δ_B^W. The general neutral D meson state $\tilde{D}^{(*)}$ decays then further to a final state which is chosen so that both $D^{0\,(*)}$ and $\bar{D}^{0\,(*)}$ contribute to the same final state. The two amplitudes add coherently, leading to interference. In analogy to r_B and δ_B^s, one also defines

$$r_D = \frac{\left|A(D^{0\,(*)} \to f)\right|}{\left|A(\bar{D}^{0\,(*)} \to f)\right|} \qquad \text{and} \qquad \delta_D^s - \delta_D^W = \arg\left(\frac{A(D^{0\,(*)} \to f)}{A(\bar{D}^{0\,(*)} \to f)}\right) \tag{4.29}$$

for the decay of the $\tilde{D}$ into the final state f. The weak phase differences result from the CKM matrix elements in the decay amplitudes. For the decays of a B^- into the neutral D meson flavour states, they can be read off Fig. 4.4. Those which occur in an example of the decay of D^0 and $\bar{D}^0$ are shown in Fig. 4.5. The CP violation potentially caused by the phase difference δ_D^W in the decay of the neutral D meson is negligibly small [149]; it will not be considered in the γ extraction methods. It is therefore set to zero from now on and will be omitted. The decay rates for B^+ and B^- into f via $\tilde{D}^{(*)}$ can then be written as

$$\Gamma_\pm = \Gamma(B^\pm \to \tilde{D}^{(*)} K^\pm) \propto r_B^2 + r_D^2 + 2 r_B r_D \cos(\delta_B^s + \delta_D^s \pm \gamma). \tag{4.30}$$

The charge averaged rate is

$$\Gamma = \frac{\Gamma_+ + \Gamma_-}{2} \propto r_B^2 + r_D^2 + 2r_B 2r_D \cos(\delta_B^s + \delta_D^s)\cos\gamma. \tag{4.31}$$

The rates r_B and strong phases δ_B^s are specific for each charged B decay. The values of r_D and δ_D^s are discussed separately for each extraction method.

Measurements on excited D^* states contribute to the input used. Since excited states in general do not have the same CP eigenvalues as ground states, the question arises if there are any peculiarities to consider in an SM4 context. In γ extractions, the D^* decays to either $D\pi^0$ or $D\gamma$. It was shown in [147] that $D^{(*)}_{CP\pm} \to D_{CP\pm}\pi^0$ due to angular momentum conservation, while $D^{(*)}_{CP\pm} \to D_{CP\mp}\gamma$ due to parity conservation. With the neutral $D^{(*)}$ meson's CP eigenstates

$$\left|D^{(*)}_{CP\pm}\right\rangle = \frac{1}{\sqrt{2}}\left(\left|D^{0\,(*)}\right\rangle \pm \left|\bar{D}^{0\,(*)}\right\rangle\right) \tag{4.32}$$

(D_{CP+} is the CP-even (+) eigenstate of the D meson system) and eq. (4.27), the general excited neutral D state can be written as

$$\tilde{D}^* = \frac{1}{\sqrt{2}}\left((D_+^* + D_-^*) + r_B e^{\mathrm{i}(\delta_B^s - \delta_B^W)}(D_+^* - D_-^*)\right). \tag{4.33}$$

In $\tilde{D}^* \to \tilde{D}\pi^0$ and $\tilde{D}^* \to \tilde{D}\pi^0$, the final states are

$$\tilde{D}_{\pi^0} = D^0 + r_B e^{\mathrm{i}(\delta_B^s - \delta_B^W)}\bar{D}^0 \tag{4.34}$$

$$\text{and} \qquad \tilde{D}_\gamma = \frac{1}{\sqrt{2}}\left((D_-^* + D_+^*) + r_B e^{\mathrm{i}(\delta_B^s - \delta_B^W)}(D_-^* - D_+^*)\right) \tag{4.35}$$

$$= D^0 + r_B e^{\mathrm{i}(\delta_B^s + \pi - \delta_B^W)}, \tag{4.36}$$

respectively. This amounts to an effective strong phase shift of π between the two cases, i.e. something that must be accounted for in the extraction of the weak phase, but which does not change due to the presence of a fourth generation of fermions.

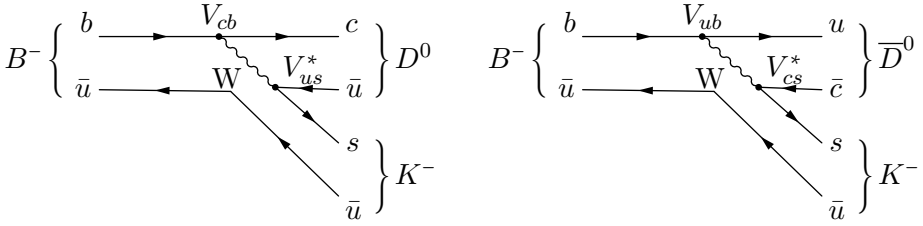

(a) $B^- \to D^0 K^-$ (b) $B^- \to \overline{D}^0 K^-$

Figure 4.4.: Tree Level Feynman graphs contributing to B^- decay. (b) is CKM suppressed. B^+ mesons decay in the CP-conjugate processes, for which every CKM matrix element has to be replaced by its complex conjugate.

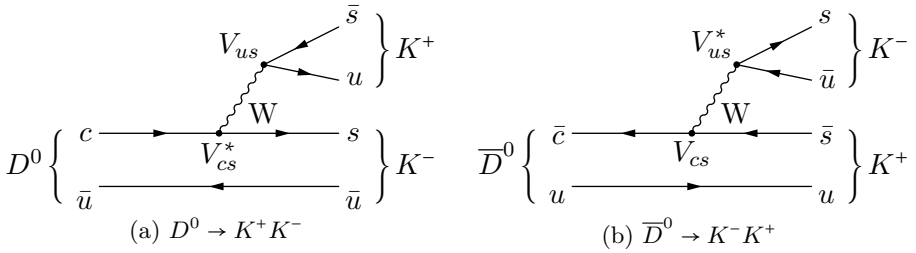

(a) $D^0 \to K^+K^-$ (b) $\overline{D}^0 \to K^-K^+$

Figure 4.5.: Decays of D^0 and $\overline{D}^0$ mesons used in γ extraction by the GLW method. For final state pions as used in the ADS method, replace s by d in the graphs and the assigned CKM matrix elements.

GLW Method

The first extraction method to be described is the "GLW" method proposed by Gronau, London and Wyler in [150] and [151], respectively. Its distinguishing feature is that the reconstructed state $\tilde{D}^{(*)}$ is a CP eigenstate $D_{CP\pm}$. The method will be explained using the decay chain $B^- \to DK^-$ and its charge conjugated process as an example. Other decay chains will be given later, with appropriate remarks. The quantities measured are the partial decay rate asymmetries

$$A_{CP+} = \frac{\Gamma(B^- \to D_{CP+}K^-) - \Gamma(B^+ \to D_{CP+}K^+)}{\Gamma(B^- \to D_{CP+}K^-) + \Gamma(B^+ \to D_{CP+}K^+)} \tag{4.37}$$

and the ratio

$$R_{CP+} = 2\frac{\Gamma(B^- \to D_{CP+}K^-) + \Gamma(B^+ \to D_{CP+}K^+)}{\Gamma(B^- \to D^0K^-) + \Gamma(B^+ \to \overline{D}^0K^+)}. \tag{4.38}$$

A_{CP-} and R_{CP-} are analogous quantities with the CP-odd (-) eigenstates of the D meson. Following this definition, the amplitude $A(B^- \to D_{CP+}K^-)$ can be decomposed into two contributing processes (cf. eq. (4.27))

$$\begin{aligned}\sqrt{2}A(B^- \to D_{CP+}K^-) &= A(B^- \to D^0K^-) + A(B^- \to \overline{D}^0K^-) \\ &= A(B^- \to D^0K^-)(e^{i\,\delta^W_{bc\bar{u}s}} + r_B e^{i\,\delta^W_{bu\bar{c}s}} e^{i\,\delta^s_B}).\end{aligned} \tag{4.39}$$

The δ^W are weak phases with their subscripts denoting the quark flavours involved in the weak interaction. They are, of course, the phases of the products of CKM matrix elements. An equivalent decomposition can be applied to the decay of the B^+ with a CP-even neutral D meson in the final state:

$$\begin{aligned}\sqrt{2}A(B^+ \to D_{CP+}K^+) &= A(B^+ \to D^0K^+) + A(B^+ \to \overline{D}^0K^+) \\ &= A(B^+ \to D^0K^+)(e^{i\,\delta^W_{\bar{b}\bar{u}c\bar{s}}} + r_B e^{i\,\delta^W_{\bar{b}\bar{c}u\bar{s}}} e^{i\,\delta^s_B}).\end{aligned} \tag{4.40}$$

Fig. 4.4 shows the Feynman graphs corresponding to the amplitudes at tree level. In the decays $B^\pm \to D_{CP-}K^\pm$, the plus sign on the right hand sides of the above two equations is replaced by a

minus sign. The final states which are identified by the detector are the final states of the D meson decay. The GLW measurements entering the value given in eq. (4.26) use the CP-even states K^+K^- and $\pi^+\pi^-$ and the CP-odd $K^0_S\pi^0$, $K^0_S\phi$, $K^0_S\eta$ and $K^0_S\omega$. CP violation in the neutral kaon system is neglected and the CP eigenvalue $\eta_{CP}(K^0_S)$ is approximated by +1. As CP violation in the decay of D mesons is neglected, the decayed D state can thus be identified as either D_{CP+} or D_{CP-}. The D's flavour eigenstate cannot be identified: Since the CP eigenstates $D_{CP\pm}$ are the superpositions in eq. (4.32), both flavour eigenstates D^0 and $\overline{D}^0$ contribute to each final state and their amplitudes have to be added coherently. In the GLW method, the negligible CP violation in the D and K^0_S meson decays leads to $r_D = 1$. Also, δ^s_D is $0 \mod \pi$ [147]. Using the above definitions, it can be shown that the asymmetries $A_{CP\pm}$ and ratios $R_{CP\pm}$ can be expressed in terms of the ratio r_B, the final state interaction phase differences δ^s_B and the weak phase difference δ^W_B:

$$R_{CP\pm} = 1 + r_B^2 \pm 2r_B \cos\delta^s_B \cos\delta^W_B \tag{4.41}$$

$$A_{CP\pm} = \frac{\pm 2r_B \cos\delta^s_B \cos\delta^W_B}{1 + r_B^2 \pm 2r_B \cos\delta^s_B \cos\delta^W_B} \tag{4.42}$$

The weak phase δ^W_B can be separated from the final state interaction phase δ^s_B by measuring several distinct decay channels. While different decays in general have different δ^s_B, the weak phase from the decay of B to D mesons only depends on the quark flavours involved in final and intermediate states by means of the corresponding CKM matrix elements. It is therefore the same for all decays measured.

In some of the actual extractions included in the combination in eq. (4.26), an approximation of $R_{CP\pm}$ is used which reduces systematic uncertainties in the measurement of branching ratio and reconstruction efficiencies while introducing a smaller systematic uncertainty of its own (see e.g. [152] and other parts of Ref. 17 in [131]).

ADS Method

The second method is the "ADS" method named for the authors Atwood, Dunietz and Soni of [153] where it was proposed. Unlike the GLW method, the ADS method does *not* reconstruct CP eigenstates. This had been proposed before in [154]. However, in [153], it was argued that the CP violating effects could be enhanced by selecting decay chains which suitably combine doubly Cabbibo suppressed and Cabbibo allowed decays. In the decay of a B^-, for example, two competing decay chains to a common final state are

$$B^- \begin{array}{l} \nearrow K^- D^0 \searrow \\ \searrow K^- \overline{D}^0 \nearrow \end{array} K^- f. \tag{4.43}$$

A dashed arrow indicates a CKM suppressed decay. While these chains result in lowered statistics in such an extraction, they make the interfering amplitudes of the decay paths more comparable and CP violating effects manifest themselves more strongly in the measured asymmetries. The common final state of (anti-) D meson decays used as an example in this description is $K^+\pi^-$.

The quantity measured in the experiments in the case of eq. (4.43) is

$$R_- = \frac{\Gamma(B^- \to (K^+\pi^-)_D K^-)}{\Gamma(B^- \to (K^-\pi^+)_D K^-)}. \tag{4.44}$$

In the charge conjugated process of eq. (4.43), the quantity R_+ is measured. Its expression follows from eq. (4.44) by reversing all charge signs. R_+ and R_- can be used to express the average decay rate R_{ADS} and the CP violating asymmetry A_{ADS}:

$$R_{ADS} = \frac{1}{2}(R_+ + R_-) \tag{4.45}$$

$$A_{ADS} = \frac{R_- - R_+}{R_- + R_+} = \frac{R_- - R_+}{2R_{ADS}} \tag{4.46}$$

With (4.30), this becomes

$$R_{ADS} = r_B^2 + r_D^2 + 2r_B r_D \cos(\delta^W)\cos(\delta_B^s + \delta_D^s) \tag{4.47}$$

$$A_{ADS}\frac{2r_B r_D \sin\delta^W \sin(\delta_B^s + \delta_D^s)}{R_{ADS}}. \tag{4.48}$$

GGSZ / Dalitz Plot Method

The third method is the "GGSZ" method, named for the authors Giri, Grossman, Soffer and Zupan who proposed it in [155]. Previously, it had been suggested by Bondar[4]. It is also known as the Dalitz plot method. At the B-factories it has the highest statistical power [156] of the three methods described here. In principle, only Cabbibo-allowed modes are needed to obtain useful data. This shortens the time needed to measure enough events to satisfy statistical requirements. Also, in final states containing only charged particles, the reconstruction efficiency is higher and the background is lower, further improving statistics.

Neutral $D^{(*)}$ mesons from $B^\pm \to D^{(*)}K^\pm$ or $B^\pm \to D\,K^{\pm\,*}$ decays are reconstruced from three-body decays with self-conjugate, common final states $D \to K_S^0\pi^+\pi^-$ and $D \to K_S^0 K^+ K^-$. For readability, this description will *not* include the cases of excited D mesons or kaons. Towards the end of this section, references for their treatment will be given. Using the invariant masses $s_+ = m(K_S^0 h^+)^2$ and $s_- = m(K_S^0 h^-)^2$ as "Dalitz plot variables", one can measure the rates $\Gamma(B^+ \to (K_S^0\pi^+\pi^-)_D K^+)$ and $\Gamma(B^+ \to (K_S^0\pi^+\pi^-)_D K^-)$ as $\Gamma_\pm(s_+, s_-)$, keeping in mind that the index $_\pm$ of the rate and, later, the amplitudes, indicates the charge of the decayed B meson while the index in $s_\pm$ denotes the charge of the pion or kaon in the Dalitz plot observable. The amplitude corresponding to $\Gamma_\pm(s_\pm, s_\mp)$ is

$$A_\pm(s_\pm, s_\mp) = A(\bar{D}^0 \to K_S^0\pi^+\pi^-)(s_\pm, s_\mp) + A(D^0 \to K_S^0\pi^+\pi^-)(s_\mp, s_\pm). \tag{4.49}$$

Assuming absence of CP violation in the neutral D and K meson systems and neglecting D mixing effects, $A(D^0 \to K_S^0\pi^+\pi^-)(s_\mp, s_\pm) = A(\bar{D}^0 \to K_S^0\pi^+\pi^-)(s_\pm, s_\mp)$. With eq. (4.28) and the phase

[4] A. Bondar, Proceedings of BINP special analysis meeting on Dalitz analysis, 24-26 Sep. 2002, unpublished

δ_B^s, eq. (4.49) becomes

$$A_\pm(s_\pm, s_\mp) = A(\bar{D}^0 \to K_S^0\pi^+\pi^-)(s_\pm, s_\mp) + r_B \cdot A(D^0 \to K_S^0\pi^+\pi^-)(s_\mp, s_\pm)e^{\mathrm{i}(\delta_B^s \pm \delta^W)}. \tag{4.50}$$

This leads to the expression for the rate as a function of the Dalitz plot variables,

$$\begin{aligned}\Gamma_\pm(s_\pm, s_\mp) = &\left|A(\bar{D}^0 \to K_S^0\pi^+\pi^-)(s_\pm, s_\mp)\right|^2 + r_B^2\left|A(\bar{D}^0 \to K_S^0\pi^+\pi^-)(s_\mp, s_\pm)\right|^2 + \\ &+ 2\cdot\left|A(\bar{D}^0 \to K_S^0\pi^+\pi^-)(s_\pm, s_\mp)\right|\left|A(\bar{D}^0 \to K_S^0\pi^+\pi^-)(s_\mp, s_\pm)\right| \mathrm{Re}\left(e^{\pm\mathrm{i}\,\delta^W + \mathrm{i}\,\delta_B^s}\right).\end{aligned} \tag{4.51}$$

In Dalitz plots, the complex quantity $r_B \cdot e^{\mathrm{i}\,\delta_B^s \pm \gamma}$ is often expressed in real and imaginary parts, i.e. as $z_\pm = x_\pm + \mathrm{i}\,y_\pm$. Once the rate $A(\bar{D}^0 \to K_S^0\pi^+\pi^-)(s_\pm, s_\mp)$ is known, events satisfying the selection criteria for the γ extraction are placed in the s_+, s_--plane, generating the actual Dalitz plot. Eq. (4.51) can then be fitted to this result and the angle δ^W can be extracted.

From Observed Rate Differences to the Angle γ

In order to extract the angle γ from the observed phase differences, it has to be separated from other contributions. These are the strong phase differences δ^s and the influence of other CKM matrix elements involved in the cascade decays of B mesons to the decay products finally observed in the detector. Also, the methods described above yield γ only up to certain ambiguities. They are discussed in the original publication of the GGSZ method [155] and, for the GLW and ADS methods and their combination, in [157].

In the context of using an SM3 extraction of γ in an SM4 context, the interesting part is the role played by the abovementioned other CKM matrix elements which appear in the processes measured [158]. The CKM matrix elements which occur in the ADS and GLW results which are included in the γ average eq. (4.26) are given in Table 4.2. The GGSZ results entering this value include determinations where the D meson decays to $K_S\pi^+\pi^-$, $K^-K^+K_S$, $K^\pm\pi^\pm$, $K_S\pi^0$, $K_S\eta$, $\pi\pi$ and KK. Table 4.2 already lists the required CKM matrix elements. Let the decay $B^- \to (K^+K^-)_{\tilde{D}}$ serve as an example on how to obtain the phase given in its third column: The weak phases of the two amplitudes interfering in the experiment can be read off the corresponding Feynman graphs (in this case, Figs. 4.4 and 4.5). Keep in mind that the intermediate D meson state is a CP eigenstate as in eq. (4.32); this is how the interference between both processes given in the first column comes to pass in the first place. The weak phase difference is given in the second column:

$$\delta^W = \arg\left(\frac{V_{cb}V_{us}^* \cdot V_{us}V_{cs}^*}{V_{ub}V_{cs}^* \cdot V_{cs}V_{us}^*}\right) = \arg\left(\frac{V_{cb}V_{us}}{V_{ub}V_{cs}}\right) \tag{4.52}$$

One realizes that there are no factors of V_{cd}^* or V_{ud}^* present which are needed to form the expression for γ (eq. (2.60)), so the fraction is expanded accordingly:

$$\delta^W = \arg\left(\frac{V_{cb}V_{cd}^* \cdot V_{ud}^*V_{us}}{V_{ub}V_{ud}^* \cdot V_{cs}V_{cd}^*}\right) \tag{4.53}$$

Interfering processes	weak phase δ^W	
GLW method, $D^0/\overline{D}^0 \to K^+K^-$		
$B^- \to (K^+K^-)_{D^0}K^-$ $B^- \to (K^+K^-)_{\overline{D}^0}K^-$	$\arg\left(\frac{V_{cb}V_{us}^*\cdot V_{us}V_{cs}^*}{V_{ub}V_{cs}^*\cdot V_{cs}V_{us}^*}\right)$	$\gamma + \pi - \arg\left(\frac{V_{ud}V_{us}^*}{V_{cd}V_{cs}^*}\right)$
GLW method, $D^0/\overline{D}^0 \to \pi^+\pi^-$		
$B^- \to (\pi^+\pi^-)_{D^0}K^-$ $B^- \to (\pi^+\pi^-)_{\overline{D}^0}K^-$	$\arg\left(\frac{V_{cb}V_{us}^*\cdot V_{ud}V_{cd}^*}{V_{ub}V_{cs}^*\cdot V_{cd}V_{ud}^*}\right)$	$\pi + \gamma - \arg\left(\frac{V_{ud}V_{us}^*}{V_{cd}V_{cs}^*}\right)$
GLW method, $D^0/\overline{D}^0 \to K_S h$		
$B^- \to (K_S h)_{D^0}K^-$ $B^- \to (K_S h)_{\overline{D}^0}K^-$	$\arg\left(\frac{V_{cb}V_{us}^*\cdot V_{ud}V_{cs}^*}{V_{ub}V_{cs}^*\cdot V_{cs}V_{ud}^*}\right)$	$\pi - \gamma + \arg\left(\frac{V_{ud}V_{us}^*}{V_{cd}V_{cs}^*}\right)$
ADS method		
$B^- \to D^0K^- \to (K^+\pi^-)_{D^0}K^-$ $B^- \to \overline{D}^0K^- \to (K^+\pi^-)_{\overline{D}^0}K^-$	$\arg\left(\frac{V_{cb}V_{us}^*V_{us}V_{cd}^*}{V_{ub}V_{cs}^*V_{cs}V_{ud}^*}\right)$	$\pi - \gamma$

Table 4.2.: CKM factors entering the extraction of UT angle γ in GLW and ADS methods. h can be one of the CP-eigenstate mesons π^0, ϕ, η or ω. Complex conjugated processes are implicit; their extracted phase carries the opposite sign.

Using $\arg(z^*) = -\arg(z) = \arg(z^{-1})$, this can be written as

$$\delta^W = \arg\left(\frac{V_{ud}V_{ub}^*}{V_{cd}V_{cb}^*}\cdot\frac{V_{cd}V_{cs}^*}{V_{ud}V_{us}^*}\right) = \pi + \arg\left((-1)\cdot\frac{V_{ud}V_{ub}^*}{V_{cd}V_{cb}^*}\cdot\frac{V_{cd}V_{cs}^*}{V_{ud}V_{us}^*}\right) = \tag{4.54}$$

$$= \pi + \gamma + \arg\left(\frac{V_{cd}V_{cs}^*}{V_{ud}V_{us}^*}\right) = \pi + \gamma - \arg\left(\frac{V_{ud}V_{us}^*}{V_{cd}V_{cs}^*}\right). \tag{4.55}$$

When extracting γ in a given scenario, one has to make sure that the quantity actually measured is reasonably close to γ. A glance at column 3 of Table 4.2 shows that the deviation from γ is

$$\delta_1 = \pi + \arg\left(\frac{V_{ud}V_{us}^*}{V_{cd}V_{cs}^*}\right) \tag{4.56}$$

or π depending on the D^0 decay channel used. In the SM3's Wolfenstein parametrisation (see eq. (A.3)), $\delta_1 < \mathcal{O}(\lambda^4) \approx 2.3\cdot 10^{-3}$ and thus certainly negligible. If the deviation of δ_1 from π can be constrained to be small enough to be dominated by the uncertainty of the measurement in the SM4, it is possible to use γ values from SM3 extractions in the fits. The Dalitz plot method effectively averages over all these possible deviations from γ, ensuring that its contribution to the deviation of the quantity extracted in measurements and γ is not greater than that of the other two methods. Anticipating the other results given in section 5.1, the Tree Level input set (cf. p.

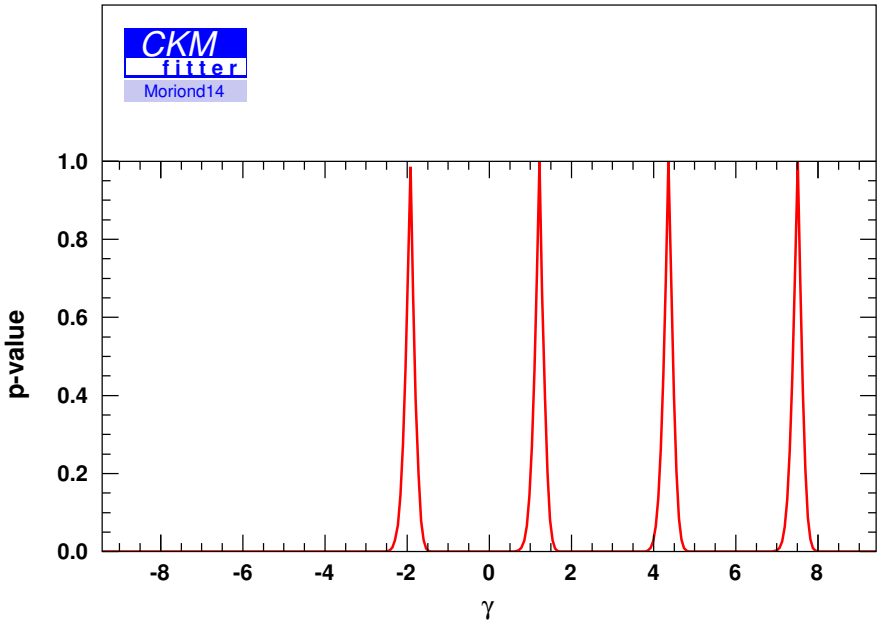

Figure 4.6.: Plot of the lookup table providing the γ input. The multiple peaks account for amibiguities modπ in the extraction from experiment. For the plot, the χ^2 provided by the lookup table was converted to a p-value.

93) can indeed constrain δ_1 to

$$\delta_1 = 0.000^{+0.017}_{-0.000} = (0.00^{+1.03}_{-0.00})^\circ \mod 360^\circ. \tag{4.57}$$

The p-value plot is shown in Fig. 4.7. The uncertainty on δ_1 is negligible compared to the uncertainty of the average eq. (4.26) obtained by CKMfitter. As experiments determine γ only up to an ambiguity of π, the input used for the fits is given to the program in the shape of a lookup table [159]. The first 1σ interval in this lookup table was already given in eq. (4.26), and the entire lookup table - converted from χ^2 to p-value - is shown in Fig. 4.6.

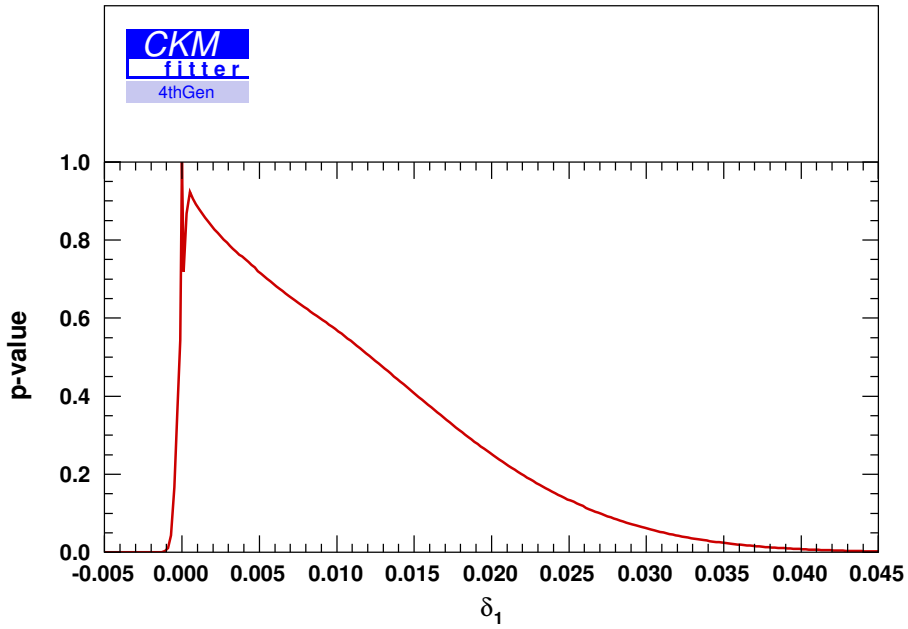

Figure 4.7.: p-value plot of the additional phase δ_1 by which the extraction of γ from experiment is blurred in the presence of a fourth generation. The limit was obtained with the TL set of inputs as described on p. 93, but omitting the γ input.

4.2. Loop Observables Respecting CP Symmetry

γ as described in the previous section 4.1.10 is the only one of the CP violating observables used as inputs in this work which can be described at Tree Level. All others do not occur below one-loop level. There are, however, a number of loop-level inputs which do not violate CP symmetry. They are described in this section.

4.2.1. Results of the Electroweak Precision Fit

The effects of the Electroweak Precision Fit on constraints of SM4 parameters are condensed into a 2D χ^2 lookup table (see section 3.2.2) correlating the modulus $|V_{t'b}|$ and the mass $m_{t'}$ of the t' quark. It is a fit result provided by Otto Eberhardt. A short description on how it was obtained seems in order. For more details, see section 2.7 and e.g. [100].

In the course of the project which also resulted in the present thesis, attempts were made to equip CKMfitter with routines to perform an Electroweak Precision Fit. Instead of writing an EWP theory package from scratch, Otto Eberhardt and Martin Wiebusch developed an interface which calls Zfitter's `DIZET` (see [160], [161] and [112]) routine to perform the calculation of quantities included in the fit. New Physics contributions, in this case SM4 terms at one-loop level, are then calculated using `FeynArts`, `FormCalc` and `LoopTools` ([162], [163] and [164]). The method is described in [102]. For the reasons given in section 2.7, the lookup table used as input in this thesis was generated without using the "oblique parameters" S, T and U [98] but by using the full set of EWP observables given in sec. 2.7. The inputs values used are given in Table 4.3. The p-value distribution corresponding to the 2D χ^2 LUT is shown in Fig. 4.8.

4.2.2. Δm_d

The difference of the mass of the two mass eigenstates of the neutral B meson system Δm_d - as defined in eq. (2.83) - can be measured in time-dependent mixing experiments as 2π times the $B_d^0 - \bar{B}_d^0$ oscillation frequency. As argued in sec. 2.5.2, the simplification given in eq. (2.86) applies here:

$$\Delta m = -2\,|M_{12}| \tag{4.58}$$

The general expression for M_{12}, eq. (2.100), can now be adapted to the B_d^0 meson system and is also simplified as permitted by the properties of the neutral B meson. The down-type constituent quarks are b and d. Both in the SM3 and the SM4, contributions from box graphs containing virtual c and u quarks can be neglected. Their mass is much smaller than the top quark mass and the still higher mass of the t', and the contribution of a quark species is governed not only by its CKM matrix elements but also the mass-dependent Inami-Lim functions in eq. (C.1). The remaining expression for M_{12} is then

$$\begin{aligned} M_{12} =& \frac{G_F^2 m_B \hat{B}_B f_B^2 m_W^2}{12\pi^2} \cdot \\ & \cdot \left(\eta_{tt}(\mu) S_0(x_t)\ {\lambda_t^{B_d}}^2 + 2\eta_{tt'}(\mu) S_0(x_t, x_{t'}) \lambda_t^{B_d} \lambda_{t'}^{B_d} + \eta_{t't'}(\mu) S_0(x_{t'})\ {\lambda_{t'}^{B_d}}^2 \right) \end{aligned} \tag{4.59}$$

Obs.	Value	Ref.
	Masses and widths [GeV]	
m_Z	(91.1876 ± 0.0021)	[46]
Γ_Z	(2.4952 ± 0.0023)	[105]
m_W	$(80.385 \pm 0.015 \pm 0.004)$	[165],[166]
Γ_W	(2.085 ± 0.042)	[167]
m_t^{pole}	$(173.07 \pm 0.52 \pm 0.72)$	[168]
$\alpha_s(m_Z)$	$0.1202 \pm 0.0006 \pm 0.0021$	[169]
σ^0_{had}	(41.541 ± 0.037) nb	[46]
$\Delta\alpha^{(5)}_{\text{had}}$	0.02757 ± 0.00010	[170]
$\mathcal{A}_\ell$	0.1499 ± 0.0018	[105],[171]

Obs.	Value
	All taken from Ref. [105].
$A^{0,b}_{\text{FB}}$	0.0992 ± 0.0016
$A^{0,c}_{\text{FB}}$	0.0707 ± 0.0035
$A^{0,\ell}_{\text{FB}}$	0.0171 ± 0.0010
$\mathcal{A}_b$	0.923 ± 0.020
$\mathcal{A}_c$	0.670 ± 0.027
R^0_b	0.21629 ± 0.00066
R^0_c	0.1721 ± 0.0030
R^0_ℓ	20.767 ± 0.025
$\sin^2\theta^{\text{eff}}_\ell$	0.2324 ± 0.0012

Table 4.3.: Inputs used to obtain the electroweak precision constraints on $|V_{tb'}|$ and $m_{t'}$.

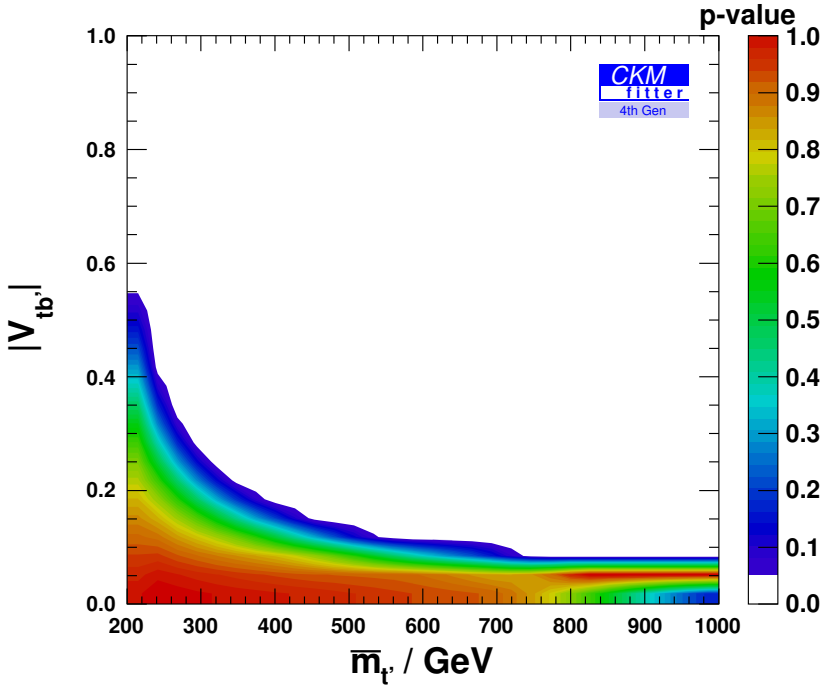

Figure 4.8.: 2D LUT used to include SM4 constraints from the EWP fit, converted to a p-value. The bar above $m_{t'}$ indicates that it is to be taken in the $\overline{MS}$ scheme (cf. eg. [43]).

with $\lambda_{\hat{u}}^{B_d} = V_{\hat{u}d}V_{\hat{u}b}^*$. $\hat{u}$ is the flavour of the virtual up-type quark in the box graph, i.e. either t or t'. The QCD corrections $\eta_{tt}^{(B)}$ are given at NLO in [172]. Like in [25], it is assumed that

$$\eta_{xx}^{(B)} = \eta_{tx}^{(B)} = \eta_{tt}^{(B)} = \eta^{(B)} \tag{4.60}$$

To arrive at the SM3 expression for Δm_d, one can simply omit the last two summands in the modulus, i.e. those in which t' occurs. The experimental input used for the fits is an average [129] of a large number of values obtained by the collaborations ALEPH, DELPHI, L3, OPAL, CDFI, D0, *BABAR*, Belle and LHCb:

$$\Delta m_d = (0.507 \pm 0.004)\ \text{ps}^{-1} \tag{4.61}$$

4.2.3. Δm_s

The theoretical expression for Δm_s is exactly analogous to the expression for Δm_d in the previous section. The main difference is that the d quark is replaced by an s quark. Therefore $\lambda_{\hat{u}}^{B_s} = V_{\hat{u}s}V_{\hat{u}b}^*$. Also, the appropriate mass, bag parameter and decay constant for the B_s meson have to be used, resulting in

$$\begin{aligned}\Delta m_s =& 2\frac{G_F^2 m_{B_s}\hat{B}_{B_s}f_{B_s}^2 m_W^2}{12\pi^2}\cdot \\ &\cdot\left|\eta_{tt}(\mu)S_0(x_t)\ {\lambda_t^{B_s}}^2 + 2\eta_{tt'}(\mu)S_0(x_t,x_{t'})\lambda_t^{B_s}\lambda_{t'}^{B_s} + \eta_{t't'}(\mu)S_0(x_{t'})\ {\lambda_{t'}^{B_s}}^2\right|\end{aligned} \tag{4.62}$$

where $\lambda_{\hat{u}}^{B_s} = V_{\hat{u}s}V_{\hat{u}b}^*$. Again, the SM3 expression can be obtained by omitting the last two summands in eq. (2.100). The experimental input used in the present thesis

$$\Delta m_s = (17.762 \pm 0.023)\ \text{ps}^{-1} \tag{4.63}$$

is an average by the CKMfitter group [131]. It includes another average from [129] of measurements performed by CDF2 and LHCb and augments it by another value published by LHCb in [173].

4.2.4. $\Gamma(b \to s\gamma)/\Gamma(b \to ce\bar{\nu})$

The inclusive decay $B \to X_s\gamma$ in which X_s is any state with strangeness $S \neq 0$ is one of three so-called rare decays used as inputs in this thesis. The qualifier "rare" refers to its branching ratio of $(360 \pm 23) \cdot 10^{-6}$ [174]. This is small enough to compare with possible effects of New Physics but still large enough to be measured. Also, it depends only on the top quark mass and α_s. These two characteristics make it suitable for putting constraints on New Physics [16, 32]. In order to reduce uncertainties due to CKM matrix elements and the dependence on m_b^5 [67], one normalizes the branching fraction $\mathcal{B}(B \to X_s\gamma)$ to that of inclusive semileptonic B-meson decays to charmed final states, $\mathcal{B}(B \to X_c e\bar{\nu})$:

$$\frac{\mathcal{B}(B \to X_s\gamma)}{\mathcal{B}(B \to X_c e\bar{\nu})} \tag{4.64}$$

For the calculation, one approximates eq. (4.64) by the ratio of the partonic decays. This is called the spectator model which was shown to correspond to the leading order approximation of an HQE expansion [5] [172]:

$$R_{b\to s\gamma} = \frac{\Gamma(b\to s\gamma)}{\Gamma(b\to ce\bar{\nu})} \tag{4.65}$$

$R_{b\to s\gamma}$ is the quantity whose theoretical expression will be used in the fits of chapter 5. The $b\to s\gamma$ decay proceeds via magnetic penguins (cf. Fig. 2.1 c)) in which the photon has to be on-shell. Any details of the calculations necessary to derive the expressions needed in the fit are beyond the scope of this work but are elaborated upon in [67] and also [172]. In the SM3, the theoretical expression is derived by using the 3×3 unitarity of the CKM matrix to eliminate the term proportional to $V_{cs}V_{cb}^*$ and then using the smallness of $V_{us}V_{ub}^*$ and its coefficient to obtain [25]

$$R_{b\to s\gamma}^{(\mathrm{SM3})} = \frac{\left|V_{ts}V_{tb}^*\right|^2}{\left|V_{cb}\right|^2}\frac{6\alpha_{EM}}{\pi f(z)}\left|C_7^{\mathrm{eff},1}(\mu,\bar{m}_t) + C_7^{\mathrm{eff},2}(\mu,\bar{m}_t) + C_7^{\mathrm{eff},3}(\mu)\right|^2. \tag{4.66}$$

In this complete leading logarithm expression, μ is as usual the scale at which the calculation is performed - some words regarding its choice will follow below. $f(z)$ is the phase space factor in $\Gamma(b\to ce\bar{\nu})$, taken at $z = m_c^2/m_b^2$ and given by [67]

$$f(z) = 1 - 8z + 8z^3 - z^4 - 12z^2\ln z. \tag{4.67}$$

The ratio z is calculated from the pole masses of the b and c quarks, but at one-loop order, the pole mass is equal to the $\overline{MS}$ mass while differences are only small at two-loop order[6]. Therefore, the SM4 expression corresponding to eq. (4.66), (4.69), is currently coded with $z = \frac{\bar{m}_c^2}{\bar{m}_b^2}$. The C_7^{eff} are effective Wilson coefficients. The contribution of the current-current operator's Wilson coefficient $C_7^{\mathrm{eff},3}\propto C_2^{(0)}$ to eq. (4.66) is dominant [25]. $C_7^{\mathrm{eff},2}$ is proportional to the Wilson Coefficient C_{8g} of the magnetic gluon penguin operator Q_{8g} and $C_7^{\mathrm{eff},1}$ to $C_{7\gamma}^{(0)}$, the electromagnetic penguin operator $Q_{7\gamma}$'s Wilson Coefficient. The C_7^{eff} are listed in Appendix C.

To go from SM3 to SM4, the first step is to make sure that approximations similar to those made in the derivation of eq. (4.66) are possible. In general, and including all quark flavours $\hat{u}$ which might appear in the loop in Fig. 4.9, the SM4 effective Hamiltonian assuming a completely general CKM matrix reads

$$\begin{aligned}\mathcal{H}_{b\to X_s\gamma}^{\mathrm{eff,SM4}} = -\frac{G_F}{\sqrt{2}}\Big(&V_{t's}V_{t'b}^*\cdot(\hat{Q}_{t'}^{(\mathrm{OPE})}(\mu,m_{t'}) - \hat{Q}_c^{(\mathrm{OPE})}(\mu,m_c)) + \\ &+ V_{ts}V_{tb}^*\cdot(\hat{Q}_t^{(\mathrm{OPE})}(\mu,m_t) - \hat{Q}_c^{(\mathrm{OPE})}(\mu,m_c)) + \\ &+ V_{us}V_{ub}^*\cdot(\hat{Q}_u^{(\mathrm{OPE})}(\mu,m_u) - \hat{Q}_c^{(\mathrm{OPE})}(\mu,m_c))\Big).\end{aligned} \tag{4.68}$$

Here, the $\hat{O}_q^{(\mathrm{OPE})}$ represent whichever operators of the OPE of the SM4 Hamiltonian come with the appropriate CKM matrix factor. 4×4-unitarity has already been used to eliminate $V_{cs}V_{cb}^*$.

[5] An expansion in $\frac{1}{m_b}$; cf. [175] for a review

[6] Ulrich Nierste, private communication

Compared to the values assumed with the other two quark masses, the coefficient of the CKM factors $V_{us}V_{ub}^*$ turns out to be negligible (see Table 4.4 for values obtained with the inputs used in the upcoming fits). Looking at the Tree Level fit results (cf. chapter 5) of $\left|V_{us}V_{ub}^*\right|$ and $\left|V_{t's}V_{t'b}^*\right|$ in Table 4.5, it seems justifiable to neglect the term proportional to $V_{us}V_{ub}^*$.
During the calculation of the leading-order effective Wilson Coefficient C_7^{eff}, contributions of the current-current operator $\hat{O}_2$ were inserted. Their (non-negligible) part has a CKM factor $V_{cs}V_{cb}^*$ which was, in the SM3 case, approximated by $-V_{ts}V_{tb}^*$ using 3×3 unitarity and the smallness of $V_{us}V_{ub}^*$ (see [172] and references therein). Above, this numerically dominant contribution is named $C_7^{\text{eff}3}$. For the SM4 expression, this has to be undone, i.e. this contribution has to be subtracted again. One then arrives at the expression published in [25] which is also used in this work:

$$\begin{aligned} R_{b\to s\gamma} =& \frac{6\alpha_{EM}}{\pi f(z)}\frac{1}{|V_{cb}|^2}\cdot \\ &\cdot\Big|V_{cs}V_{cb}^* C_7^{\text{eff},3}(\mu) - V_{ts}V_{tb}^*(C_7^{\text{eff},1}(\mu,m_t)+C_7^{\text{eff},2}(\mu,m_t))- \\ &\quad -V_{t's}V_{t'b}^*(C_7^{\text{eff},1}(\mu,m_{t'})+C_7^{\text{eff},2}(\mu,m_{t'}))\Big|^2 . \end{aligned} \tag{4.69}$$

As for the scale μ, this work - like [25] - follows an approximation proposed in [32]: While only LO expressions are used for the Wilson Coefficients involved, a scale μ_{LO} is chosen in such a way that in the limit of neglecting the contribution of 4th Generation particles, the LO expression reproduces the numerical value of the NNLO SM3 calculation in [176]. This particular scale is found to be

$$\mu_{LO} = (3.14 \pm 0.001 \pm 0.03)\ \text{GeV}, \tag{4.70}$$

where the small statistical uncertainty was only introduced to prevent fit problems. The theoretical error was adjusted in such way that the precision of the result in [176] was reproduced. The selection of an otherwise arbitrary scale in order to numerically reproduce a higher order result is justified in [32][7] as follows:

> "The 4G effects will then be included through the modification of the SM3 Wilson coefficients at $\mu = M_W$ without the inclusion of additional QCD corrections. As the dominant QCD corrections to $\mathcal{B}(B\to X_S\gamma)$ come anyway from the renormalisation group evolution from M_W down to μ_{eff}, and from the matrix elements of the operators Q_2 and $Q_{7\gamma}$ at μ_{eff}, these dominant corrections are common to the SM3 and the SM4. While not exact, this treatment of QCD corrections in the SM4 should be sufficient for our purposes."

The experimental input

$$R_{b\to s\gamma} = (3.19 \pm 0.21)\cdot 10^{-4} \tag{4.71}$$

was calculated from the current PDG value [50] of $\mathcal{B}(b\to s\gamma) = (3.40\pm 0.21)\cdot 10^{-4}$ and the HFAG average [177] of the branching fraction of the decay of both charged and neutral B mesons to charmed final states $\mathcal{B}(B^{\pm/0}\to X_c\ell^+\nu) = (10.65\pm 0.16)\%$ which is dominated by $\ell = e$.

[7] Symbols used where changed from the original quote to fit in with the symbols used in the rest of the present thesis.

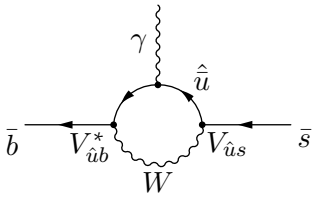

Figure 4.9.: Feynman graph contributing to $B \to X_s\gamma$ at lowest order. $\hat{u}$ can be any up-type quark, but graphs with a heavy $\hat{u} = t$ and $\hat{u} = t'$ dominate strongly.

$\hat{u}$ mass	$C_7^{\text{eff},1}$	$C_7^{\text{eff},2}$	$C_7^{\text{eff},3}$
2.3 MeV $\approx \overline{m}_u$	$-1.4 \cdot 10^{-10}$	$-2.1 \cdot 10^{-11}$	
1.285 GeV $\approx \overline{m}_c$	$-4.5 \cdot 10^{-5}$	$-6.7 \cdot 10^{-6}$	
165.95 GeV $\approx \overline{m}_t$	-0.11	-0.010	-0.212
400 GeV	-0.16	-0.012	
900 GeV	-0.19	-0.013	

Table 4.4.: Values of the effective Wilson coefficients at various quark masses and the scale $\mu = 3.14$ GeV. The last two masses were selected to lie within the allowed $m_{t'}$ regions of the Electroweak Precision fit (see sec. 4.2.1 and Fig. 4.8). $C_7^{\text{eff},3}$ does not depend on the quark mass.

	1σ	2σ	3σ
$\left\lvert V_{us}V^*_{ub}\right\rvert$	$0.000897^{+0.000027}_{-0.000074}$	$0.000897^{+0.000054}_{-0.000157}$	$0.000897^{+0.000081}_{-0.000190}$
$\left\lvert V_{t's}V^*_{t'b}\right\rvert$	$0.000^{+0.016}_{-0.000}$	$0.000^{+0.039}_{-0.000}$	$0.000^{+0.062}_{-0.000}$

Table 4.5.: Tree Level results from sec. 5.1 as justification for the approximations used in the derivation of the SM4 expression for $R_{b\to s\gamma}$.

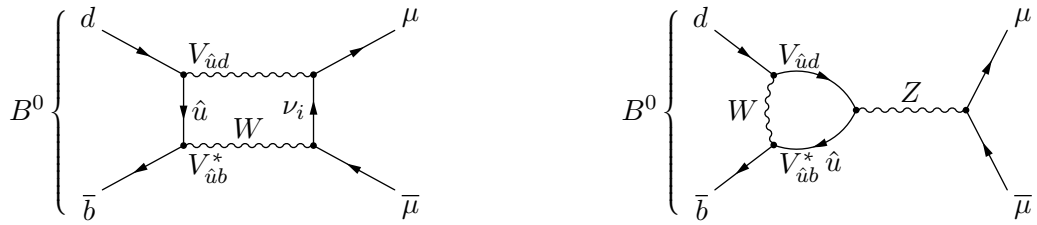

(a) Box contribution (b) Penguin graph

Figure 4.10.: Feynman graphs contributing to the decay $B_{(s)} \to \mu\bar{\mu}$. For the B_s decay, every d quark is replaced by an s quark. $\hat{u}$ can be any up-type quark.

4.2.5. $\mathcal{B}(\mathbf{B_d} \to \mu^+\mu^-)$ and $\mathcal{B}(\mathbf{B_s} \to \mu^+\mu^-)$

The decays $B_d \to \mu^+\mu^-$ and $B_s \to \mu^+\mu^-$ are very similar to each other and will thus be described together. Both are helicity suppressed and hence very rare, with the SM3 fit by the CKMfitter group [131][8] predicting branching ratios of $\mathcal{B}(B_d \to \mu^+\mu^-) = (1.087^{+0.063}_{-0.097}) \cdot 10^{-10}$ and $\mathcal{B}(B_s \to \mu^+\mu^-) = (3.65^{+0.18}_{-0.30}) \cdot 10^{-9}$. Since the theoretical prediction of these decays suffers only from relatively small uncertainties (e.g. [72], [67]), any sizeable deviation would indicate effects of New Physics. This motivated many attempts at measuring them, but for roughly 30 years these efforts only succeeded in pushing down the upper limits on the branching fractions. In 2012, the LHCb experiment finally reported first evidence of the decay $B_s \to \mu^+\mu^-$[178]. The values used in this thesis [179],

$$\mathcal{B}(B_d \to \mu^+\mu^-) = (3.6^{+1.6}_{-1.4}) \cdot 10^{-10} \text{ and} \tag{4.72}$$

$$\mathcal{B}(B_s \to \mu^+\mu^-) = (2.9 \pm 0.7) \cdot 10^{-9}, \tag{4.73}$$

average results from LHCb [180] and CMS [181]. For details on the combination procedure see the former, for the work of the two experiments the latter publication.
Both decays receive contributions both from box graphs and electroweak penguin diagrams as shown in Fig. 4.10. Penguin graphs with a photon instead of the Z^0 boson vanish due to vector current conservation. In the SM3, $\mathcal{B}(B_d \to \mu^+\mu^-)$ is given by [67]

$$\mathcal{B}(B_d \to \mu^+\mu^-) = \tau_{B_d} \frac{G_F^2}{\pi} \left(\frac{\alpha_{EM}}{4\pi \sin^2\theta_W} \right)^2 f_{B_d}^2 m_\mu^2 m_{B_d} \sqrt{1 - 4\frac{m_\mu^2}{m_{B_d}^2}} \cdot Y(x_t)^2 \cdot |V_{td}V_{tb}^*|^2 \tag{4.74}$$

where τ_{B_d} and f_{B_d} are the mean life and the decay constant of the B_d meson, respectively. $Y(x_t)$ is an Inami-Lim function governing the m_t dependence of the decay. The Inami-Lim function

[8] This is more precise than the predictions in [32] which were not obtained by means of a global fit: $\mathcal{B}(B_d \to \mu^+\mu^-) = (1.0 \pm 0.1) \cdot 10^{-10}$ and $\mathcal{B}(B_s \to \mu^+\mu^-) = (3.2 \pm 0.2) \cdot 10^{-9}$. Note the deviation between the values of $\mathcal{B}(B_s \to \mu^+\mu^-)$.

used in this thesis includes QCD corrections of $\mathcal{O}(\alpha_S)$:

$$Y(x,\mu_t^{(\ell\ell)}) = Y_0(x) + \frac{\alpha_S}{4\pi} Y_1(x,\mu_t^{(\ell\ell)}) \tag{4.75}$$

The dependence on the scale $\mu_t^{(\ell\ell)} = \mathcal{O}(m_t)$ enters in Y so that, at the order considered, the scale dependence of the leading term Y_0 is cancelled [182]. The allowed range for this parameter is set to $[80, 320]$ GeV. This choice by the CKMfitter group in their input data is roughly the range examined in [182]. Contributions from graphs with c and u quarks in the loop were neglected as $Y(x_t)$ makes the top quark loop dominant. The expression for $\mathcal{B}(B_s \to \mu^+\mu^-)$ is exactly analogous to eq. (4.74). It follows from the latter expression by replacing τ_{B_d}, f_{B_d} and m_{B_d} by τ_{B_s}, f_{B_s} and m_{B_s}, respectively, and V_{td} by V_{ts}.
In the SM4, there are contributions from graphs with t' in the loops of Fig. 4.10 and the neutrino in the penguin graph can be a ν_4. Assuming no or negligible mixing between the 4th generation neutrino and the SM3 neutrinos, i.e. unitarity of the SM3 submatrix $U_{3\times3}$, eq. (4.74) adapted to the SM4 reads

$$\begin{aligned}\mathcal{B}(B_d \to \mu^+\mu^-) =& \tau_{B_d} \frac{G_F^2}{\pi} \left(\frac{\alpha}{4\pi \sin^2\theta_W}\right)^2 f_{B_d}^2 m_\mu^2 m_{B_d} \sqrt{1 - 4\frac{m_\mu^2}{m_{B_d}^2}} \cdot \\ & \cdot \left| V_{td} V_{tb}^* \cdot Y(x_t, \mu_t^{(\ell\ell)}) + V_{t'd} V_{t'b}^* \cdot Y(x_{t'}, \mu_t^{(\ell\ell)}) \right|^2 .\end{aligned} \tag{4.76}$$

Once more, the expression for the B_s decay is exactly analogous. The procedure is practically identical to obtaining the SM3 expression for $\mathcal{B}(B_s \to \mu^+\mu^-)$ from eq. (4.74) except now one also has to replace $V_{t'd}$ by $V_{t's}$.

4.3. CP violating Loop observables

This section describes loop observables in which CP violation can be observed and which can be used to constrain CP violating phases. The only CP violating input observable not described in this section is the UT angle γ. Unlike all other CP violating observables, it can be extracted from tree level processes which were already described in section 4.1.

4.3.1. $|\epsilon_K|$

CP violation was first observed in the neutral kaon system in the decay $K_L \to \pi\pi$ (cf. sections 2.4 and 2.5). $|\epsilon_K|$ is the observable from this system which is used in the fits described here. Both

$$\eta_{+-} = \frac{\langle \pi^+\pi^- | \mathcal{H} | K_L \rangle}{\langle \pi^+\pi^- | \mathcal{H} | K_S \rangle} \qquad \text{and} \qquad \eta_{00} = \frac{\langle \pi^0\pi^0 | \mathcal{H} | K_L \rangle}{\langle \pi^0\pi^0 | \mathcal{H} | K_S \rangle} \tag{4.77}$$

would be 0 if CP symmetry was not violated by the weak interaction. They can be combined to

$$\epsilon_K = \frac{2\eta_{+-} + \eta_{00}}{3}. \tag{4.78}$$

In [68] and [93], the expression for ϵ_K in terms of the formalism given in section 2.5 is derived.

Due to WATSON's theorem [183], the amplitudes in equation (4.77) can be expressed in terms of amplitudes of neutral kaon decays to final states classified by their isospin I:

$$\left\langle (\pi\pi)_I \left| \mathcal{H} \right| K^0 \right\rangle = A_I \cdot e^{\mathrm{i}\delta_I} \tag{4.79}$$

The phase δ_I is determined only by strong final state interactions. The amplitude of the anti-particle process of eq. (4.79) is $\overline{A}_I$ and it carries the same strong phase δ_I because the strong interaction which generates it does obey CP symmetry. A CP-violating phase is implicit in A_I ($\neq \overline{A}_I$).

With the spin of K mesons being zero, the orbital angular momentum and hence the total angular momentum of the final state pions is defined. Because pions obey Bose statistics, symmetry requires the S wave two-pion final state to have an isospin of $I = 0$ or 2. Assuming - as everywhere in the present work unless stated otherwise - CPT symmetry leads to

$$\left\langle (\pi\pi)_I \left| \mathcal{H} \right| K^0_{S\atop L} \right\rangle = e^{\mathrm{i}\delta_I} \left(pA_I \pm q\overline{A}_I \right). \tag{4.80}$$

An isospin decomposition of the two-pion final states yields then

$$\langle \pi^+\pi^- | \mathcal{H} | K_L \rangle = \sqrt{\frac{2}{3}} e^{\mathrm{i}\delta_0} pA_0 \left(\Delta_0 + \frac{1}{\sqrt{2}} e^{\mathrm{i}(\delta_2-\delta_0)} \omega \Delta_2 \right) \tag{4.81}$$

$$\left\langle \pi^0\pi^0 \left| \mathcal{H} \right| K_L \right\rangle = \sqrt{\frac{2}{3}} e^{\mathrm{i}\delta_0} pA_0 \left(\Delta_0 - \sqrt{2} e^{\mathrm{i}(\delta_2-\delta_0)} \omega \Delta_2 \right) \tag{4.82}$$

with $\Delta_I = 1 - \frac{q}{p}\frac{\overline{A}_I}{A_I}$ and $\omega = \frac{A_2}{A_0}$.

An analogous decomposition can be performed on $\langle \pi^+\pi^- | \mathcal{H} | K_S \rangle$ and $\left\langle \pi^0\pi^0 \left| \mathcal{H} \right| K_S \right\rangle$. It is then possible to write down the expressions in eq. (4.77) and also eq. (4.78) in terms of strong phases δ_I, Δ_I, p and q. The resulting unwieldy expression can be further simplified thanks to specific properties of the Kaon system: Firstly, $\Delta\Gamma_K \approx 2\Delta m_K$ while $|p/q|^2 \approx 1$, reflecting the smallness of CP violation. Together, these observations imply that the relative phase ζ between Γ_{12} and M_{12} (cf. eq. (2.85)) must be close to zero. Secondly, there is the empirically found relation $\omega \approx 1/22$ [93] (known as $\Delta I = \frac{1}{2}$ rule and still an area of research [184]). Using, thirdly, the ratio of the decay widths of K_L and K_S $\Gamma_L/\Gamma_S \ll 1$, one can expand the expression for ϵ_K. Defining $\xi_0 = \arg A_0$, one obtains

$$\epsilon_K \simeq \left[\frac{1}{\sqrt{1 + \left(\frac{\Delta\Gamma}{2\Delta m_K}\right)^2}} \left(-\frac{\mathrm{Im}\,(M_{12})}{\Delta m_K} + \xi_0 \right) \right] e^{\mathrm{i}\,\Phi_{\epsilon_K}}. \tag{4.83}$$

Obviously, the term in square brackets is the absolute value $|\epsilon_K|$. The phase is given by

$$\Phi_{\epsilon_K} = \arctan \frac{2\Delta m_K}{\Delta\Gamma_K}. \tag{4.84}$$

It can be shown [68] that ξ_0 is too small to generate the observed magnitude of ϵ_K alone, so a sizeable contribution must come from $-\frac{\mathrm{Im}(M_{12})}{\Delta m_K}$. With $m_{t'}, m_t, m_c > m_K$, the effective operator responsible for the oscillation of the K mesons is local and can be used to evaluate $\mathrm{Im}\,(M_{12})$ as in equation (2.100). In the SM4, the expression used in the CKMfitter code is [36]

$$\begin{aligned}|\epsilon_K| = &\frac{G_F^2 m_W^2}{6\sqrt{2}\pi^2 \Delta m_K} f_K^2 m_K \hat{B}_K \kappa_{\epsilon_K} \cdot \\ &\cdot \Big|\mathrm{Im}\Big(\eta_{cc}^{(K)} S_0(x_c)\cdot (V_{cs}V_{cd}^*)^2 + \eta_{tt}^{(K)} S_0(x_t)\cdot (V_{ts}V_{td}^*)^2 + \eta_{t't'}^{(K)} S_0(x_{t'})\cdot (V_{t's}V_{t'd}^*)^2 + \\ &+ \eta_{ct}^{(K)} S_0(x_c, x_t)\cdot V_{cs}V_{cd}^* V_{ts}V_{td}^* + \eta_{ct'}^{(K)} S_0(x_c, x_{t'})\cdot V_{cs}V_{cd}^* V_{t's}V_{t'd}^* + \\ &+ \eta_{tt'}^{(K)} S_0(x_t, x_{t'})\cdot V_{ts}V_{td}^* V_{t's}V_{t'd}^*\Big)\Big| \end{aligned} \tag{4.85}$$

As usual, f_K is a meson decay constant and $\hat{B}_K$ is the kaon bag parameter. $\eta_{qq'}^{(\mathrm{K})}$ are QCD corrections. Among these, the scale dependence of $\eta_{cc}^{(\mathrm{K})}$ is explicitely parametrized in the CKMfitter software. The parametrization is based on [185][9] and reads

$$\eta_{cc}^{(\mathrm{K})} \simeq (1.44 \pm \delta_{cc}^{(\mathrm{K})}) \left(1 - 1.2\left(\frac{\bar{m}_c(m_c)}{1.25} - 1\right)\right) \cdot (1 + 52 \cdot (\alpha_s(m_Z) - 0.118))\,, \tag{4.86}$$

with the uncertainty

$$\delta_{cc}^{(\mathrm{K})} = 0.22 \left(1 - 1.8\left(\frac{\bar{m}_c(m_c)}{1.25} - 1\right)\right) \cdot (1 + 80 \cdot (\alpha_s(m_Z) - 0.118))\,. \tag{4.87}$$

The SM3 expression is simpler than eq. (4.85) as all terms involving t' can be omitted. Most quantities are familiar from section 2.5 except for κ_{ϵ_K}. This is a parameter used to express various deviations from simplifying assumptions. It is equal to 1 if [146]

- the phase $\phi_{\epsilon_K} = \pi/4 (= 45°)$,
- the final state phase $\xi_0 = 0$,
- $\mathrm{Im}\left(M_{12}^{(K)}\right)$ is calculated using only the lowest-dimension d=6 operator in the effective Hamiltonian.

The value used in the fits in this work,

$$\kappa_{\epsilon_K} = 0.940 \pm 0.013 \pm 0.023, \tag{4.88}$$

was also taken from [146] where it is assumed that ϵ'_K is not affected by New Physics. Using the same value in the SM4 context must be justified in view of the assumptions it is based on.

[9] The term in the original publication was adapted to the purpose on hand and numerical values were calculated following some private communication between the CKMfitter group and Ulrich Nierste.

The phase ϕ_{ϵ_K} is experimentally known to be [50]

$$\phi_{\epsilon_K} = (43.14 \pm 0.05)^\circ. \tag{4.89}$$

The approximation $\phi_{\epsilon_K} = \pi/4$ is therefore as good in the SM4 as it is in SM3. The condition that only the lowest-dimension d=6 operator can be used is also satisfied - no higher-dimension operators were used in the SM4 than in the SM3 case. The assumption concerning the final state phase ξ_0 must be examined more closely as it may change depending on the relative size and phase of new graphs which contribute to the decay $K_S \to \pi\pi$ in the SM4 as shown in Fig. 4.11. The penguin graphs in subfigures b) and c) receive a new contribution from $\hat{u} = t'$. An additional observable,

$$\epsilon'_K = \frac{1}{3}(\eta_{+-} - \eta_{00}), \tag{4.90}$$

helps to place a limit on this contribution. It measures channel dependent, direct CP violation [68] in the neutral kaon system and measures the difference of the contribution of gluonic and electroweak penguins which interfere destructively [32]. For heavy $\hat{u} = t, t'$ and neglecting QCD corrections, the Z penguin scales $\propto x_{\hat{q}} = \left(\frac{m_{\hat{q}}}{m_W}\right)^2$. The gluonic penguin does not show this behaviour[10]. With a sizeable contribution from a new quark heavier than a top quark one would thus expect the experimental value of $\frac{\epsilon'}{\epsilon}$ to be larger than the value predicted by the SM3. The authors of [186] find values between $1.23{\cdot}10^{-3}$ and $1.67{\cdot}10^{-3}$, depending on their choice of parameters. These values agree with the experimental value quoted by the PDG: [92]

$$\frac{\epsilon'_K}{\epsilon_K} \approx \mathrm{Re}\left(\frac{\epsilon'_K}{\epsilon_K}\right) = (1.65 \pm 0.26) \cdot 10^{-3} \tag{4.91}$$

This, in turn allows one to assume only negligible effects of the fourth generation on the phase of ϵ_K. Using the SM3 value for κ_{ϵ_K} in this work is therefore justified.

The $|\epsilon_K|$ input used in this work,

$$|\epsilon_K| = (2.228 \pm 0.011) \cdot 10^{-3}, \tag{4.92}$$

was obtained by the PDG [46, 187] (see the review "CP violation in K_L decays") in a fit to a large number of different measurements of $K_{S,L}$ lifetimes and branching fractions.

4.3.2. $\sin(2\beta)$ and $\sin(2\beta - 2\theta_{\mathrm{d}})$

SM3 situation

The extraction of the angle

$$\beta = \arg\left(-\frac{V_{cd}V_{cb}^*}{V_{td}V_{tb}^*}\right) \tag{4.93}$$

of the SM3 Unitarity Triangle from experiment has to be reconsidered in an SM4 context. The SM extraction will shortly be recalled here, if only to avoid confusion of notation. $\sin(2\beta)$ is

[10] Ulrich Nierste, private communication

extracted from a measurement of the time-dependent asymmetry

$$a_f(t) = \frac{\Gamma(B^0(t) \to J/\psi K_S) - \Gamma(\overline{B}_0(t) \to J/\psi K_S)}{\Gamma(B^0(t) \to J/\psi K_S) + \Gamma(\overline{B}_0(t) \to J/\psi K_S)}. \tag{4.94}$$

The common final state $J/\psi K_S$ is a CP eigenstate. The underlying processes at quark level are $b \to c\bar{c}s$ and its charge conjugated process. Two decay processes of a B^0 contribute to the reaction rates:

$$B^0 \xrightarrow[\text{decay}]{b\to c\bar{c}s} J/\psi K^0 \xleftarrow[\text{oscillation}]{K^0} J/\psi \overline{K}^0 \xleftarrow[\text{decay}]{\bar{b}\to \bar{c}c\bar{s}} \overline{B}_0 \xleftarrow[\text{oscillation}]{B^0} \overline{B}^0 \tag{4.95}$$

Their charge-conjugated processes contribute to the decay of $\overline{B}^0$. The interference of these processes is the cause of the asymmetry observed. From eqs. (2.88) and (2.89), one can derive an expresssion for the reaction rates Γ (see [68] for the explicit calculation) in which the main exponential time dependence of the decay rate is factored out:

$$\Gamma(B^0(t) \to f) \propto \frac{1}{2} e^{-\Gamma_1 t} \cdot G_f(t) \tag{4.96}$$

$$\Gamma(\overline{B}^0(t) \to f) \propto \frac{1}{2} e^{-\Gamma_1 t} \cdot \overline{G}_f(t) \tag{4.97}$$

where

$$\overset{(-)}{G}_f(t) = \overset{(-)}{a} + \overset{(-)}{b}\, e^{\Delta\Gamma_B t} + \overset{(-)}{c}\, e^{\Delta\Gamma_B t/2} \cos(\Delta m_d t) + \overset{(-)}{d}\, e^{\Delta\Gamma_B t/2} \sin(\Delta m_d t). \tag{4.98}$$

This is considerably simplified by two features of the decay $B^0 \to J/\psi K_S$. Firstly, the underlying process $b \to c\bar{c}s$ is isoscalar and hence the final state is described by a single isospin amplitude. Thus it is unlikely for direct CP violation to occur in this decay even in the presence of New Physics [68]. The amplitudes of the decay should therefore satisfy

$$|A(J/\psi K_S)| = \left|\overline{A}(J/\psi K_S)\right|. \tag{4.99}$$

Secondly, one can use the experimental facts that, in the B_d^0 system,

$$\Delta\Gamma_{B_d} \ll \Delta m_d \approx \Gamma_{B_d} \tag{4.100}$$

which finally leads to

$$G_{J/\psi K_S}(t) = |A(J/\psi K_S)|^2 \cdot \left(1 - \mathrm{Im}\left(\frac{q}{p}\frac{\overline{A}(J/\psi K_S)}{A(J/\psi K_S)}\right)\sin(\Delta m_d t)\right) \tag{4.101}$$

$$\overline{G}_{J/\psi K_S}(t) = |A(J/\psi K_S)|^2 \cdot \left(1 + \mathrm{Im}\left(\frac{q}{p}\frac{\overline{A}(J/\psi K_S)}{A(J/\psi K_S)}\right)\sin(\Delta m_d t)\right). \tag{4.102}$$

It might be noted in passing that CP violation can only be observed if $\Delta m_d \neq 0$ and that it is

also time dependent. Another consequence of eq. (4.100) is that

$$\frac{q}{p} = \sqrt{\frac{M_{12}^*}{M_{12}}} + \mathcal{O}\left(\frac{\Gamma_{12}}{M_{12}}\right) \approx \frac{V_{td}V_{tb}^*}{V_{td}^*V_{tb}} \tag{4.103}$$

where the approximation follows from the SM3 version of eq. (4.59).

The phase of $\frac{\overline{A}(J/\psi K_S)}{A(J/\psi K_S)}$ is the result of the interference of several processes contributing to the decay of B^0 and $\overline{B}^0$ each. Their lowest-order Feynman graphs are drawn in Fig. 4.12. They serve to illustrate that the phases of the contributing processes are not identical. The tree level graph in Fig. 4.12 a) has the CKM phase resulting from the contributing matrix elements $V_{cs}V_{cb}^*$ while, at the next order, the penguin's CKM phase depends on the flavour of the up-type quark in the loop, denoted in Fig. 4.12 c) as $\hat{u}$. Within SM3, the possible phases are $V_{us}V_{ub}^*$, $V_{cs}V_{cb}^*$ and $V_{ts}V_{tb}^*$. One can now perform an Operator Product Expansion (cf. sec. 2.3), ordering the individual contributing operators by their CKM phase [72]:

$$A(f) = V_{us}V_{ub}^*M^{(u)} + V_{cs}V_{cb}^*M^{(c)} + V_{ts}V_{tb}^*M^{(t)} \tag{4.104}$$

$$\overline{A}(f) = V_{ub}V_{us}^*M^{(u)} + V_{cb}V_{cs}^*M^{(c)} + V_{tb}V_{ts}^*M^{(t)} \tag{4.105}$$

$M^{(\hat{u})}$ are those parts of the remaining effective operators which remain after stripping off the CKM matrix elements. $M^{(c)}$ contains the contribution of the tree diagram. Using 3×3 unitarity ($V_{ts}V_{tb}^*$=-$V_{us}V_{ub}^*$-$V_{cs}V_{cb}^*$), $M^{(t)}$ can be absorbed into the other two terms:

$$A(f) = V_{us}V_{ub}^*(M^{(u)} - M^{(t)}) + V_{cs}V_{cb}^*(M^{(c)} - M^{(t)}), \tag{4.106}$$

and $\overline{A}(f)$ is treated accordingly. Utilizing the "language" of the SM3 Wolfenstein parametrization (cf. Appendix A.2) for a moment, one can quickly analyze the relative magnitudes of the terms contributing to (4.106). With $(M^{(c)} - M^{(t)})$ dominating over $(M^{(u)} - M^{(t)})$ due to $M^{(c)}$'s tree level contribution and $\frac{V_{us}V_{ub}^*}{V_{cs}V_{cb}^*} \approx \mathcal{O}(\lambda^2)$, there is a clear hierarchy between the contributions. The phase difference between the decay amplitudes of $b \to c\bar{c}s$ and its conjugated process is therefore well approximated by the phase difference between the corresponding tree level graphs, i.e.

$$\frac{\bar{A}}{A} \approx \frac{V_{cb}V_{cs}^*}{V_{cs}V_{cb}^*}. \tag{4.107}$$

As those B ($\bar{B}$) mesons which oscillated into their antimeson state before decaying did decay into $\bar{K}$ (K) mesons, the kaons have to oscillate into the "right" kaon state before they can actually interfere in the final state. K^0 oscillation is dominated by the box graph with c quarks in the loop (cf. Fig. 2.5, $\hat{u} = c$) and its mixing is controlled by a pure phase ($\left|\frac{q}{p}\right| - 1 = \mathcal{O}(10^{-3})$, [93]). Neglecting CP violation in K^0 oscillation, this third phase contribution is

$$\phi_{K^0}^{\text{osc}} = \frac{V_{cs}V_{cd}^*}{V_{cd}V_{cs}^*}. \tag{4.108}$$

A fourth contribution arises because J/ψ is a CP odd state ($\eta_{CP} = -1$): In an SM3 context, the asymmetry $a_f(t)$ is therefore governed by the expression

$$\frac{q}{p}\frac{\overline{A}}{A} \propto \eta_{CP}\frac{V_{td}V_{tb}^*}{V_{td}^*V_{tb}} \cdot \frac{V_{cb}V_{cs}^*}{V_{cs}V_{cb}^*} \cdot \frac{V_{cs}V_{cd}^*}{V_{cd}V_{cs}^*} = \eta_{CP}\frac{V_{td}V_{tb}^*}{V_{td}^*V_{tb}} \cdot \frac{V_{cb}V_{cd}^*}{V_{cd}V_{cb}^*}. \tag{4.109}$$

This can be written as the defining equation for β,

$$-e^{-2i\beta} = \left(\frac{q}{p}\frac{\overline{A}}{A}\right)_{B^0 \to J/\psi K_S}. \tag{4.110}$$

SM4

The presence of fourth generation quarks has two ways to influence the experiment. Firstly, the CKM matrix elements may change in size and phase and secondly, additional Feynman graphs contribute because the quark denoted as $\hat{u}$ in Fig. 4.12 c) can now also be a t'. From another perspective, the two ways are the effect on the mixing phase (4.103) and the effect on the phase from the decay, i.e. the phase of $\frac{\overline{A}(J/\psi K_S)}{A(J/\psi K_S)}$, respectively. The value extracted in the decay $B \to J/\psi K_S$ in the presence of New Physics can be expressed as

$$\sin(2\beta - \phi_{\text{osc,SM4}} - \phi_{\text{decay,SM4}}). \tag{4.111}$$

Here β is the angle in the Unitarity Triangle and the ϕ_{SM4} are the contribution of New Physics (here, of course: 4th generation fermions) in mixing and in the decay of the B meson, respectively, to the measured asymmetry. As for the decay, penguin graphs with t' in the loop might cause an additional phase contribution. Using the unitarity in a similar manner as in the SM3 case, one can eliminate [32] the contributions of the u-quark penguin:

$$A(f) = V_{cs}V_{cb}^*(M^{(c)} - M^{(u)}) + V_{ts}V_{tb}^*(M^{(t)} - M^{(u)}) + V_{t's}V_{t'b}^*(M^{(t')} - M^{(u)}) \tag{4.112}$$

It is not a-priori clear that contributions from the t- and t' penguins are sufficiently CKM-suppressed, either compared to the Tree Level contribution or compared to each other. [32] states that these contributions might change the result of the above (SM3) extraction by ≈10% if $\frac{V_{t's}V_{t'b}^*}{V_{ts}V_{tb}^*} \sim \mathcal{O}(1)$. However, since fits including only Tree Level observables (see section 5.1) suggest that this ratio is only $\mathcal{O}(0.2)$, the 10% can be considered a worst-case scenario. This means that the contribution of the additional graphs to the extracted $\sin 2\beta$ is smaller. Therefore, any effect of 4th generation fermions on the experiment will manifest itself in mixing.

With the approximation in eq. (4.103), the phase caused by New Physics in mixing is

$$\eta_{CP}e^{-2\,\mathrm{i}(\beta+\theta_d)} = \exp(-\,\mathrm{i}\,\phi_{\text{osc,SM4}}) \cdot \exp(\mathrm{i}\,\phi_{\text{decay}}) \cdot \exp(\mathrm{i}\,\phi_{K^0}) \tag{4.113}$$

where the three factors in (4.109) were expressed as exponential terms while keeping them in the same order. The CKM matrix elements which occur in ϕ_{decay} and ϕ_{K^0} are V_{cb} and V_{cd}. V_{cb} has the same phase in the SM4 as in the SM3; they are both exactly real in the Hou/Soni parametrization

and in the SM3 standard parametrization given in eq. (A.1). The imaginary part of V_{cd} is very small both in the SM3 and the SM4 - see e.g. Wolfenstein parameter values quoted in [131] and Table 5.3, respectively. One can therefore approximate that a fourth generation has no effects on ϕ_{decay} and ϕ_{K^0}. Then,

$$\eta_{CP} e^{-2i\beta} = \exp(-\mathrm{i}\,\phi_{\text{osc,SM3}}) \cdot \exp(\mathrm{i}\,\phi_{\text{decay}}) \cdot \exp(\mathrm{i}\,\phi_{K^0}). \tag{4.114}$$

This can be inserted into the previous equation to yield the NP (in mixing) phase in the SM4 framework,

$$2\theta_d = -\arg\left(\frac{\phi_{\text{osc,SM4}}}{\phi_{\text{osc,SM3}}}\right). \tag{4.115}$$

Inserting the expressions for $M_{12}^{B_d}$ in SM3 and SM4, eq. (4.59), one obtains (see e.g. [36])

$$2\theta_d = -\arg\left(\frac{\eta_{tt}(\mu) S_0(x_t)\, {\lambda_t^{B_d}}^2 + 2\eta_{tt'}(\mu) S_0(x_t, x_{t'}) \lambda_t^{B_d} \lambda_{t'}^{B_d} + \eta_{t't'}(\mu) S_0(x'_t)\, {\lambda_{t'}^{B_d}}^2}{\eta_{tt}(\mu) S_0(x_t)\, {\lambda_t^{B_d}}^2}\right). \tag{4.116}$$

In summary, any $\sin(2\beta)$ input from an SM3 context will in the SM4 be interpreted as $\sin(2\beta - 2\theta_d)$ with θ_d given by equation (4.116) and assumed to be caused by 4th generation effects in $B^0 - \overline{B}^0$ mixing only.

The fits in chapter 5 will use as experimental input an average provided by HFAG online [188]:

$$\sin(2\beta - 2\theta_d) = \sin(2\beta)_{\text{SM3}} = 0.682 \pm 0.019 \tag{4.117}$$

where the stated error contains a statistical contribution of 0.017. Measurements included are from ALEPH, OPAL, CDF, LHCb and Belle.

4.3.3. Semileptonic Charge Asymmetry a_{SL}^s

The semileptonic charge asymmetry in the B_s^0 system a_{SL}^s is extracted from a measurement of the time integrated charge asymmetry in the flavour specific, semileptonic decay $B_s^0 \to D_s^- \mu^+ X$ and its charge-conjugated process. No initial-state tagging is used. The determinations entering the average used in the fits of the next chapter [189, 190] measure the asymmetry

$$A_{\text{meas}} = \frac{N(\mu^+ D_s^-) - N(\mu^- D_s^+)}{N(\mu^+ D_s^-) + N(\mu^- D_s^+)}, \tag{4.118}$$

where the N are the recorded count of $\mu^\pm D_s^\mp$ pairs. The D mesons are reconstructed in their $D_s^- \to \phi\pi^- \to K^+K^-\pi^-$ decays and the charge-conjugated process. After correcting for efficiencies like those of trigger, tracking and muon identification, the corrected asymmetry A_{corr} can be expressed [191] in terms of the asymmetry

$$a_{SL}^s = \frac{\Gamma_{\text{int}}(\bar{B}_s^0 \to B_s^0 \to D_s^- \mu^+ X) - \Gamma_{\text{int}}(B_s^0 \to \bar{B}_s^0 \to D_s^+ \mu^- X)}{\Gamma_{\text{int}}(\bar{B}_s^0 \to B_s^0 \to D_s^- \mu^+ X) + \Gamma_{\text{int}}(B_s^0 \to \bar{B}_s^0 \to D_s^+ \mu^- X)} = A_{\text{corr}}/\chi_s. \tag{4.119}$$

χ_s is the time-integrated probability that a meson which was a B_s^0 ($\bar{B}_s^0$) at production time has oscillated into its antiparticle state by the time it decays. In case of B_s^0 mesons, it is very close to 0.5 (cf. e.g. [50]) as its oscillation frequency is much higher than its inverse mean life.

In order to express a_{SL}^s in terms of the formalism presented in section 2.5, one can use eqs. (2.88), (2.89) and (2.82) to obtain

$$a_{SL}^s = \frac{1-|\frac{q}{p}|^4}{1+|\frac{q}{p}|^4} = \frac{\mathrm{Im}\left(M_{12}^* \Gamma_{12}\right)}{2\left|M_{12}\right|^2 + 1/2\left|\Gamma_{12}\right|^2}. \tag{4.120}$$

Since in both B-meson systems $|\Gamma_{12}| \ll |M_{12}|$, one can use this for an approximation. The result is the expression commonly used for semileptonic charge asymmetries (also see [93], chapter 1, for a different derivation):

$$a_{SL}^s = \frac{2\mathrm{Im}\left(\frac{\Gamma_{12}M_{12}^*}{M_{12}M_{12}^*} \cdot |M_{12}|^2\right)}{2\left|M_{12}\right|^2\left(1+\frac{|\Gamma_{12}|^2}{4|M_{12}|^2}\right)} \simeq \mathrm{Im}\left(\frac{\Gamma_{12}}{M_{12}}\right) \tag{4.121}$$

The individual ingredients for eq. (4.121) can be read off eqs. (4.59) and (2.101), each time remembering to insert the correct quantities for B_s^0. As stated already in sec. 2.6.1, a full listing of the Γ_{12}^{ab} is long, unwieldy and beyond the scope of this work. For an in-depth discussion, see [95] and references cited there. The Γ_{12}^{ab} depend on a number of parameters:

$$\begin{aligned}\Gamma_{12}^{ab} = \Gamma_{12}^{ab}(&G_F, \overline{m}_b, m_B, f_{B_d}, \hat{B}_d, \widetilde{B}_S^d, \bar{z}, \alpha_S(mW), \alpha_S(\mu_1), x_{\mu_1}, x_{\mu_2}, \mu_1, \mu_2, \\ &\Lambda_{QCD}, \overline{m}_q, \overline{m}_q, m_b^{\mathrm{pow}}, B_{\widetilde{R}_0}, B_{\widetilde{R}_1}, B_{\widetilde{R}_1}, B_{\widetilde{R}_2}, B_{\widetilde{R}_2}, B_{\widetilde{R}_3}, B_{\widetilde{R}_3})\end{aligned} \tag{4.122}$$

Those quantities not introduced up to now - e.g. in sec. 2.6.1 - , while used as inputs for the fits in this thesis, are specific to the operator basis proposed in [95]. They will only be listed here for quick reference. Again, see the original publication and its references for details.

- $\bar{z} = \frac{\overline{m}_c(\overline{m}_b)^2}{\overline{m}_b(\overline{m}_b)^2}$ - Parametrizes the quark mass dependence of the $G_{(S)}^{ab}$ from eq. (2.103) in another renormalization scheme which reduces uncertainties [95].
- μ_1 - Renormalization scale.
- μ_2 - Scale at which the operators of the new basis in [95] are defined. Here, $\mu_2 = \overline{m}_b$.
- m_q - Mass of the non-b quark in the decaying meson - here $\overline{m}_{d,s}$. Enters calculation of $\widetilde{\Gamma}_{12,1/m_b}^{ab}$.
- $\overline{m}_b$ - Value of the b quark mass that enters the calculation of the bag factor

$$\widetilde{B}_S'(\mu_2) = \frac{m_{B_q}^2}{\left(\overline{m}_b(\mu_2) + \overline{m}_q(\mu_2)\right)^2} \cdot \widetilde{B}_S(\mu_2). \tag{4.123}$$

- $\overline{m}_q$ - Mass of non-b quark entering eq. (4.123).

- B_{R_i}, $B_{\widetilde{R}_i}$ - Bag parameters of operators R_i, $\widetilde{R}_i$ at order $1/m_b$ which parametrize the deviation of the matrix elements $\langle B_s | R_i | \overline{B}_S \rangle$ and $\langle B_s | \widetilde{R}_i | \overline{B}_S \rangle$ from their vacuum insertion value.
- m_b^{pow} - Serves to calibrate the overall size of the matrix elements of the operators R_i, $\widetilde{R}_i$ so that the numerical values of the bag parameters B_{R_i}, $B_{\widetilde{R}_i}$ are close to 1.

Parameter values used in the fits presented in this thesis are given in Table 5.2.

The a_{SL}^s input in this thesis is a weighted average of results from 10.4 fb^{-1} of $p\bar{p}$ at D0 [189] and 1 fb^{-1} of proton-proton-collisions at LHCb [190]:

$$a_{SL}^s = (-4.8 \pm 4.8) \cdot 10^{-3} \tag{4.124}$$

The details of the extraction methods differ - not surprisingly, due to different initial states. a_{SL}^s is in both cases extracted from the asymmetry defined in eq. (4.119).

4.3.4. Semileptonic Charge Asymmetry a_{SL}^d

a_{SL}^d is to the B_d system what a_{SL}^s is to the B_s system. The quantity extracted from measurements is defined analogously:

$$a_{SL}^d = \frac{\Gamma_{\text{int}}(\bar{B}_d^0 \to B_d^0 \to D^{(*)-}\mu^+ X) - \Gamma_{\text{int}}(B_d^0 \to \bar{B}_d^0 \to D^{(*)+}\mu^- X)}{\Gamma_{\text{int}}(\bar{B}_d^0 \to B_d^0 \to D_d^{(*)-}\mu^+ X) + \Gamma_{\text{int}}(B_d^0 \to \bar{B}_d^0 \to D^{(*)+}\mu^- X)} \tag{4.125}$$

The theoretical expression describing a_{SL}^d is the same as the ones given for a_{SL}^s in the previous section except that one has to insert the correct masses and CKM matrix elements for the B_d^0 system.

The experimental input value used in this work is

$$a_{SL}^d = (2.3 \pm 2.6) \cdot 10^{-3}, \tag{4.126}$$

an average published by the CKMfitter group in [159]. It includes values from the experiments D0 [192] and *BABAR* [193] as well as another average [129] by the HFAG group which in turn considers results from the B factory experiments CLEO, *BABAR* and Belle. The D0 result [192] is obtained from two separately analysed decay channels, $B_s \to D^- \mu^+ X$ (charge-conjugated processes always implicitely assumed) and $B_s \to D^{*-} \mu^+ X$. The D^- decays further into $K^+\pi^-\pi^+$, while the D^{*-} decays in $D^{*-} \to \overline{D}^0 \pi^- \to (K^+\pi^-)_{\overline{D}^0}\pi^-$. The value published is the average of the results obtained in the two channels.

The *BABAR* result was extracted from the decay $B_d \to D^{*-}\ell^+ X$ where ℓ may either be an electron or a muon.

The average given in [129] is formed from results similarly obtained by partial or full hadronic reconstruction or by measuring the like-sign dilepton asymmetry discussed in sec. 4.4.4 for the case of the measurement on a mixture of B_s^0 and B_d^0 mesons.

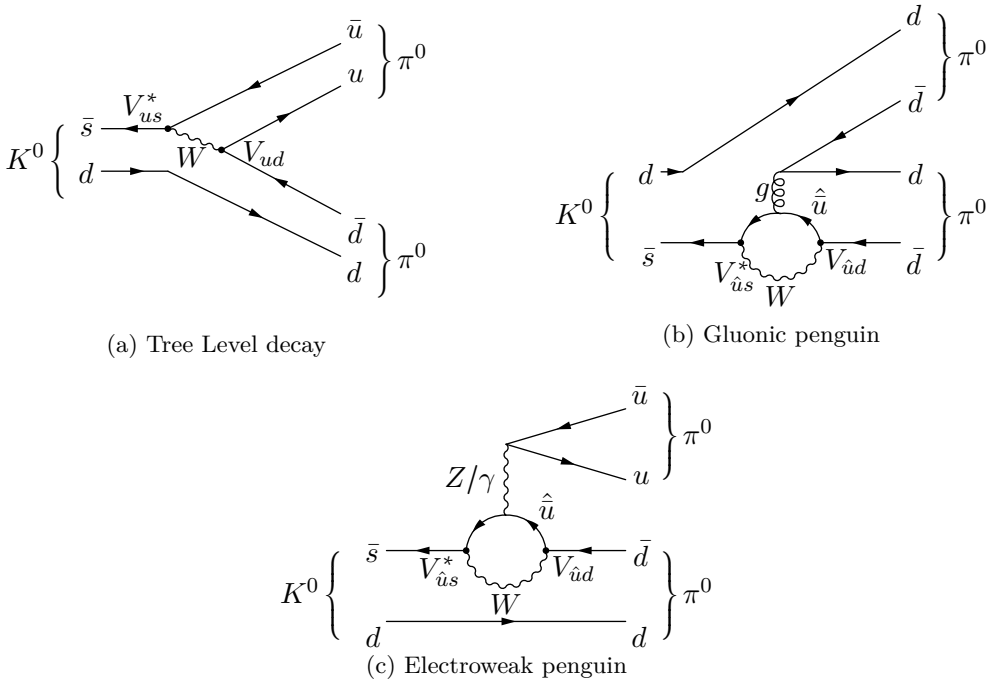

(a) Tree Level decay

(b) Gluonic penguin

(c) Electroweak penguin

Figure 4.11.: Feynman graphs contributing to the decay $K^0 \to \pi\pi$. $\hat{u}$ is any up-type quark.

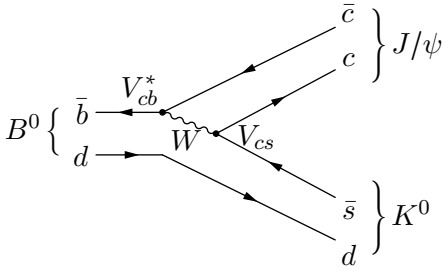

(a) Tree Level B^0 decay

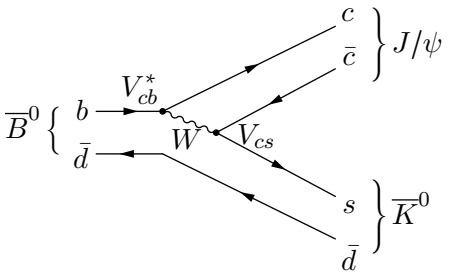

(b) Tree Level $\overline{B}^0$ decay

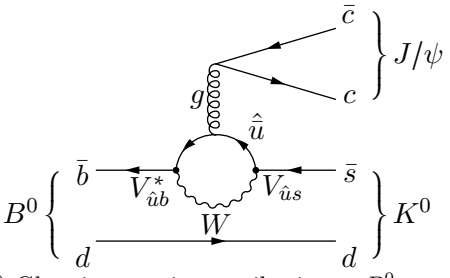

(c) Gluonic penguin contribution to B^0 meson decay. $\overline{B}^0$ analogous. $\hat{u}$ is any up-type quark.

Figure 4.12.: Relevant Feynman graphs which contribute to the B^0 and $\bar{B}^0$ decays in eq. (4.95). Their interference causes the asymmetry a_f (eq. (4.94)) from which $\sin(2\beta)$ is extracted. Note different CKM phases.

4.4. A Few Words on the Choice of Inputs

The present chapter closes with a few words on the selection of inputs. A reader familiar with the area of Flavour Physics Beyond the Standard Model will likely miss some inputs which seem to be popular to constrain New Physics. Their omission will now be motivated and/or justified.

4.4.1. Phase ϕ_s between mixing and decay in the B_s^0 system

The CP violating relative phase between mixing and the decay $b \to c\bar{c}s$ in the neutral B_s meson system is given by (e.g. [146])

$$\phi_s = \arg\left(\frac{-M_{12}^s}{\Gamma_{12}^s}\right). \tag{4.127}$$

It can be extracted by means of a full angular analysis of the decay products in $B_s^0 \to J/\psi\phi$ and a number of other channels [177]. Within the SM3, and neglecting a number of penguin contributions, this is equal to

$$\beta_s = \arg\left(-\frac{V_{ts}V_{tb}^*}{V_{cs}V_{cb}^*}\right). \tag{4.128}$$

This is the B_s^0 system's analogon to the B_d^0 Unitarity Triangle's angle β (cf. eq. (2.60)). With increasing experimental precision, neglecting the penguin contributions becomes questionable even within an SM3 context without New Physics [194, 195] - the SM3 penguins can change the angle extracted from $B_s^0 \to J/\psi$ to $2\beta_s - \delta_s^{PSM}$ where PSM means "Penguins, Standard Model". If they are not under good control theoretically, they might obscure any phase ϕ_s^Δ from New Physics in mixing (under whose inclusion the extraction would yield $2\beta_s - \phi_s^\Delta$, provided δ_s^{PSM} can be separated out). More penguins arise in the SM4 as there is one more flavour which can appear in the penguin's loop, adding another contribution to the extracted angle which now reads $2\beta_s \to 2\beta_s - \phi_s^\Delta - \delta_s^{PSM} - \delta^{PNP_s}$, where δ_s^{PNP} denotes penguin contributions from New Physics. Unless all these phases are under good theoretical control, it is not clear what the angle extracted from $B_s^0 \to J/\psi\phi$ actually is, and any constraint it provides may be misleading.

4.4.2. The UT angle α

Just like β_s, the extraction of the UT angle α (cf. section 2.4.6) is affected by penguin pollution. In this case, however, it is not the QCD penguins, but the electroweak penguins which may become sizeable in the SM4. The angle α can be extracted in several ways from decays involving $b \to u$. One possibility is to measure time-dependent asymmetries

$$\mathcal{A}_f(\Delta t) = \frac{\Gamma_{\bar{B}^0 \to f}(\Delta t) - \Gamma_{B^0 \to f}(\Delta t)}{\Gamma_{\bar{B}^0 \to f}(\Delta t) + \Gamma_{B^0 \to f}(\Delta t)} \tag{4.129}$$

which can be written as

$$\mathcal{A}_f(\Delta t) = \frac{2\mathrm{Im}\left(\lambda_f\right)}{1 + \left|\lambda_f\right|^2} \sin(\Delta m_d \cdot \Delta t) - \frac{1 - \left|\lambda_f\right|^2}{1 + \left|\lambda_f\right|^2 \cos(\Delta m_d \cdot \Delta t)}. \tag{4.130}$$

Assuming that the decay is described by only one tree-level graph, e.g. $S_{\pi^+\pi^-} = \sin(2\alpha)$, but there is a contribution from penguin graphs with a different phase. The ratio of their amplitude contribution P_{EW} to the tree level amplitudes T can be estimated by [196]

$$\frac{P_{EW}}{T} = \frac{3}{2}\frac{C_9^t(\mu) + C_{10}^t(\mu)}{C_1(\mu) + C_2(\mu)} \cdot \frac{|V_{td}|}{|V_{ub}|} \cdot e^{\mathrm{i}\,\alpha} \tag{4.131}$$

where the C_i are the relevant Wilson coefficients. The modulus of P_{EW}/T is - in SM3 - roughly 3 %. Given the current experimental precision, this justifies neglecting the contribution from electroweak Penguins. The contribution from QCD penguins is not negligible. They can, however, be eliminated by means of an isospin analysis [197, 198, 196].

Another way to extract the CP violating phase α is performing a time dependent Dalitz plot analysis (e.g. [199]). This method also employs isospin symmetries.

In the presence of a fourth generation, more electroweak penguin graphs contribute because the t' can occur as an internal quark, changing the ratio in eq. (4.131) to

$$\left(\frac{P_{EW}}{T}\right)_{SM4} = \frac{3}{2}\left(\frac{C_9^t(\mu, m_t) + C_{10}^t(\mu, m_t)}{C_1(\mu) + C_2(\mu)} \cdot \frac{V_{td}V_{tb}^*}{V_{ud}V_{ub}^*} + \frac{C_9^{t'}(\mu, m_{t'}) + C_{10}^{t'}(\mu, m_{t'})}{C_1(\mu) + C_2(\mu)} \cdot \frac{V_{t'd}V_{t'b}^*}{V_{ud}V_{ub}^*}\right). \tag{4.132}$$

Assuming that the $m_{t'}$ dependence of the relevant Wilson coefficents $C_{9,10}^{t'}$ is the same as the m_t dependence of $C_{9,10}^t$ and using the linear parametrisation given on p. 1164 of ref. [172] at $m_{t'} = 450$ GeV,

$$C_9^{t'}(\mu, m_{t'}) + C_{10}^{t'}(\mu, m_{t'}) \approx 2.7 \cdot (C_9^t(\mu, m_t) + C_{10}^t(\mu, m_t)). \tag{4.133}$$

At the same time, the magnitude of the CKM factor $V_{t'd}V_{t'b}^*$ can well be comparable to $V_{td}V_{tb}^*$. Therefore, the contribution from electroweak penguins cannot safely be neglected in the SM4. This makes an extraction of α in such a context more complicated and results in larger uncertainties. Therefore, the result of an SM3 extraction of α will not be used as an input in an SM4 context.

4.4.3. Mass Difference in the Neutral D Meson System

The mass difference in the neutral D meson system, usually given by the parameter [37, 25]

$$x_D = \frac{\Delta m_D}{\Gamma_D} \leq \frac{2\left|M_{12}^D\right|}{\Gamma_D}, \tag{4.134}$$

could in principle place a direct constraint on elements of the 4th column of the CKM matrix. In the SM4, x_D is described by an expression analogous to Δm_s and Δm_d, with down type quarks

in the loops of the corresponding box diagrams:

$$M_{12}^D = \frac{G_F^2 m_D \hat{B}_D f_B^2 m_W^2}{12\pi^2}\eta(m_c, m_W)\cdot$$
$$\cdot\Big(S_0(x_s)\ {\lambda_s^D}^2 + 2S_0(x_s, x_b)\lambda_s^D\lambda_b^D + S_0(x_b)\ {\lambda_b^D}^2 + LD + \tag{4.135}$$
$$+ 2S_0(x_s, x_{b'})\lambda_s^D\lambda_{b'}^D + 2S_0(x_b, x_{b'})\lambda_b^D\lambda_{b'}^D + LD \tag{4.136}$$
$$S_0(x_{b'})\ {\lambda_{b'}^D}^2\Big) \tag{4.137}$$

with $\lambda_{\hat{d}}^D = V_{c\hat{d}}V_{u\hat{d}}^*$. $\hat{d}$ is the flavour of the virtual down-type quark in the box graph, i.e. either s, b or b'. The first line is purely from SM3 contribution, the second stems from mixing between the SM3 particles and the 4th generation. The third line is the 4th generation's effect. The problem with the input x_D lies in large long distance corrections LD which are difficult to estimate or calculate (see [37] and references given there). Without any precise values available, the use of this input regrettably had to be refrained from.

4.4.4. Dimuon Charge Asymmetry A_{SL}

A_{SL} is measured e.g. at the Tevatron [177] in the charge asymmetry of like-sign dimuon events [200]

$$A = \frac{N^{++} - N^{--}}{N^{++} + N^{--}} \tag{4.138}$$

where N^{--} (N^{++}) denotes the number of events with two muons (anti-muons) detected. In $p\bar{p}$ collisions, most dimuon events are expected to come from the decay of $b\bar{b}$ pairs. After subtracting the background contributions - from several detector-related charge asymmetries, particles such as K, π or protons misidentified as muons and like-sign dimuons which both originate from a chain decay of a single b-quark - the CP violating asymmetry

$$A_{SL} = \frac{\Gamma(b\bar{b} \to X\mu^+\mu^+) - \Gamma(b\bar{b} \to X\mu^-\mu^-)}{\Gamma(b\bar{b} \to X\mu^+\mu^+) + \Gamma(b\bar{b} \to X\mu^-\mu^-)} \tag{4.139}$$

remains. The X in eq. (4.139) comprise all other final state particles. If both members of a $b\bar{b}$ pair decayed into muonic final states directly (or after hadronisation), one would end up with a pair of "right-sign" muons $\mu^+\mu^-$ in the final state:

$$b \to X_1\mu^- \qquad\qquad \bar{b} \to X_2\mu^+ \tag{4.140}$$

Their indices serve as reminder that they are, in general, not each other's anti-particles. In the following, the indices will not be printed explicitely again. As the time scale of the strong interaction responsible for hadronisation is much shorter than the time scale of the weak interaction responsible for b quark decay, the b (or $\bar{b}$) quark decays only after having hadronised into a $B_{d,s}^0$ meson ($\overline{B}_{d,s}^0$).

Until recently, only one way was considered how a dimuon event - i.e. an event containing a

"wrong sign" muon - could come to pass: After hadronisation, the meson can oscillate into its anti-particle and decay:

$$b \to B^0_{d,s} \to \overline{B}^0_{d,s} \to \overline{X}\mu^+ \tag{4.141}$$

The final state then contains a "wrong-sign" muon, making the entire decay of the $b\bar{b}$ pair a like-sign dimuon event. As A_{SL} is measured in mixtures of B^0_d and B^0_s mesons, its theoretical expression is a linear combination of a^d_{SL} and a^s_{SL}. Note that this means that the like-sign dimuon charge asymmetry is interpreted as a case of CP violation in mixing (only). The corresponding expression used in this work to predict A_{SL} and given in [201] is based on four assumptions:

- There is no production asymmetry between mesons and anti-mesons, i.e. the experiment's production fractions f_d and f_s ($\bar{f}_d$ and $\bar{f}_s$) of $B^0_{d,s}$ ($\overline{B}^0_{d,s}$) satisfy $\bar{f}_q = f_q$.
- No direct CP violation occurs in the decays involved.
- There is only small CP violation in mixing.
- $\Gamma^d_{(SL)} = \Gamma^s_{(SL)}$ is satisfied to a very good approximation. This seems justified since this $SU(3)$ flavour equality is violated only by terms of $\mathcal{O}(\frac{\Lambda_{QCD} m_s}{m_b^2})$.

The first three assumptions are confirmed experimentally (also, cf. sec. 2.5.2). Then,

$$A_{SL} = \frac{f_d Z_d a^d_{SL} + f_s Z_s a^s_{SL}}{f_d Z_d + f_s Z_s} \tag{4.142}$$

where the coefficients are

$$Z_q = \frac{1}{1 - y_q^2} - \frac{1}{1 + x_q^2} \tag{4.143}$$

with $y_q = \frac{\Delta\Gamma_q}{2\Gamma_q}$ and $x_q = \frac{\Delta m_q}{\Gamma_q}$ [201]. The input values of $Z_{d,s}$ were computed from $x_d = 0.771 \pm 0.007$, $y_d \approx 0$, $x_s = 26.3 \pm 0.4$ (all from [129]). The value $y_s = 0.061 \pm 0.005$ was taken from the more recent source [177] as no average was given in the previous one. The values thus obtained and used in the fits are given in Table 5.2. The expressions for $a^{d,s}_{SL}$ were given in the previous two sections.

The A_{SL} measurement of the D0 collaboration deviates from the SM prediction by almost 4 σ [202]:

$$A^{\mathrm{D0}}_{SL} = (-7.87 \pm 1.72 \pm 0.93) \cdot 10^{-3} \qquad A^{\mathrm{SM3}}_{SL} = (-2.8^{+0.5}_{-0.5}) \cdot 10^{-4} \tag{4.144}$$

Contribution From CPV in Interference of Decays of Mixed and Unmixed B Mesons

In 2013, a candidate for an additional contribution to the like-sign dimuon charge asymmetry was put forward by Hoeneisen and Borissov [203]. They observed that in the decay $B^0(\bar{B}^0) \to c\bar{c}d\bar{d}$ - for example

$$\begin{array}{rcl} & \nearrow \quad \mu^- X & \qquad\qquad \mu^- X \\ p\bar{p} \longrightarrow & b\bar{b}X & \qquad\qquad \nearrow \\ & \searrow \quad B^0_d & \to \bar{B}^0_d \to D^+ D^- \end{array} \tag{4.145}$$

and its charge conjugated process - the CP-even state D^+D^- is accessible both from $B^0_{d,s}$ and its antimeson. Consequently, CP symmetry could be violated in the interference of the following two decays (charge conjugated processes assumed):

$$B^0 \to c\bar{c}d\bar{d} \qquad \text{and} \qquad B^0 \to \bar{B}^0 \to c\bar{c}d\bar{d}$$

which would contribute to the like-sign dimuon asymmetry observed. There should be no contributions to the measured asymmetry from the quark level decay $b \to c\bar{c}s$ because each CP-even final state (e.g. in $B^0 \to J/\psi K_S$) is cancelled by a CP-odd state (in the example, $J/\psi K_L$). At the same time, the effect is shown not to contribute to the inclusive muon charge asymmetry measured between positive and negative muons

$$a = \frac{n^+ - n^-}{n^+ + n^-}. \tag{4.146}$$

The entire like-sign dimuon charge asymmetry then consists of one part from mixing and one part from interference of decays with mixing and without mixing: $A = A^{\text{mix}} + A^{\text{int}} = A_{SL} + A^{\text{int}}$. In the SM3, the charge asymmetry in the decay of a B^0_d to a final state f_i can be shown to obey [204]

$$A^{\text{int}} \propto -\eta_{CP}\frac{\Delta\Gamma}{\Gamma} \cdot \frac{\text{Im}\left(M^d_{12}\right)}{\left|M^d_{12}\right|} \cdot \frac{P_b - P_{\bar{b}}}{P_b P_{\bar{b}}}. \tag{4.147}$$

P_b ($P_{\bar{b}}$) is the probability that the decay of an initial b quark produces a final-state right-sign (wrong-sign) muon μ^-. η_{CP} denotes the final state's CP eigenvalue. Neglecting (cf. sec. 5.3) the small imaginary part of V_{cd}, the phase of M^d_{12} is $\sin 2\beta$ in the SM3. In the SM4, the value of the phase is the same except it must now be interpreted as $\sin(2\beta - 2\theta_d)$. Based on measurements of various branching rations and decay widths, the authors of [203] give some estimations of the contribution of CPV in interference of decays with mixing and decays without mixing in the B^0_d system. All are significantly larger than what is predicted by the mixing contribution a^d_{SL} to eq. (4.142) in the SM3, and the uncertainty interval of one of them overlaps with that of the measurement in [202]. In the SM3 B^s_0 system's contribution from CP violation in interference is suppressed by the small values of $\sin(2\beta_s)$ and time dilution term $x_s/(1 + x^2)$, with $x_s = \Delta m_s/\Gamma_s$. D0 took this into account in their latest extraction of the dimuon charge asymmetry [200]. The authors of [200] state that their publication's most important results are the two model-independent quantities

$$a_{CP} = (-3.2 \pm 4.2 \pm 6.1) \cdot 10^{-4} \quad \text{and} \quad A_{CP} = (-2.35 \pm 0.64 \pm 0.55) \cdot 10^{-3}. \tag{4.148}$$

They are what remains after background contributions are subtracted from eqs. (4.138) and (4.146).

Very soon, the approach in [203] was critized by Ulrich Nierste on the following grounds[11]: The Jarlskog criterion for CP violation [57] states that CP violation disappears if any two up-type quark flavours or any two down-type quark flavours have the same mass. In the limit $m_c = m_u$, the interference contribution to A_{SL} from processes such as eq. (4.145) should thus

[11] private communication, see also [204].

disappear as do $a_{SL}^{(d)}$ and $a_{SL}^{(s)}$. However, it does not. The reason is that the authors of [203] considered only $c\bar{c}$ final states, but overlooked the other contributions $u\bar{c}$ and $u\bar{u}$ which must interfere destructively, leading to the desired cancellation. Another hint to the incorrectness pointed out by Ulrich Nierste is that the observable depends on $\sin(2\beta)$ which cannot be the case for an observable with untagged charm.
In [204], the contribution to A_{SL} from interference is corrected by the addition of the missing terms. Both in SM3 and SM4, the absorptive part of the effective Hamiltonian Γ_{12}^d (eq. (2.101), with $M = B_0^d$) is dominated by the charm contribution. Using

$$\Delta\Gamma_d = -\Delta m_d \cdot \mathrm{Re}\left(\frac{\Gamma_{12}}{M_{12}}\right), \tag{4.149}$$

this leads to the SM3 expression

$$A_d^{\mathrm{int}} = -(P_{c\to\mu} - P_{u\to\mu})\frac{2\Gamma_{12,d}^{cc}}{\Gamma_d}\left|\lambda_c^{B_d}\lambda_t^{B_d}\right|\sin\beta\frac{x_d}{1-x_d^2} \tag{4.150}$$

given in [204]. $P_{c\to\mu}$ and $P_{u\to\mu}$ are the probabilities for an u quark and a c quark to decay to a muonic final state, respectively. The term $\left|\lambda_c^{B_d}\lambda_t^{B_d}\right|$ enters by using the 3×3 unitarity of the CKM matrix. At the end of the day, this reduces the prediction of A_d^{int} by a factor of 0.49 to a lower limit of

$$A_d^{\mathrm{int}} > (-2.2 \pm 0.8)\cdot 10^{-4}. \tag{4.151}$$

In the SM4, at least a few modifications to eq. (4.150) are required. $\sin\beta$ must be replaced by $\sin(\beta-\theta_d)$, but as this is just the SM4 interpretation of the input value, there is no numerical effect. Also, 3×3 unitarity is not valid any more and $\left|\lambda_c^{B_d}\lambda_t^{B_d}\right|$ must be replaced by the original term:

$$\left|\lambda_c^{B_d}\left(\lambda_c^{B_d}+\lambda_u^{B_d}\right)\right| \tag{4.152}$$

The other relations which went into eq. (4.150) should remain valid in an SM4 context, leading to

$$A_d^{\mathrm{int}} = -(P_{c\to\mu} - P_{u\to\mu})\frac{2\Gamma_{12,d}^{cc}}{\Gamma_d}\left|\lambda_c^{B_d}\left(\lambda_c^{B_d}+\lambda_u^{B_d}\right)\right|\sin\beta\frac{x_d}{1-x_d^2}. \tag{4.153}$$

Also, due to the rather small ratio $\lambda_{t'}^{B_d}/\lambda_t^{B_d} \approx 0.2$ and a $|V_{tb}|$ value "reasonably close" to the SM3 value (cf. sec. 5.4), one can expect the SM4 prediction to be roughly in the same ballpark as eq. (4.151).

Additional sources of CPV identified in [203] -

1. interference of B_s^0 decays with and without mixing,
2. direct CP violation in $\bar{b}\to c\bar{c}\bar{q}$ ($q = d$ or s) with subsequent decay $\bar{c}\to\mu^- X$,
3. direct CP violation in semileptonic decays of b and c quarks

- were shown to be negligibly small in the SM3. The dominance of the charm contribution in the absorptive term Γ_{12}^s is even more pronounced than in Γ_{12}^d, permitting the same approximation

as in the derivation of eq. (4.150). The phase $\sin(\beta - \theta_d)$ must be replaced by the phase of the mixing amplitude $M_{12}^{B_s}$. HFAG published [177] an average of the CP violating phase between the mixing amplitude and the $b \to c\bar{c}s$ decay amplitude,

$$\phi_s^{c\bar{c}s} = -0.015 \pm 0.035. \tag{4.154}$$

With the dominance of this decay in $\Gamma_{12}^{B_s}$ and the phase $\arg\left(\lambda_c^{B_s}\right) = \arg\left(V_{cs}V_{cb}^*\right) \approx 0$ (cf. eq. (2.43) and Tab. 5.3), one can approximate

$$\phi_s = \arg\left(\frac{-M_{12}^{B_s}}{\Gamma_{12}^{B_s}}\right) \approx \arg\left(\frac{-M_{12}^{B_s}}{\Gamma_{12}^{c\bar{c}s}}\right) = \phi_s^{c\bar{c}s} \approx \arg(-M_{12}^{B_s}). \tag{4.155}$$

The HFAG value eq. (4.154) is even smaller than the value used in the estimate in [203], and x_s is the same in SM3 and SM4. There is therefore no reason to expect a significantly larger contribution to CP violation from interference in the SM4 than in the SM3. As for 2, the CP violation involves penguin graphs which may well contribute more strongly in the SM4 than in the SM3, and a more thorough analysis seems necessary. On the other hand, even an increase of this contribution - estimated at 0.0002% in [203] - by a factor of 10 would not change the observation that it would have no effect at the current experimental precision. As Ref. [204] was only brought to the attention of the author when fit results and coding were almost complete, a thorough and consistent SM4 treatment is beyond the scope of this thesis and is unlikely to be undertaken, given the demise of the model. Given all of the above, the A_{SL} input from [200] will not be used as input to any fit, and A_{SL} will be only predicted by means of eq. (4.142). The prediction will, however, be compared to an SM4 estimate of the A_{SL} based on [200].

An SM4 Estimate of A_{SL} With CP Violation in Interference

To obtain this estimate, the analysis in [200] is retraced, albeit not in a consistent fit. As a first step, the numerical difference between eqs. (4.150) and (4.153) is calculated. Then, the analysis of [200] will be retraced. In the comparison of the SM3 and SM4 expressions, the question is how eq. (4.152) compares to its SM3 equivalent. Using e.g. PDG input values [50] or fit results by the CKMfitter group such as [131], one obtains

$$\left|\lambda_c^{B_d,\mathrm{SM3}} \cdot \lambda_t^{B_d,\mathrm{SM3}}\right| \approx 8 \cdot 10^{-5}, \tag{4.156}$$

with an uncertainty of $\mathcal{O}(5 \cdot 10^{-6})$ which turns out to be negligible compared to the error of the estimate eq. (4.151). In order to obtain the corresponding SM4 value, a fit result of $\left|\lambda_d^{B_d}\right|$ to the complete set of inputs (cf. Chapter 5) was used. Except for V_{ub}, all CKM matrix elements entering $\lambda_c^{B_d}\left(\lambda_c^{B_d} + \lambda_u^{B_d}\right)$ are approximately real in the Hou/Soni parametrisation. The phase of

$|V_{ub}|$ is equal to the CKM matrix parameter $-\delta$. Therefore,

$$\left|\lambda_c^{B_d}\left(\lambda_c^{B_d}+\lambda_u^{B_d}\right)\right| = \left|\lambda_c^{B_d}\right|\cdot\sqrt{\left|\lambda_c^{B_d}\right|^2+\left|\lambda_u^{B_d}\right|^2+2\left|\lambda_c^{B_d}\right|\left|\lambda_u^{B_d}\right|\cos\delta} \tag{4.157}$$

$$\approx 9.96^{+0.8}_{-1.2}\cdot 10^{-5}. \tag{4.158}$$

The error was estimated by inserting the boundaries of the uncertainty intervals into the above expressions, i.e. it is larger than what is to be expected in the correct Gaussian error propagation. Still, the relative uncertainty is much smaller than the relative error of the original estimate in [203] and, like in [204], it was neglected. As the probabilities $P_{u\to\mu}$ and $P_{c\to\mu}$ in eq. (4.150) can be experimentally determined, the SM4 value of A_d^{int} is then obtained by

$$A_d^{\text{int,SM4}} = A_d^{\text{int,SM3}}\cdot\frac{\left|\lambda_c^{B_d}\left(\lambda_c^{B_d}+\lambda_u^{B_d}\right)\right|_{\text{SM4}}}{\left|\lambda_c^{B_d}\lambda_t^{B_d}\right|_{\text{SM3}}} \gtrapprox (-2.2\pm 0.8)\cdot 10^{-3}\cdot 1.245$$

$$A_d^{\text{int,SM4}} \gtrapprox (-2.7\pm 1.0)\cdot 10^{-3} \tag{4.159}$$

which constitutes the lower limit in the SM4. With an estimate now available of $A_d^{\text{int,SM4}}$, one can try to retrace the analysis of [200] to obtain an SM4-compatible A^{mix}.

Only if the muons detected in the experiment stem from decays *within* the beampipe can one assume that the CP violating asymmetries observed in their counting is certainly caused by the underlying physical process and not an interaction of e.g. intermediate states with the detector material. The asymmetries measured are therefore extracted from counts of such "short distance" (S) muons. Muons which are produced by longer-lived particles which travel further are referred to as "long" distance (L) muons. The connection between this A_S and A_{CP} on the one hand and a_S and a_{CP} on the other hand is given by

$$a_{CP} = f_S a_S \quad \text{and} \quad A_{CP} = F_{SS}A_S + F_{SL}a_S, \tag{4.160}$$

respectively. Here, f_S is the fraction of the muons which are S muons, and F_{SL} and F_{SS} are fractions of dimuon events which contain one L muon and one S muon, and two S muons, respectively. Values of these and other parameters will be taken from [200] and are given in Table 4.6. Solving the above equations yields

$$a_S = (-6.4\pm 8.4\pm 12.2)\cdot 10^{-4} \quad \text{and} \quad A_S = (3.2\pm 1.5)\cdot 10^{-3}. \tag{4.161}$$

This is the point where the analysis in [200] starts to differ visibly from what will be done here. Up to now, the main difference was that, in the original D0, measurements of A_{CP} and a_{CP} and also the parameters recorded are binned. On these binned results, a fit is performed to obtain the results. Here, the numbers taken from [200] are those obtained without dividing into bins, and the uncertainties given here are simply calculated by error propagation. In order to check if the results obtained in this way are comparable to the results obtained by D0, the SM3 value of A_{SL} is calculated under the assumption that CP violation from interference and mixing is as

Parameter	Value
f_S	0.4997 ± 0.0186
F_{SS}	0.6914 ± 0.0149
F_{SL}	0.2269 ± 0.0110
c_b	$(6.3 \pm 0.7) \cdot 10^{-2}$
C_b	0.524 ± 0.040

Table 4.6.: Parameter values from Ref. [200] to retrace the analysis performed there.

obtained in their SM3 simulation ([200], Table XVI):

$$A_S^{\text{int}} = (-5.0 \pm 1.2) \cdot 10^{-4} \tag{4.162}$$

The value obtained from the measured A_S in the procedure lined out above is

$$A_{SL}^{\text{SM3,D0}} = (-5.2 \pm 2.4) \cdot 10^{-3} \tag{4.163}$$

where the dominant relative error of eq. (4.161) is taken as relative error of A_{SL}. This agrees well with the fit result $A_{SL}^{\text{SM3}} = (-4.96 \pm 1.53 \pm 0.72) \cdot 10^{-3}$ given by D0. Including the correction in [204] (cf. eq. (4.150)), the prediction eq. (4.162) is reduced by 49%:

$$A_S^{\text{int}} = (2.45 \pm 0.59) \cdot 10^{-4}, \tag{4.164}$$

corresponding to

$$A_{SL}^{\text{SM3}} = (-5.6 \pm 2.6) \cdot 10^{-3}. \tag{4.165}$$

In the SM4, finally, the predicted contribution to CP violation from interference is increased by a factor of 1.245. Applying this factor to the value obtained in the simulation by D0 yields (cf. eq. (4.159)):

$$A_{SL}^{\text{SM4}} = (-5.5 \pm 2.6) \cdot 10^{-3}. \tag{4.166}$$

Simply assuming that there is no CP violation from interference and interpreting the measured asymmetries purely in terms of mixing gives

$$A_{SL}^{\text{NoInt}} = (-6.1 \pm 2.9) \cdot 10^{-3}. \tag{4.167}$$

As can be seen, even the smaller error of the original number quoted in [200] covers all other values within its 1 σ interval. Given the even larger uncertainty of a_S and the low weight of an A_{SL} value computed from it (cf. eqs. (4.160) and (4.161)), the value

$$A_{SL}^{\text{single-muon}} = -0.010 \pm 0.013 \pm 0.019 \tag{4.168}$$

will not be used to form an average with any of the above.

Now that the description of the inputs is complete, the next chapter will describe the fits themselves.

5. SM4 Fits and their Results

This chapter describes the fits performed in the SM4 framework which was described in chapter 2, using the inputs described in chapter 4. In order to distinguish between the effects of different sets of inputs, several series of fits were performed:

Tree Level inputs only For this series of fits, only those quantities were included whose lowest-order contribution comes from tree-level processes. These are the CKM matrix element moduli $|V_{ud}|$, $|V_{us}|$, $|V_{ub}|$, $|V_{cd}|$, $|V_{cs}|$, $|V_{cb}|$ and $|V_{tb}|$, the branching fraction of the leptonic B meson decay $\mathcal{B}(B \to \tau\nu)$ and those of the three leptonic W boson decays $\mathcal{B}(W \to \ell\nu)$. The angle γ of the Unitarity Triangle is also extracted from tree level processes and is therefore also included in this series' inputs. Its input value is given as a χ^2 Lookup Table. It is plotted in Fig. 4.6. All these inputs are described in sec. 4.1. For brevity, this set of inputs will be referred to as "TL" in the following.

CP conserving loop observables The inputs used in this series include, in addition to those in the Tree Level scenario, CP conserving observables induced by processes which do not occur at tree level. These observables are the oscillation frequencies of neutral B_d and B_s mesons, Δm_d and Δm_s, the branching fractions of dimuonic decays of those mesons $\mathcal{B}(B_d \to \mu^+\mu^-)$ and $\mathcal{B}(B_s \to \mu^+\mu^-)$ and the ratio $\frac{\mathcal{B}(B\to X_s\gamma)}{\mathcal{B}(B\to X_c e\bar{\nu})}$. Also, the effects of the Electroweak Precision Observables are included. More detailed descriptions of the inputs can be found in sec. 4.2. This input set will from now on be referred to as LoopNoCPV.

CP violating observables, semileptonic asymmetries not included This adds to the above LoopNoCPV set two CP-violating inputs: The SM4-reinterpretation of the SM3 extraction of the UT angle β, $\sin(2\beta - 2\theta_d)$, and $|\epsilon_K|$. A more detailed description can be found in sec. 4.3. The short name of this input set is LoopCPV.

Full set of observables including semileptonic asymmetries Due to previously encountered convergence problems - see appendix B - some CP-violating observables were considered problematic and were not included in the previous series of fits but are only added in this last step. These observables are a^d_{SL}, a^s_{SL} and A_{SL}. As there is no physical reason to distinguish this input set from the previous one, the descriptions of the inputs can be found in the same place, i.e. section 4.2. This will be referred to as "complete set of inputs".

For quick overview and reference, the input values are also given in Table 5.1. The theoretical expressions of most observables contain certain parameters whose particular meaning is explained in section 4. Their values and references are given in Table 5.2.

No.	Observable	Value ±Error / CL	Ref.
		Tree Level input set / "TL"	
-	$\lvert V_{ud}\rvert$	$0.97421^{+0.00034}_{-0.00029}$	[59], see sec. 4.1.1
-	$\lvert V_{us}\rvert$	$0.2247 \pm 0.0006 \pm 0.0011$	[131]
-	$\lvert V_{ub}\rvert$	$(3.70 \pm 0.12 \pm 0.26) \cdot 10^{-3}$	cf. sec. 4.1.3
-	$\lvert V_{cd}\rvert$	0.230 ± 0.011	[84]
-	$\lvert V_{cs}\rvert$	$0.98 \pm 0.01 \pm 0.1$	[84]
-	$\lvert V_{cb}\rvert$	$(41.00 \pm 0.33 \pm 0.74) \cdot 10^{-3}$	[84]
-	$\lvert V_{tb}\rvert$	1.017 ± 0.028	See sec. 4.1.8
-	γ	LUT $(69.9^{+8.0}_{-9.2}\,^{\circ})$	[131], cf. sec. 4.1.10
1	$\mathcal{B}(B \to \tau\nu)$	$(1.15 \pm 0.23) \cdot 10^{-4}$	[123]
2	$\mathcal{B}(\mathrm{W} \to \mathrm{e}\nu)$	(10.75±0.13) %	[46]
3	$\mathcal{B}(\mathrm{W} \to \mu\nu)$	(10.57±0.15) %	[46]
4	$\mathcal{B}(\mathrm{W} \to \tau\nu)$	(11.25±0.20) %	[46]
		CP conserving loop observables / New in input set "LoopNoCPV"	
5	$\frac{\mathcal{B}(B\to X_s\gamma)}{\mathcal{B}(B\to X_c e\bar{\nu})}$	0.00319 ± 0.00021	cf. sec. 4.2.4, [46]
6	$\mathcal{B}(B_s \to \mu^-\mu^+)$	$(2.9 \pm 0.7) \cdot 10^{-9}$	[179]
7	$\mathcal{B}(B_d \to \mu^-\mu^+)$	$(3.6^{+1.6}_{-1.4}) \cdot 10^{-10}$	[179]
8	Δm_d	$(0.507 \pm 0.004) \cdot 10^{-12} s$	HFAG Spring 2012
9	Δm_s	$(17.762 \pm 0.023) \cdot 10^{-12} s$	[131]
-	Constraints from Electroweak Precision Fit		See sec. 4.2.1
		CP violating inputs excl. semileptonic Asymmetries / New in input set "LoopCPV"	
10	$\sin(2\beta - 2\theta_d)$	0.682 ± 0.0019	[188], cf. sec. 4.3.2
11	$\lvert\epsilon_K\rvert$	$(2.228 \pm 0.011) \cdot 10^{-3}$	[46]
		Semileptonic charge symmetries in neutral B meson decays	
12	a^d_{SL}	$(2.3 \pm 2.6) \cdot 10^{-3}$	See sec. 4.3.4
13	a^s_{SL}	$(-4.8 \pm 4.8) \cdot 10^{-3}$	See sec. 4.3.3

Table 5.1.: Input values of observables used in different input sets. The numbers given in the first column relate this table to Table 5.2, where these numbers are used to denote the observable(s) in which a parameter is used.

Parameter	Value ±Error / CL	used in obs. No.	Ref.
$\hat{B}_s$	$1.320 \pm 0.017 \pm 0.040$	8,9,12-14	[131]
f_{B_s}	$0.2256 \pm 0.0011 \pm 0.0054$	6-9,12-14	[131]
Λ_{QCD}	(0.2315 ± 0.0090) GeV	2-4,5-7,11	see caption
f_{B_s}/f_{B_d}	$1.205 \pm 0.003 \pm 0.007$	6-8, 12, 14	[131]
$\hat{B}_s/\hat{B}_d$	$1.023 \pm 0.013 \pm 0.014$	7, 8, 12, 14	[131]
η_B	[0.5488,0.5532]	8,9,10,12,13	[172]
$\overline{m}_t$	$(165.95 \pm 0.35 \pm 0.64)$ GeV	5-14	[205]
$\overline{m}_{t'}$	$[200, 1000]$ GeV	5-14	see text
$\overline{m}_b$	(4.222 ± 0.051) GeV	5, 9, 12-14	HFAG FPCP2009
$\overline{m}_c$	$1.286 \pm 0.013 \pm 0.040$	5, 11	[131]
$\overline{m}_s$	(0.080 ± 0.003) GeV	9	[206]
$\overline{m}_d$	$(4.8^{+0.5}_{-0.3})$ MeV	9, 12-14	[46]
η_B	$[0.5488, 0.5532]$	8, 9, 10, 12-14	cf. sec. 4.2.4
$\mu_{b\to s\gamma}$	$(3.13 \pm 0.001 \pm 0.03)$ GeV	5	see sec. 4.2.4
$\mu_t^{(\ell\ell)}$	$(200 \pm 1 \pm 120)$ GeV	6, 7	see sec. 4.2.5
$\hat{B}_K$	$0.7615 \pm 0.0027 \pm 0.0137$		[159]
η_{ct}	$[0.45, 0.544]$		[207]
η_{tt}	$[0.57, 0.5830]$	11	[131]
κ_{ϵ_K}	$0.940 \pm 0.013 \pm 0.023$		[159]
m_b^{pow}	$[4.60, 4, 80]$ GeV	12-14	[95]
μ_1	$[2.111, 8.444]$ GeV	12-14	[95]
$\bar{z}$	$0.0482 \pm 0.0015 \pm 0.0030$	12-14	CKMfitter internal
f_s	0.107 ± 0.005	14	[129]
f_d	0.407 ± 0.007	14	[129]
Z_d	0.3728 ± 0.0042	14	see Sec. 4.4.4
Z_s	1.0023 ± 0.0006	14	

Cont. next page

Table 5.2.: Parameter values used as inputs in the fits of this chapter. The bar over masses indicates that masses are defined in the $\overline{MS}$ renormalization scheme (see e.g. [43]). The value of Λ_{QCD} was calculated from $\alpha_S(m_Z) = 0.1184 \pm 0.0007$ [46].

Parameter	Value ±Error / CL	used in obs. No.	Ref.
$B^d_{R_0}$			
$B^d_{R_1}$		12,14	
$\tilde{B}^d_{\widetilde{R}_1}$	1.0 ± 0.5		
$B^s_{R_0}$			
$B^s_{R_1}$		13,14	[95]
$\tilde{B}^s_{\widetilde{R}_1}$			
$\tilde{B}^d_{R_2}$		12,14	
$\tilde{B}^d_{\widetilde{R}_3}$	$1.0 \pm 0.0 \pm 0.5$		
$\tilde{B}^s_{\widetilde{R}_2}$		13,14	
$\tilde{B}^s_{\widetilde{R}_3}$			
$\Delta B^d_{R_2}$		12,14	
$\Delta B^d_{R_2}$	$0.0 \pm 0.0 \pm 0.2$		[95]
$\Delta B^s_{R_2}$		13,14	
$\Delta B^s_{R_3}$			
$\widetilde{B}^s_S(m_b)$	$0.91 \pm 0.03 \pm 0.12$	12-14	[208]
$\frac{\tilde{B}^s_S}{\tilde{B}^d_S}(m_b)$	$1.01 \pm 0.0 \pm 0.03$	12,14	

Table 5.2.: Parameter values used as inputs in the fits of this chapter. Continuation of previous page.

Several inputs used in those series are correlated. These are

- $\mathcal{B}(W \to \ell\nu)$ The correlations used in the fit are given in equation (4.25).
- f_s and f_d (cf. sec. 4.4.4 on A_{SL}) obey the correlation matrix

$$\begin{pmatrix} 1 & 0.224 \\ 0.224 & 1 \end{pmatrix}. \tag{5.1}$$

For each input set the fit results are provided in tables containing numerical constraints in the form of best-fit values and 1, 2 and 3 σ intervals. In cases where this is not possible, a p-value plot is given. Such plots will also be shown whenever an interesting feature makes this advisable, or to support an argumentation. As it is sometimes interesting to characterise the influence which a certain input has on a fit, tables are provided giving, for each input set, the following quantities for each input observable:

- $\frac{\hat{x}_{\text{pred}} - \hat{x}_{\text{exp}}}{\Delta x_{\text{exp}}}$, called the "pull" of an input. Here, $\hat{x}_{\text{pred}}$ is the best fit value of the observable x as obtained in a fit where x is *not* used as an input. $\hat{x}_{\text{exp}}$ is the central value of the experimental input for x, and Δx_{exp} is the quoted uncertainty. The pull is, in other words, the discrepancy between the preferred value of the fit and the central value of experimental input expressed in units of the experimental uncertainty.

- The reduction of the χ^2 value if the input is omitted.

They should be enough to quantify the influence of an input on the fit, and whether otherwise free parameters are constrained or if there is any tension with the other inputs.

In section 5.5, the p-value plots of all scanned (and constrained) quantities are shown in common coordinate systems. This way, it is easier to tell how constraints change with the input set.

For the statistical reliability of the results presented here, see sec. 3.1. In short, *within* the SM4, the limits given are statistically reliable in the sense of the *R*fit scheme.

5.1. Tree Level Inputs only

This section describes the first and simplest series of fits. The interpretation of the numerical input values in an SM4 framework has already been discussed in sec. 4.1.

5.1.1. Interplay of Tree Level Inputs

Here, the aim is to point out the mechanisms by which the parameters of the CKM matrix are constrained and how the global fit "predicts" values of observables for which no input values are used. For the first purpose, one can subdivide the inputs of this series into three classes, i.e.

1. Inputs in which the experiments extract only the squared modulus of an individual matrix element $|V_{ij}|^2$, or the product of such a matrix element with a decay constant or similar.

2. Inputs in which a sum of $|V_{ij}|^2$ is measured.

3. The special case of γ where a relative phase between products of CKM matrix elements is measured.

The first category covers the seven matrix elements as described in section 4.1, i.e. $|V_{ud}|$, $|V_{us}|$, $|V_{ub}|$, $|V_{cd}|$, $|V_{cs}|$, $|V_{cb}|$ and $|V_{tb}|$, as well as the branching fraction $\mathcal{B}(B \to \tau\nu)$. As for constraining the parameters of the CKM matrix, a look at its parametrisation eq. (2.43) shows that the elements of the third row, i.e. $|V_{ub}|$, $|V_{cb}|$ and $|V_{tb}|$, consist only of one summand. They are products of sines and cosines of the rotation angle parameters and, in case of $|V_{ub}|$, also an exponential function with a complex argument. Obviously, none of the measurements of these three matrix elements can by itself constrain any of the phases δ, ϕ_2 or ϕ_3.

The other four CKM matrix elements consist, in this parametrisation, of two, three or five summands of different phases, respectively. For the discussion of phase constraints, it is useful to introduce a nomenclature to denote these summands. Let a, b, c, d and f be the real-valued coefficients of the complex exponential functions in the summands as in Table 5.3. In the following, an a denotes the summand with no complex phase, b the coefficient of $e^{\mathrm{i}\,\delta}$, c the coefficient of $e^{\mathrm{i}\,\phi_2}$ and d the coefficient of $e^{\mathrm{i}\,\phi_3}$. Any coefficients of exponential functions with a more "complicated" argument are denoted by f with a superscript indicating which phase factor comes with it, and

they all bear subscripts denoting to which matrix element they belong. For example,

$$\begin{aligned} V_{td} \quad &= a_{td} + b_{td} \cdot e^{\mathrm{i}\,\delta} + d_{td} \cdot e^{\mathrm{i}\,\phi_3} + f_{td}^{(\phi_3-\phi_2)} \quad \cdot e^{\mathrm{i}(\phi_3-\phi_2)} + f_{td}^{(\delta+\phi_3-\phi_2)} \cdot e^{\mathrm{i}(\delta+\phi_3-\phi_2)} \\ & a_{td} = c_w s_{12} s_{23} \qquad\qquad f_{td}^{(\phi_3-\phi_2)} = c_{12} s_{23} s_v s_w \\ & b_{td} = -c_{12} c_{23} c_w s_{13} \qquad\qquad f_{td}^{(\delta+\phi_3-\phi_2)} = c_{23} s_{12} s_{13} s_v s_w \\ & d_{td} = -c_{13} c_{23} c_v s_u s_w \end{aligned} \tag{5.2}$$

and (note bars where exponential factors have a negative argument)

$$\begin{aligned} V_{ub'} = &\bar{b}_{ub'} \cdot e^{-\mathrm{i}\,\delta} + \bar{c}_{ub'} \cdot e^{-\mathrm{i}\,\phi 2} + \bar{d}_{ub'} \cdot e^{-\mathrm{i}\,\phi_3}, \\ & \bar{b}_{ub'} = c_v c_w s_{13} s_u \\ & \bar{c}_{ub'} = c_{13} c_w s_{12} s_v \\ & \bar{d}_{ub'} = c_{12} c_{13} s_w. \end{aligned} \tag{5.3}$$

Occasionally, in the following, quantities with a "vector arrow" on top such as $\vec{b}_{td}$ will be encountered. These are *not* actually vectors, but just a shorthand notation for the summand including its phase - in this case $\vec{b}_{td} = b_{td} \cdot e^{\mathrm{i}\,\delta}$.

If the expression for a matrix element V_{ij} is numerically dominated by at least two summands of comparable magnitude, but different phases, then the phase difference between the summands can be constrained by only measuring the modulus $|V_{ij}|$. This was checked not to be the case for any of the seven measured matrix elements by constraining each summand in a global fit for which the Tree Level set of inputs was further reduced by the omission of the angle γ. No significant constraint of any of the phases was found. There is always one summand which clearly dominates over the others (cf. Tables 5.3). This confirms the absence of phase constraints.

In the second category, there is only the leptonic branching ratio of W decays, $\mathcal{B}(W \to \ell\bar{\nu}_\ell)$. For such a constraint to have any effect on a particular matrix element, the other elements which appear in the sum have to be well-constrained from the beginning. This is how the constraint on $|V_{cs}|$ is improved (cf. sec. 4.1.9). Phases can only be constrained by such an input if e.g. two of the matrix elements in an expression $\sum_i |V_{ij}|^2$ consist of summands of comparable magnitude which have the same phase difference.

In case of γ, the input's power to constrain an individual phase parameter again depends on the summands which make up the matrix elements involved. A look at their relative magnitude makes it clear that the phase parameter constrained by a γ input is δ:

$$\gamma \simeq \arg\left(-V_{ub}^*\right) = \delta + \pi. \tag{5.4}$$

This is very similar to the SM3 because the phases of the CKM matrix elements involved, i.e. V_{ud}, V_{ub}, V_{cd} and V_{cb}, are roughly the same as in the SM3 - any summands of their parametrization as in eq. (2.43) whose phase *differs* from the SM3-like phase are simply too small to have a noticable effect on the overall phase of the matrix element and, hence, cannot "absorb" a constraint on δ imposed by γ. Correspondingly, there is no constraint on either ϕ_2, ϕ_3, or their difference.

The matrix elements which are *not* given as inputs are constrained by the unitarity of the CKM matrix. Such a constraint affects only the modulus of the CKM matrix element (or elements, as in case of the first and second column) concerned. A bound on phases could result from summands of comparable magnitude, as in the case of $|V_{td}|$ and $|V_{ts}|$. The reverse is also possible: A phase constraint as placed on δ by a γ input can provide bounds on the absolute value of a matrix element if its summands' magnitudes are otherwise fixed (e.g. in a global fit).

V_{ud}	$c_{12}c_{13}c_w$	$-c_{13}e^{-\mathrm{i}(\phi_2-\phi_3)}s_{12}s_vs_w$	$-c_ve^{-\mathrm{i}(\delta-\phi_3)}s_{13}s_us_w$		
$\hat{\theta}$	≈ 1.000	0	$\mathcal{O}(10^{-6})$		
2σ	> 0.997	$\mathcal{O}(10^{-3})$	$\mathcal{O}(10^{-4})$		
V_{us}	$c_{13}c_vs_{12}$	$-e^{-\mathrm{i}(\delta-\phi_2)}s_{13}s_us_v$			
$\hat{\theta}$	1	$\mathcal{O}(10^{-5})$			
2σ	> 0.999	$\mathcal{O}(10^{-3})$			
$V_{ub'}$	$c_{12}c_{13}e^{-\mathrm{i}\phi_3}s_w$	$c_{13}c_we^{-\mathrm{i}\phi_2}s_{12}s_v$	$c_vc_we^{-\mathrm{i}\delta}s_{13}s_u$		
$\hat{\theta}$					
2σ	unconstrained	unconstrained	unconstrained		
V_{cd}	$-c_{23}c_ws_{12}$	$-c_{12}c_{23}e^{-\mathrm{i}(\phi_2-\phi_3)}s_vs_w$	$-c_{13}c_ve^{\mathrm{i}\,\phi_3}s_{23}s_us_w$	$-c_{12}c_we^{\mathrm{i}\delta}s_{13}s_{23}$	$e^{\mathrm{i}\delta-\mathrm{i}(\phi_2-\phi_3)}s_{12}s_{13}s_{23}s_vs_w$
$\hat{\theta}$	0.999	0	$\mathcal{O}(10^{-4})$	$\mathcal{O}(10^{-3}$	$\mathcal{O}(10^{-5})$
2σ	> 0.945	< 0.046	$< 3\cdot 10^{-3}$	$\mathcal{O}(10^{-3})$	$\mathcal{O}(10^{-5})$
V_{cs}	$c_{12}c_{23}c_v$	$-c_{13}e^{\mathrm{i}\phi_2}s_{23}s_us_v$	$-c_ve^{\mathrm{i}\delta}s_{12}s_{13}s_{23}$		
$\hat{\theta}$	≈ 1	$\mathcal{O}(10^{-4})$	$\mathcal{O}(10^{-5})$		
2σ	> 0.998	$\mathcal{O}(10^{-4})$	$\mathcal{O}(10^{-4})$		
$V_{cb'}$	$c_{12}c_{23}c_we^{-\mathrm{i}\phi_2}s_v$	$-c_{23}e^{-\mathrm{i}\phi_3}s_{12}s_w$	$c_{13}c_vc_ws_{23}s_u$	$-c_{12}e^{\mathrm{i}\delta-\mathrm{i}\phi_3}s_{13}s_{23}s_w$	$-c_we^{\mathrm{i}\delta-\mathrm{i}\phi_2}s_{12}s_{13}s_{23}s_v$
$\hat{\theta}$				$\mathcal{O}(10^{-5})$	$\mathcal{O}(10^{-3})$
2σ	unconstrained	unconstrained	unconstrained	$\mathcal{O}(10^{-5})$	$\mathcal{O}(10^{-3})$
V_{td}	$c_ws_{12}s_{23}$	$-c_{12}c_{23}c_we^{\mathrm{i}\delta}s_{13}$	$-c_{13}c_{23}c_ve^{\mathrm{i}\phi_3}s_us_w$	$c_{12}e^{-\mathrm{i}(\phi_2-\phi_3)}s_{23}s_vs_w$	$c_{23}e^{\mathrm{i}\delta-\mathrm{i}(\phi_2-\phi_3)}s_{12}s_{13}s_vs_w$
$\hat{\theta}$	0.701	0.299	0	0	0
2σ	$\in (0.333, 0.747)$	$\in (0.14, 0.314)$	< 0.51	< 0.033	$< 7.5\cdot 10^{-4}$
V_{ts}	$-c_{12}c_vs_{23}$	$-c_{23}c_ve^{\mathrm{i}\delta}s_{12}s_{13}$	$-c_{13}c_{23}e^{\mathrm{i}\phi_2}s_us_v$		
$\hat{\theta}$	0.978	0.023	0		
2σ	< 0.49	< 0.024	≈ 0.5		
$V_{tb'}$	$c_{13}c_{23}c_vc_ws_u$	$-c_{12}c_we^{-\mathrm{i}\phi_2}s_{23}s_v$	$e^{-\mathrm{i}\phi_3}s_{12}s_{23}s_w$	$-c_{23}c_we^{\mathrm{i}(\delta-\phi_2)}s_{12}s_{13}s_v$	$-c_{12}c_{23}e^{\mathrm{i}(\delta-\phi_3)}s_{13}s_w$
$\hat{\theta}$			≤ 0.73		
2σ	unconstrained	unconstrained	≤ 0.75	≤ 0.024	≤ 0.32

Table 5.3.: Relative magnitude of summands of the CKM matrix elements, normalized to the sum of their absolute values. Matrix elements of third column and fourth row are not listed as they consist only of one summand each; see eq. (2.43) for their parametrisation. The values were obtained by means of a global fit in the "Tree Level" set of inputs, further reduced by the omission of the angle γ.

5.1.2. Results of the Global Fit With the Tree Level Input Set

This section, finally, contains the results obtained by a global fit with all Tree Level inputs used. The optimum χ^2 found in each case is $\chi^2_{\text{min}} = 7.3682$ which reduces to 0.7840 if the leptonic W decays are not used as inputs. This is because the experimental value of $\mathcal{B}(W \to \tau\bar{\nu})$ is larger than the theory prediction. The constraints on the moduli of the matrix elements are given at the 1-, 2-, and 3 σ level in Table 5.4.

The only phase that is constrained in this input set is δ which contains a $\mod \pi$ ambiguity. The values are given in Table 5.5. One feature that perhaps requires a special mention is the dip between the two peaks of $|V_{td}|$ as shown in Fig. 5.1 a). It disappears when the input γ is omitted and becomes much deeper in the SM3 limit, i.e. with $\theta_u = \theta_v = \theta_w = 0$. Also, not surprisingly any more at this point, there is a correlation between $|V_{td}|$ and δ (see Fig. 5.1 b)). The reason for the dip is the ambiguity in γ: The first and the second summand of V_{td} (cf. Tab. 5.3) add up to different $|V_{td}|$, depending on which value γ (and thus δ) takes. Any violation of unitarity which might result can be "absorbed" by the uncertainties on the other elements of the 3rd row and 1st column of the CKM matrix (at the price of an increase in χ^2). As soon as θ_u, θ_v and θ_w are allowed to vary, the other three summands (as in Table 5.3) can, by means of their unconstrained phase ϕ_3, alleviate any tension between the first two summands (whose relative phase is $\approx \delta$ and hence constrained) on one side and the $|V_{td}|$ value required by unitarity on the other side. Therefore, the dip is less pronounced in this case. The whole argument is illustrated in Fig. 5.2. The dip should be reflected in other matrix elements - again, by virtue of unitarity - but its width is so small that it is not visible at the granularity used and also easily "absorbed" by the uncertainty on $|V_{tb}|$ and especially $|V_{tb'}|$.

The angles α and β of the Unitarity Triangle are badly constrained, but preferred regions show themselves in the fits. With their definitions in eq. (2.60) and the magnitudes of the matrix elements involved, one can approximate

$$\alpha \approx \arg\left(-\frac{a_{ud}b_{ub}e^{\mathrm{i}\,\delta}}{(a_{cd}+f_{cd}^{(-(\phi_3-\phi_2))}e^{\mathrm{i}(\phi_3-\phi_2)})a_{cb}}\right) = \arg\left(-\frac{e^{\mathrm{i}\,\delta}}{a_{cd}+f_{cd}^{(-(\phi_3-\phi_2))}e^{\mathrm{i}(\phi_3-\phi_2)}}\right) \tag{5.5}$$

$$\beta \approx \arg\left(-\frac{a_{cb}(a_{cd}+f_{cd}^{(-(\phi_3-\phi_2))}e^{\mathrm{i}(\phi_3-\phi_2)})}{a_{tb}(a_{td}+b_{td}e^{\mathrm{i}\,\delta}+d_{td}e^{\mathrm{i}\,\phi_3})}\right) = \arg\left(-\frac{a_{cd}+f_{cd}^{(-(\phi_3-\phi_2))}e^{\mathrm{i}(\phi_3-\phi_2)}}{a_{td}+b_{td}e^{\mathrm{i}\,\delta}+d_{td}e^{\mathrm{i}\,\phi_3}}\right). \tag{5.6}$$

The hierarchy of the coefficients involved (once more, cf. Table 5.3) together with the freely varying phases ϕ_2 and ϕ_3 make it clear that the deviations of α and β from $\delta \simeq \gamma$ are governed by the relative sizes of $f_{cd}^{(-(\phi_3-\phi_2))}$ and a_{td} and d_{td}, respectively. The 1 σ limits - there are no better limits within the interval $[-\pi, \pi]$ with Tree Level inputs only - are given in Table 5.6.

	1 σ	2 σ	3 σ
$\lvert V_{ud}\rvert$	$0.97420^{+0.00033}_{-0.00028}$	$0.97420^{+0.00060}_{-0.00057}$	$0.97420^{+0.00075}_{-0.00086}$
$\lvert V_{us}\rvert$	$0.22567^{+0.00065}_{-0.00261}$	$0.2257^{+0.0012}_{-0.0032}$	$0.2257^{+0.0017}_{-0.0038}$
$\lvert V_{ub}\rvert$	$0.00397^{+0.00012}_{-0.00033}$	$0.00397^{+0.00023}_{-0.00067}$	$0.00397^{+0.00035}_{-0.00081}$
$\lvert V_{ub'}\rvert$	$0.000^{+0.038}_{-0.000}$	$0.000^{+0.046}_{-0.000}$	$0.000^{+0.052}_{-0.000}$
$\lvert V_{cd}\rvert$	$0.2255^{+0.0011}_{-0.0058}$	$0.2255^{+0.0023}_{-0.0108}$	$0.2255^{+0.0034}_{-0.0154}$
$\lvert V_{cs}\rvert$	$0.97340^{+0.00075}_{-0.00982}$	$0.9734^{+0.0010}_{-0.0210}$	$0.9734^{+0.0013}_{-0.0321}$
$\lvert V_{cb}\rvert$	$0.04026^{+0.00181}_{-0.00033}$	$0.04026^{+0.00214}_{-0.00066}$	$0.04026^{+0.00247}_{-0.00099}$
$\lvert V_{cb'}\rvert$	$0.00^{+0.14}_{-0.00}$	$0.00^{+0.20}_{-0.00}$	$0.00^{+0.25}_{-0.00}$
$\lvert V_{td}\rvert$	$0.0086^{+0.0081}_{-0.0044}$	$0.0086^{+0.0160}_{-0.0084}$	$0.009^{+0.023}_{-0.009}$
$\lvert V_{ts}\rvert$	$0.040^{+0.016}_{-0.017}$	$0.040^{+0.038}_{-0.040}$	$0.040^{+0.060}_{-0.040}$
$\lvert V_{tb}\rvert$	$0.99918^{+0.00034}_{-0.01537}$	$0.99918^{+0.00084}_{-0.04095}$	$0.9992^{+0.0011}_{-0.0681}$
$\lvert V_{tb'}\rvert$	$0.00^{+0.17}_{-0.00}$	$0.00^{+0.28}_{-0.00}$	$0.00^{+0.36}_{-0.00}$
$\lvert V_{t'd}\rvert$	$0.000^{+0.051}_{-0.000}$	$0.000^{+0.071}_{-0.000}$	$0.000^{+0.085}_{-0.000}$
$\lvert V_{t's}\rvert$	$0.00^{+0.14}_{-0.00}$	$0.00^{+0.20}_{-0.00}$	$0.00^{+0.25}_{-0.00}$
$\lvert V_{t'b}\rvert$	$0.00^{+0.17}_{-0.00}$	$0.00^{+0.28}_{-0.00}$	$0.00^{+0.36}_{-0.00}$
$\lvert V_{t'b'}\rvert$	$1.0000^{+0.0010}_{-0.0172}$	$1.0000^{+0.0020}_{-0.0453}$	$1.0000^{+0.0028}_{-0.0748}$

Table 5.4.: 1 , 2 and 3 σ constraints on moduli of CKM matrix elements if only Tree Level inputs are used in the fit. The minimum χ^2 in the fit is $\chi^2_{\text{min}} = 7.3682$.

	1 σ	2 σ	3 σ
δ	$(69.9^{+8.0}_{-8.6})^\circ$	$(70^{+16}_{-18})^\circ$	$(70^{+22}_{-28})^\circ$
	$(249.8^{+7.4}_{-9.2})^\circ$	$(250^{+15}_{-18})^\circ$	$(250^{+22}_{-28})^\circ$

Table 5.5.: Limits on δ as obtained in the Tree Level fit. Note the $\pm\pi$ ambiguity.

	1 σ	2 σ	3 σ
α	$(84^{+42}_{-39})^\circ$		
	$(-50^{+32}_{-29})^\circ$		
β	$(25^{+43}_{-76})^\circ$		

Table 5.6.: Limits on α and β as obtained in the Tree Level fit. No part of the interval $[-\pi, \pi]$ is excluded at 2σ level.

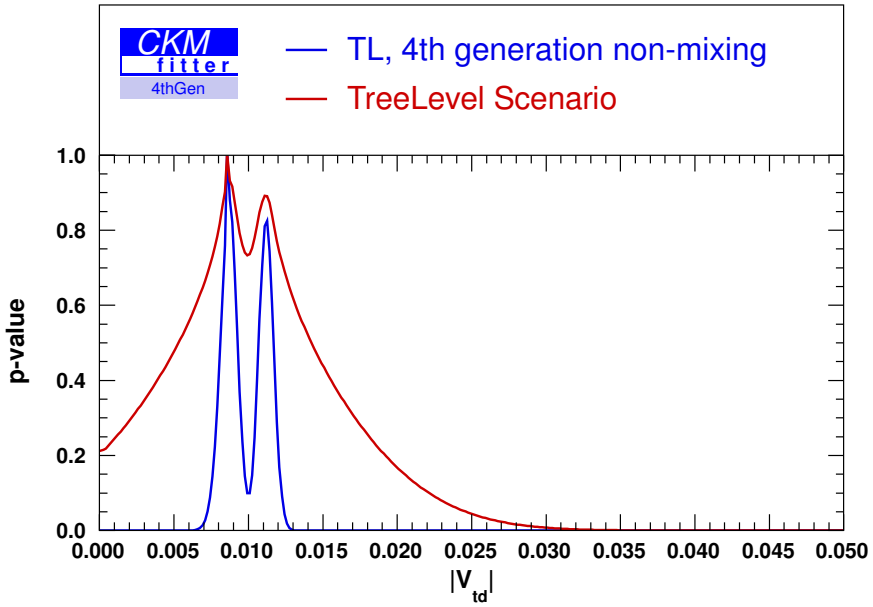

(a) 1D p-value graph. The dip is more pronounced if the angles describing mixing with the 4th generation are set to zero.

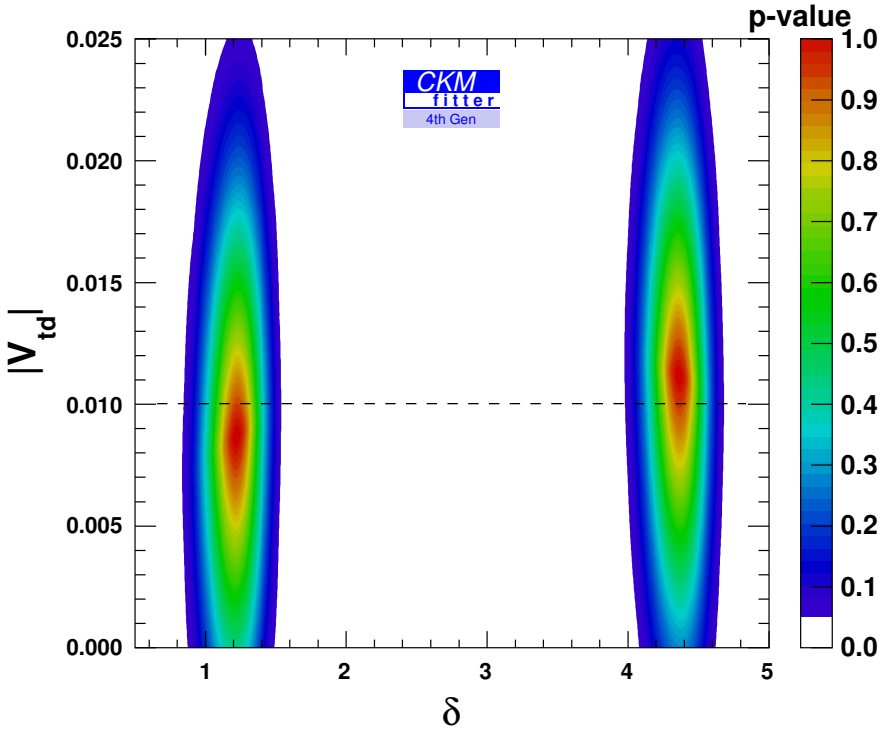

(b) Correlation with δ.

Figure 5.1.: Dip in p-Value graph of $|V_{td}|$ in the TL set of inputs (red curve in a)) and in a modified TL set of inputs in which the 4th generation quarks are not allowed to mix ($\theta_u = \theta_v = \theta_w = 0$, SM3 limit). The latter graph is the blue curve in a).

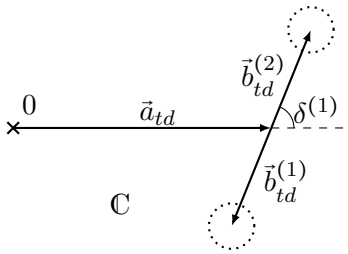

Figure 5.2.: Illustration of the discussion of the "dip" in the p-value plot of $|V_{td}|$, roughly to scale. As γ and hence δ are only determined up to a phase factor π, $|V_{td}|$ can assume two different values. The dashed circles around $\vec{a}_{td} + \vec{b}_{td}$ indicate the contribution by the other three summands which contain a factor $e^{\mathrm{i}\,\phi_3}$ with ϕ_3 unconstrained in the TL set.

5.2. More Input: CP-*non*violating Loop Observables

This is the second step of the programme outlined at the beginning of the present Chapter, i.e. the LoopNoCPV set of inputs. Now that the mass of the t' quark is present in the loop expressions (cf. Section 4.2), this mass can in principle be constrained. Mostly, this constraint is due to the Electroweak Precision fit (cf. Section 4.2.1) which enters the input set in the shape of the Lookup Table discussed in sec. 4.2.1, i.e. a correlated constraint on $|V_{tb'}|$ and the mass of the t' quark.

5.2.1. The Effects of the Electroweak Precision Fit

The input from the Electroweak Precision Fit differs from the other inputs added in the LoopNoCPV set of inputs in two ways. Firstly, no Electroweak Observables are actually included as inputs in the fits presented in this work. Instead, the correlated constraints on $|V_{t'b}|$ and $m_{t'}$ are provided by the lookup table described in sec. 4.2.1. In that sense, the Electroweak Precision fit could be described as a "black box". Secondly, as far as the CKM matrix itself is concerned, the EWP input constrains only one CKM matrix element directly and thus is rather like a Tree Level input (which it physically certainly is not!). All other inputs in the present section 5.2 - and also all of the next sets - constrain *linear combinations of products of CKM matrix elements* as will be described below. As the rather tight constraint on $|V_{t'b}|$ has, by means of the unitarity of the CKM matrix, a notable effect on the limits on other matrix elements, it seems advisable to perform another series of fits combining the inputs from the previous chapter with only the EWP input - from the fit program's point of view, an "effective Tree Level" fit - to identify the EWP input's effect on the fit results. As the lookup table from the Electroweak Precision fit contains *two* preferred t' mass ranges, the constraint on $|V_{t'b}|$ - and hence, by unitarity, also on other $|V_{ij}|$ - depends on this mass. Therefore, this fit was performed once for $\bar{m}_{t'} = 300 \pm 5$ GeV and once for $\bar{m}_{t'} = 900 \pm 5$ GeV. Typically, $\chi^2_{\text{min}} \approx 7.373$ and $\chi^2_{\text{min}} \approx 7.41$, respectively. This constitutes an increase over the χ^2_{min} of the TL scenario of less than 1 permille and 5 permille respectively. Relative to $\chi^2_{\text{min}} = 0.7840$ obtained with TL inputs without $\mathcal{B}(W \to \ell\nu)$, the increase is still below 1% and around 5%, respectively. The smallness of the increase is not surprising as m'_t does not enter any observables in the TL input set and unitarity still allows plenty of freedom for the 4th row and column matrix elements. Where limits changed compared to the "pure" Tree Level scans of the previous section, the new values are given in Table 5.7. In short, the last two rows of the CKM matrix are better constrained with the exact effect depending on $m_{t'}$. The phases ϕ_2 and ϕ_3 are still not constrained.

5.2.2. Constraining More Phases

All inputs of the LoopNoCPV set except the Electroweak Precision Fit's result are described by the absolute values of linear combinations of products of CKM matrix elements λ_q^M of the form

$$\left| \sum_q \left(\lambda_q^M\right)^{p(q)} \cdot \varrho_q \right| \tag{5.7}$$

	$m_{t'}$/GeV	1 σ	2 σ	3 σ
$\lvert V_{td}\rvert$	300	$0.0086^{+0.0063}_{-0.0042}$	$0.009^{+0.012}_{-0.009}$	$0.009^{+0.018}_{-0.009}$
	900	$0.0086^{+0.0052}_{-0.0021}$	$0.0086^{+0.0063}_{-0.0024}$	$0.0086^{+0.0071}_{-0.0033}$
$\lvert V_{ts}\rvert$	300	$0.040^{+0.012}_{-0.012}$	$0.040^{+0.028}_{-0.029}$	$0.040^{+0.045}_{-0.040}$
	900	$0.0396^{+0.0088}_{-0.0082}$	0.040 ± 0.011	$0.040^{+0.011}_{-0.014}$
$\lvert V_{tb}\rvert$	300	$0.99909^{+0.00035}_{-0.00786}$	$0.99909^{+0.00083}_{-0.02172}$	$0.9991^{+0.0012}_{-0.0354}$
	900	$0.9984^{+0.0010}_{-0.0012}$	$0.9984^{+0.0015}_{-0.0016}$	$0.9984^{+0.0019}_{-0.0022}$
$\lvert V_{tb'}\rvert$	300	$0.0132^{+0.1133}_{-0.0043}$	$0.0132^{+0.1951}_{-0.0064}$	$0.0132^{+0.2519}_{-0.098}$
	900	$0.0396^{+0.0211}_{-0.0048}$	$0.040^{+0.027}_{-0.031}$	$0.040^{+0.034}_{-0.033}$
$\lvert V_{t'd}\rvert$	900	$0.000^{+0.051}_{-0.000}$	$0.000^{+0.071}_{-0.000}$	$0.000^{+0.085}_{-0.000}$
$\lvert V_{t's}\rvert$	900	$0.03^{+0.11}_{-0.03}$	$0.03^{+0.18}_{-0.03}$	$0.03^{+0.22}_{-0.03}$
$\lvert V_{t'b}\rvert$	300	$0.00132^{+0.1131}_{-0.0024}$	$0.0132^{+0.1948}_{-0.0048}$	$0.0132^{+0.2517}_{-0.0072}$
	900	$0.0396^{+0.0204}_{-0.0048}$	$0.040^{+0.025}_{-0.031}$	$0.040^{+0.032}_{-0.033}$
$\lvert V_{t'b'}\rvert$	300	$0.99991^{+0.00084}_{-0.01134}$	$0.9999^{+0.0016}_{-0.0290}$	$0.9999^{+0.0023}_{-0.0478}$
	900	$0.9992^{+0.0013}_{-0.0104}$	$0.9992^{+0.0023}_{-0.0212}$	$0.9992^{+0.0030}_{-0.0326}$

Table 5.7.: 1 , 2 and 3 σ constraints on moduli of CKM matrix elements obtained by combining the Tree Level inputs combined only with the LUT from the electroweak precision fit. $|V_{ij}|$ which are not included did not change appreciably compared to the "pure" Tree Level fits. As the LUT contains two preferred mass ranges, the fit was performed for two values of $m_{t'}$ The minimum χ^2 in the fit is $\chi^2_{\text{min}} = 7.373$ for $m_{t'} = 300 \pm 5$ GeV and $\chi^2_{\text{min}} = 7.40$ for $m_{t'} = 900 \pm 5$ GeV. In case of $|V_{t'b}|$ and $|V_{tb'}|$, there is another area just above the 1 σ level where the matrix element is almost zero (see plots in sec. 5.5.1). This stems directly from the EWP lookup table.

(cf. eq. (2.100)). The $p(q)$ only serves as a reminder that in some expressions, squares of λ_q^M occur (**p**ower) and the ϱ represents any coefficients of the λ_q^M such as (products of) Inami-Lim functions, QCD correction factors and similar. As the moduli of all CKM matrix elements are more or less fixed by the Tree Level inputs already and constrained further by the EWP input, the "levers" by which a term like the expression for $\mathcal{B}(B \to \mu^+\mu^-)$ (cf. eq. (4.76)) can be brought to reflect the value observed by experiment are

- Changing the values of QCD corrections or masses, so that the coefficients ϱ_q of the $\lambda_{\hat{u}}^M$ bring the expression to the correct value.
- Adjusting any free phase differences between the individual $\lambda_{\hat{u}}^M$ occuring in the expression.

Obviously, the first approach is at best very limited: Particle masses and QCD corrections are mostly rather well constrained already. The second approach is what actually happens in the global fit of the CKM matrix. Obviously, a single observable of the form (5.7) will always lead to ambiguous constraints on the phases of the summands, so combining it with others of the same kind or an input like γ is desirable. Varying masses or corrections do indeed play a role, but rather as a nuisance which *limits* the precision one can obtain on the phase differences of the $\lambda_{\hat{u}}^M$. The λ_q^M which occur in the observables of this section (cf. the SM4 expressions given in section 4.2) are given in Table 5.8. Their CKM phases can again be read off their dominant summands as given in Tables 5.3 and the parametrisation (eq. (2.43)), respectively. If several summands of a CKM matrix element are of comparable size and different phase, the resulting phase of the $\lambda_{\hat{u}}^M$ depends on each of those as in case of $\lambda_t^{B_d}$. The phases of the numerically relevant summands are also listed in Table 5.8. Even if the relative phase of two $\lambda_{\hat{u}}^M$ in a theoretical expression can be expressed in terms of a phase used in the parametrization, an angle of the Unitarity Triangle or similar, there is no guarantee that it can be cleanly extracted. Similar to the summands of which the parametrisation of a CKM matrix element consist, both the magnitudes of the matrix elements forming the $\lambda_{\hat{u}}^M$ and the magnitude of the respective coefficient function play a role in this matter. If, say, the summand $\lambda_t^{B_d} \cdot Y(x_t, \mu_t^{(\ell\ell)})$ in the expression for $\mathcal{B}(B \to \mu^+\mu^-)$ (cf. eq. (4.76)) was very much smaller than the t' contribution $\lambda_{t'}^{B_d} \cdot Y(x_{t'}, \mu_t^{(\ell\ell)})$, then the phase difference between them would be impossible to measure.

In order to attribute the constraints obtained in a fit to a certain input (in other words: to assess the constraining power of an input), the relative magnitude of such summands was numerically compared. The magnitudes $\left|\lambda_{\hat{u}}^M\right|$ were determined by a global fit of the CKM matrix in which the Electroweak Precision Fit's result was combined with the Tree Level input scenario. As the Inami-Lim functions in the expressions for the observables $S_0(x_i, x_j)$ and $Y(x)$ as well as the Wilson coefficients C_7^{eff} depend on the mass of the quark occuring in the loop (see Appendix C), the t' mass may have a dramatic effect on the relative size of the summands in the expressions eqs. (4.59), (4.63), (4.69) and (4.76). As this relative size is crucial for the ability of such an input to constrain the phases ϕ_2 and ϕ_3, the relative size of the summands was again calculated in the two t' mass scenarios which were defined in sec. 5.2.1. The second mass should not be taken too seriously in a physical way as it is well beyond the mass range in which perturbative calculations as used here should be trusted. However, since the global fit seems to prefer high masses, this can be considered a legitimate scenario to simply estimate which observable is responsible for which constraint obtained in such a fit.

$\lambda_{\hat{u}}^{M}$	approximate phase(s)	$\left\lvert\lambda_{\hat{u}}^{M}\right\rvert\,(\bar{m}_t' = 300\text{ GeV})$	$\left\lvert\lambda_{\hat{u}}^{M}\right\rvert\,(\bar{m}_t' = 900\text{ GeV})$
$\lambda_t^{B_d} = V_{td}V_{tb}^*$	$a_{td} + b_{td}\cdot e^{\mathrm{i}\,\delta} + d_{td}\cdot e^{\mathrm{i}\,\phi_3}$	< 0.01	$\approx 0.01 \pm 0.004$
$\lambda_{t'}^{B_d} = V_{t'd}V_{t'b}^*$	$d_{t'd}\cdot e^{\mathrm{i}\,\phi_3}$	< 0.01	< 0.0035
$\lambda_t^{B_s} = V_{ts}V_{tb}^*$	$a_{ts} + b_{ts}\cdot e^{\mathrm{i}\,\delta} + c_{ts}\cdot e^{\mathrm{i}\,\phi_2}$	0.039 ± 0.028	0.040 ± 0.011
$\lambda_{t'}^{B_s} = V_{t's}V_{t'b}^*$	$c_{t's}\cdot e^{\mathrm{i}\,\phi_2}$	< 0.028	< 0.011
$\lambda_c^{B_s} = V_{cs}V_{cb}^*$	a_{cs}	0.0397 ± 0.0016	0.0397 ± 0.0016
$\left(\lambda_t^{B_d}\right)^2$	$\left(a_{td}^2 + b_{td}^2 e^{2\,\mathrm{i}\,\delta} + d_{td}^2 e^{2\,\mathrm{i}\,\phi_3} + 2a_{td}b_{td}e^{\mathrm{i}\,\delta} + 2a_{td}d_{td}e^{\mathrm{i}\,\phi_3} + 2b_{td}d_{td}e^{\mathrm{i}(\delta+\phi_3)}\right)\cdot a_{tb}^2$		
	$\approx \left(\mathcal{O}(0.5) + \mathcal{O}(0.1)e^{2\,\mathrm{i}\,\delta} + \mathcal{O}(0.01)e^{\mathrm{i}\,\phi_3} + \mathcal{O}(0.3)e^{\mathrm{i}\,\delta} + \mathcal{O}(0.1)e^{\mathrm{i}\,\phi_3} + \right.$		
	$\left. + \mathcal{O}(0.1)e^{\mathrm{i}(\delta+\phi_3)}\right)\cdot\left\lvert\lambda_t^{B_d}\right\rvert^2$		
$\left(\lambda_{t'}^{B_d}\right)^2$	$d_{t'd}^2 a_{t'b}^2 e^{2\,\mathrm{i}\,\phi_3}$		
$\left(\lambda_t^{B_s}\right)^2$	$\left(a_{ts}^2 + 2a_{ts}b_{ts}e^{\mathrm{i}\,\delta} + 2b_{ts}c_{ts}e^{\mathrm{i}\,\phi_2} + c_{ts}^2 e^{2\,\mathrm{i}\,\phi_2}\right)\cdot a_{tb}^2$		
	$\approx \left(\mathcal{O}(0.5) + \mathcal{O}(0.01)e^{\mathrm{i}\,\delta} + \mathcal{O}(0.01)e^{\mathrm{i}(\delta+\phi_2)} + \mathcal{O}(0.5)e^{2\,\mathrm{i}\,\phi_2}\right)\cdot\left\lvert\lambda_t^{B_s}\right\rvert^2$		
$\left(\lambda_{t'}^{B_s}\right)^2$	$a_{t'b}^2 c_{t's}^2 e^{2\,\mathrm{i}\,\phi_2}$		
$\lambda_t^{B_d}\cdot\lambda_{t'}^{B_d}$	$a_{tb}a_{t'b}d_{t'd}e^{\mathrm{i}\,\phi_3}\left(a_{td} + b_{td}e^{\mathrm{i}\,\delta} + d_{td}e^{\mathrm{i}\,\phi_3}\right)$		
	$\approx \left(\mathcal{O}(0.7)e^{\mathrm{i}\,\phi_3} + \mathcal{O}(0.3)e^{\mathrm{i}(\phi_3+\delta)} + \mathcal{O}(0.1)e^{2\,\mathrm{i}\,\phi_3}\right)\left\lvert\lambda_t^{B_d}\right\rvert\left\lvert\lambda_{t'}^{Bd}\right\rvert$		
$\lambda_t^{B_s}\cdot\lambda_{t'}^{B_s}$	$a_{tb}a_{t'b}c_{t's}e^{\mathrm{i}\,\phi_2}\left(a_{ts} + b_{ts}e^{\mathrm{i}\,\delta} + c_{ts}e^{\mathrm{i}\,\phi_2}\right)$		
	$\approx \left(\mathcal{O}(0.5)e^{\mathrm{i}\,\phi 2} + \mathcal{O}(0.01)e^{\mathrm{i}(\delta+\phi_2)} + \mathcal{O}(0.5)e^{2\,\mathrm{i}\,\phi_2}\right)\left\lvert\lambda_t^{B_s}\right\rvert\left\lvert\lambda_{t'}^{Bs}\right\rvert$		

Table 5.8.: Approximate phases of the $\lambda_{\hat{u}}^{M}$ which occur in the observables of sec. 5.2. The notation is as described just after eq. (5.5). The magnitudes in the 3rd and 4th column were determined in a global fit with the Tree Level set of inputs augmented by the result of the Electroweak Precision fit. Either a best-fit value with 2-σ error or, if the best-fit value is zero, the 2σ upper limit is given. The lower section gives the most important contributions to the phases of products of $\lambda_{\hat{u}}^{M}$ for a coarse estimation of the constraints on phases provided by an input.

Fit results of the $\left|\lambda_{\hat{u}}^{M}\right|$ are also given in Table 5.8. The coefficient functions of the $\lambda_{\hat{u}}^{M}$ were then evaluated at the same $\bar{m}_{t'}$. The resulting hierarchy of the contributions to each observable is given in Table 5.9. As can be seen, there is no individual summand of any of the theoretical expressions predicting an observable which can a priori be neglected, possibly excepting the t' quark contribution of $\frac{\mathcal{B}(B\to X_s\gamma)}{\mathcal{B}(B\to X_c e\bar{\nu})}$. This was checked not to change when the rather loosely constrained input parameter $\mu_t^{(\ell\ell)}$ is varied throughout its allowed range (cf. Tab. 5.2).

As δ is fixed by the γ input already in the TL set of inputs, the lower section of Table 5.9 shows that the inputs Δm_d and $\mathcal{B}(B_d \to \mu^+ u^-)$ can be expected to constrain ϕ_3 while Δm_s, $\mathcal{B}(B_s \to \mu^+ u^-)$ and the ratio $\frac{\mathcal{B}(B\to X_s\gamma)}{\mathcal{B}(B\to X_c e\bar{\nu})}$ should constrain ϕ_2.

5.2.3. Global Fit Results

With the addition of six new inputs, some of which have quite a history of being used to constrain New Physics, the χ^2_{min} value achieved in these fits is slightly higher than in the TL fits at 7.70. To put this in perspective, Table 5.10 contains the χ^2_{min} values achieved in a number of modifications of the TL and LoopNoCPV input sets. As shown there, the lion's share of the TL χ^2_{min} comes from the $\mathcal{B}(W \to \ell\nu)$ input (see also sec. 5.1.2 and 6.3). Compared to the "rest" given in the TL$\backslash\mathcal{B}(W \to \ell\nu)$ column, the increase from adding the Electroweak Precision Fit is not a marginal increase but quite a "jump". The same is true for the χ^2 increase from adding only the non-EWP inputs from the LoopNoCPV set (fourth column). The EWP input seems to have more impact on the χ^2_{min} obtained in the LoopNoCPV set than in the TL set. This is because the t' quark mass now enters the expressions for the observables via the Inami-Lim functions and, therefore, the EWP input does not only put an upper limit on $|V_{t'b}|$ as in the TL input set. The constraint placed on the phase ϕ_3 causes some tension between unitarity and the relative phase of the summands of e.g. V_{td}. The mechanisms involved will be discussed below in more detail. The constraints on the moduli of the CKM matrix elements enforced by the LoopNoCPV input set are shown in Table 5.11. Constraints on angles of the unitarity triangle, phases and other parameters are given in Table 5.12.

It turns out that, while ϕ_3 does indeed receive some constraints (cf. Tab. 5.12 and Fig. 5.7 a)), ϕ_2 does not. This difference can be explained as follows: ϕ_3 is constrained by Δm_d (relative uncertainty $\delta(\Delta m_d) \approx 0.78\%$) and $\mathcal{B}(B_d \to \mu^+\mu^-)$ (relative uncertainty $\delta(\mathcal{B}(B_d \to \mu^+\mu^-)) \approx 42\%$). Looking at Tables 5.8 and 5.9, one sees that none of the contributions given in the latter can be neglected. The lower part of Tab. 5.8 reveals that the terms carrying the free phase ϕ_3 - i.e. $2a_{td}d_{td}\cdot a_{tb}^2$, $2b_{td}d_{td}\cdot a_{tb}^2$, $d_{t'd}^2 a_{t'b}^2$ and $a_{tb}a_{t'b}d_{t'd}d_{td}$ - contribute to the whole expression in eq. (4.59) (and thus Δm_d) on a scale comparable to terms with a previously constrained phase δ or 0. The precise Δm_d input can therefore constrain ϕ_3. ϕ_2, on the other hand, occurs in the expressions for Δm_s (relative uncertainty $\delta(\Delta m_s) \approx 0.13\%$), $\frac{\mathcal{B}(B\to X_s\gamma)}{\mathcal{B}(B\to X_c e\bar{\nu})}$ (relative uncertainty $\approx 6.5\%$) and $\mathcal{B}(B_s \to \mu^+\mu^-)$ (relative uncertainty $\delta(\mathcal{B}(B_s \to \mu^+\mu^-)) \approx 24\%$). Starting with the most precisely measured input Δm_s and again consulting Table 5.8, one again finds that no contribution in Table 5.9 is negligible. The lower part of Table 5.8, however, shows that almost all terms contributing to Δm_s as described by eq. (4.63) carry a phase of ϕ_2 or $2\phi_2$. Therefore, the total magnitude of terms with another phase is relatively small, rendering the precise input powerless to constrain ϕ_2. The ratio $\frac{\mathcal{B}(B\to X_s\gamma)}{\mathcal{B}(B\to X_c e\bar{\nu})}$ suffers from a similar problem. Here, the approximately real c quark

Contrib. to $M_{12}^{B_d}$	$S_0(x_t)\ {\lambda_t^{B_d}}^2$	$2S_0(x_t, x_{t'})\lambda_t^{B_d}\lambda_{t'}^{B_d}$	$S_0(x_{t'})\ {\lambda_{t'}^{B_d}}^2$
$\bar{m}_{t'}$ = 300 GeV	0.40	0.45	0.14
$\bar{m}_{t'}$ = 900 GeV	0.29	0.39	0.32
Contrib. to $M_{12}^{B_s}$	$S_0(x_t)\ {\lambda_t^{B_s}}^2$	$2S_0(x_t, x_{t'})\lambda_t^{B_s}\lambda_{t'}^{B_s}$	$S_0(x_t{}')\ {\lambda_{t'}^{B_s}}^2$
$\bar{m}_{t'}$ = 300 GeV	0.50	0.41	0.09
$\bar{m}_{t'}$ = 900 GeV	0.48	0.36	0.17
Contrib. to $\frac{\Gamma(b\to s\gamma)}{\Gamma(b\to ce\bar{\nu})}$	$\lambda_c^{B_s} C_7^{\text{eff},3}(\mu)$	$\lambda_t^{B_s}(C_7^{\text{eff},1} + C_7^{\text{eff},2})$	$\lambda_{t'}^{B_s}(C_7^{\text{eff},1} + C_7^{\text{eff},2})$
$\bar{m}_{t'}$ = 300 GeV	0.83	0.12	0.06
$\bar{m}_{t'}$ = 900 GeV	0.83	0.12	0.06
Contrib. to $\mathcal{B}(B_d \to \mu^+\mu^-)$	$\lambda_t^{B_d} Y(x_t, \mu_t^{(\ell\ell)})$	$\lambda_{t'}^{B_d} Y(x_{t'}, \mu_t^{(\ell\ell)})$	
$\bar{m}_{t'}$ = 300 GeV	0.53	0.47	
$\bar{m}_{t'}$ = 900 GeV	0.21	0.79	
Contrib. to $\mathcal{B}(B_s \to \mu^+\mu^-)$	$\lambda_t^{B_s} Y(x_t, \mu_t^{(\ell\ell)})$	$\lambda_{t'}^{B_s} Y(x_{t'}, \mu_t^{(\ell\ell)})$	
$\bar{m}_{t'}$ = 300 GeV	0.61	0.39	
$\bar{m}_{t'}$ = 900 GeV	0.33	0.67	

Table 5.9.: Relative Magnitudes of the contributions to the observables added in the "CPV-nonviolating loop observables" series of fits. "Relative Magnitude" here means that the number given is the size of the contribution normalized to the sum of the moduli of all contributions of an expression.

Input set	TL\$\mathcal{B}(W \to \ell\nu)$	TL	TL + EWP	LnoCPV\ EWP	LnoCPV
χ^2_{min}	0.7840	7.3682	≈ 7.40	7.58	7.70

Table 5.10.: Comparison of χ^2_{min} values achieved with different input configurations. A backslash \ is to be understood as "without".

	1 σ	2 σ	3 σ
$\lvert V_{ud}\rvert$	$0.97419^{+0.00033}_{-0.00029}$	$0.97419^{+0.00054}_{-0.00057}$	$0.97419^{+0.00069}_{-0.00085}$
$\lvert V_{us}\rvert$	$0.2247^{+0.0015}_{-0.0016}$	$0.2247^{+0.0021}_{-0.0022}$	$0.2247^{+0.0027}_{-0.0028}$
$\lvert V_{ub}\rvert$	$0.00397^{+0.00012}_{-0.00032}$	$0.00397^{+0.00023}_{-0.00067}$	$0.00397^{+0.00035}_{-0.00081}$
$\lvert V_{ub'}\rvert$	$0.021^{+0.018}_{-0.017}$	$0.021^{+0.026}_{-0.021}$	$0.021^{+0.032}_{-0.021}$
$\lvert V_{cd}\rvert$	$0.2246^{+0.0015}_{-0.0042}$	$0.2246^{+0.0015}_{-0.0092}$	$0.2246^{+0.0035}_{-0.0133}$
$\lvert V_{cs}\rvert$	$0.97368^{+0.0004}_{-0.00328}$	$0.97368^{+0.00061}_{-0.00964}$	$0.97368^{+0.00082}_{-0.02411}$
$\lvert V_{cb}\rvert$	$0.04027^{+0.00177}_{-0.00034}$	$0.04027^{+0.00211}_{-0.00067}$	$0.04027^{+0.00245}_{-0.00100}$
$\lvert V_{cb'}\rvert$	$0.005^{+0.085}_{-0.005}$	$0.005^{+0.145}_{-0.005}$	$0.005^{+0.21}_{-0.005}$
$\lvert V_{td}\rvert$	see text	$0.0086^{+0.0065}_{-0.0018}$	$0.0086^{+0.0119}_{-0.0074}$
$\lvert V_{ts}\rvert$	$0.03948^{+0.00228}_{-0.00078}$	$0.0395^{+0.0044}_{-0.0047}$	$0.039^{+0.016}_{-0.019}$
$\lvert V_{tb}\rvert$	$0.99785^{+0.00090}_{-0.00106}$	$0.9978^{+0.0016}_{-0.0164}$	$0.9978^{+0.018}_{-0.0458}$
$\lvert V_{tb'}\rvert$	$0.055^{+0.013}_{-0.026}$	$0.055^{+0.130}_{-0.046}$	$0.055^{+0.246}_{-0.048}$
$\lvert V_{t'd}\rvert$	$0.021^{+0.027}_{-0.011}$	$0.021^{+0.045}_{-0.021}$	$0.021^{+0.060}_{-0.021}$
$\lvert V_{t's}\rvert$	$0.007^{+0.075}_{-0.007}$	$0.007^{+0.143}_{-0.007}$	$0.007^{+0.203}_{-0.007}$
$\lvert V_{t'b}\rvert$	$0.054^{+0.015}_{-0.024}$	$0.054^{+0.134}_{-0.043}$	$0.054^{+0.249}_{-0.045}$
$\lvert V_{t'b'}\rvert$	$0.99829^{+0.00097}_{-0.00337}$	$0.9983^{+0.0017}_{-0.0179}$	$0.9983^{+0.0021}_{-0.0471}$

Table 5.11.: 1 , 2 and 3 σ constraints on moduli of CKM matrix elements if the inputs from CP-nonviolating loop observables are added to the Tree Level inputs. The minimum χ^2 in the fit is $\chi^2_{\rm min} = 7.70$.

loop contribution dominates already in Tab. 5.9 so that terms carrying a phase of ϕ_2 or $2\phi_2$ - according to Tab. 5.8 - will not contribute much to eq. (4.69). Once more, this results in an unfavorable condition to constrain ϕ_2. The situation is similar in case of $\mathcal{B}(B_s \to \mu^+\mu^-)$ where it is compounded by the large error of the input.

Having explained the failure of the LoopNoCPV set of inputs to constrain ϕ_2 in any way, one's attention can turn once more to the p-value plot of $|V_{td}|$ whose structure gets even more interesting than in the previous section: The peak develops a distict "Trident" shape with incisions falling below the 1-σ level as shown in Fig. 5.3 a). The reason can be found by looking at the new constraints on ϕ_3 given in Table 5.12: The ambiguity in δ, together with the three distinct preferred values of ϕ_3, coincide so that three distinct ranges of preferred values of $|V_{td}|$ arise - see also Fig. 5.4 as an illustration.

The ambiguity in δ is now under pressure from unitarity: With $|V_{td}|$ more strictly constrained from above (an effect of the Electroweak Precision input, see Tab. 5.7), $\delta = 1.20$ is now favoured over $\delta = 4.35$. $\delta = 1.20$ leads to smaller $|V_{td}|$ - see also the correlation plot Fig. 5.3 b). This is reflected in the p-value contour of γ. The ambiguity in the LUT is partially resolved - see δ plot in section 5.5.2.

The fit result $m_{t'} = 986.6^{+2.4}_{-436.1}$ now gives a justification for using $m_{t'} = 900$ GeV as one mass scenario in the previous section. While dubious with regard to perturbation theory as stated above, the fit slightly prefers high mass values and if understanding the result of a fit to whatever flawed model is a step to understanding the physics, then setting $m_{t'}$ =900 GeV is part of the analysis needed here. Also, the constraint on the mass is not really different from what is used as an input in the LUT, indicating that, in the LoopNoCPV series of fits, the flavour observables do not place additonal constraints on $m_{t'}$: No part of the interval allowed for $\bar{m}_x$ is excluded even at the 2 σ level.

The LoopNoCPV set of inputs also allows a first prediction of a^d_{SL} and a^s_{SL}. The ambiguity in the prediction of a^d_{SL} (see Table 5.12 and Fig. 5.5) is due to the ambiguity in γ and thus δ. E.g. by replacing the γ input by a δ input which constrains it to one of the two preferred intervals given in Table 5.5, it can be shown that the 1 σ interval $a^d_{SL} = -0.0122^{+0.0041}_{-0.0043}$ corresponds to $\delta = 4.37^{+0.12}_{-0.17}$ while $a^d_{SL} = -0.0054^{+0.0067}_{-0.0039}$ corresponds to $\delta = 1.24^{+0.14}_{-0.16}$. The phases of the matrix elements which occur in the expression for a^d_{SL} are functions of δ and ϕ_3 (cf. Sec. 4.3.4, eq. (2.43)). The dependence on δ agrees well with the observation just described. The dependence on ϕ_3 reflects the correlation of δ and ϕ_3 in the LoopNoCPV set. That said, the prediction in the LoopNoCPV series of fits covers the experimental central value with its own 1 σ interval while lying slightly above the experimental value's own 1 σ limit. The prediction of a^s_{SL} does not show any ambiguities. It is covered by the experimental input's 1σ range, but its own uncertainty does not cover the central value of the experimental input.

With ϕ_3 constrained, another prediction of the angles α and β of the Unitarity Triangle and the SM4 "contamination" of β and θ_d (cf. section 4.3.2) was attempted. The results are displayed in Table 5.12 and, as they cannot be described simply in terms of a central value and an uncertainty interval, the p-value plots are shown in Fig. 5.7 together with that of ϕ_3.

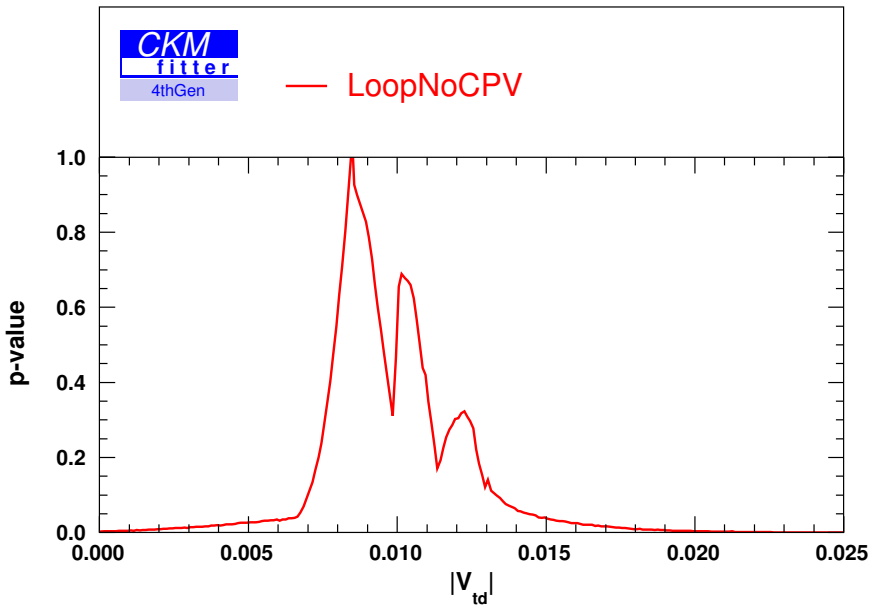

(a) The conspicuous "trident" contour of $|V_{td}|$'s p-value.

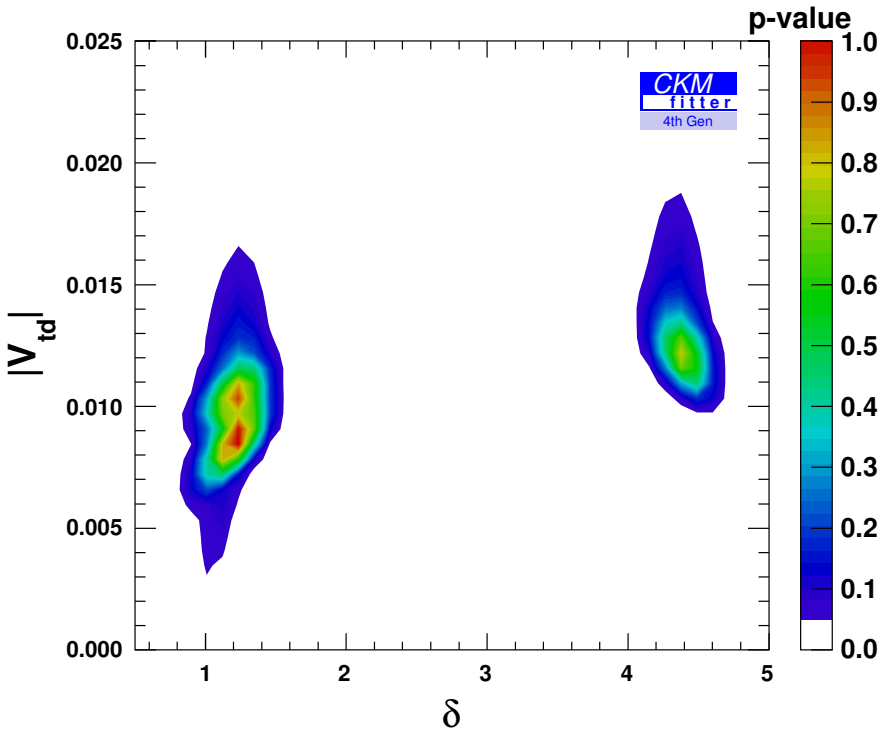

(b) Correlation of $|V_{td}|$ and δ.

Figure 5.3.: P-value plots of $|V_{td}|$ in the LoopNoCPV series of fits.

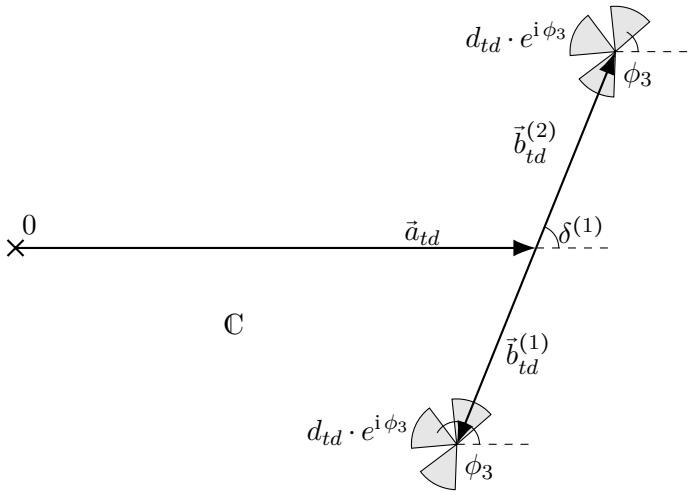

Figure 5.4.: Sketch to explain the "trident" structure in Fig. 5.3, roughly to scale. Instead of an unconstrained ϕ_3 as in the TL series of fits which leads to the dip explained in the previous section, there are now preferred and disfavoured ranges of ϕ_3 (see also Tab. 5.12). The preferred ranges are indicated as gray arcs. As $|V_{td}|$ corresponds to the modulus of the sum of the complex numbers drawn here, the fit of this quantity can indeed lead to the observed pattern.

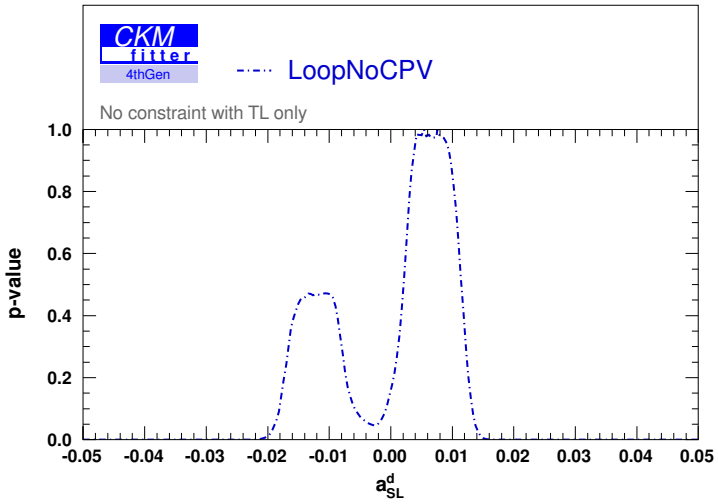

Figure 5.5.: Constraint on a_{SL}^d predicted in the LoopNoCPV series of fits. The ambiguity reflects the ambiguity in δ and thus the γ input.

	1σ	2σ	3σ
$\bar{m}_x$ [GeV]	$986.6^{+2.4}_{-436.1}$	$986.6^{+3.4}_{-770.8}$	$986.6^{+3.6}_{-773.8}$
δ	$1.24^{+0.12}_{-0.18}$ $4.440^{+0.047}_{-0.123}$	$1.24^{+0.24}_{-0.33}$ $4.44^{+0.18}_{-0.27}$	$1.24^{+0.36}_{-0.50}$ $4.44^{+0.29}_{-0.46}$
ϕ_3	$1.00^{+0.67}_{-0.28}$ $2.70^{+0.53}_{-0.48}$ $4.42^{+0.26}_{-0.64}$	unconstrained	unconstrained
α	$1.35^{+0.48}_{-0.18}$	$1.35^{+1.02}_{-0.59}$	$1.3^{+1.7}_{-1.1}$
β	$0.313^{+0.067}_{-0.180}$ $-0.565^{+0.170}_{-0.088}$ $-0.461^{+0.018}_{-0.040}$	$0.313^{+0.86}_{-0.63}$ $0.472^{+0.094}_{-0.318}$ $-0.461^{+0.084}_{-0.332}$	0.5 ± 1.8
θ_d	-0.39 ± 0.22 $-0.024^{+0.111}_{-0.064}$ $0.39^{+0.34}_{-0.22}$	$0.39^{+1.62}_{-0.72}$	$-0.4^{+2.0}_{-1.2}$
a^d_{SL}	$0.0054^{+0.0067}_{-0.0039}$ $-0.0122^{+0.0041}_{-0.0043}$	$0.0054^{+0.0082}_{-0.0077}$ $-0.0122^{+0.0092}_{-0.0065}$	$0.0054^{+0.0097}_{-0.0265}$
a^s_{SL}	$(-9^{+22}_{-19}) \cdot 10^{-4}$	$(-9^{+45}_{-41}) \cdot 10^{-4}$	$(-9^{+59}_{-55}) \cdot 10^{-4}$

Table 5.12.: Constraints on SM4-related parameters obtained in the LoopNoCPV series of fits. See also Fig. 5.7 and the plots in Sec. 5.5.

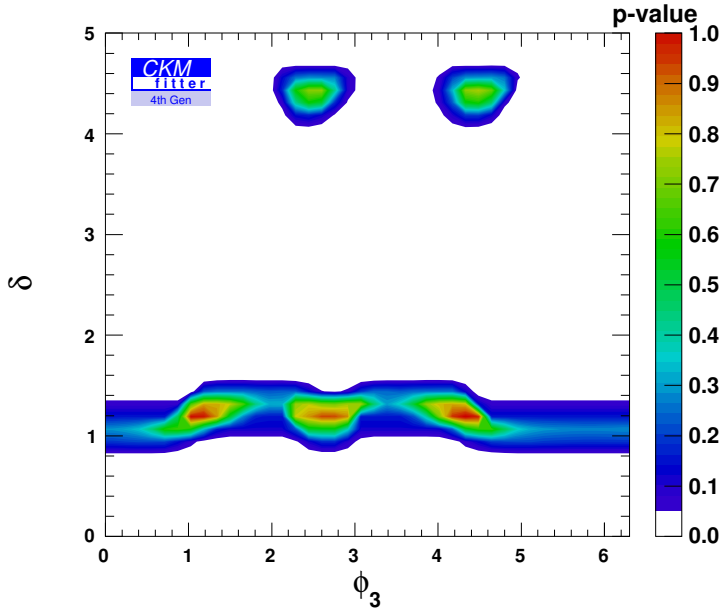

Figure 5.6.: Correlation of δ and ϕ_3 in the LoopNoCPV input set.

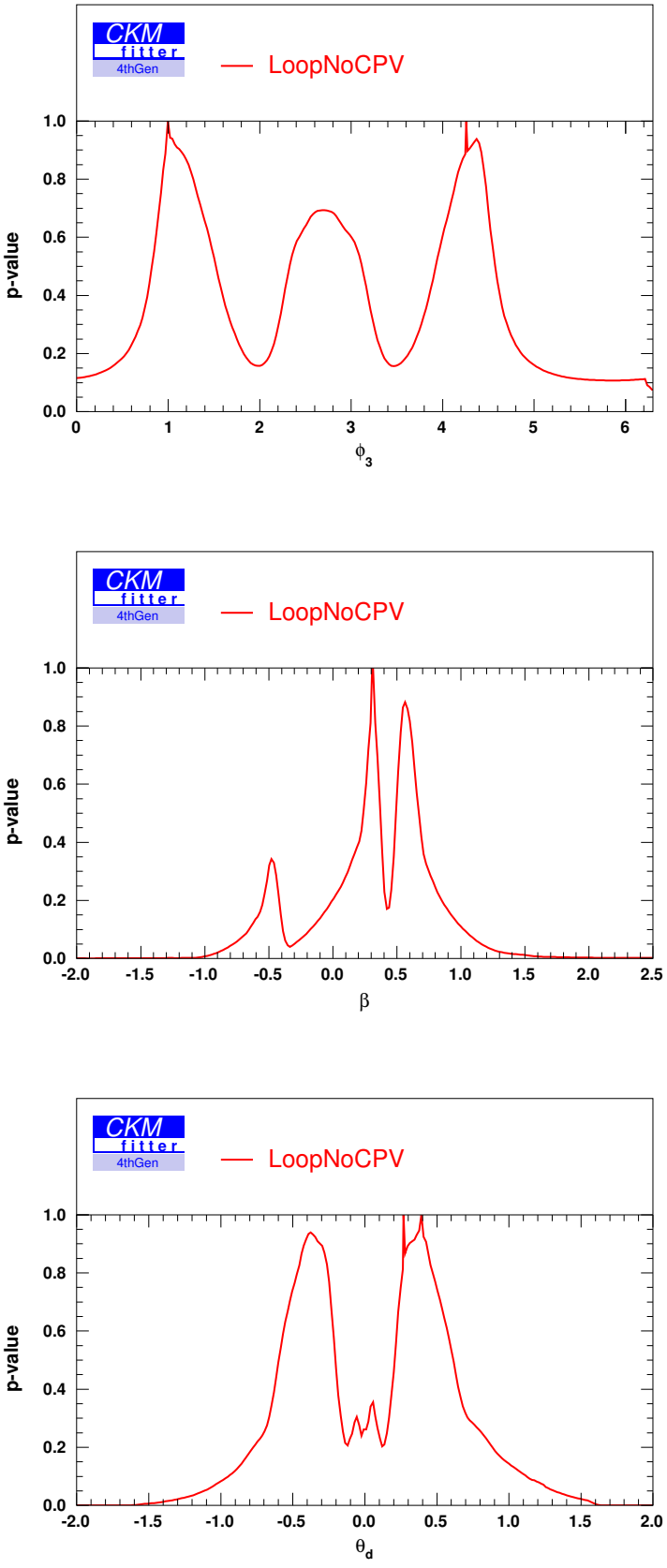

Figure 5.7.: P-value plots of ϕ_3, θ_d and the Unitarity Triangle β obtained with the LoopNoCPV set of inputs. For numerical values, see Table 5.12.

5.3. Adding CP Violating Loop Observables

While the fits of the previous section did not use any CP violating observables as input, those are added here. As stated at the beginning of this chapter, the inputs in question are $|\epsilon_K|$ and $\sin(2\beta - 2\theta_d)$. The CKM matrix elements occuring in $\sin(2\beta - 2\theta_d)$ are the same as in the B_d-system related variables in the previous section. It is therefore not to be expected that this input will constrain ϕ_2, but an improved constraint on ϕ_3 might be achieved. Unlike the Δm_d which measures the absolute value of

$$\eta_{tt}(\mu) S_0(x_t)\ {\lambda_t^{B_d}}^2 + 2\eta_{tt'}(\mu) S_0(x_t, x_{t'}) \lambda_t^{B_d} \lambda_{t'}^{B_d} + \eta_{t't'}(\mu) S_0(x'_t)\ {\lambda_{t'}^{B_d}}^2, \tag{5.8}$$

$\sin(2\beta - 2\theta_d)$ measures its phase (up to a negligible $2 \cdot \arg(V_{cd})$, cf. eqs. (4.109), (2.43) and Table 5.3). The two inputs thus complement each other.

$|\epsilon_K|$, from the neutral K system, does in principle provide a means to constrain ϕ_2. An analysis of relative magnitudes of contributions as in the "LoopNoCPV" section is made unfeasible by too many individual terms with too many different phases and similar magnitudes whose hierarchy depends sensitively on the mixing angles. However, looking at the structure of the CKM matrix in the Hou/Soni parametrisation - if necessary, aided by Table 5.3 - leads to following picture:

The matrix elements occurring in B_d system observables are marked in purple, those occurring

$$\begin{pmatrix} V_{ud} & V_{us} & V_{ub} & V_{ub'} \\ V_{cd} & V_{cs} & V_{cb} & V_{cb'} \\ V_{td} & V_{ts} & V_{tb} & V_{tb'} \\ V_{t'd} & V_{t's} & V_{t'b} & V_{t'b'} \end{pmatrix}$$

in B_s system observables are blue and anything appearing in $|\epsilon_K|$ is yellow. While the B_d system by itself can only constrain ϕ_3 and the B_s system observables used here are unable to even constrain ϕ_2, the neutral Kaon system connects these two sectors and might therefore constrain ϕ_2 indirectly. For any noticable effect on the fit results, no phase should dominate the expression for ϵ_K and good precision of the $|\epsilon_K|$ input is required. If this indirect constraint of ϕ_2 is indeed at work here, and if the inputs are precise enough, there should be a correlation between ϕ_2 and ϕ_3 in the fit result.

5.3.1. Fit results

The constraints on the moduli of CKM matrix elements obtained in the LoopCPV series are given in Table 5.13 while other constraints can be found in Table 5.14.

Comparing the one-dimensional p-value plots of ϕ_2 and ϕ_3 with the result of the two-dimensional scan of both phase angles (Fig. 5.8) shows that there is indeed a correlation visible now which had not been there in the LoopNoCPV scan. This lends some credibility to the mechanism of indirectly constraining ϕ_2 just described. The CKMfitter flags `globalMinSearches` and `nbOfFits` (cf. section 3.2.3) had to be set to extremely high values if fits were to be reproducible. This indicates either that, once more, a non-optimal parametrisation reaches the limits of its numerical

suitability for the problem, or that the input set used is hard-pressed to provide constraints on at least one particular parameter.

Compared to the LoopNoCPV result, the constraints on both a_{SL}^d and a_{SL}^s improve: The predictions read

$$a_{SL}^d = \left(5.9^{+5.5}_{-1.8}\right) \cdot 10^{-3} \quad \text{and} \quad a_{SL}^s = \left(-5.7^{+4.5}_{-9.9}\right) \cdot 10^{-4}. \tag{5.9}$$

They benefit from the almost complete resolution of the ambiguity in δ (see p-value plot in sec. 5.5.2) and the improved constraint on ϕ_3. Based on the respective width of the 1 σ interval, the relative uncertainty of $a_{SL}^d$is now reduced by more than a third and only about half that of the experimental result. This increases the tension between the prediction and the experimental value, but their 1 σ intervals still overlap. The prediction of a_{SL}^s is covered by the 1 σ range of the experimental result. The prediction's relative uncertainty is roughly 25% larger than the experimental input's, and its central value is only about 1/8 of the experimental central value. Finally, one can compare the SM4 predictions to the SM3 predictions given in [95] and the rest of Ref. [9] of [200]:

$$a_{SL}^d = (-4.1 \pm 0.6) \cdot 10^{-4} \qquad a_{SL}^s = (1.9 \pm 0.3) \cdot 10^{-4} \tag{5.10}$$

The SM3 predictions have a much smaller relative uncertainty - 15% vs. 123% in case of a_{SL}^d and 16% vs. 253% for a_{SL}^s. This "improves" the SM4's compatibility with the experimental inputs. The SM4 prediction of a_{SL}^d is of the correct order of magnitude and carries the correct sign, unlike the SM3 prediction. In case of a_{SL}^s, the SM4 prediction's central value is too small by a factor of roughly eight compared to a factor larger than 25 in the SM3 prediction. Also, the SM4 prediction is the one whose sign is correct. In that sense, the SM4 does better at predicting $a_{SL}^{d,s}$. There is now a preferred value of $\bar{m}_{t'}$ clearly below the upper limit of the allowed range. While this may indicate that there is now a constraint from above, it is not strong enough to have any pronounced effect even on the 1 σ range.

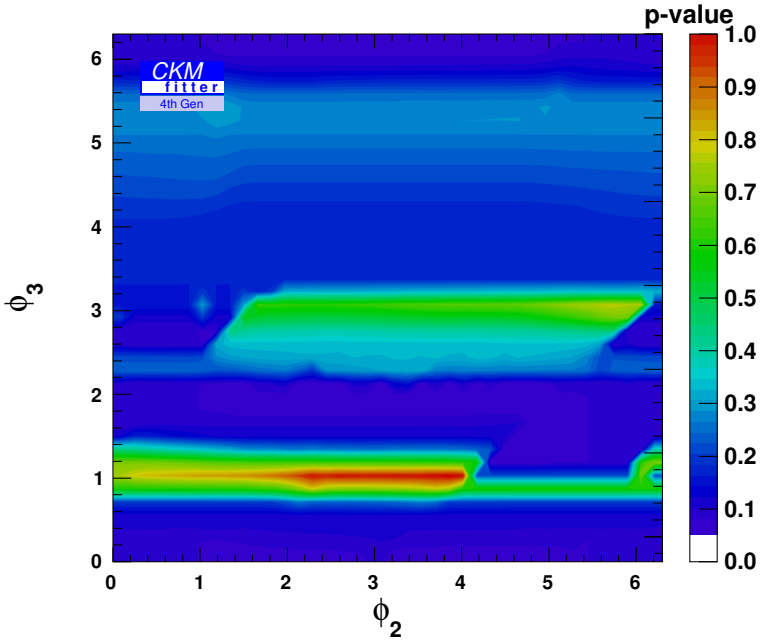

Figure 5.8.: 2-dimensonal p-value scan of ϕ_2 vs. ϕ_3 with the LoopCPV input set. While no combination of values is excluded even at 2 σ, there are clearly preferred values for both angles. As "predicted" in sec. 5.3, they are indeed correlated.

	1 σ	2 σ	3 σ
$\lvert V_{ud}\rvert$	$0.97416^{+0.00019}_{-0.00026}$	$0.97416^{+0.00038}_{-0.00055}$	$0.97416^{+0.00068}_{-0.00083}$
$\lvert V_{us}\rvert$	$0.22370^{+0.00144}_{-0.00071}$	$0.2237^{+0.0026}_{-0.0013}$	$0.2237^{+0.0034}_{-0.0019}$
$\lvert V_{ub}\rvert$	$0.00398^{+0.00012}_{-0.00032}$	$0.00398^{+0.00023}_{-0.00067}$	$0.00398^{+0.00035}_{-0.00081}$
$\lvert V_{ub'}\rvert$	$0.0296^{+0.0097}_{-0.0062}$	$0.030^{+0.016}_{-0.030}$	$0.030^{+0.023}_{-0.030}$
$\lvert V_{cd}\rvert$	$0.22282^{+0.00028}_{-0.00098}$	$0.2228^{+0.0035}_{-0.0020}$	$0.2228^{+0.0053}_{-0.0090}$
$\lvert V_{cs}\rvert$	$0.97382^{+0.00024}_{-0.00061}$	$0.97382^{+0.00042}_{-0.00572}$	$0.97382^{+0.00060}_{-0.02812}$
$\lvert V_{cb}\rvert$	$0.04029^{+0.00171}_{-0.00036}$	$0.04029^{+0.00207}_{-0.00069}$	$0.0403^{+0.0024}_{-0.0010}$
$\lvert V_{cb'}\rvert$	$0.009^{+0.015}_{-0.009}$	$0.009^{+0.093}_{-0.009}$	$0.01^{+0.20}_{-0.01}$
$\lvert V_{td}\rvert$	see text	$0.0085^{+0.0041}_{-0.0018}$	$0.0085^{+0.0083}_{-0.0072}$
$\lvert V_{ts}\rvert$	$0.03924^{+0.00281}_{-0.00071}$	$0.0392^{+0.0048}_{-0.0063}$	$0.039^{+0.018}_{-0.018}$
$\lvert V_{tb}\rvert$	$0.99785^{+0.00070}_{-0.00127}$	$0.9978^{+0.0015}_{-0.0062}$	$0.9978^{+0.0018}_{-0.0434}$
$\lvert V_{tb'}\rvert$	$0.051^{+0.019}_{-0.010}$	$0.051^{+0.070}_{-0.041}$	$0.051^{+0.249}_{-0.043}$
$\lvert V_{t'd}\rvert$	$0.0334^{+0.0101}_{-0.0055}$	$0.033^{+0.024}_{-0.031}$	$0.033^{+0.044}_{-0.033}$
$\lvert V_{t's}\rvert$	$0.011^{+0.023}_{-0.011}$	$0.011^{+0.094}_{-0.011}$	$0.01^{+0.21}_{-0.01}$
$\lvert V_{t'b}\rvert$	$0.049^{+0.022}_{-0.011}$	$0.049^{+0.073}_{-0.038}$	$0.049^{+0.246}_{-0.041}$
$\lvert V_{t'b'}\rvert$	$0.99807^{+0.00049}_{-0.00115}$	$0.9981^{+0.0020}_{-0.0065}$	$0.9981^{+0.0023}_{-0.0441}$

Table 5.13.: 1 , 2 and 3 σ constraints on moduli of CKM matrix elements after inputs from CP-violating loop observables $|\epsilon_K|$ and $\sin(2\beta - 2\theta_d)$ are added. The minimum χ^2 in the fit is $\chi^2_{\rm min} = 7.87$.

	$1\ \sigma$	$2\ \sigma$	3σ
$\bar{m}_x$/GeV	810^{+180}_{-261}	810^{+180}_{-590}	810^{+180}_{-600}
δ	1.21 ± 0.15	$1.21^{+0.26}_{-0.31}$ $4.2053^{+0.0123}_{-0.0036}$ $4.41^{+0.13}_{-0.15}$	$1.21^{+0.37}_{-0.48}$ $4.41^{+0.30}_{-0.38}$
ϕ_3	$1.00^{+0.18}_{-0.19}$ $3.01^{+0.13}_{-0.15}$	$1.00^{+0.42}_{-0.35}$ $3.01^{+2.86}_{-0.83}$	unconstrained
α	$1.29^{+0.26}_{-0.13}$	$1.29^{+0.55}_{-0.24}$	$1.29^{+0.75}_{-0.37}$ $2.48^{+0.45}_{-0.28}$
β	$0.642^{+0.040}_{-0.031}$ $0.378^{+0.014}_{-0.036}$	$0.642^{+0.140}_{-0.073}$ $0.38^{+0.16}_{-0.10}$	$0.64^{+0.17}_{-0.41}$
θ_d	$-0.555^{+0.042}_{-0.031}$ $-0.0005^{+0.0025}_{-0.0329}$	$-0.555^{+0.138}_{-0.074}$ $0.00^{+0.16}_{-0.10}$	$0.00^{+1.59}_{-1.59}$
$a^d_{SL}(\cdot 10^{-3})$	$5.9^{+5.5}_{-1.8}$	$5.9^{+6.6}_{-2.7}$	$5.9^{+7.5}_{-3.7}$ $-11.5^{+6.4}_{-5.8}$
$a^s_{SL}(\cdot 10^{-4})$	$-5.7^{+4.5}_{-9.9}$	-6^{+10}_{-17}	-6^{+38}_{-32}

Table 5.14.: Constraints on SM4-related quantities obtained in the LoopCPV series of fits.

5.4. All In: Including Semileptonic Charge Asymmetries

In this final step, the complete set of inputs chosen for this thesis will be used, i.e. a^s_{SL} (cf. Section 4.3.3) and a^d_{SL} (cf. Section 4.3.4) are added to the "LoopCPV" set. For the reasons given in Section 4.4.4, the dimuon charge asymmetry A_{SL} is not used as an input. A predicted value will be given below. The constraints on the moduli of CKM matrix elements and other SM4 related quantities from the complete set of inputs are given in Tables 5.15 and 5.16. As was found during the computations for the pull of each input, the prediction of a^d_{SL} receives a considerable shift from its "LoopCPV" predictions once the a^s_{SL} input is included. There is no such effect of the a^d_{SL} input on the prediction of a^s_{SL}. The respective constraints are

$$a^s_{SL} = (-6.0^{+5.2}_{-5.7}) \cdot 10^{-4} \quad \text{and} \quad a^d_{SL} = (8.4^{+3.4}_{-4.5}) \cdot 10^{-3}. \tag{5.11}$$

Again, the relative uncertainties are well comparable to those of the experimental inputs. As the preferred value of a^d_{SL} is now located more "centrally" in the 1 σ interval compared to the result in the LoopCPV fits, the shift doesn't change much concerning the overlap of the uncertainty intervals.

The fit results of a^d_{SL} and a^s_{SL} *with* their own experimental inputs included are given in Table 5.16.

The prediction for A_{SL} reads

$$A_{SL} = 2.47^{+0.80}_{-0.50} \cdot 10^{-3}. \tag{5.12}$$

The ambiguity in the γ input LUT is now resolved; only a $\mod(2\pi)$ ambiguity remains. This also removed what had remained of the $|V_{td}|$ "trident" structure discussed in sec. 5.2, further narrowing the constraint. The ambiguities in the UT angle β and its SM4/New Physics related "contamination" θ_d are also reduced compared to the LoopCPV input set. Both the UT angle α and the phase parameter ϕ_2 are now slightly better constrained, but in the latter case the effect is only seen in the plot in sec. 5.5.2. Interestingly, the constraint on $|V_{cb'}|$ is now *wider* than in the previous input set (cf. plot in sec. 5.5.1). The p-value plot of $\bar{m}_{t'}$ in sec. 5.5.4 shows now stronger hints on a constraint from above. However, since it is very weak and also above the mass range in which the perturbative expressions used are considered reliable, it should not be taken too seriously at this point.

	$1\ \sigma$	$2\ \sigma$	$3\ \sigma$
$\lvert V_{ud}\rvert$	$0.97418^{+0.00022}_{-0.00028}$	$0.97418^{+0.00050}_{-0.00057}$	$0.97418^{+0.00071}_{-0.00084}$
$\lvert V_{us}\rvert$	$0.22362^{+0.00164}_{-0.00061}$	$0.2236^{+0.0027}_{-0.0012}$	$0.2236^{+0.0034}_{-0.0018}$
$\lvert V_{ub}\rvert$	$0.00397^{+0.00012}_{-0.00038}$	$0.00397^{+0.00023}_{-0.00068}$	$0.00397^{+0.00035}_{-0.00082}$
$\lvert V_{ub'}\rvert$	$0.02940^{+0.00901}_{-0.00641}$	$0.029^{+0.016}_{-0.029}$	$0.029^{+0.023}_{-0.029}$
$\lvert V_{cd}\rvert$	$0.2231^{+0.0015}_{-0.0012}$	$0.2231^{+0.0034}_{-0.0044}$	$0.2231^{+0.0052}_{-0.0105}$
$\lvert V_{cs}\rvert$	$0.97382^{+0.00022}_{-0.00061}$	$0.97382^{+0.00041}_{-0.00719}$	$0.97382^{+0.00058}_{-0.02373}$
$\lvert V_{cb}\rvert$	$0.04039^{+0.00161}_{-0.00046}$	$0.04039^{+0.00197}_{-0.00079}$	$0.0404^{+0.0023}_{-0.0011}$
$\lvert V_{cb'}\rvert$	$0.020^{+0.0022}_{-0.020}$	$0.020^{+0.094}_{-0.020}$	$0.02^{+0.19}_{-0.02}$
$\lvert V_{td}\rvert$	$0.00825^{+0.00091}_{-0.00090}$	$0.0083^{+0.0019}_{-0.0017}$	$0.0083^{+0.0079}_{-0.0073}$
$\lvert V_{ts}\rvert$	$0.03950^{+0.00160}_{-0.00015}$	$0.0395^{+0.0039}_{-0.071}$	$0.040^{+0.016}_{-0.02}$
$\lvert V_{tb}\rvert$	$0.99794^{+0.00059}_{-0.00073}$	$0.9979^{+0.0014}_{-0.0078}$	$0.9979^{+0.0016}_{-0.0452}$
$\lvert V_{tb'}\rvert$	$0.0500^{+0.0110}_{-0.0019}$	$0.050^{+0.083}_{-0.040}$	$0.050^{+0.251}_{-0.041}$
$\lvert V_{t'd}\rvert$	$0.0345^{+0.0091}_{-0.0081}$	$0.035^{+0.023}_{-0.033}$	$0.035^{+0.044}_{-0.035}$
$\lvert V_{t's}\rvert$	$0.014^{+0.021}_{-0.014}$	$0.01^{+0.10}_{-0.01}$	$0.01^{+0.20}_{-0.01}$
$\lvert V_{t'b}\rvert$	$0.049^{+0.013}_{-0.011}$	$0.049^{+0.085}_{-0.038}$	$0.049^{+0.252}_{-0.040}$
$\lvert V_{t'b'}\rvert$	$0.99812^{+0.00043}_{-0.00058}$	$0.9981^{+0.0019}_{-0.0104}$	$0.9981^{+0.0022}_{-0.0465}$

Table 5.15.: 1 , 2 and 3 σ constraints on moduli of CKM matrix elements obtained with the complete set of inputs. The minimum χ^2 in the fit is $\chi^2_{\rm min} = 9.56$.

	1σ	2σ	3σ
$\bar{m}_x$/GeV	$807^{+164.2}_{-212}$	810^{+180}_{-590}	810^{+180}_{-600}
δ	1.172 ± 0.145	$1.17^{+0.27}_{-0.30}$	$1.17^{+0.39}_{-0.45}$
ϕ_2			
ϕ_3	$0.96^{+0.15}_{-0.19}$ $2.99^{+2.94}_{-0.80}$	$0.96^{+0.41}_{-0.37}$ $3.01^{+2.86}_{-0.83}$	unconstrained
α	$1.32^{+0.15}_{-0.13}$	$1.32^{+0.31}_{-0.25}$ $1.700^{+0.173}_{-0.064}$	$1.32^{+1.66}_{-0.37}$
β	$0.645^{+0.020}_{-0.039}$	$0.645^{+0.143}_{-0.083}$ $0.422^{+0.021}_{-0.047}$	$0.65^{+0.18}_{-0.11}$ $0.422^{+0.034}_{-0.087}$
θ_d	$0.001^{+0.017}_{-0.050}$	$0.00^{+0.16}_{-0.11}$	$-0.00^{+0.22}_{-0.15}$
a^d_{SL}	$(4.73^{+1.29}_{-0.80}) \cdot 10^{-3}$	$(4.7^{+3.4}_{-1.8}) \cdot 10^{-3}$	$(4.7^{+5.6}_{-2.6}) \cdot 10^{-3}$
a^s_{SL}	$(-8.7^{+7.5}_{-3.7}) \cdot 10^{-4}$	$(-9^{+12}_{-15}) \cdot 10^{-4}$	$(-9^{+27}_{-43}) \cdot 10^{-4}$

Table 5.16.: Constraints on SM4-related quantities obtained with the complete set of inputs.

5.5. Overview Of Results

As announced at the beginning of the present chapter, this section contains the plots of p-value curves of some observable constrained in the fits, combined in common coordinate systems. While this is a lot more convenient than the long tables containing numbers shown in the previous sections, there is one caveat: The p-values are given with respect to the χ^2_{min} achieved in the respective scan, so a given p-value does *not* mean the same χ^2 value for two different curves. However, unlike in the tables, it is possible to see at a glance how the constraints on individual quantities change with the input set.

The χ^2 values achieved are approximately

- 7.36819 ± 0.00001 in the TL input set,
- 7.69 ± 0.01 for LoopNoCPV,
- 7.87 ± 0.03 for LoopCPV and
- 9.56 ± 0.01 for the complete set of inputs.

The error intervals state which χ^2 values were considered acceptable in view of reproducibility and any irregularities in the p-value plots obtained. While the TL input set led to almost perfect convergence each time, the others would obviously have required even higher settings of `globalMinSearches`, `nbOfFits` and `granularity`. While this would have significantly increased the time required, some experimentation showed that the reproducibility of the fits was sufficient with the settings used.

5.5.1. CKM Matrix Elements

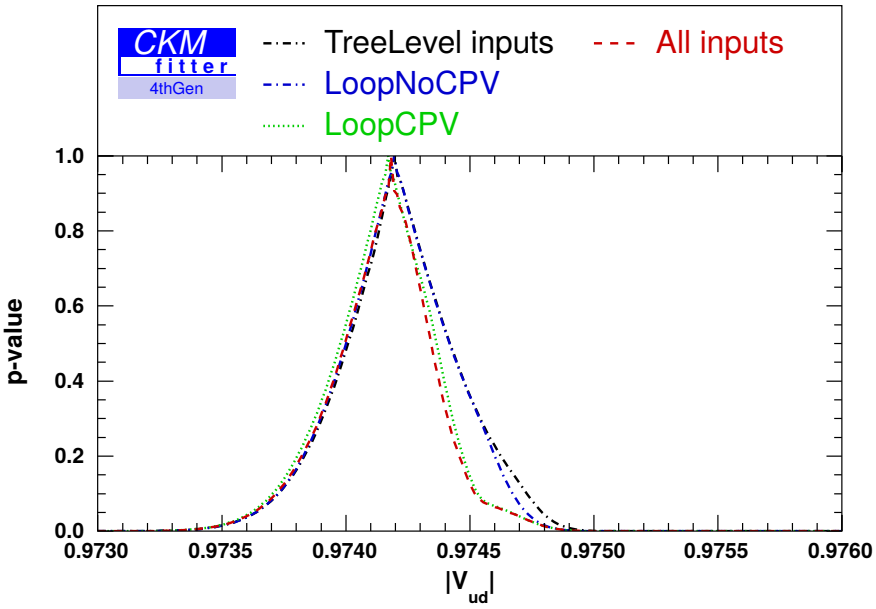

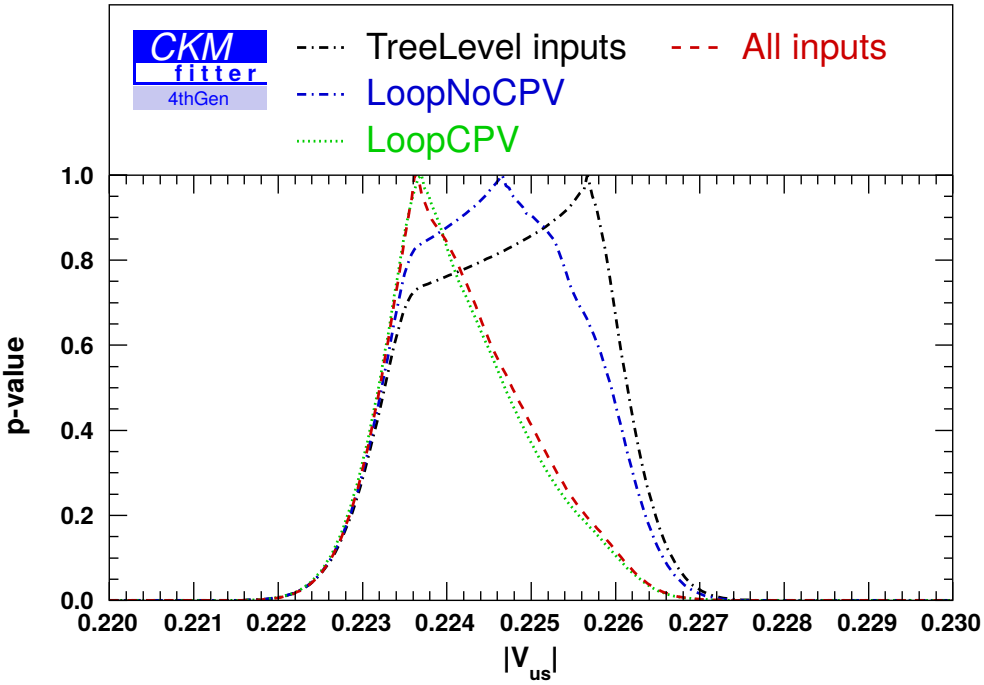
CKM fitter
4thGen
TreeLevel inputs
All inputs
LoopNoCPV
LoopCPV
p-value
1.0
0.8
0.6
0.4
0.2
0.0
0.220 0.221 0.222 0.223 0.224 0.225 0.226 0.227 0.228 0.229 0.230
|V_us|

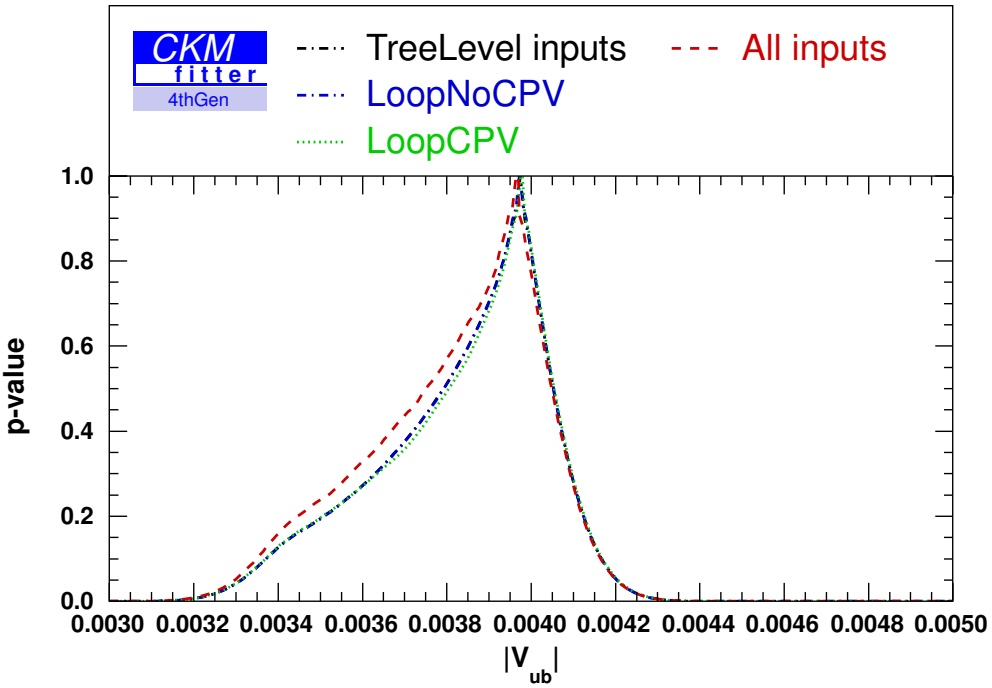
CKM fitter
4thGen
TreeLevel inputs
All inputs
LoopNoCPV
LoopCPV
p-value
1.0
0.8
0.6
0.4
0.2
0.0
0.0030 0.0032 0.0034 0.0036 0.0038 0.0040 0.0042 0.0044 0.0046 0.0048 0.0050
|V_ub|

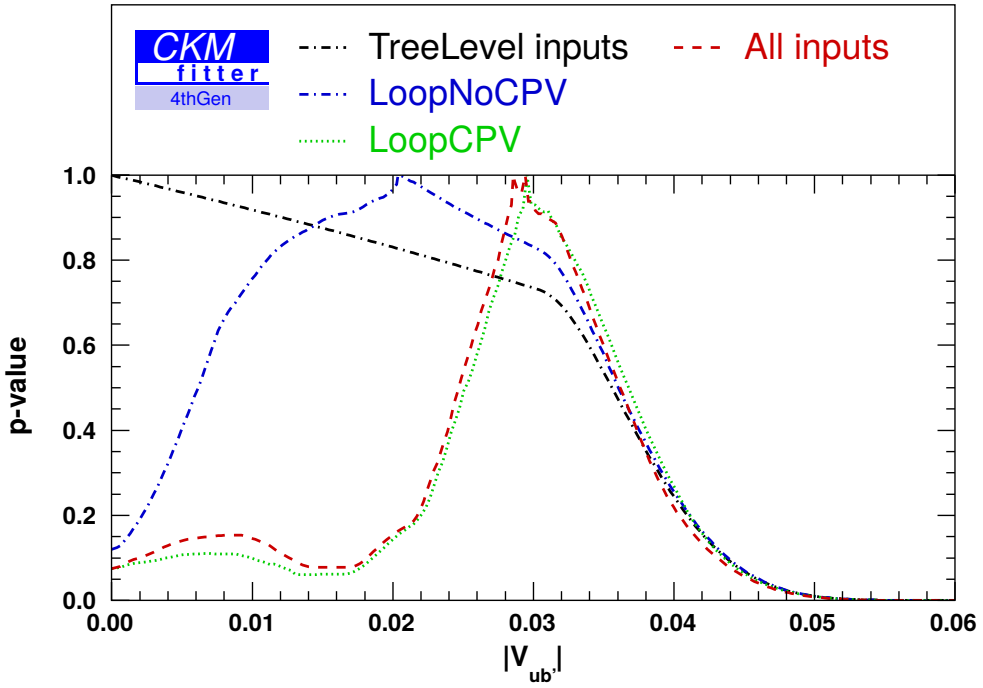
CKM fitter
4thGen
TreeLevel inputs
All inputs
LoopNoCPV
LoopCPV
p-value
1.0
0.8
0.6
0.4
0.2
0.0
0.00
0.01
0.02
0.03
0.04
0.05
0.06
|V_ub'|

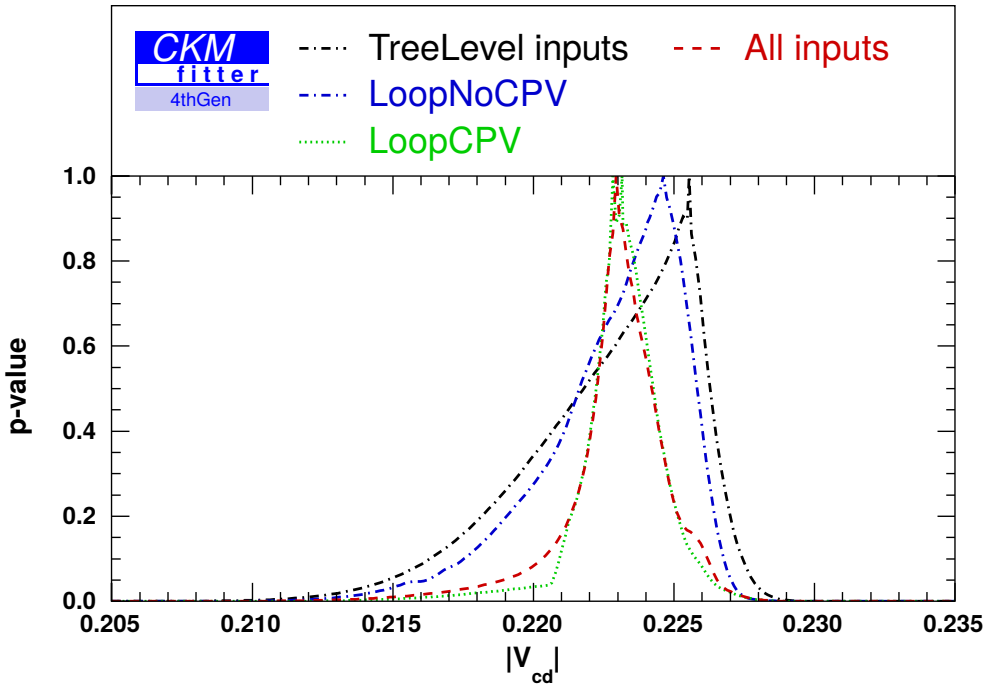
CKM fitter
4thGen
TreeLevel inputs
All inputs
LoopNoCPV
LoopCPV
p-value
1.0
0.8
0.6
0.4
0.2
0.0
0.205
0.210
0.215
0.220
0.225
0.230
0.235
|V_cd|

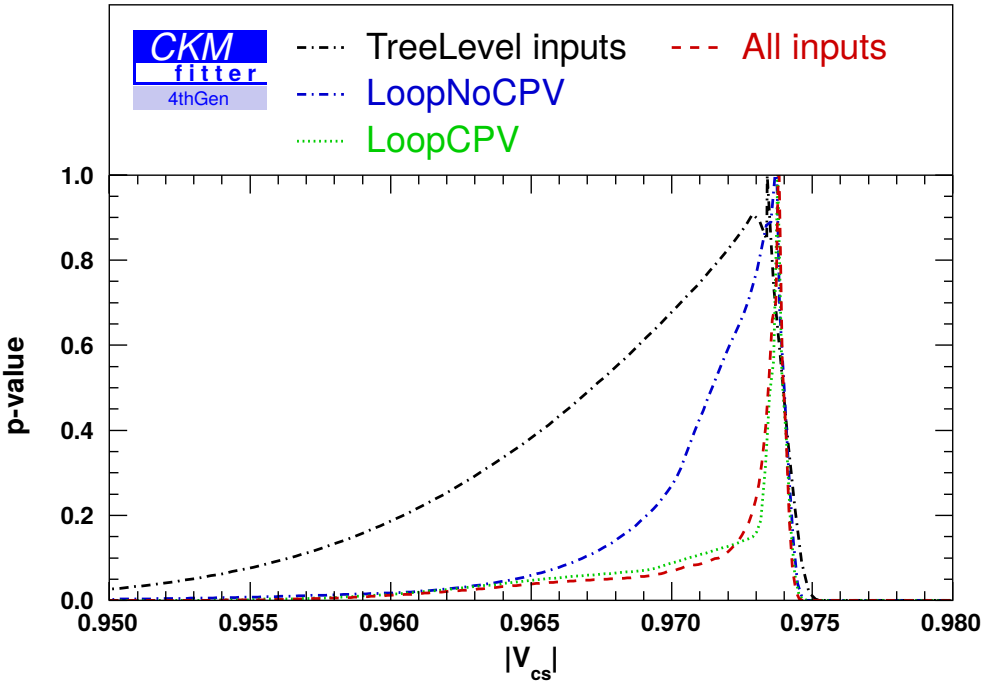
CKM fitter
4thGen
TreeLevel inputs
All inputs
LoopNoCPV
LoopCPV
p-value
1.0
0.8
0.6
0.4
0.2
0.0
0.950
0.955
0.960
0.965
0.970
0.975
0.980
|V_cs|

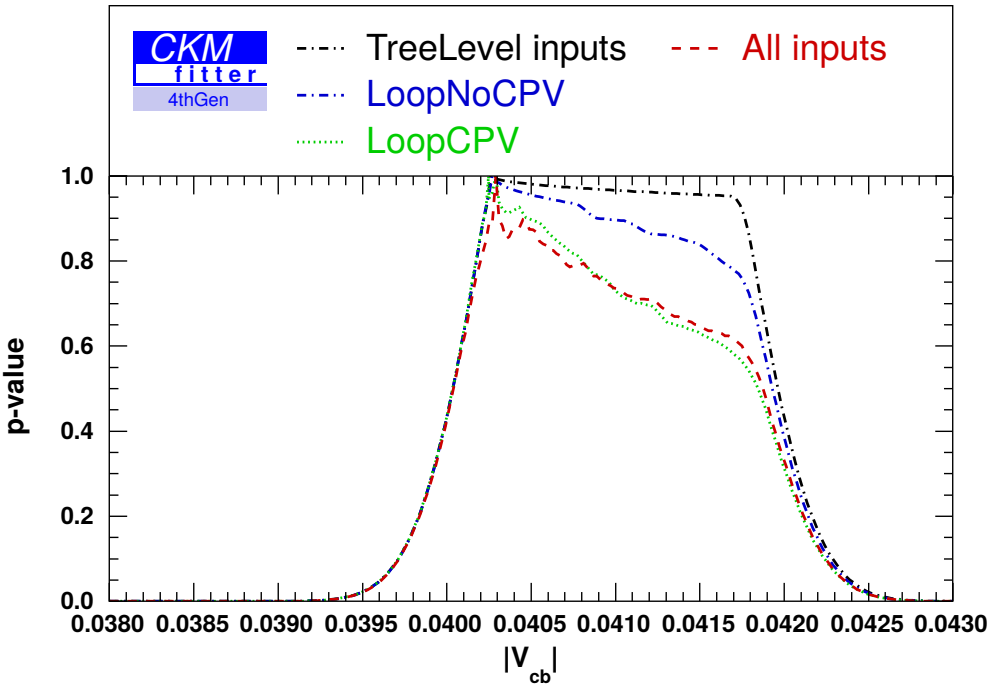
CKM fitter
4thGen
TreeLevel inputs
All inputs
LoopNoCPV
LoopCPV
p-value
1.0
0.8
0.6
0.4
0.2
0.0
0.0380
0.0385
0.0390
0.0395
0.0400
0.0405
0.0410
0.0415
0.0420
0.0425
0.0430
|V_cb|

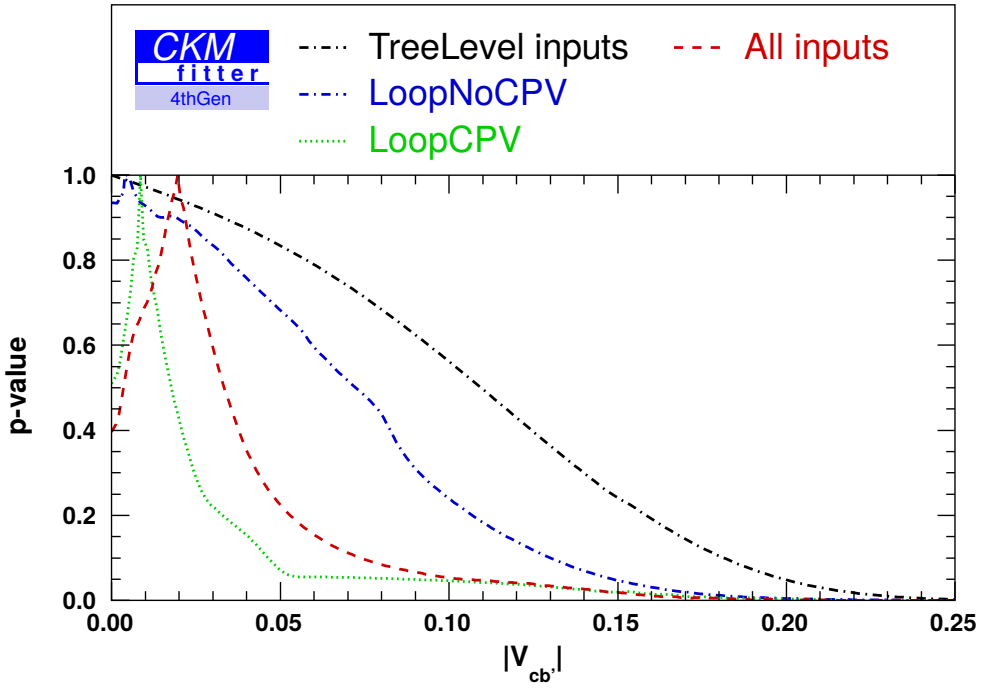
CKM fitter
4thGen
TreeLevel inputs
All inputs
LoopNoCPV
LoopCPV
p-value
1.0
0.8
0.6
0.4
0.2
0.0
0.00
0.05
0.10
0.15
0.20
0.25
|V_cb'|

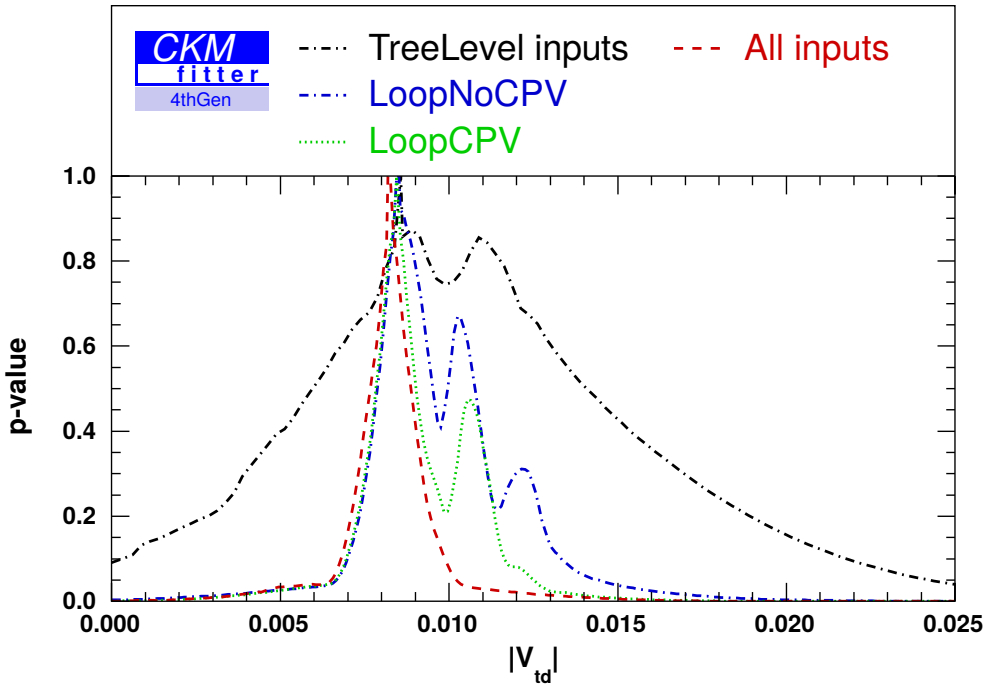
CKM fitter
4thGen
TreeLevel inputs
All inputs
LoopNoCPV
LoopCPV
p-value
1.0
0.8
0.6
0.4
0.2
0.0
0.000
0.005
0.010
0.015
0.020
0.025
|V_td|

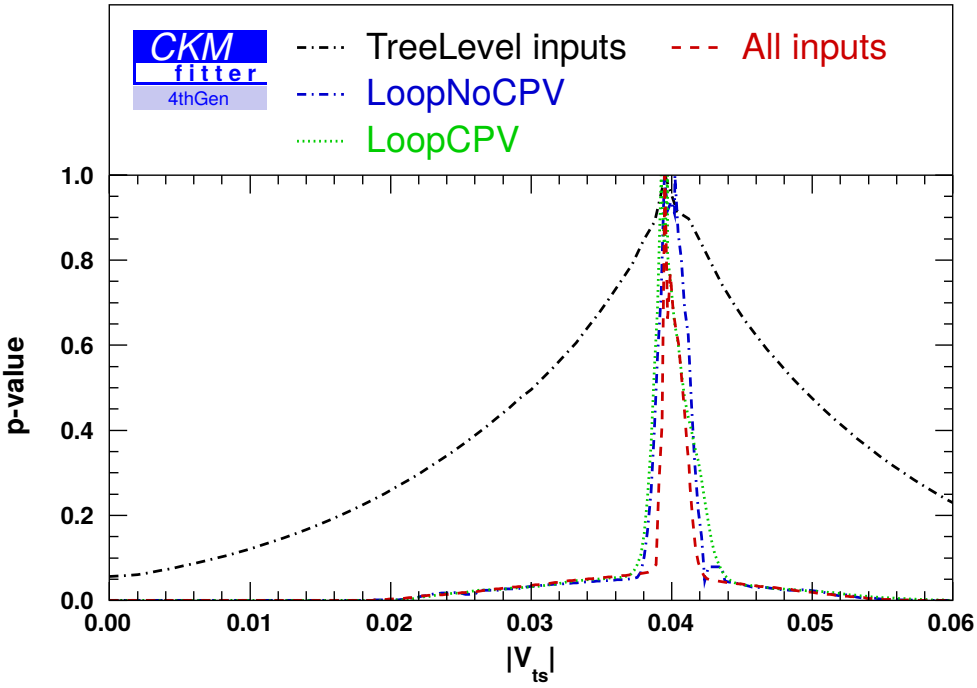
CKM
fitter
4thGen
TreeLevel inputs
All inputs
LoopNoCPV
LoopCPV
p-value
1.0
0.8
0.6
0.4
0.2
0.0
0.00
0.01
0.02
0.03
0.04
0.05
0.06
|V_ts|

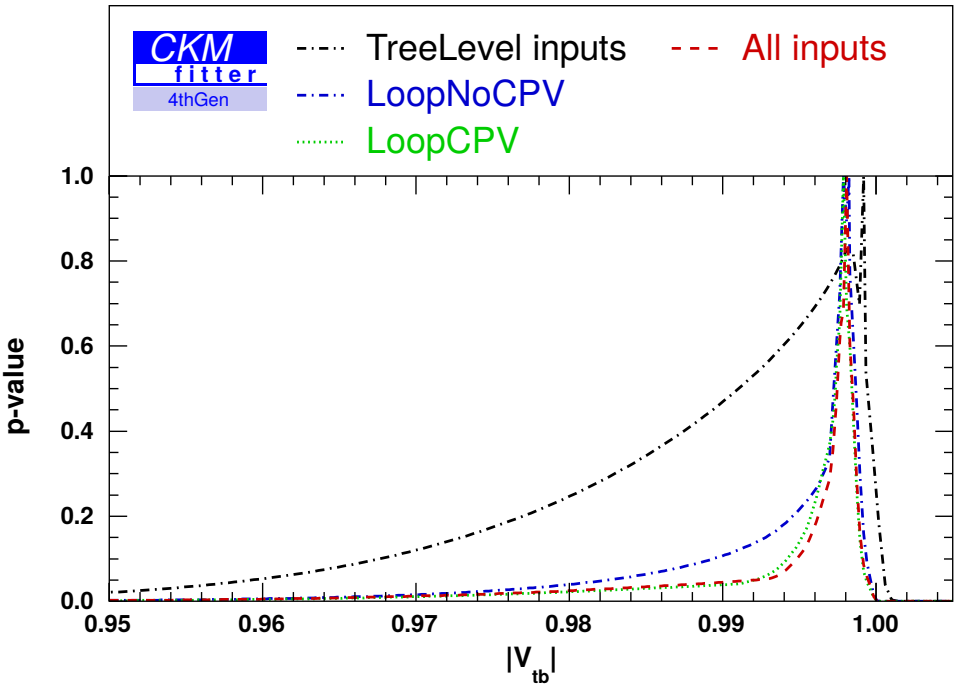
CKM
fitter
4thGen
TreeLevel inputs
All inputs
LoopNoCPV
LoopCPV
p-value
1.0
0.8
0.6
0.4
0.2
0.0
0.95
0.96
0.97
0.98
0.99
1.00
|V_tb|

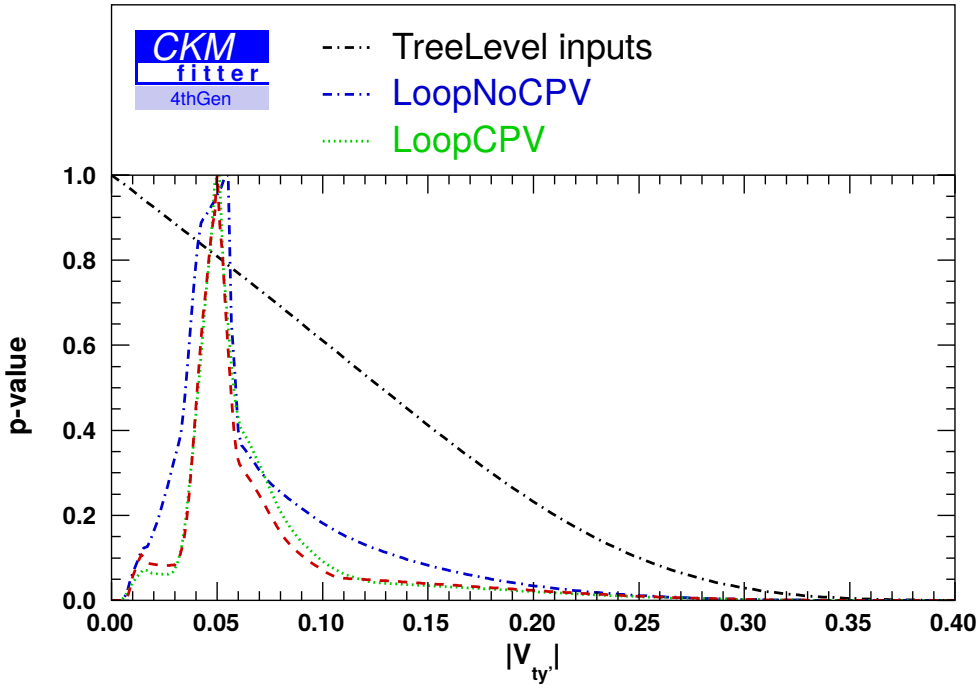
CKM
fitter
4thGen
TreeLevel inputs
LoopNoCPV
LoopCPV
p-value
1.0
0.8
0.6
0.4
0.2
0.0
0.00
0.05
0.10
0.15
0.20
0.25
0.30
0.35
0.40
|V_ty'|

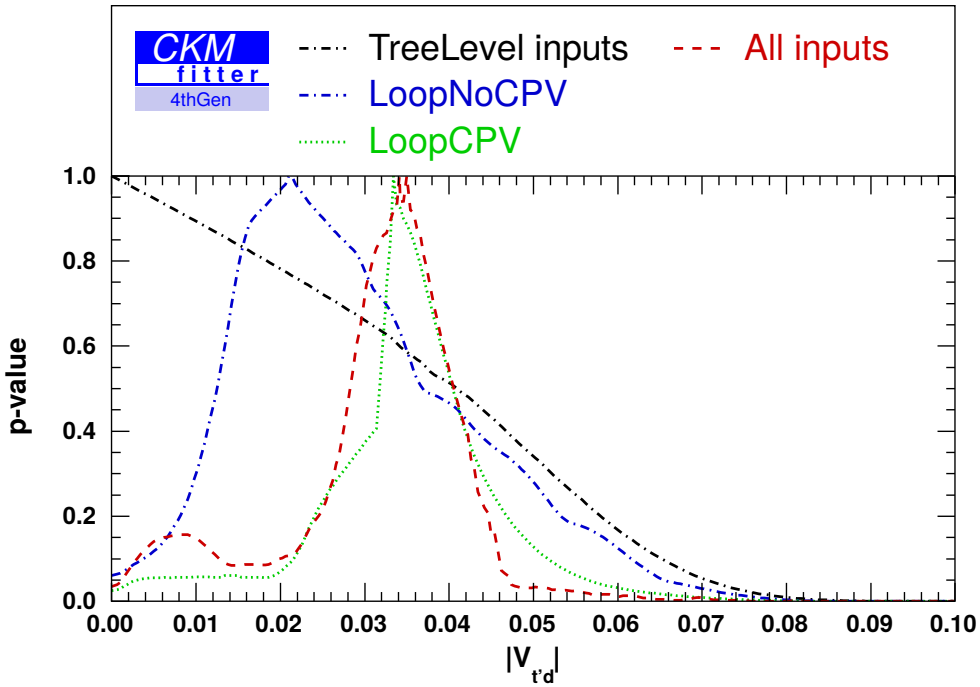
CKM
fitter
4thGen
TreeLevel inputs
All inputs
LoopNoCPV
LoopCPV
p-value
1.0
0.8
0.6
0.4
0.2
0.0
0.00
0.01
0.02
0.03
0.04
0.05
0.06
0.07
0.08
0.09
0.10
|V_t'd|

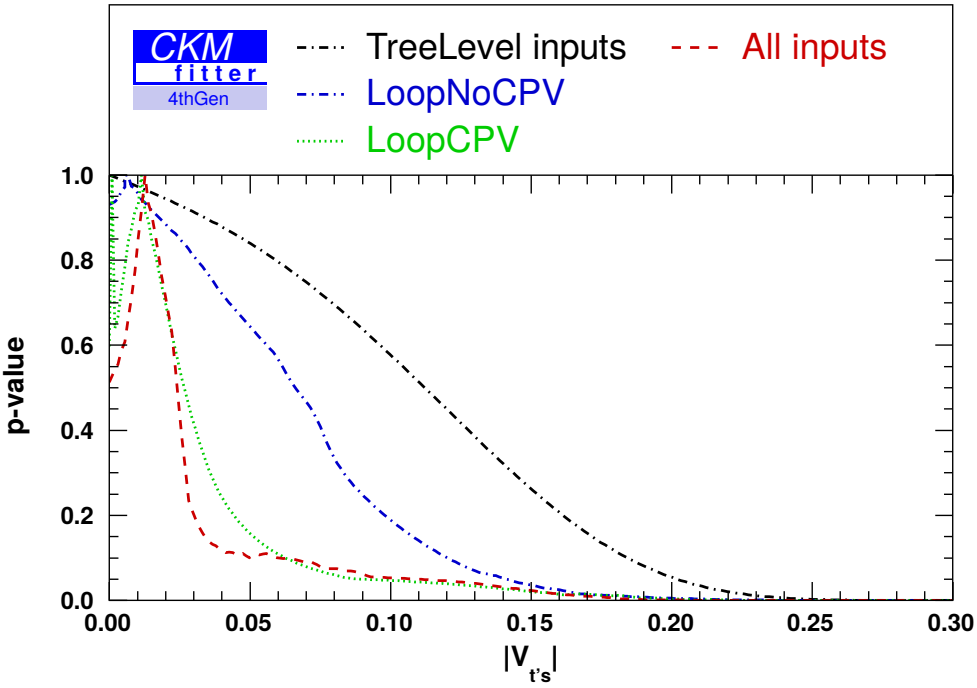
CKM fitter
4thGen
TreeLevel inputs
All inputs
LoopNoCPV
LoopCPV
p-value
1.0
0.8
0.6
0.4
0.2
0.0
0.00
0.05
0.10
0.15
0.20
0.25
0.30
|V_t's|

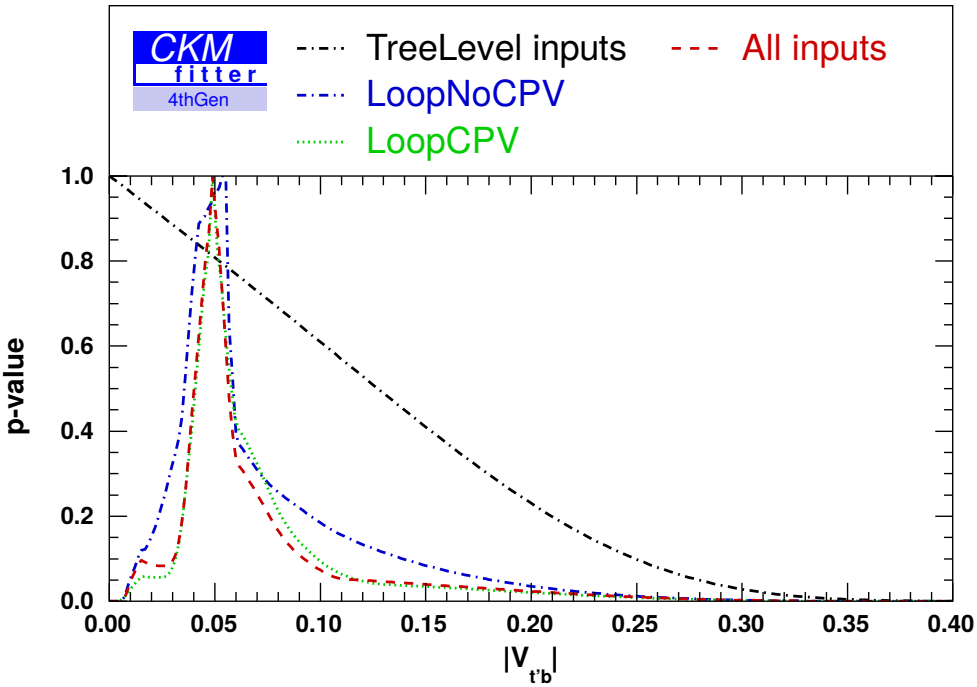
CKM fitter
4thGen
TreeLevel inputs
All inputs
LoopNoCPV
LoopCPV
p-value
1.0
0.8
0.6
0.4
0.2
0.0
0.00
0.05
0.10
0.15
0.20
0.25
0.30
0.35
0.40
|V_t'b|

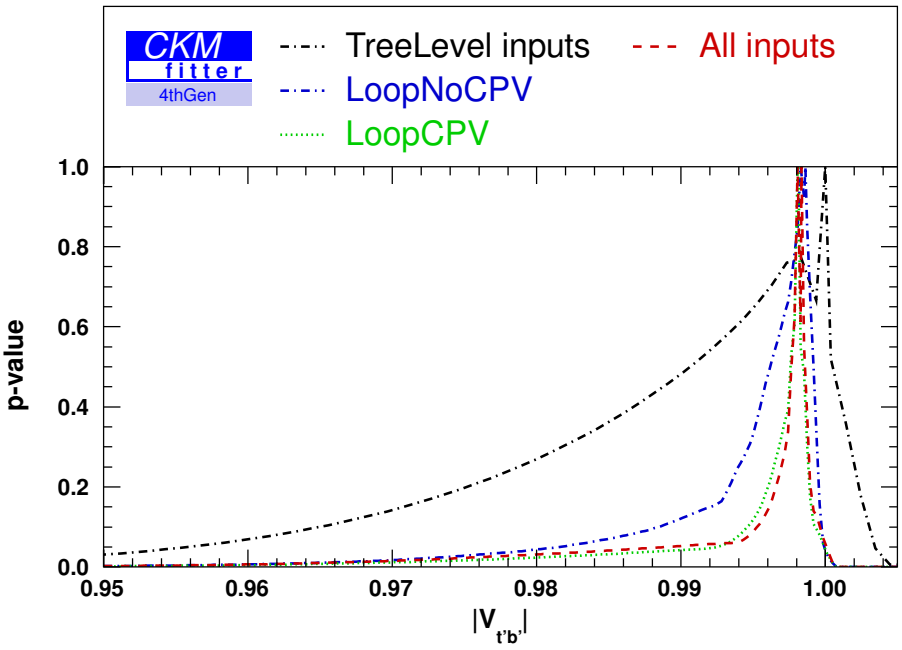

5.5.2. CKM Matrix Parameters δ, ϕ_2 and ϕ_3

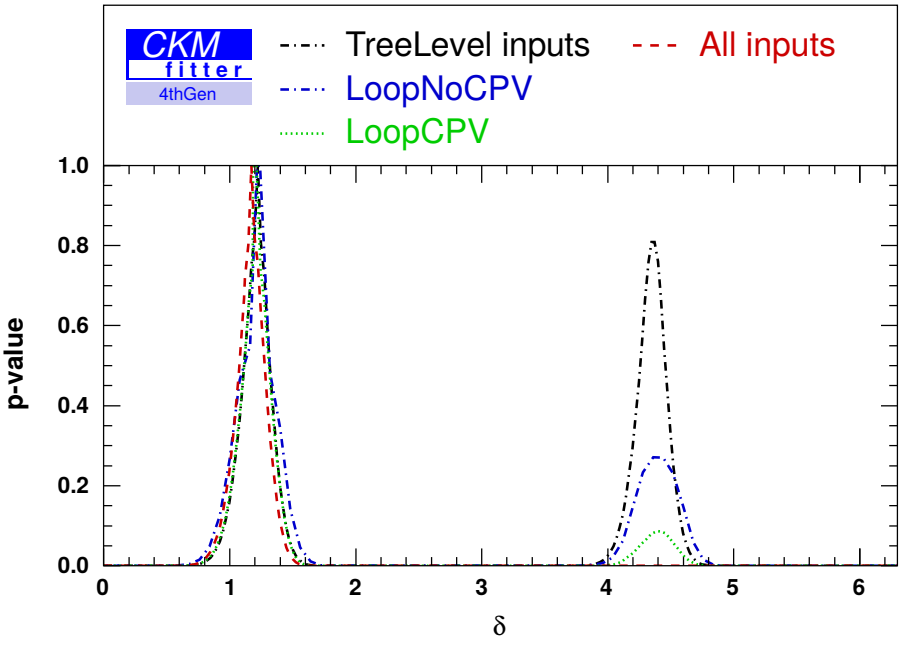

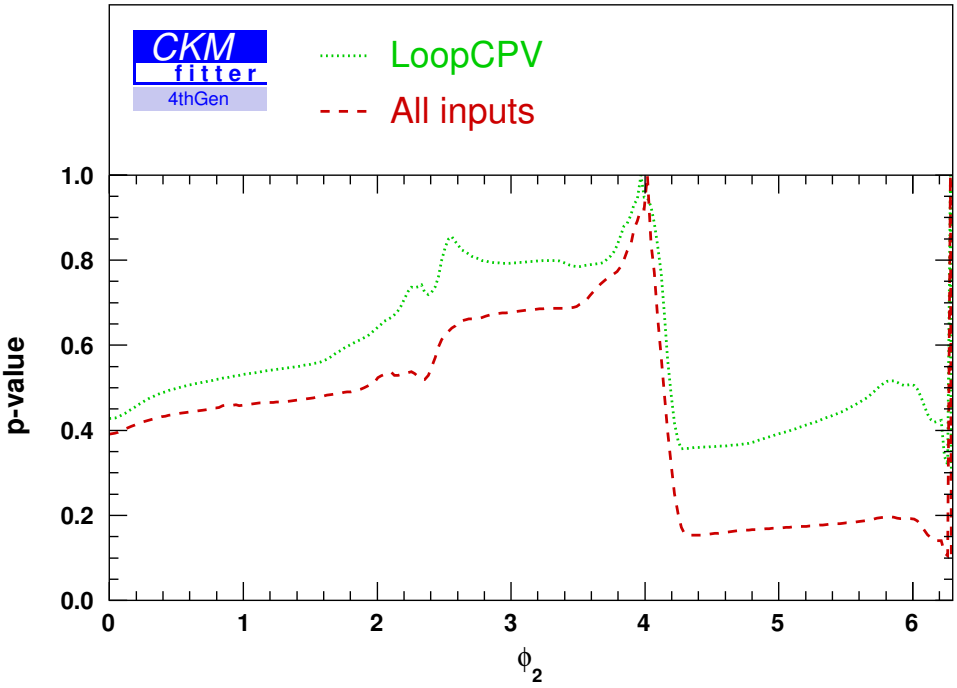
CKM
fitter
4thGen
LoopCPV
All inputs
p-value
1.0
0.8
0.6
0.4
0.2
0.0
0
1
2
3
4
5
6
ϕ_2

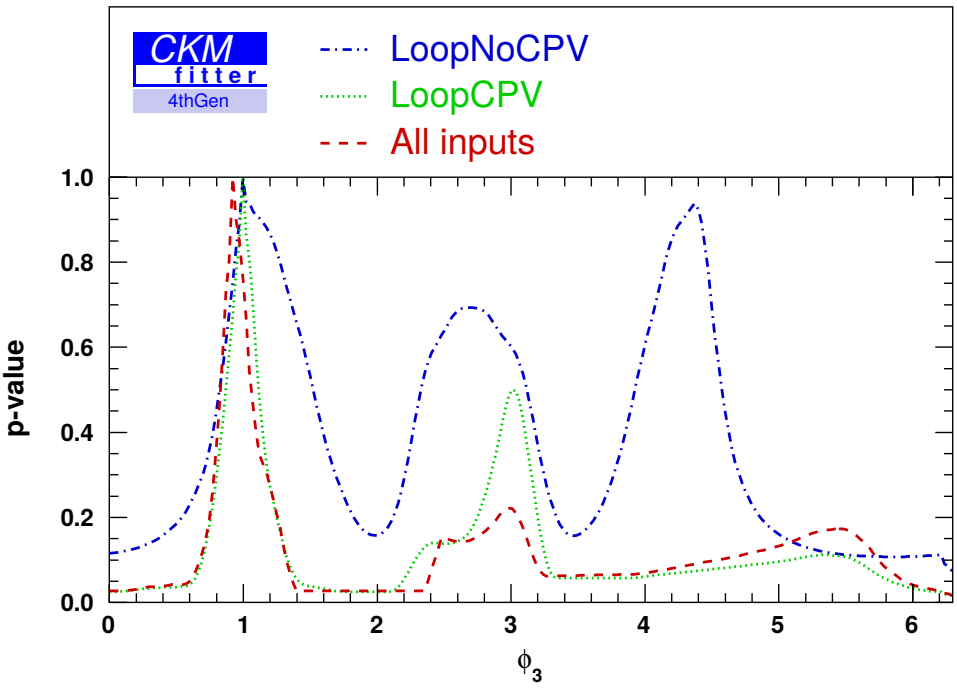
CKM
fitter
4thGen
LoopNoCPV
LoopCPV
All inputs
p-value
1.0
0.8
0.6
0.4
0.2
0.0
0
1
2
3
4
5
6
ϕ_3

5.5.3. UT Angles and Related

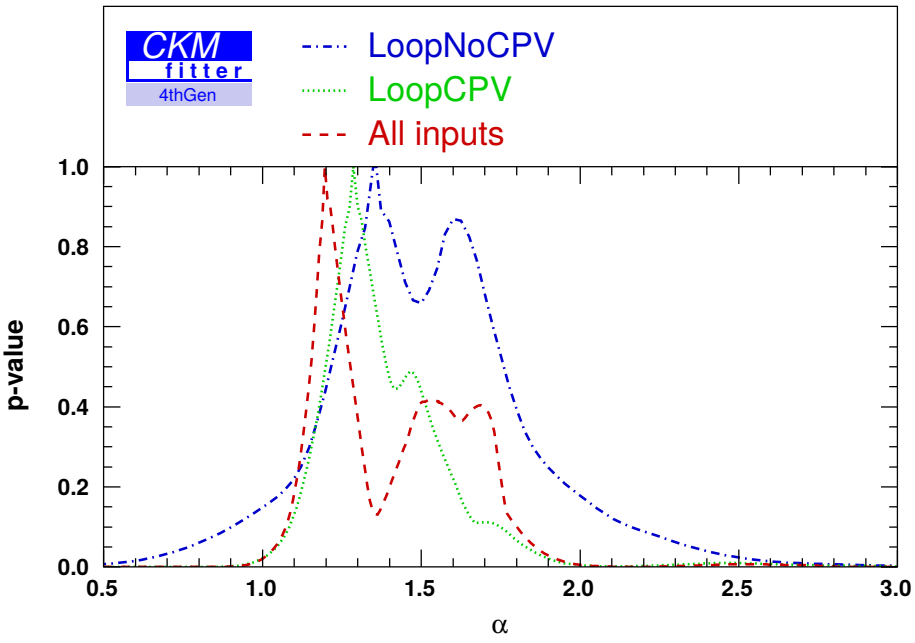

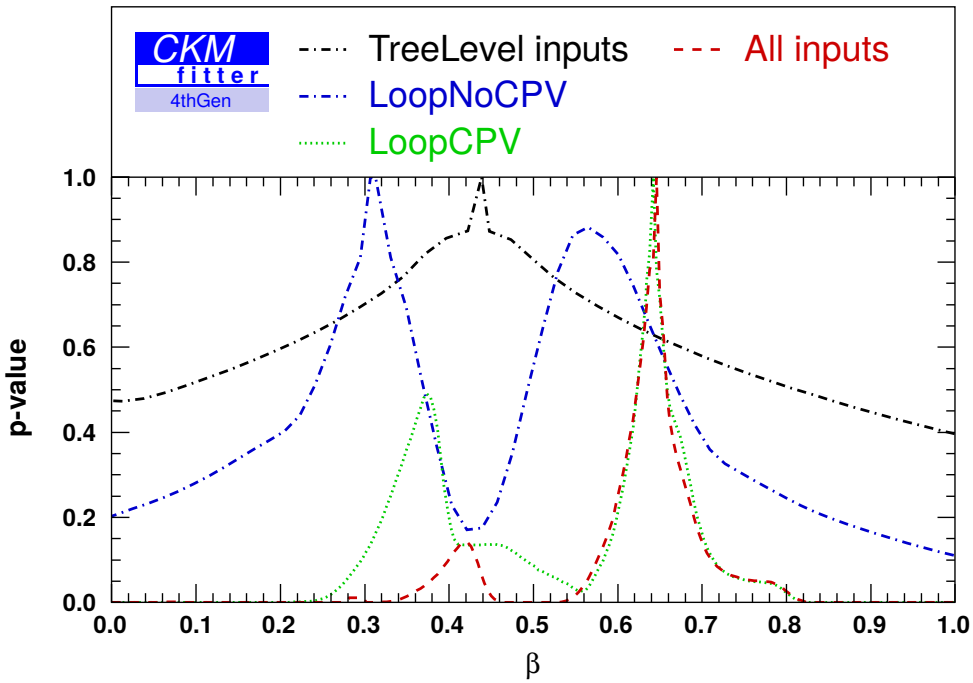

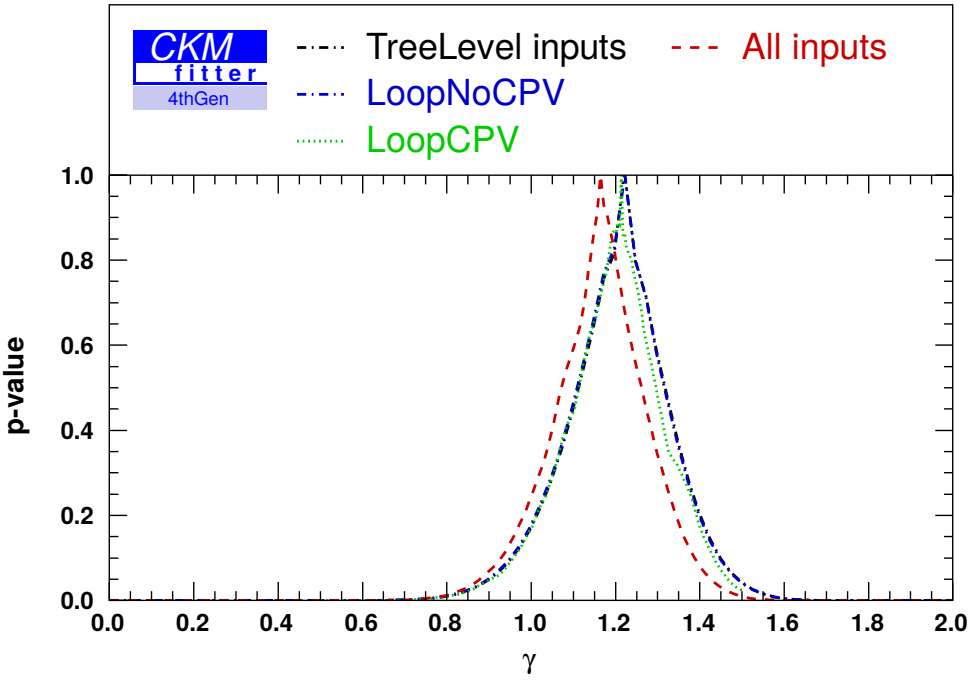
CKM
fitter
4thGen
TreeLevel inputs
All inputs
LoopNoCPV
LoopCPV
p-value
γ

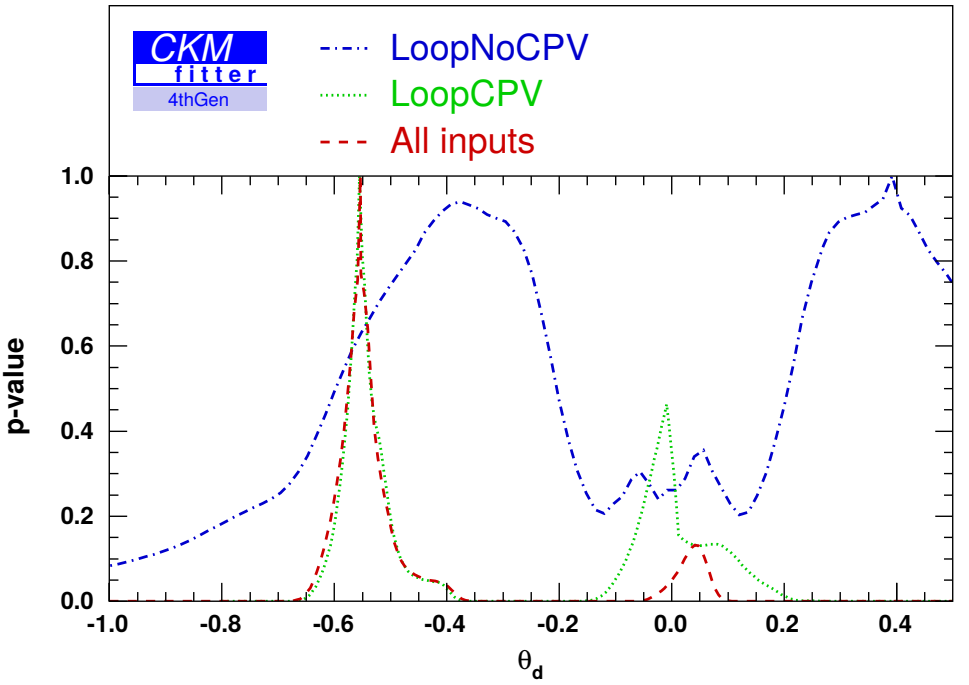
CKM
fitter
4thGen
LoopNoCPV
LoopCPV
All inputs
p-value
θd

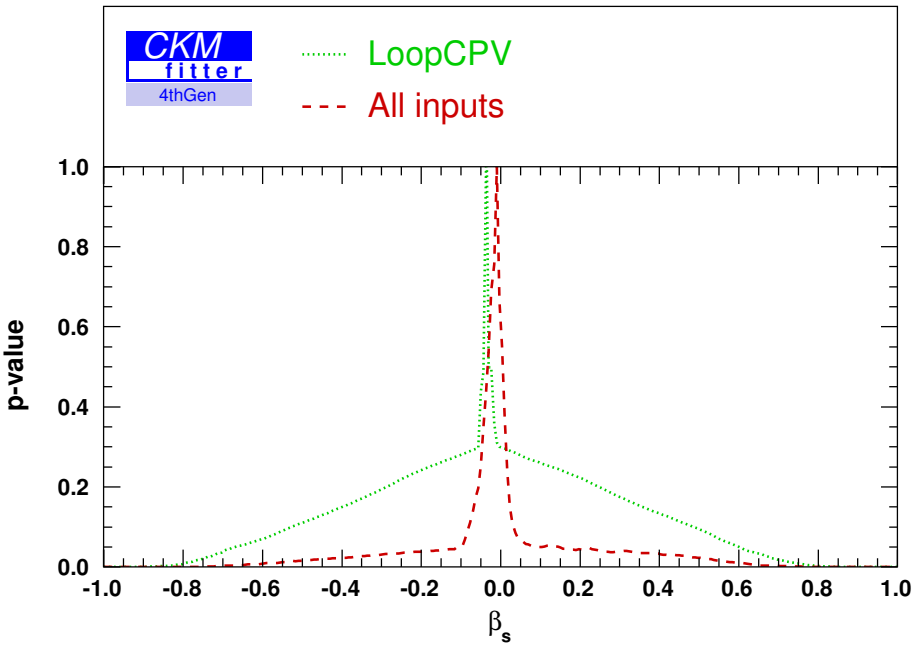

5.5.4. t' Quark Mass

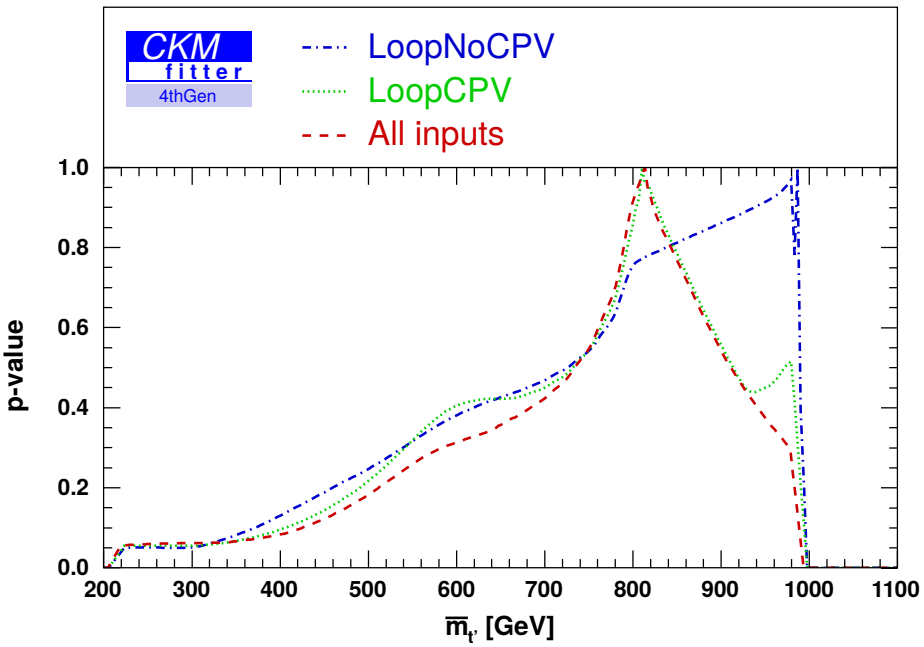

5.5.5. A_{SL} and Related

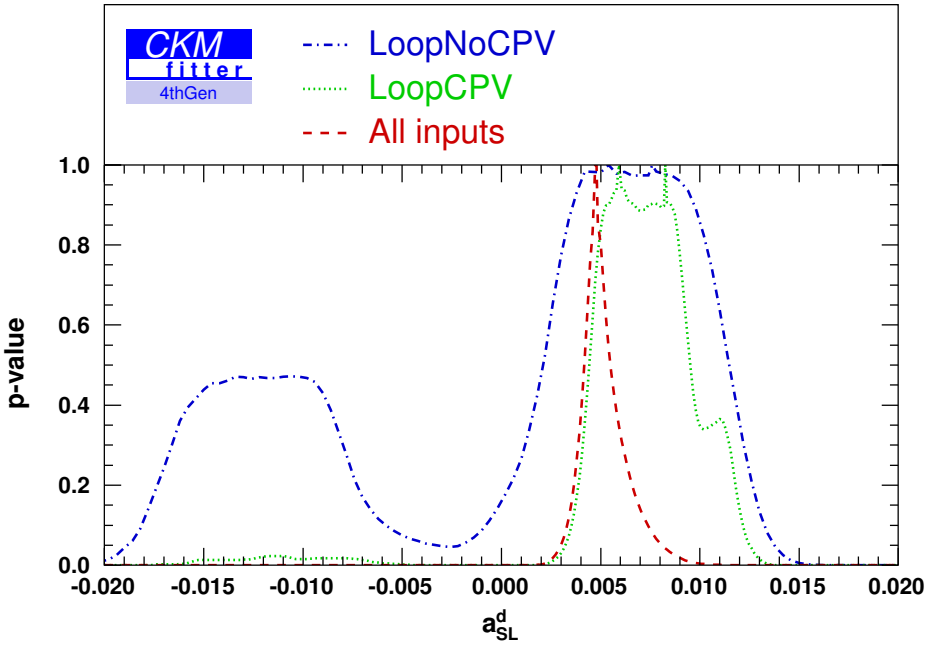

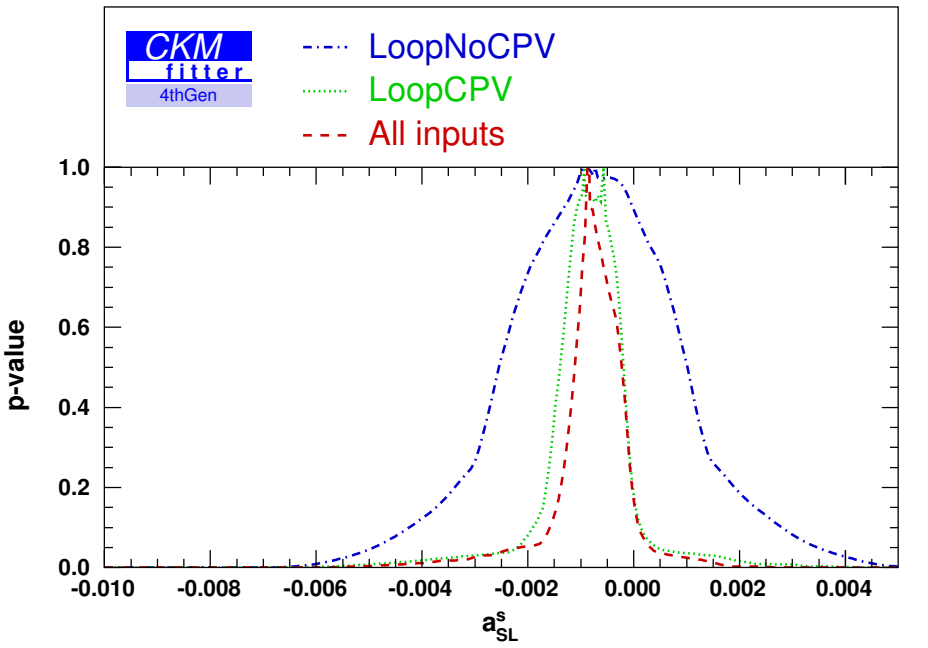

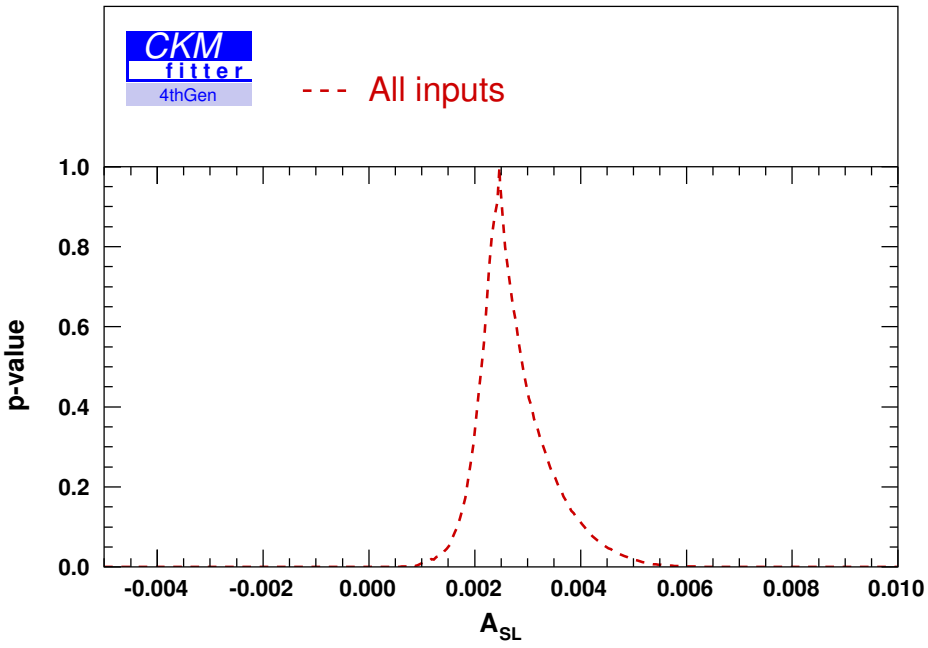

5.5.6. Effects of Individual Inputs on the Fit

Each input value which is not perfectly reproduced by its prediction in the global fit will increase the global χ^2_{min} found. The omission of any input will usually decrease this value by a shift $\Delta\chi^2$ compared to the χ^2_{min} found with the full set of inputs. The direction of the tension between the prediction and the input is characterised by the "pull" as defined at the beginning of Chapter 5.

The $\Delta\chi^2$ and pulls of each input observable are separately given for each input set in Table 5.17. For convenience, the contents are also represented graphically in Fig. 5.9.

The χ^2 shift $\Delta\chi^2$ and the pull together can help to judge the influence of a quantity x on the fit.

- A small $\Delta\chi^2$ together with a small pull means that within its uncertainty Δx_{exp}, the experimental result is well predicted by the fit, both in terms of the uncertainty Δx_{pred} and the preferred value $\hat{x}_{\text{pred}}$. One could obtain the same fit results without this input. Example: $|V_{cs}|$ in all input sets.
- A small $\Delta\chi^2$ together with a large pull implies that x is poorly constrained by the other inputs used. The input often can constrain one or more parameters which are not properly constrained by other inputs. Example: $|\epsilon_K|$.
- A large $\Delta\chi^2$ with a large pull indicates a tension between x_{exp} and other inputs. Example: Δm_d with the complete set of inputs.
- A large $\Delta\chi^2$ with a small pull does not occur.

Input	TL		LoopNoCPV		LoopCPV		All	
	Pull	$\Delta\chi^2$	Pull	$\Delta\chi^2$	Pull	$\Delta\chi^2$	Pull	$\Delta\chi^2$
$\|V_{ud}\|$	-3.48	0.0486	-2.10	0.13	-2.79	0.276	-1.93	0.19
$\|V_{us}\|$	0.80	0.00	0.16	0.00	-1.04	0.02	-1.12	0.00
$\|V_{ub}\|$	1.75	0.212	1.85	0.22	2.16	0.30	1.67	0.17
$\|V_{cd}\|$	-0.41	0.167	-0.59	0.29	-0.64	0.40	-0.65	0.39
$\|V_{cs}\|$	-0.066	0.000	-0.0647	0.00	-0.06	0.00	-0.062	0.00
$\|V_{cb}\|$	-50.6	0.045	-1.85	0.02	-1.97	0.08	-0.96	0.00
$\|V_{tb}\|$	-18.5	0.405	-0.68	0.46	-0.61	0.22	-0.679	0.45
$\mathcal{B}(W \to e\bar{\nu})$	0.61	0.0126	0.66	0.02	0.677	0.03	0.686	0.00
$\mathcal{B}(W \to \mu\bar{\nu})$	2.29	2.85	1.78	2.25	1.79	2.13	1.79	2.21
$\mathcal{B}(W \to \tau\bar{\nu})$	-2.08	3.29	-2.07	3.25	-2.06	3.19	-2.06	3.17
$\mathcal{B}(B \to \tau\bar{\nu})$	-1.78	0.213	-0.63	0.21	-1.61	0.22	-1.96	0.72
γ	-	0.01	-3.86	0.12	-1.87	0.28	-0.37	0.79
Δm_d			55.8	0.06	60.75	0.23	68.25	1.12
Δm_s			-20.0	0.01	-27.7	0.02	-15.7	0.01
$\frac{\Gamma(b\to s\gamma)}{\Gamma(b\to ce\bar{\nu})}$			-1.52	0.22	-1.00	0.15	-0.810	0.16
$\mathcal{B}(B_d \to \mu^+\mu^-)$			1.5	0.12	0.875	0.29	2.13	0.31
$\mathcal{B}(B_s \to \mu^+\mu^-)$			7.57	0.08	0.43	0.02	12.71	0.02
$\sin(2\beta - 2\theta_d)$					146.3	0.17	-543	0.96
$\|\epsilon_K\|$					$\mathcal{O}(10^3)$	0.0	$\mathcal{O}(10^5)$	0.06
$a_{SL}^{(s)}$							0.875	0.68
$a_{SL}^{(d)}$							2.35	1.07

Table 5.17.: Pulls and χ^2 shifts by individual inputs in each input set. See the beginning of Chapter 5 for the definitions. No pull is given for γ in the TL case because it is completely unconstrained if the input is not used. Note the following examples of the description on page 141 of how an input's influence can be judged by its pull and its $\Delta\chi^2$: $|V_{cs}|$ in all input sets, $|\epsilon_K|$ in the LoopCPV set and Δm_d in the complete input set. For a graphical representation of this Table, see Fig. 5.9.

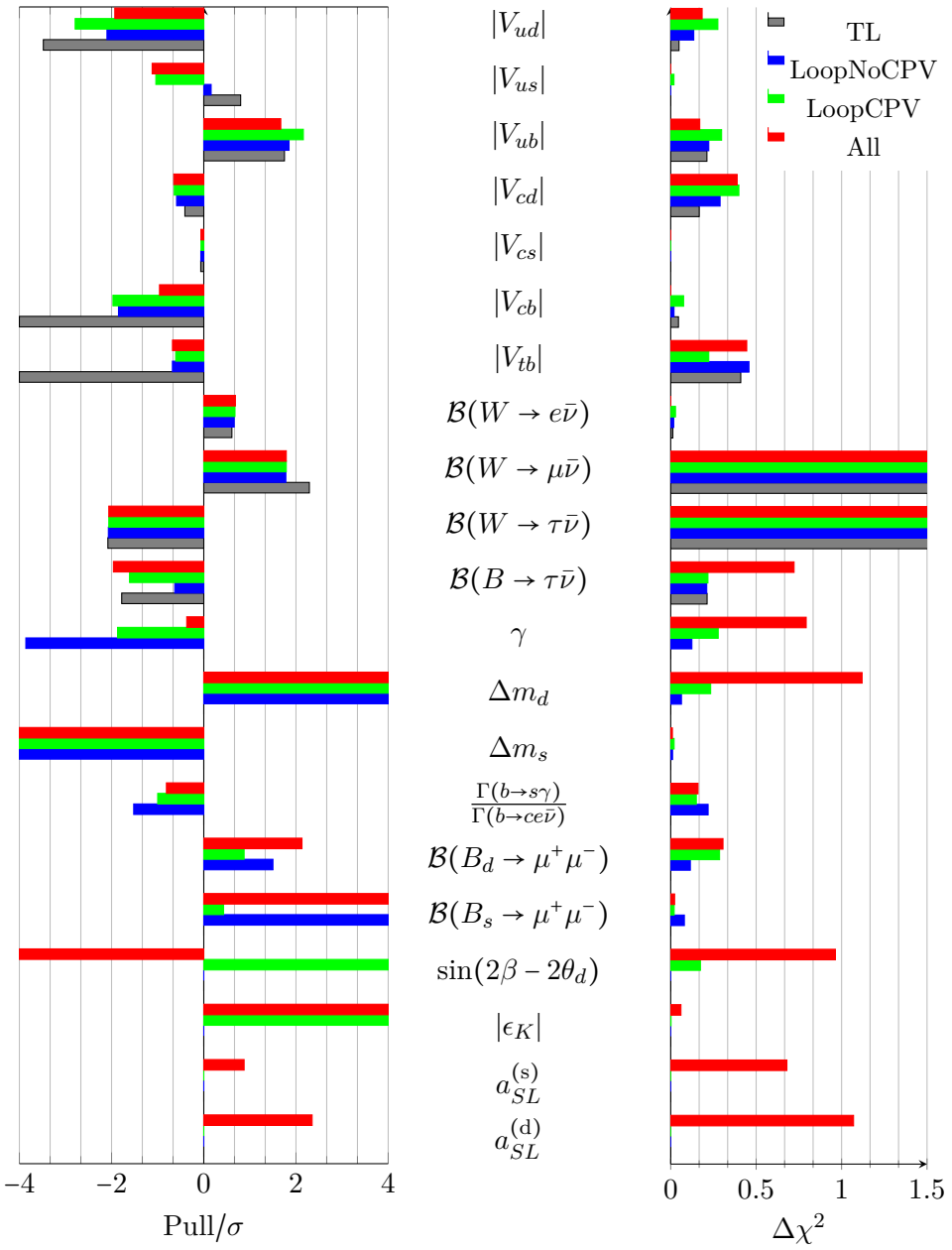

Figure 5.9.: Pulls and χ^2 shifts by individual inputs in each input set. Note that the horizontal axes are truncated. See Table 5.17 for numerical values.

6. SM4 vs. SM3 using Flavour Physics, EWP Fit and Higgs Decays

This chapter compares the performance of the SM3 to that of the SM4 in the combined fit to Flavour Physics and Electroweak Precision Observables. It also recalls the exclusion of the SM4 in [40] in fits to the same Electroweak Precision Observables combined with Higgs signal strengths measured at the Tevatron and the LHC.

In order to be able to do such a comparison, the fits presented previously were repeated in the SM3 framework. The comparison itself is limited to a comparison of the χ^2_{min} values achieved. It is not an exhaustive statistical analysis. As will be explained below, a full quantitative analysis cannot be done by CKMfitter at that point.

6.1. Statistical Caveats in Comparing SM3 and SM4

In addition to the debatable treatment of systematic errors in the *R*fit scheme as described in sec. 3.1, a comparison of the SM3 and the SM4 faces an additional problem: It is not a comparison of realisations of different parameter values within one model but a comparison of two different models, with different parameter spaces, by means of a likelihood ratio test. The goal would be to give a p-value for the exclusion of one of the models. Under certain conditions, Wilks' theorem [209] states that a likelihood ratio

$$S(x_{exp}) = -2 \ln \frac{\max_{y_{mod}} \mathcal{L}_1(x_{exp})}{\max_{y_{mod}} \mathcal{L}_2(x_{exp})} \tag{6.1}$$

follows a χ^2 distribution. A p-value can then easily be calculated. During the work on [101], our collaboration realized that those conditions are not satisfied. More specifically, the application of Wilks' theorem requires

- that the theory used to construct $\mathcal{L}_1$ is *nested* in the theory behind $\mathcal{L}_2$. Applied to the present problem, the SM3 would have to be nested in the SM4, i.e. it would have to be a realisation of the SM4 with certain parameters fixed to specific values.
- that the likelihood components of the experimental inputs are Gaussians.
- that both theory manifolds as described by

  $$M = \{x_{theo}(y_{mod}) | y_{mod} \in \Omega\}, \tag{6.2}$$

  where Ω is the allowed parameter space, are hyperplanes.

At least two of the condition are violated by the physics scenario investigated here: The first condition is not satisfied because the heavy particles of the 4th generation do not decouple. Even in the limit of a non-mixing 4th generation with infinitely heavy member particles, i.e. $\theta_{u,v,w} \to 0$ and $m_{t'}, m_{b'} \to \infty$, they contribute to Electroweak Precision Observables, the Higgs production channel $gg \to H$ and the Higgs decay $H \to \gamma\gamma$[35]. The second condition is neither satisfied in the study presented here, nor in the earlier study [101] published by our collaboration. For the calculation of p-values in the subsequent publications [35] and [40], Martin Wiebusch developed the C++ library *my*Fitter. This was presented in [210] which contains also a thorough discussion of the above arguments. The numerical methods of *my*Fitter are especially advantageous at small p-values. It enabled us to exclude the SM4 at the 5.3 σ level as described in sec. 6.2.1.

The present study does not make use of *my*Fitter because most of the theoretical expressions presented in Chapter 4 are not yet implemented in *my*Fitter. The limited time and manpower available to our project did not permit this.

6.2. Fourth Generation and the Higgs At Tevatron and LHC - The Demise of the Sequential Fourth Generation

As hinted in the Introduction in Chapter 1, the subject of this study, a sequential fourth generation, has in the meantime been ruled out. This section gives background information needed to understand the exclusion of a sequential fourth generation in late 2012, i.e. list the effects of SM4 particles on those observables which led to the exclusion of the SM4. This, in the context needed here, amounts to examining products of cross sections $\sigma(X \to H)$ of Higgs production processes (with the initial state $X = pp$ at the LHC and $X = p\bar{p}$ at the Tevatron) and branching fractions of the Higgs boson to final states Y, $\mathcal{B}(H \to Y)$.

At hadron colliders such as the LHC and the Tevatron, gluon-gluon fusion $gg \to H$ is the most important Higgs production mechanism [212]. At a center of mass energy of $\sqrt{s} = 8$ TeV at the LHC, the relative contrubution is 87.5% [213], while at the Tevatron's $\sqrt{s} = 1.96$ TeV, it is 74.8% [214]. In the SM3, the Higgs production cross section is dominated by the triangle diagram in Fig. 6.1 a) with $q = t$. While its amplitude decreases proportional to $1/m_q$ for $m_q \to \infty$, this is compensated by the quark's Yukawa coupling to the Higgs which is $y_q \propto m_q$ [215, 216]. The heavy t' and b' quarks contribute in similar diagrams with $q = t'$ and $q = b'$.

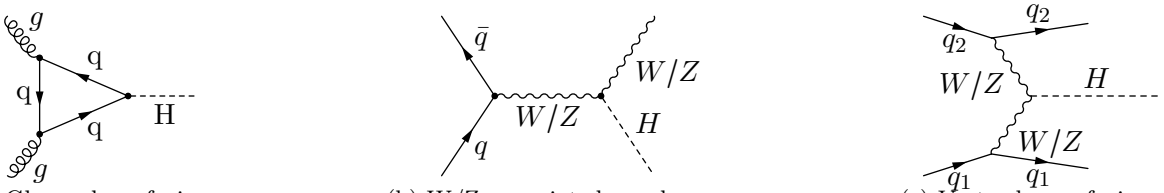

(a) Gluon-gluon fusion (b) W/Z associated production (c) Vector boson fusion

Figure 6.1.: Main Higgs production processes at Tevatron and LHC at first order. Vector boson fusion is sometimes referred to as "Higgs-Strahlung".

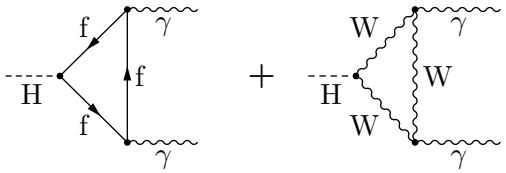

Figure 6.2.: Lowest-order contributions to $H \to \gamma\gamma$ which accidentally almost cancel in the SM4.

This leads to an increase of the cross section prediction by a factor of approximately 9 [217]. All other things unchanged (and keeping in mind that the other Higgs production channels do not receive this enhancement), one might expect a corresponding increase in the products $\sigma(gg \to H \to Y) = \sigma(gg \to H) \cdot \mathcal{B}(H \to Y)$ and, hence, the signals observed at the LHC. It was shown [218, 219], however, that the large Yukawa couplings y_q of such heavy quarks lead to sizeable higher-order corrections. They cause a suppression of the effective couplings HWW and HZZ. Therefore, the branching ratios $\mathcal{B}(H \to WW^*, ZZ^*)|_{\mathrm{SM4}}$ are reduced by a factor of 0.2 or smaller compared to the SM3. By the same mechanism, the cross sections of Higgs production in vector boson fusion and W/Z associated production are suppressed compared to the SM3.

Such a suppression is not possible for the decay $H \to \tau\bar{\tau}$ so that $\sigma(gg \to H \to \tau\bar{\tau})$ should indeed be enhanced along with $\sigma(gg \to H)$.

In case of the decay $H \to \gamma\gamma$, an accidental cancellation between fermion and gauge boson mediated contributions (see Fig. 6.2) takes place in the SM4 [218, 219]. It would make the Higgs unobservable in this decay channel at ATLAS and CMS [219].

Provided the 4th generation's neutrino ν_4 is light enough, i.e. $m_{\nu_4} \leq m_H/2$, the Higgs boson can decay in the process $H \to \nu_4\bar{\nu}_4$. If, then, the 4th generation's charged lepton is heavier than the ν_4 and neutrino mixing is small, then the ν_4 is sufficiently long-lived to escape detection by experiment. The Higgs boson's decay width Γ_H would, however, increase while the branching ratios of all visible Higgs decay channels would decrease by a common factor.

6.2.1. Higgs Discovery and the SM4

In 2012, a Higgs candidate was observed at ATLAS [220] and CMS [39] at a mass of ≈126 GeV. Assuming that the excesses observed did indeed stem from a Standard Model-like Higgs boson, three increasingly sophisticated analyses [101, 35, 40] of its measured branching fractions succeeded in ruling out a sequential fourth generation. Their salient points are shortly repeated here, with an emphasis on the last of the three publications.

In these publications, results of global fits were presented which combined Electroweak Precision Observables and a number of Higgs detection channels used for measurements at the LHC and the Tevatron (see Table 6.1 for a listing), both in an SM3 and an SM4 framework. The obtained χ^2 values were used as a test statistic to compare the performance of the models. In [40], the fit parameters were the Z mass m_Z, the top quark mass, the strong coupling constant α_s, the hadronic contribution to the fine structure constant $\Delta\alpha^{(5)}_{\mathrm{had}}(m_Z)$ and the Higgs mass m_H. In the SM4 fit, this was augmented by the masses of the fourth generation fermions. For all of them, an upper limit of 800 GeV was chosen. As lower limits, $m_E > 100$ GeV, $m_{\nu 4} > m_Z/2$ and the t' and b' quarks were required to be heavier than 400 GeV. Mixing between the 4th generation and the three SM generations of quarks was neglected as suggested by the results in [101]. The

Electroweak Precision inputs were almost the same as the input used to generate the lookup table used for the fits in the present thesis. They are listed in Table 4.3. The differences between Table 4.3 and the inputs in [40] are given in Table 6.2. They should be tiny enough to be ignored, i.e. to consider the EWP constraints provided by the Lookup Table used in this thesis (cf. sec. 4.2.1) as identical to the constraints one would obtain with the input values used in [40].

The Higgs sector input were several signal strengths $\hat{\mu}(X \to H \to Y)$. A measured (predicted) signal strength is defined as the observed (predicted) product $\sigma(X \to H) \cdot \mathcal{B}(H \to Y)$ divided by its SM3 prediction

$$\hat{\mu} = \frac{\sigma(X \to H)\mathcal{B}(H \to Y)|_{\text{exp(pred)}}}{\sigma(X \to H)\mathcal{B}(H \to Y)|_{\text{SM3}}}. \tag{6.3}$$

The predicted SM4 signal strength which was then fitted to the data was obtained as follows: For each Higgs production mechanism $H \to X$ considered, the SM3 prediction of the production cross section $\sigma(X \to H)|_{\text{SM3}}$ was multiplied with the SM4/SM3 ratio of the decay width of the reversed production mechanism, i.e. $H \to X$:

$$\sigma(X \to H)|_{\text{SM4}} = \sigma(X \to H)|_{\text{SM3}} \frac{\Gamma(H \to X)|_{\text{SM4}}}{\Gamma(H \to X)|_{\text{SM3}}} \tag{6.4}$$

The fraction in this equation is the modification of the effective coupling in the SM4 and was calculated by HDECAY v4.45 [225]. In order to obtain the SM4's prediction of the signal strength, eq. (6.4) was multiplied by the SM4 branching fraction $\mathcal{B}(H \to Y)|_{\text{SM4}}$ which was also computed by HDECAY:

$$\hat{\mu}(X \to H \to Y)|_{\text{SM4}} = \sigma(X \to H)|_{\text{SM3}} \frac{\Gamma(H \to X)|_{\text{SM4}}}{\Gamma(H \to X)|_{\text{SM3}}} \cdot \mathcal{B}(H \to Y)|_{\text{SM4}} \tag{6.5}$$

It turns out that the χ^2 value achieved by the SM4 is significantly higher than the SM3 value if the observed excesses at $\sqrt{s} \approx 126$ GeV are assumed to be indeed caused by an SM-like Higgs. Both are plotted against m_H in Fig. 6.3.

On a physical level, the incompatibility of the SM4 with the observation can be described as follows: The experimental results prefer a slightly reduced signal strength in the $pp \to H \to WW^*, ZZ^*$ decay. This could be e.g. accomodated by an appropriately light ν_4 which would lead to invisible decays. This would also suppress the event rate in the $pp \to H \to \gamma\gamma$ decay where the factor of 9 in the Higgs production cross section is overcompensated by the reduction of the branching fraction $\mathcal{B}(H \to \gamma\gamma)$ due to destructive interference between W boson and heavy fermion loops, but one observes an excess in the $\gamma\gamma$ final state. This disfavours the "light ν_4" scenario significantly. The SM4 predicts a slight reduction of the HW/HZ associated production cross section in $\hat{\mu}(p\bar{p} \to H \to b\bar{b})$ at the Tevatron compared to the SM3. The measurement, however, shows a dramatic increase. Finally, the decay $H \to \tau\tau$ is not affected by the cancellation which overcompensates the SM4 increase of the gluon-gluon fusion cross section, so the signal strength $gg \to H \to \tau\bar{\tau}$ should reflect this increase. Instead, a reduced signal is observed. At the end of the day, both the SM4 and the SM3 struggle to describe the excesses (see Fig. 6.4), but the SM3 fares a lot better.

Using the *my*Fitter software described in sec. 6.1, we succeeded at excluding the SM4 with a

Process	Reference(s)	Combined $\hat{\mu}$ at 126 GeV
$pp \to H \to \gamma\gamma$	[220, 221]	$1.583^{+0.337}_{-0.345}$
$pp \to H \to WW^*$	[220, 39]	$0.905^{+0.323}_{-0.294}$
$pp \to H \to ZZ^*$	[220, 39]	$0.861^{+0.391}_{-0.285}$
$p\bar{p} \to HV \to Vb\bar{b}$	[222]	$2.127^{+0.806}_{-0.763}$
$pp \to HV \to Vb\bar{b}$	[220, 39]	$0.478^{+0.783}_{-0.680}$
$pp \to H \to \tau\tau$	[39, 223]	$0.100^{+0.714}_{-0.699}$

Table 6.1.: Experimental inputs for Higgs signal strengths used in [40] in the fit which excluded the SM4 at 5.3 σ level. Except for $H \to \gamma\gamma$, CMS had only provided signal strengths at 125.5 GeV. ATLAS had not published a 2012 update on $H \to \tau\bar{\tau}$ and $H \to b\bar{b}$ data, so 2011 data was used. Table reproduced from [40].

Quantity	LUT input	Ref.	Input in [40]	Ref.
$\sin^2\theta_\ell^{\text{eff}}$	0.2324 ± 0.0012	[105]	$0.2324 \pm 0.0012 \pm 0.000047$	[171],[105]
m_t^{pole}	$(173.07 \pm 0.52 \pm 0.72)$ GeV	[168]	$(173.18 \pm 0.56 \pm 0.75)$ GeV	[224]

Table 6.2.: Differences between the input set used to obtain the lookup table used in the fits of chapter 5 (cf. sec. 4.2.1) and the input set used to exclude the SM4 in [40].

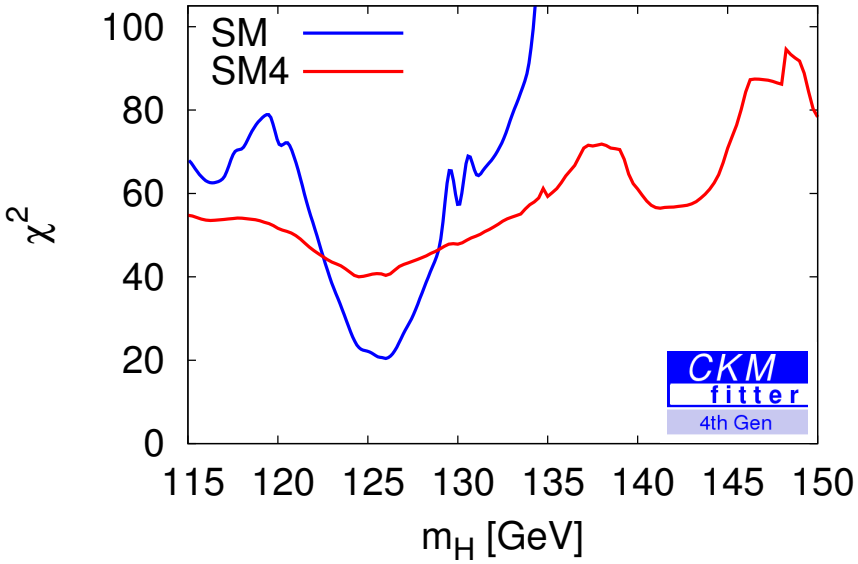

Figure 6.3.: Higgs mass scan for the SM (blue line) and the SM4 (red line) based on the input set in Table 6.1. Reproduced from [40].

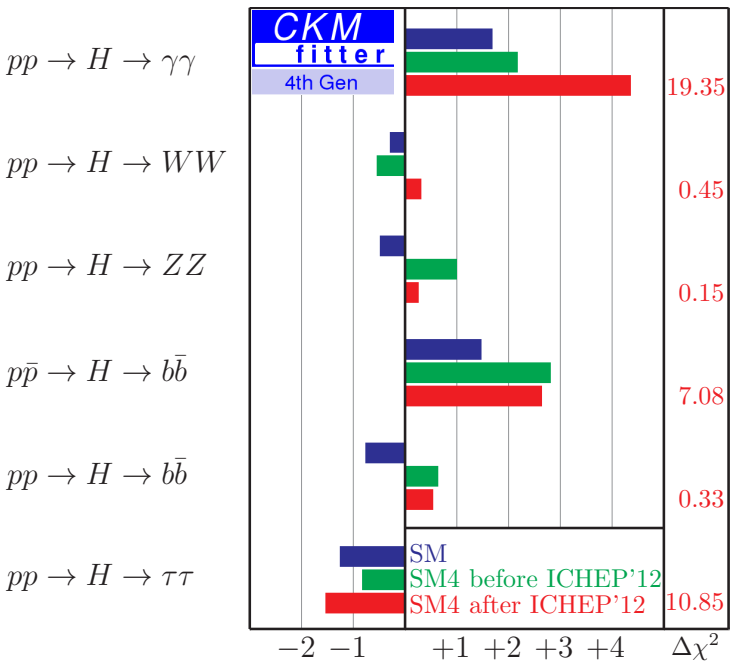

Figure 6.4.: "Pulls" of the Higgs signal strengths for the SM (blue) and for the SM4 (red) at a fixed Higgs mass of 126 GeV. For comparison the results of the fit to pre-ICHEP2012 data from [35] are also shown in green. In the right column we show, for the SM4 fit to current data, the change in the minimum χ^2 value when the corresponding signal strength is removed from the fit. Plot reproduced from [40].

significance of 5.3 σ based on the Higgs measurements [40].

6.3. Comparison of SM4 and SM3 fit results

The SM3 χ^2 minimum $\chi^2_{min;\mathrm{SM3}}$ to which the result of the previous chapter,

$$\chi^2_{min;\mathrm{SM4,All}} = 9.56, \tag{6.6}$$

will be compared was obtained by repeating the fits of sec. 5.4 within an SM3 framework. For modifications of the "standard" CKMfitter SM3 theory packages, see sec. 3.3.

The inputs are identical to those of the SM4 fits except in case of V_{ud}, where the origina result from [118] as given in eq. (4.2) was used. The SM3 achieved

$$\chi^2_{min;\mathrm{SM3}+\mathcal{B}(\mathrm{W}\to\ell\nu)} = 15.53. \tag{6.7}$$

Naively, the numbers N_{dof} of degrees of freedom in both fits satisfy

$$N^{\mathrm{SM4}}_{dof} = N^{\mathrm{SM3}}_{dof} - 6 \tag{6.8}$$

because there are six parameters more in the SM4 fits than in the SM3, namely the five additional CKM matrix parameters and the t' quark mass; and both fits use the same number of inputs. If all likelihood components are Gaussians (cf. eq. (3.3)) and if no input uncertainties are overestimated or underestimated, one expects $\chi^2/N_{dof} = 1$. Comparing the χ^2_{min} values above, their difference is almost exactly 6, so this estimate suggests that both SM4 and SM3 describe the inputs equally well.

Besides the χ^2 comparison, the pulls of the individual inputs in both models were compared in Table 6.3. A graphical representation is shown in Fig. 6.5. In the SM3, there are more inputs which do not have any impact on the χ^2 value than in the SM4. All of them are "tree level observables" as described in Chapter 4. Also, in general, the pulls in the SM3 tend to be smaller - in cases of the CP-violating observables $|\epsilon_K|$ and $\sin(2\beta - 2\theta_d)$, quite dramatically so. In loop observables in general, there is a tendency that the pulls in the SM4 fit are larger. In case of the $\Delta\chi^2$, it is the SM3 values which tend to be larger. Exceptions are Δm_s and $\frac{\Gamma(b\to s\gamma)}{\Gamma(b\to ce\bar{\nu})}$. The general picture should not be too surprising: In the SM3, the lower number of parameters y_{mod} enables fewer precise inputs to constrain other less precisely measured quantities. As a result, it is more likely that tensions between inputs arise. In the SM4, on the other hand, the the additional parameters cause less precise predictions - and hence, larger pulls despite low χ^2 values. Other points to note are:

- $\frac{\Gamma(b\to s\gamma)}{\Gamma(b\to ce\bar{\nu})}$, $\mathcal{B}(B\to\tau\nu)$, γ, Δm_d and $|V_{cb}|$ cause more tension in the SM4 than in the SM3, but only once the $a^{d,s}_{SL}$ inputs are added (cf. Tab. 5.17 and Fig. 5.9).
- $|V_{ud}|$ and $|V_{cd}|$ also have a higher $\Delta\chi^2$ in the SM4, but *not* due to the a_{SL} inputs.

Input	SM4		SM3	
	Pull	$\Delta\chi^2$	Pull	$\Delta\chi^2$
$\lvert V_{ud}\rvert$	-1.93	0.19	-0.172	0.00
$\lvert V_{us}\rvert$	-1.12	0.00	0.878	0.00
$\lvert V_{ub}\rvert$	1.67	0.17	-0.524	0.00
$\lvert V_{cd}\rvert$	-0.65	0.39	-0.400	0.16
$\lvert V_{cs}\rvert$	-0.062	0.00	-0.0664	0.00
$\lvert V_{cb}\rvert$	-0.96	0.00	0.370	0.00
$\lvert V_{tb}\rvert$	-0.679	0.45	-0.638	0.41
$\mathcal{B}(W \to e\bar{\nu})$	0.686	0.00	0.64	0.01
$\mathcal{B}(W \to \mu\bar{\nu})$	1.79	2.21	1.76	2.19
$\mathcal{B}(W \to \tau\bar{\nu})$	-2.06	3.17	-2.08	3.30
$\mathcal{B}(B \to \tau\bar{\nu})$	-1.96	0.72	-1.774	2.14
γ	-0.37	0.79	-0.60	0.39
Δm_d	68.25	1.12	19.3	0.65
Δm_s	-15.7	0.01	-37.5	0.18
$\frac{\Gamma(b\to s\gamma)}{\Gamma(b\to ce\bar{\nu})}$	-0.810	0.16	-1.00	0.12
$\mathcal{B}(B_d \to \mu^+\mu^-)$	2.13	0.31	-1.82	3.30
$\mathcal{B}(B_s \to \mu^+\mu^-)$	12.71	0.02	1.04	0.78
$\sin(2\beta - 2\theta_d)$	-543	0.96	46.8	1.79
$\lvert\epsilon_K\rvert$	$\mathcal{O}(10^5)$	0.06	-13.45	0.12
$a_{SL}^{(\mathrm{s})}$	0.875	0.68	1.00	1.01
$a_{SL}^{(\mathrm{d})}$	2.35	1.07	-1.09	1.19

Table 6.3.: Pulls and $\Delta\chi^2$ of all input observables in SM4 and SM3 fits. For a graphical representation, see Fig. 6.5.

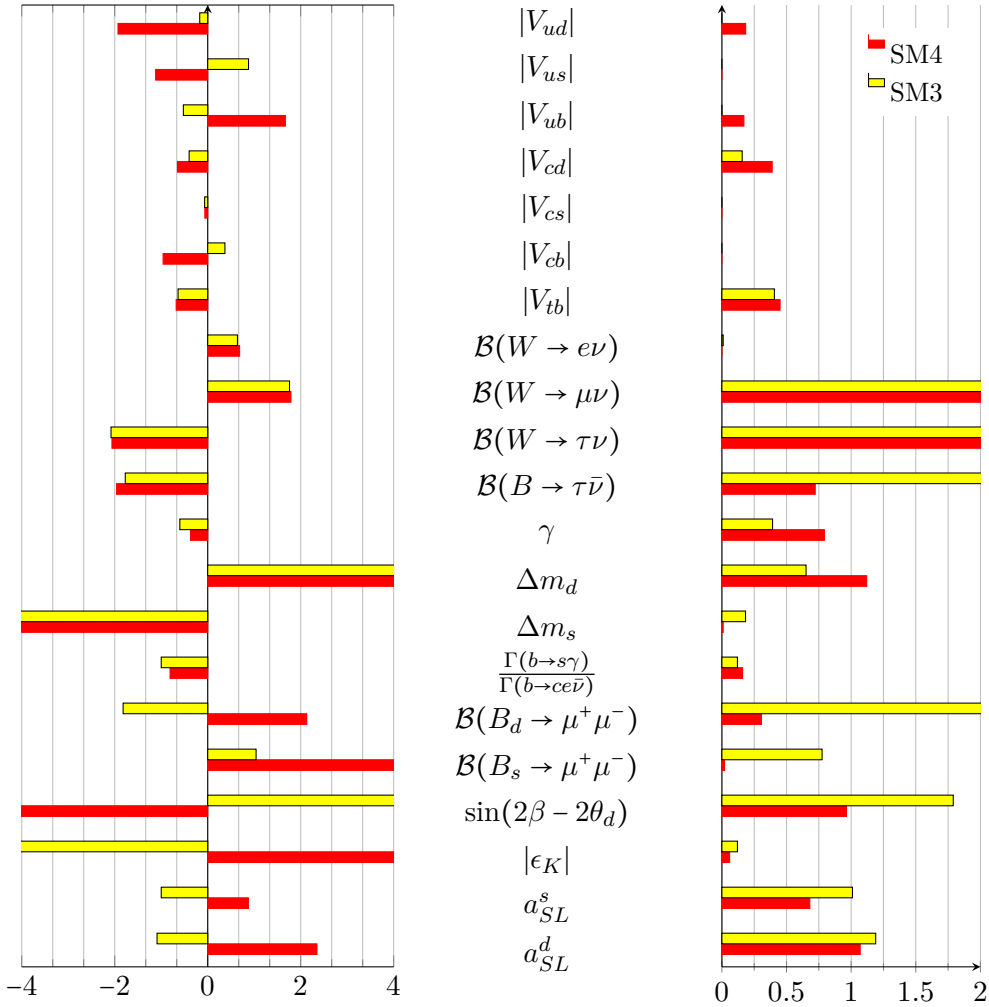

Figure 6.5.: Pulls (left) and $\Delta\chi^2$ (right) of all input observables in SM4 and SM3 fits. As only a few inputs show pulls or $\Delta\chi^2$ outside of the plotted ranges, the horizontal axes are truncated for better readability. See Table 6.3 for numerical values.

6.4. A_{SL} and $a_{SL}^{d,s}$ Predictions in the SM4 and the SM3

As SM3 predictions of the dimuon charge asymmetry A_{SL} are currently several standard deviations away from the experimental results (cf. e.g. eq. (4.144)), such a prediction provides another test for the SM4's comparative performance. The "normal" procedure would be to include it in the fit as an input and examine its influence on the χ^2 and its pull as was done with other inputs. However, due to the reasons described in sec. 4.4.4, it was finally decided to merely use the fit to predict A_{SL}. In this section, such a prediction is given and compared to the SM3 prediction and various other extractions.

The prediction of A_{SL} in an SM3 fit with the complete set of inputs as defined in the previous Chapter is

$$A_{SL}^{\mathrm{SM3}} = (-3.02^{+0.25}_{-1.62}) \cdot 10^{-4}, \tag{6.9}$$

corresponding to a relative uncertainty of ≈ 31 %[1]. Compared to the SM4 prediction with the complete set of inputs,

$$A_{SL}^{\mathrm{SM4}} = (2.47^{+0.80}_{-0.50}) \cdot 10^{-3}, \tag{6.10}$$

(relative error: ≈ 26 %) the sign is different and the modulus is smaller by a factor of 8. As for a comparison to experimental results, the new contribution to A_{SL} put forward in [203] (cf. sec. 4.4.4) rises the question: To which experimental result is the prediction to be compared? Table 6.4 contains a set of candidates.

Fig. 6.6, illustrating the contents of Table 6.4, shows that the choice between them is not very important: All values extracted from the A_{CP} measurement in [200] (i.e. No. 1, 2, 3, 4 and 6) are covered by the 1 σ interval of No. 1, the smallest of them all. Value 7, extracted from a_{CP}, is the only exception but its own uncertainty is much larger than the others'. Value 8 was obtained by inserting the $a_{SL}^{d,s}$ and parameter inputs used in the fits (cf. Tabs. 5.1 and 5.2) into eq. (4.142). Value 5, an older average of extractions from CDF [211] and D0[202] without considering A_d^{int}, does not quite agree with all of the others but it also points in the same general direction as the rest of Tab. 6.4:

The SM3 prediction is either covered by the 2 σ or the 3 σ range of most values. Exceptions are value No. 7 whose huge uncertainty covers eq. (6.9) even with its 1 σ range, and value No. 5 whose 3 σ interval does not come close. With its positive sign, the SM4 prediction deviates even more from the experimental values.

With such significant discrepancies between both predictions and the various experimental results quoted above, it seems worthwile to look one step below, i.e. at a_{SL}^d and a_{SL}^s. The relevant numerical values are listed in Table 6.5 and plotted in Fig. 6.7. In case of a_{SL}^d, all SM4 fit results's 1 σ intervals overlap with that of the input. This is not true for the SM3 predictions because the absolute width of the error intervals of the predictions are very small. Unlike the SM3, the central values of the SM4 predictions carry the same sign and order of magnitude as the experimental input. However, in terms of the χ^2 achieved in each fit, the SM4 does not benefit from this "success" because the distance between the experimental 1 σ limit and the predicted central value is larger than in case of the SM3 predictions. In case of a_{SL}^s, the preferred value of each SM4 fit is covered by the input's 1 σ value, but the reverse is not true: The central value of

[1] In case of asymmetric error intervals, this will be given based on *half* the 1σ interval's width.

No.		Value	Source
1	$A_{SL}^{\mathrm{SM3,D0}}$	$(-4.96 \pm 1.53 \pm 0.72) \cdot 10^{-3}$	Ref. [200], note sec. 4.4.4
2		$(-5.2 \pm 2.4) \cdot 10^{-3}$	Analysis of [200] retraced (no fit)
3	A_{SL}^{SM3}	$(-5.6 \pm 2.6) \cdot 10^{-3}$	Like No. 2, but corrected A_d^{int}
4	A_{SL}^{NoInt}	$(-6.1 \pm 2.9) \cdot 10^{-3}$	Assuming CPV in mixing only
5	A_{SL}^{2013}	$(-7.4 \pm 1.9) \cdot 10^{-3}$	[159]
6	A_{SL}^{SM4}	$(-5.5 \pm 2.6) \cdot 10^{-3}$	Corrected A_d^{int}, SM4
7	$A_{SL}^{\mathrm{single-muon}}$	$-0.010 \pm 0.013 \pm 0.019$	From a_{CP} measured in [200].
8	$A_{SL}^{\mathrm{eq.\ (4.142)}}$	$(-4.2 \pm 2.0) \cdot 10^{-3}$	From equation (4.142)

Table 6.4.: Results of various extractions of A_{SL} from experiment. For definitions, see text and also sec. 4.4.4. For a graphical representation, see Fig. 6.6.

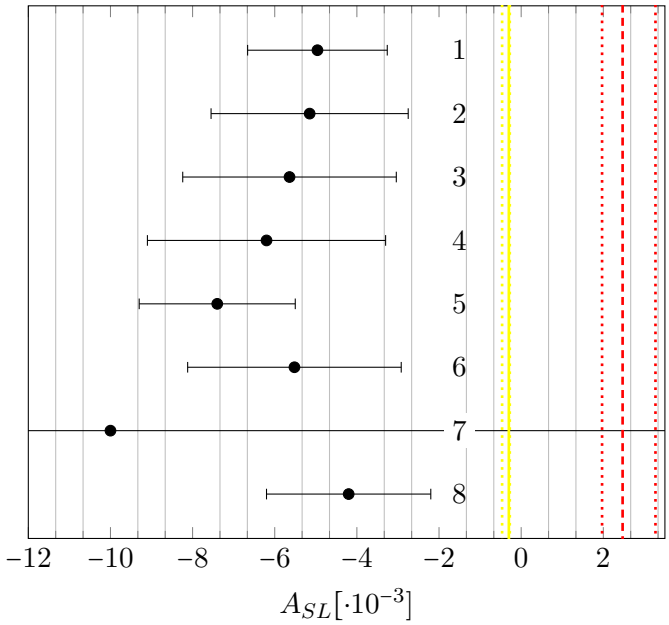

Figure 6.6.: Graphical representations of the experimental results of A_{SL} listed in Tab. 6.4. Statistical and systematic errors of values 1 and 7 were added quadratically. The yellow lines represent the central value and 1 σ range of the SM3 prediction given in eq. (6.9). The red lines show the location of the SM4 prediction.

	a_{SL}^d	δa_{SL}^d	a_{SL}^s	δa_{SL}^s
SM3 LoopCPV	$(-6.5 \pm 1.7) \cdot 10^{-4}$	0.26	$(2.6^{+2.6}_{-1.8}) \cdot 10^{-5}$	0.85
SM3 Complete	$(-5.4^{+0.49}_{-2.79}) \cdot 10^{-4}$	0.30	$(2.33^{+1.23}_{-0.19}) \cdot 10^{-5}$	0.30
SM4 LoopCPV	$(5.9^{+5.5}_{-1.8}) \cdot 10^{-3}$	0.62	$(-5.7^{+4.5}_{-9.9}) \cdot 10^{-4}$	1.26
SM4 Complete	$(8.4^{+3.4}_{-4.5}) \cdot 10^{-3}$	0.43	$(-6.0^{+5.2}_{-5.7}) \cdot 10^{-4}$	0.90
Exp. input in fits	$(2.3 \pm 2.6) \cdot 10^{-3}$	1.13	$(-4.8 \pm 4.8) \cdot 10^{-3}$	1.00
SM4 result with exp. input	$(4.73^{+1.29}_{-0.80}) \cdot 10^{-3}$	0.44	$(-8.7^{+7.5}_{-3.7}) \cdot 10^{-4}$	1.29

Table 6.5.: Constraints of a_{SL}^d and a_{SL}^s obtained in fits with LoopCPV and complete set of inputs, both in SM3 and SM4, in comparison with the experimental input (cf. Tab. 4.3). The last line was obtained using the experimental input of the quantity constrained as given in the fifth line. The values above are predictions from the fit. The third and fifth column contain the relative errors. For a graphical version, see Fig. 6.7.

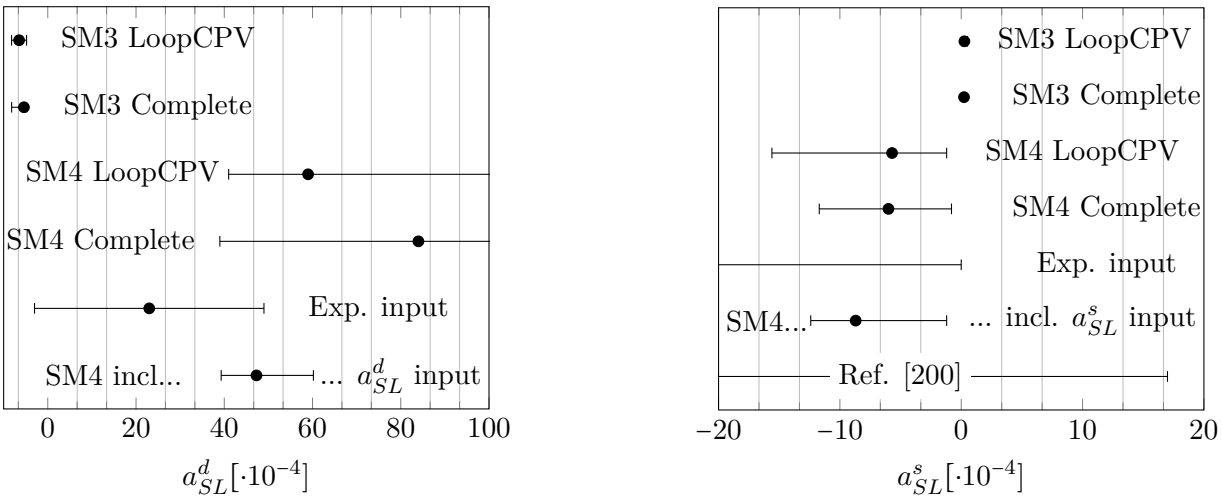

Figure 6.7.: Graphical representation of the results of a_{SL}^d and a_{SL}^s given in Table 6.5. "SM4 incl. a_{SL}^s input" refers to the result of the fit including the experimental input of the quantity to be constrained (sixth row in Table 6.5). The horizontal axes were truncated to contain only the range of a_{SL}^d and a_{SL}^s in which the 1 σ intervals overlap in order to keep both the plots' widths and their readability to acceptable levels.

the experimental input is not even covered by the 3σ range of the fits. Again, the SM4 predictions both carry the same sign as the experimental inputs while the SM3 predictions do not. The SM3 predictions' 1 σ intervals overlap neither with those of the experimental inputs nor those of the SM4 fit results. The agreement of the SM4 prediction with experiment is therefore better, but only marginally so.

In both the SM4 and the SM3, the fits predict a_{SL}^{d} to be an order of magnitude larger than a_{SL}^{s}. The experimental inputs show now sign of this, but given their current precision, it cannot be excluded that the predictions are correct. Thus, on the level of a_{SL}^{d} and a_{SL}^{s}, and judging by their influence of the global χ^2, the SM4 describes the observed physics marginally better than the SM3 does.

Returning to A_{SL}, the situation can be described as follows: The sign of the SM3's $a_{SL}^{d,s}$ predictions, which are in conflict with experiment, and the likewise unobserved difference in their magnitudes happen to bring the SM3's prediction of A_{SL} closer to the experimental values. As value No. 8 in Table 6.4 shows, expression (4.142) - which was used for the various SM3 and SM4 predictions - reproduces the experimental A_{SL} values well when the experimental results for a_{SL}^{s} and a_{SL}^{d} are inserted.

Given the above discussion of A_{SL} and $a_{SL}^{d,s}$ inputs and predictions by both models, there is still no argument found in the fits performed in this thesis to rule out the SM4, but neither does show much promise to resolve the tensions between the measured A_{SL} and its predictions.

7. Conclusion

The number of fermion generations in nature is highly non-trivial to predict. While three generations are a lower limit if e.g. CP violation in charged currents is to be incorporated, an upper limit has long been subject to research. In recent years, for the case of additional sequential generations of Dirac fermions, the question had been boiled down to the decision between three and four e.g. by fits to Electroweak Precision data (e.g. [4, 5, 6]). The Standard Model with four sequential generations - referred to as "the SM4" in this thesis - had indeed undergone a period of revived interest after it had been shown e.g. in [4] that it was on one hand compatible with experimental limits of the day and that it was, on the other hand, likely to be confirmed or excluded by the LHC which was just about to commence operation. Also, a fourth generation had been suggested as a source of the amount of CP violation needed for Baryogenesis, an explanation for a number of discrepancies in flavour physics and a number of other puzzles. However, shortly after the Higgs boson had been discovered and its production and decay channels had been measured, we succeeded at excluding the SM4 at the 5.3 σ level based on Electroweak Precision data and Higgs cross sections [40]. A remaining question was whether this exclusion of the SM4 would stand the test of including Precision Flavour physics observables in the fit. If the SM4 was sufficiently superior to the SM3 in its ability to describe Flavour physics, the 5.3 σ exclusion could at least have been reduced, given that the SM3 has e.g. difficulties at describing the semileptonic charge asymmetries a_{SL}^d, a_{SL}^s and A_{SL}.

This thesis thus examined the ability of the SM4 to globally fit a combination of a typical set of Precision Flavour Physics inputs and the result of a fit of Electroweak Precision observables without resorting to their parametrisation in terms of the "oblique parameters" S, T and U [98]. As a result of previous work, the effect of the Electroweak Precision input on the SM4 had been condensed into a non-trivial correlation of the fourth generation's up-type quark mass with the mixing between the 3rd and 4th quark family. All Flavour physics related measurements used as experimental inputs were re-interpreted in terms of an SM4 framework if necessary. The fits were performed with the CKMfitter software which, in the standard setting used, gives constraints on observables and parameters by means of the frequentist *R*fit scheme. The quantities constrained in this way are free parameters of the Standard Model with a sequential fourth fermion generation. To determine which input is responsible for which constraint, four series of fits were produced. Starting with fits using only "Tree Level" observables - i.e. observables which can be at lowest order described by Tree Level Feynman graphs -, subsequent sets added "Loop" inputs which are only described at higher order, i.e. by Feynman graphs containing at least one loop. The fits to Loop observables were subdivided into an input set including only CP-nonviolating observables and another which also included inputs extracted from CP violating processes. The latter class of inputs was split into two steps for technical reasons, with the semileptonic charge asymmetries a_{SL}^s and a_{SL}^d added last.

The global minimum χ^2 achieved in the SM4 fits,

$$\chi^2_{\mathrm{SM4}} = 9.56$$

is lower than the SM3's value

$$\chi^2_{\mathrm{SM3}} = 15.53.$$

As elaborated in sec. 6.3, this is consistent with the SM4 and the SM3 describing the input data equally well but the SM4 having six free parameters more. As the SM3 is not nested in the SM4, a statistically stringent p-value cannot be given on the basis of a likelihood comparison, and it is not possible to correctly state the influence of the Flavour input on the significance on the SM4's exclusion by the fit to Higgs cross sections and the EWP data in [40]. A consistent study would require a combination of the present inputs with Higgs sector inputs e.g. in a computation using the *my*Fitter software [210] which had been developed specifically compare non-nested models and which made the 5.3 σ exclusion in [40] possible. At the time of writing, however, most flavour observables are not implemented in *my*Fitter, and the present project's time and manpower budgets did not allow to change this state of affairs.

The interpretation of the dimuon charge asymmetry A_{SL} was subject to discussion - see sec. 4.4.4 - at the time of writing. Therefore, A_{SL} was not used as an input in the present thesis. Instead, A_{SL} was predicted in both the SM4 and the SM3 as another means of comparing them. While the exact numbers depend the choice of the experimental input and its interpretation, the SM3's prediction is typically too large by approximately 2 σ, and the SM4's by around 3 σ.

Finally, even with the statistical caveats outlined above and disregarding the tensions with A_{SL}, it seems unlikely that the reduction of the χ^2 minimum achieved by replacing the SM3 by the SM4 is enough to make up for the SM4's bad agreement with experiment in the Higgs sector (cf. Sec. 6.2) which led to its exclusion.

If the need arises, the present work can be used as a basis for a statistically more precise study. With *my*Fitter available, this is only a question of someone taking the time to implement the SM4 expressions in this software. Furthermore, this thesis underlines once more the importance of the Higgs discovery and the measurement of its branching fractions, since it was shown that a combined fit of EWP and Flavour physics data would not have permitted a clear verdict in favour of or against the SM4.

Appendices

A. Other Parametrisations of the CKM Matrix

As the parametrisation of a mixing matrix is a matter of choice and four different possibilities are mentioned in this work, this Appendix lists all of them and prints those which are not explicitely printed in other sections.

A.1. Standard SM3 parametrisation

In the SM3, the standard parametrisation in terms of three rotation angles and one phase used e.g. by the PDG is the one proposed by Chau and Keung in [61]:

$$\begin{pmatrix} c_{12}c_{13} & s_{12}c_{13} & s_{13}e^{-i\delta} \\ -s_{12}c_{23} - c_{12}s_{23}s_{13}e^{i\delta} & c_{12}c_{23} - s_{12}s_{23}s_{13}e^{i\delta} & s_{23}c_{13} \\ s_{12}s_{23} - c_{12}c_{23}s_{13}e^{i\delta} & -c_{12}s_{23} - s_{12}c_{23}s_{13}e^{i\delta} & c_{23}c_{13} \end{pmatrix} \tag{A.1}$$

A.2. Wolfenstein Parametrisation

Wolfenstein proposed [226] an expansion of the elements of the CKM matrix in terms of the parameter

$$\lambda = V_{us} \simeq 0.22. \tag{A.2}$$

The hierarchy in size of the CKM matrix elements and the requirement that the CKM matrix be unitary resulted in the choice of a parameter $A \approx 4/5$ to obtain the correct magnitude $|V_{cb}|$, and ρ and η. The original Wolfenstein parametrization reads

$$V_{CKM3} = \begin{pmatrix} 1 - \frac{\lambda^2}{2} & \lambda & A\lambda^3(\rho - \mathrm{i}\,\eta) \\ -\lambda & 1 - \frac{\lambda^2}{2} & A\lambda^2 \\ A\lambda^3(1 - \rho - \mathrm{i}\,\eta) & -A\lambda^2 & 1 \end{pmatrix}. \tag{A.3}$$

Unlike the standard parametrisation, there are no periodic functions used in eq. (A.3) which may be an advantage in numerically difficult fits - see Appendix B. Also, the expression is only unitary up to $\mathcal{O}(\lambda^4)$.

The SM3 part of the CKMfitter program uses a development of the original Wolfenstein parametrisation proposed in [227]. It was used to obtain the SM3 fits to which the SM4 results were compared in Chapter 6, so it is shortly given here. With $\cos\theta_{13} = 1 - \mathcal{O}(\lambda^6)$, the relations

$$\sin\theta_{12} = \lambda, \qquad \sin\theta_{23} = A\lambda^2 \quad \text{and} \quad \sin\theta_{13}e^{-\mathrm{i}\,\delta} = A\lambda^3(\rho - \mathrm{i}\,\eta) \tag{A.4}$$

are assumed to hold at all orders in λ. This results in the following relations which also hold up

to at least $\mathcal{O}(\lambda^6)$:

$$\begin{aligned} V_{us} &= \lambda & V_{cb} &= A\lambda^2 \\ V_{ub} &= A\lambda^3(\rho - \mathrm{i}\,\eta) & \mathrm{Im}\,(V_{cd}) &= -A^2\lambda^5\eta \\ \mathrm{Im}\,(V_{ts}) &= -A\lambda^4\eta \end{aligned}$$

Defining

$$\bar{\rho} = \rho(1 - \lambda^2/2) \quad \text{and} \quad \bar{\eta} = \eta(1 - \lambda^2/2), \tag{A.5}$$

$$V_{td} = A\lambda^3(1 + \bar{\rho} - \mathrm{i}\,\bar{\eta}). \tag{A.6}$$

Finally, one can then rewrite eq. (A.3) in terms of the parameters $A, \lambda, \bar{\rho}, \bar{\eta}$, which is the form used in CKMfitter. For more details, see [110].

A.3. Botella-Chau parametrization

This parametrisation for the SM4's CKM matrix was proposed by Botella and Chau [62][1] and others. It is obtained by multiplying the same matrices as those used for the Hou/Soni parametrization given in eq. (2.42) in a different order:

$$\begin{aligned} V_{CKM4} = &\begin{pmatrix} 1 & 0 & 0 & 0 \\ 0 & 1 & 0 & 0 \\ 0 & 0 & c_u & s_u \\ 0 & 0 & -s_u & c_u \end{pmatrix} \cdot \begin{pmatrix} 1 & 0 & 0 & 0 \\ 0 & c_v & 0 & s_v e^{-i\phi_3} \\ 0 & 0 & 1 & 0 \\ 0 & -s_v e^{i\phi_3} & 0 & c_v \end{pmatrix} \cdot \\ &\begin{pmatrix} c_w & 0 & 0 & s_w e^{-i\phi_2} \\ 0 & 1 & 0 & 0 \\ 0 & 0 & 1 & 0 \\ -s_w e^{i\phi_2} & 0 & 0 & c_w \end{pmatrix} \cdot \begin{pmatrix} & & & 0 \\ & V_{CKM3} & & 0 \\ & & & 0 \\ 0 & 0 & 0 & 1 \end{pmatrix} \end{aligned} \tag{A.7}$$

[1] There is an error in the matrix element V_{td} in the original publication.

Looking at the resulting CKM matrix in Botella/Chau form,

$$\left(\begin{array}{c:c:c:c}
c_w c_{12} c_{13} & c_w s_{12} c_{13} & c_w s_{13} e^{-i\delta} & s_w e^{-i\phi_2} \\ \hdashline
-s_v s_w c_{12} c_{13} e^{i(\phi_2-\phi_3)} & -s_v s_w s_{12} c_{13} e^{i(\phi_2-\phi_3)} & -s_v s_w s_{13} e^{i(\phi_2-\phi_3-\delta)} & s_v c_w e^{-i\phi_3} \\
-c_v s_{12} c_{23} & +c_v c_{12} c_{23} & +c_v s_{23} c_{13} & \\
-c_v c_{12} s_{23} s_{13} e^{i\delta} & -c_v s_{12} s_{23} s_{13} e^{i\delta} & & \\ \hdashline
-s_u c_v s_w c_{12} c_{13} e^{i\phi_2} & -s_u c_v s_w s_{12} c_{13} e^{i\phi_2} & -s_u c_v s_w s_{13} e^{i(\phi_2-\delta)} & s_u c_v c_w \\
+s_u s_v s_{12} c_{23} e^{i\phi_3} & -s_u s_v c_{12} c_{23} e^{i\phi_3} & -s_u s_v s_{23} c_{13} e^{i(\phi_3)} & \\
+s_u s_v c_{12} s_{23} s_{13} e^{i(\phi_3+\delta)} & +s_u s_v s_{12} s_{23} s_{13} e^{i(\phi_3+\delta)} & +c_u c_{23} c_{13} & \\
+c_u s_{12} s_{23} & -c_u c_{12} s_{23} & & \\
-c_u c_{12} c_{23} s_{13} e^{i\delta} & -c_u s_{12} c_{23} s_{13} e^{i\delta} & & \\ \hdashline
-c_u c_v s_w c_{12} c_{13} e^{i\phi_2} & -c_u c_v s_w s_{12} c_{13} e^{i\phi_2} & -c_u c_v s_w s_{13} e^{i(\phi_2-\delta)} & c_u c_v c_w \\
+c_u s_v s_{12} c_{23} e^{i\phi_3} & -c_u s_v c_{12} c_v e^{i\phi_3} & -c_u s_v s_{23} c_{13} e^{i\phi_3} & \\
+c_u s_v c_{12} s_{23} s_{13} e^{i(\phi_3+\delta)} & +c_u s_v s_{12} s_{23} s_{13} e^{i(\phi_3+\delta)} & -s_u c_{23} c_{13} & \\
-s_u s_{12} s_{23} & +s_u c_{12} s_{23} & & \\
+s_u c_{12} c_{23} s_{13} e^{i\delta} & +s_u s_{12} c_{23} s_{13} e^{i\delta} & &
\end{array}\right), \tag{A.8}$$

shows a very simple first row and fourth column. This parametrisation satisfies the criteria for a parametrisation given in [64] but, in the context of the present thesis, caused numerical problems (see Sec. B.1).

B. Convergence Problems with an Unsuited Parametrization

The work on the present thesis had long been bogged down by what turned out to be numerical problems. When including in the input the quantities $|\epsilon_K|$, a^d_{SL}, a^s_{SL} or A_{SL}, the result was erratic behaviour in fits, such as clearly unphysical spikes and discontinuities in both 1D and 2D plots. The first reaction was to subject the expressions implemented in the theory package `BBbarKKbarDDbarMixing4D` to thorough scrutiny, both by the author and Otto Eberhardt. Although a bug was found and, additionally, the expressions were changed to be numerically less expensive to compute, this did not solve the problem. From previous experience with CKMfitter, it seemed possible to succeed by adjusting the scan range in fits, changing their `granularity` or narrowing down the `startRanges` (cf. sec. 3.2.3). This turned out not to be the case. After a lenghty time of fruitless scrutiny did one plot, generated accidentally, show the magnitude and character of the problem. When a fit with all inputs except $\frac{\mathcal{B}(B\to X_s\gamma)}{\mathcal{B}(B\to X_c e\bar{\nu})}$ and $\mathcal{B}(B\to\mu^+\mu^-)$ was repeated ten times, all p-value curves were plotted together. A similar plot is shown in Fig. B.1. A number of features observed in the plot were thought of as clues for the solution. They are discussed here in some detail in order to provide some information to any reader facing similar problems at some point.

- There are several distict locations of the peak, i.e. 1-CL=1, corresponding to $\chi^2_{min;y_{mod}}$.
- p-value curves (i.e. technically: scan results) which are indistinguishable from each other for one value of the scanned quantity can separate from each other at another value. As an example, see the gray, magenta and turquoise curves in Fig. B.1 around $|V_{t'b'}| = 0.88$.

Before further discussing the behaviour of such problematic fits, it seems necessary to define some notation in order to avoid confusion. The values of parameters and observables which lead to $\chi^2 = \chi^2_{min;y_{mod}}$ will be denoted by a superscript ^{opt}, such as θ_{12}^{opt} or $|V_{t'b'}|^{opt}$. As discussed in sec. 3.1.1, a point or domain in parameter space (i.e. a vector of such observables and parameters) leading to $\chi^2 = \chi^2_{min;y_{mod}}$ will be named y^{opt}_{mod}. Any point or domain in parameter space which the minimizer claims to be the global minimum will be denoted as $\hat{y}$. The $\hat{}$ will also denote the associated values of observables and χ^2. A $\hat{y}$ clearly identified as false will bear a subscript f (false) as will the related values of observables and χ^2.

Returning to the two observations described above, the first one can a priori mean one of two things: Firstly, there could exist a subset of the parameter space in which the parameters could vary so that several values of $|V_{t'b'}|$ have the same χ^2, at least within machine accuracy. Secondly, and both simpler and more likely, the p-value maximum (corresponding to $\chi^2_{min;y_{mod}}$ in the language of section 3.1.1) is not found reliably. A closer examination ruled out the possibility

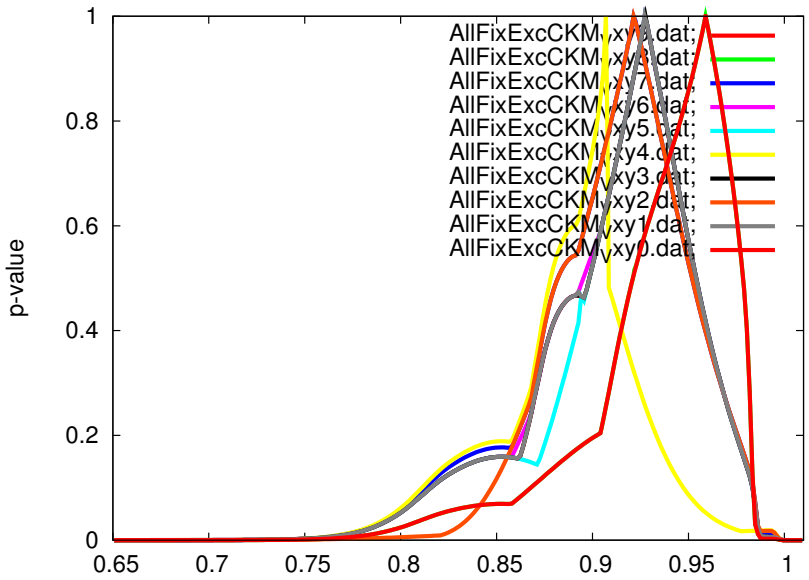

Figure B.1.: Ten p-value plot of $|V_{t'b'}|$ with identical settings and inputs. Plot and legend generated automatically with `ckmgnuplot`.

of several different values $|V_{xy}|$ corresponding to the same χ^2, let alone $\chi^2_{min;y_{mod}}$, identifying the second possibility as the immediate reason for different locations of the "peak".

The next step was to remove input observables one by one to find out if there was any particular one or any combination of observables that leads to trouble. Here, $|\epsilon_K|$ proves slightly problematic while the inclusion of any one of the inputs A_{SL}, a^d_{SL} or a^s_{SL} produced convergence problems reliably. Deactivating the use of the analytically computed gradient of χ^2 in CKMfitter didn't help in such cases. The following measure to track down the source of the trouble was to fix all parameters of the fit except the 9 CKM matrix parameters (θ_{12}, θ_{13}, θ_{23}, θ_u, θ_v, θ_w, δ, ϕ_2, ϕ_3) and assigning only Gaussian errors to input observables. This might have simplified the fit somewhat but it did nothing to visibly alleviate the problems. Increasing the setting `globalMinSearches` to 60000 - an unusually high value - improved the results only slightly while dramatically slowing down the fit. The same was found to be the case for increasing the values of the flags `granularity`, `nbOfFits` and `nbOfScans`. No correlation was found between the fluctuations in $\hat{\chi}^2$ and the location of the associated $\hat{y}$ in parameter space.

Following these results, the subsequent tests of the software were not performed in full scans of a quantity, but only in the search of the global minimum. This was perceived as a way to save computing time and, since the search for the global minimum $\chi^2_{min;y_{mod}}$ will always start at a random initial point y_i (within the `startRange` interval defined in the analysis datacard), it does not in any way interfere with the meaning of the results. In order to generate enough statistics, the CKMfitter code was slightly modified. For the ith global minimum search ($i = 1...10^6$), the code now recorded both the random initial point y_i with the associated χ^2_i and the parameter values $\hat{y}_i$ and $\hat{\chi}^2_i$ found by the minimizer. The statistics done on the results of these global

minimum searches were somewhat surprising. As illustrated by the histograms in Fig. B.2, there are two main observations to be made.

- The lowest $\hat{\chi}^2$ found in a series of otherwise identical fits was definitely *not* the one found most frequently.
- The histograms suggest that were are thousands of distinct local minima.

A crude shell/awk [228] script was used to quantify these observations. It reads the ordered list of $\hat{\chi}_i^2$ values which occurred in the minimizer runs into an array and then loops over its entries. In each step, the average value of the entries and their average deviation from said average are calculated. Then, the next χ^2 value is added and its deviation from the average is compared to the average deviation. If a - somewhat arbitrarily - selected threshold is exceeded, the entry is classified as new minimum. The script counts how often each $\hat{\chi}^2$ value occurs. By these slightly crude and probably not optimal means, it was observed that

- The lowest $\hat{\chi}^2$, hereafter referred to as $\hat{\chi}_0^2$, was only found in 18 (out of 10^6!) cases.
- The next-higher minimum $\hat{\chi}_1^2$ was found 30 times
- Typically, the resulting $\hat{\chi}^2$ within one group agreed to a very high precision: All 18 entries of the former group, for example, read $\chi^2_{min,0}$ = 13.88194674... while those of the latter group read $\chi^2_{min,1}$ = 13.887615990....
- A few minima could not be assigned to such a group. None such were found below the group at 13.88194674, however.

This indicates that the gradient search itself is not to blame for the bad reproducibility of a given $\hat{\chi}^2$. To a certain degree, this would have been surprising because the same minimizer had been used by `CKMfitter` for more than eight years and this kind of difficulty had not been encountered before. The low probability to find $\hat{\chi}_0^2$ - we never found a better one, but that does not mean $\hat{\chi}_0^2 = \chi^2_{min;y_{mod}}$! - explains why increasing the settings `globalMinSearches`, `granularity`, `nbOfFits` and `nbOfScans` did not improve the results a lot. Together with the run time of $\approx$ 31 hours, this means that simply generating more random points or increasing the granularity were not a feasible way to resolve the convergence problems. As for the location of this particular minimum, Table B.1 seems to show that $\hat{y}_0$ comprises more than one point in parameter space. In fact, this χ^2-wise equivalence is due to the ambiguities of trigonometric functions. All points within $\hat{y}_0$ are either symmetric with respect to a plane through the origin of the parameter space and perpendicular to one of the parameter axes (sign ambiguity) or the values of a given parameter differ by multiples of π. The next attempts at determining the source of the problem centered around the assumption of either a faulty computation of χ^2 or underconstrained physics. To come to grips with the latter, the correlation of the 9 CKM matrix parameters were examined in 2D plots. When no clear result was observed, some of the parameters were constrained while the others were left unconstrained and the process was repeated. Results remained unconclusive. The behaviour of the χ^2 function was examined by fixing all parameters except one to a previously determined point within $\hat{y}$ and generating random values within the allowed interval for the remaining parameter, thus effectively

doing a Monte-Carlo scan of an axis-parallel line in parameter space. The resulting χ^2 values were then plotted. No unexpected behaviour was to be seen. In particular, no "high-frequency" oscillation of the graph - as one might expect due to the presence of a myriad of $\hat{\chi}^2_f$s - was observed.

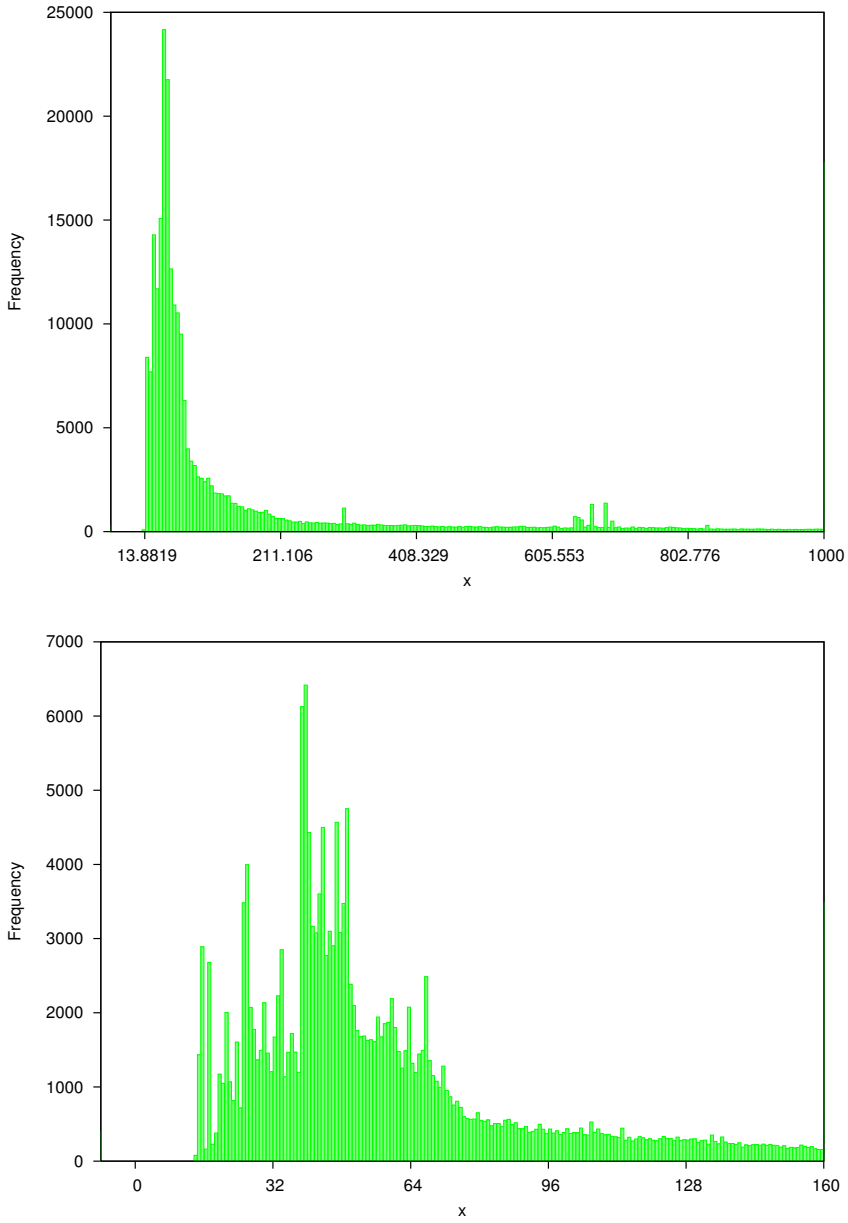

Figure B.2.: Histograms showing the frequency with which a given $\hat{\chi}^2$ value was returned as result of the global minimum search with 10^6 random initial points. The `x` label on the horizontal axes here denotes χ^2. b) is the same plot zoomed in.

θ_{12}	θ_{13}	θ_{23}	δ	θ_u	θ_v	θ_w	ϕ_2	ϕ_3
-0.2265638	$3.1372 \cdot 10^{-3}$	$4.16117 \cdot 10^{-2}$	1.0653	0.27666	0.076026	0.022316	1.46246	0.60313
0.2265638	$-4.3853 \cdot 10^{-3}$	$4.16117 \cdot 10^{-2}$	1.0653	-0.27666	3.06557	0.022316	1.46246	3.74472
0.2265638	$-4.3853 \cdot 10^{-3}$	$-4.16117 \cdot 10^{-2}$	-2.07623	0.27666	-0.076026	0.022316	-1.67913	0.60313
0.2265638	$4.3853 \cdot 10^{-3}$	$4.16117 \cdot 10^{-2}$	-2.07623	0.27666	-0.076026	0.022316	1.46246	3.74472
0.2265638	$-4.3853 \cdot 10^{-3}$	$4.16117 \cdot 10^{-2}$	1.0653	0.27666	0.076026	0.022316	1.46246	0.60313
0.2265638	$4.3853 \cdot 10^{-3}$	$-4.16117 \cdot 10^{-2}$	7.3485	0.27666	0.076026	0.022316	4.604	3.74472
-0.2265638	$4.3853 \cdot 10^{-3}$	$4.16117 \cdot 10^{-2}$	1.0653	-0.27666	0.076026	-0.022316	4.604	3.74472
0.2265638	$4.3853 \cdot 10^{-3}$	$4.16117 \cdot 10^{-2}$	-2.07623	0.27666	0.076026	-0.022316	-1.67913	0.60313
0.2265638	$-4.3853 \cdot 10^{-3}$	$4.16117 \cdot 10^{-2}$	1.0653	0.27666	0.076026	0.022316	1.46246	0.60313
0.2265638	$4.3853 \cdot 10^{-3}$	$-4.16117 \cdot 10^{-2}$	1.0653	0.27666	-0.076026	-0.022316	1.46246	0.60313
0.2265638	$4.3853 \cdot 10^{-3}$	$4.16117 \cdot 10^{-2}$	-2.07623	0.27666	-0.076026	0.022316	1.46246	3.74472
-0.2265638	$-4.3853 \cdot 10^{-3}$	$-4.16117 \cdot 10^{-2}$	1.0653	-0.27666	0.076026	0.022316	4.604	0.60313
0.2265638	$4.3853 \cdot 10^{-3}$	$-4.16117 \cdot 10^{-2}$	1.0653	0.27666	0.076026	0.022316	-1.67913	3.74472
0.2265638	$4.3853 \cdot 10^{-3}$	$4.16117 \cdot 10^{-2}$	-2.07623	-0.27666	0.076026	0.022316	4.604	3.74472
0.2265638	$-4.3853 \cdot 10^{-3}$	$4.16117 \cdot 10^{-2}$	1.0653	0.27666	0.076026	0.022316	1.46246	0.60313
0.2265638	$4.3853 \cdot 10^{-3}$	$4.16117 \cdot 10^{-2}$	-2.07623	0.27666	0.076026	0.022316	1.46246	0.60313
0.2265638	$4.3853 \cdot 10^{-3}$	$-4.16117 \cdot 10^{-2}$	1.0653	0.27666	0.076026	-0.022316	1.46246	3.74472
-0.2265638	$-4.3853 \cdot 10^{-3}$	$4.16117 \cdot 10^{-2}$	-2.07623	0.27666	0.076026	-0.022316	1.46246	0.60313

Table B.1.: Location of $\hat{\chi}^2_0$ in the parameter space as found in the 18 (of 10^6) instances when the search succeeded. All χ^2 values listed lie within $[0.138819467434, 0.138819467440]$.

B.1. A Surprisingly Late Solution

The solution was found when another parametrization of the CKM matrix was tried instead of the Botella/Chau proposal shown in eq. (A.8). The adoption of the Hou/Soni parametrization immediately solved or strongly alleviated the convergence problems. In retrospect, this is not very surprising: The Botella/Chau parametrisation keeps the first row and the fourth column of the CKM matrix very simple, the parametrisations of each element get more and more complicated the further down and to the left it is. Looking at how often each element of the CKM matrix appears in an input quantity,

$$\begin{pmatrix} 3 & 2 & 5 & - \\ 5 & 5 & 6 & - \\ 5 & 4 & 8 & - \\ 5 & 4 & 9 & - \end{pmatrix} \tag{B.1}$$

this seems awkward because for the calculation of χ^2, each matrix element which occurs in an input observable contributes to the latter's prediction which is then numerically compared to the input value. Many competing terms of (phase related) possibly opposite sign can cause numerical errors in this prediction and thus upset the χ^2 minimisation.

The Hou/Soni parametrisation, on the other hand, "relocates" potential numerical awkwardness to columns 1 and 4. As long as no $D^0\bar{D}^0$-mixing input is used, the fourth column is not compared to any input, so numerical errors will not upset the fit. In the first column, there is - possibly by sheer coincidence - only one element V_{td} where similarly-sized summands occur (cf. Table 5.3). Finally, column 3 contains only very simple terms which is useful as many different inputs depend on them. Similarly, row 4 is kept simple.

With these things in mind, it should be possible to construct a parametrisation with optimized numerical behaviour as even the Hou/Soni parametrisation may not be the best (cf. secs. 3.2.3 and 5.3.1). However, with the Hou/Soni parametrisation satisfying the requirements of the present work and the exclusion of the SM4, this is hereby declared to be beyond the scope of this work.

Reviewing the ideas that went into the scrutiny of the convergence problems in view of the history of the SM4 implementation in CKMfitter does shed some light on why the true nature of the problem was not discovered earlier: The first parametrization of the SM4 CKM matrix was a Wolfenstein style expansion. It was replaced by the Botella/Chau version only after having proven to be unsuitable. One symptom were jagged, ugly and unpredictable plots not unlike what was encountered during the work on the present thesis. However, in case of the Wolfenstein parametrization, such plots always were associated with a single $\hat{y}$ found containing parameter values of very different orders of magnitude - a perfect condition for numerical trouble to occur. Widely varying parameter values were not encountered with the Botella/Chau parametrisation, but inferring from this that the parametrisation was numerically suitable was wrong: As this parametrisation is built from trigonometric functions which are periodic, there is no reason to expect numerical problems to produce huge values of either the rotation angles θ or the phases δ and $\phi_{2,3}$.

This part of the appendix can be thought of as documentation of work that left no useful traces elsewhere but took a lot of time. Also, the search for the source of an ultimately simple problem

was described in some detail for others who might, in the future, find it useful as a “checklist” to diagnose the behaviour of awkward fits of any kind they might encounter, even though specialised work by much more competent authors - as demonstrated above - should be easy to find.

C. Loop Functions and Wilson Coefficients

This is a collection of the Inami-Lim functions used in this thesis, and their plots. Throughout this Appendix, $x_i = \frac{m_i^2}{m_W^2}$.

C.0.1. Meson Oscillation

$$S_0(x_i, x_j) = x_i x_j \Bigg[\frac{1}{x_j - x_i}\left(\frac{1}{4} + \frac{3}{2}\frac{1}{1-x_j} - \frac{3}{4}\frac{1}{(1-x_j)^2}\right)\ln x_j + \\ + \frac{1}{x_i - x_j}\left(\frac{1}{4} + \frac{3}{2}\frac{1}{1-x_i} - \frac{3}{4}\frac{1}{(1-x_i)^2}\right)\ln x_i - \\ - \frac{3}{4}\frac{1}{1-x_j}\frac{1}{1-x_i}\Bigg] \tag{C.1}$$

$$S_0(x) = \lim_{x_j \to x} S(x, x_j) = \frac{4x - 11x^2 + x^3}{4(1-x)^2} - \frac{3x^3 \ln x}{2(1-x)^3}. \tag{C.2}$$

C.0.2. Di-Leptonic Meson Decay

$$Y(x, \mu_t^{(\ell\ell)}) = Y_0(x) + \frac{\alpha_S}{4\pi} Y_1(x, \mu_t^{(\ell\ell)}) \tag{C.3}$$

The dependence on the scale $\mu_t^{(\ell\ell)}$ cancels the scale dependence of the leading term Y_0 at the order considered [229].

C.0.3. Effective Wilson Coefficients in $\Gamma(b \to s\gamma)/\Gamma(b \to ce\bar{\nu})$

$$C_7^{\text{eff},1}(\mu) = \eta^{\frac{16}{23}} C_{7\gamma}^{(0)}(m_W) \tag{C.4}$$

$$C_7^{\text{eff},2}(\mu) = \frac{8}{3}\left(\eta^{\frac{14}{23}} - \eta^{\frac{16}{23}}\right) C_g^{(0)}(m_W) \tag{C.5}$$

$$C_7^{\text{eff},3}(\mu) = \sum_{i=1}^{8} h_i \eta^{a_i} C_2^{(0)}(m_W) \tag{C.6}$$

Here,

$$\eta(\mu) = \frac{\alpha_s(m_W)}{\alpha_s(\mu)} \tag{C.7}$$

and the h_i and a_i in eq. (C.6) are given in Table XXVII [172], the relevant part of which is reproduced here as Table C.1. The initial conditions of the Wilson coefficients above read

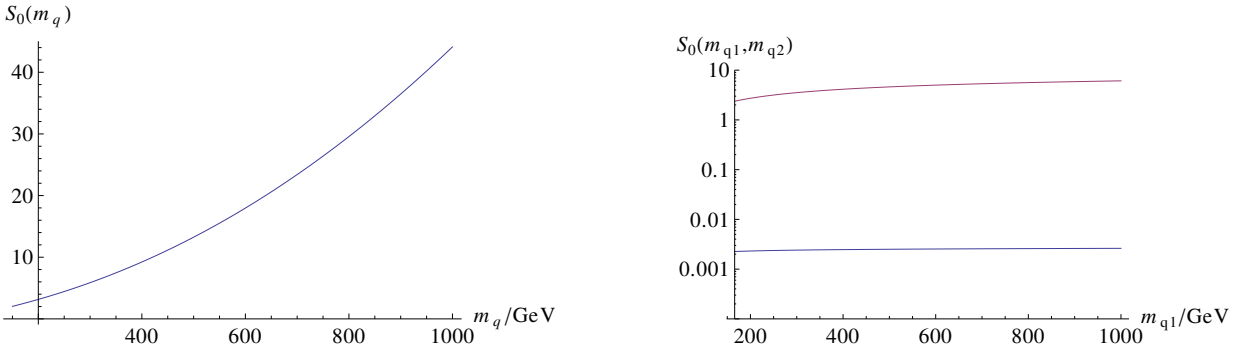

Figure C.1.: Quark mass dependence of the Inami-Lim functions S_0 needed e.g. in eqs. (2.100) and (4.85). The left plot shows $S_0(m_q)$ for two identical quarks in the corresponding box graph (cf. Fig. 2.5). The right plot shows $S_0(m_{q_1}, m_{q_2})$, i.e. non-identical virtual quarks occur in the graph. In the upper curve, the second quark mass m_{q_2} is set to $\bar{m}_t$. In the lower curve, $m_{q_2} = \bar{m}_c$.

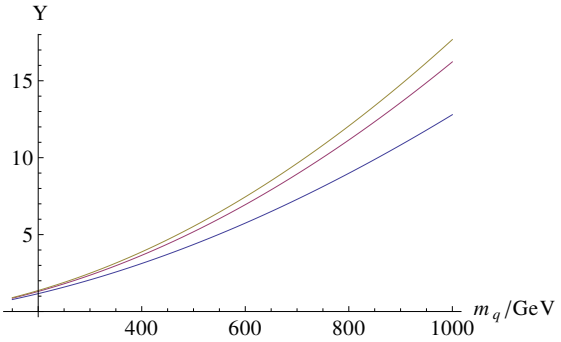

Figure C.2.: Quark mass dependence of the Inami-Lim function Y which occurs in the expression for $\mathcal{B}(B^0_{d,s} \to \mu^+\mu^-)$ in eq. (4.76). From top to bottom, the three curves are for the $\mu_t^{(\ell\ell)}$ value 80, 200 and 320 GeV.

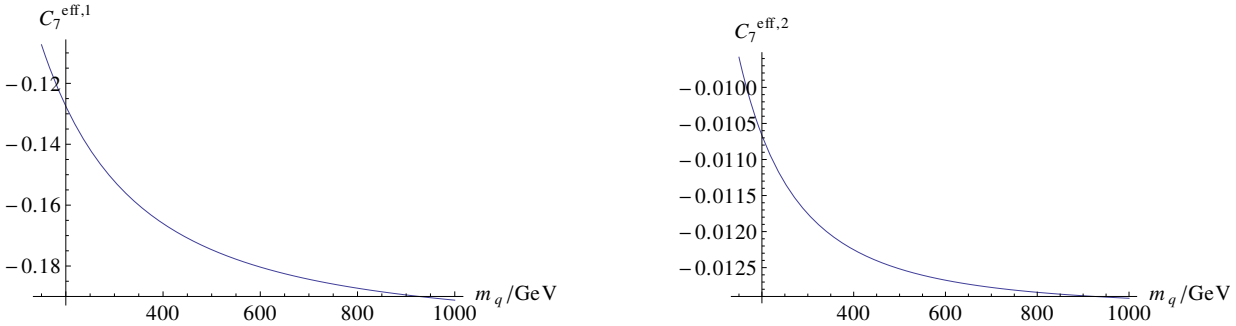

Figure C.3.: Quark mass dependence of the effective Wilson coefficients $C_7^{\text{eff},1}$ and $C_7^{\text{eff},2}$ at the scale $\mu_{LO} = 3.14$ GeV.

$$C_2^{(0)}(m_W) = 1, \tag{C.8}$$

$$C_{7\gamma}^{(0)}(mW) = -\frac{1}{2}D_0'(x_t) \text{ and} \tag{C.9}$$

$$C_{8g}^{(0)} = -\frac{1}{2}E_0'(x_t). \tag{C.10}$$

The Inami-Lim functions D_0' and E_0' read

$$D_0'(x) = -\frac{-7x + 5x^2 + 8x^3}{12(1-x)^3} + \frac{x^2(2-3x)}{2(1-x)^4}\ln(x) \text{ and} \tag{C.11}$$

$$E_0'(x) = \frac{2x + 5x^2 - x^3}{4(1-x)^3} + \frac{3x^2}{2(1-x)^4}\ln(x). \tag{C.12}$$

i	1	2	3	4	5	6	7	8
a_i	$\frac{14}{23}$	$\frac{16}{23}$	$\frac{6}{23}$	$-\frac{12}{23}$	0.4086	-0.4230	-0.8994	0.1456
h_i	2.2996	-1.0880	$-\frac{3}{7}$	$-\frac{1}{14}$	-0.6494	-0.0380	-0.0185	-0.0057

Table C.1.: Numerical constants in the expansion of the Wilson coefficient $C_7^{\text{eff},3}$ - reproduced from [172].

Bibliography

[1] M. Kobayashi and T. Maskawa. *Prog. Theor. Phys.*, (49):652, 1973.

[2] Jong-Mann Yang, David N. Schramm, Gary Steigman, and Robert T. Rood. Constraints on Cosmology and Neutrino Physics from Big Bang Nucleosynthesis. *Astrophys.J.*, 227:697–704, 1979.

[3] B. Holdom, W.S. Hou, T. Hurth, M.L. Mangano, S. Sultansoy, et al. Four Statements about the Fourth Generation. *PMC Phys.*, A3:4, 2009. (arXiv: 0904.4698).

[4] Graham D. Kribs, Tilman Plehn, Michael Spannowsky, and Timothy M.P. Tait. Four generations and Higgs physics. *Phys.Rev.*, D76:075016, 2007. (arXiv: 0706.3718).

[5] V.A. Novikov, A.N. Rozanov, and M.I. Vysotsky. Once more on extra quark-lepton generations and precision measurements. *Phys.Atom.Nucl.*, 73:636–642, 2010. (arXiv: 0904.4570).

[6] M.I. Vysotsky. Fourth quark-lepton generation and precision measurements. 2009. (arXiv: 0910.3100).

[7] Harald Fritzsch. Light neutrinos, nonuniversality of the leptonic weak interaction and a fourth massive generation. *Phys.Lett.*, B289:92–96, 1992.

[8] Amitava Datta. Flavor democracy calls for the fourth generation. *Pramana*, 40:L503–L509, 1993. (arXiv: hep-ph/9207248).

[9] A. Celikel, A.K. Ciftci, and S. Sultansoy. A Search for fourth SM family. *Phys.Lett.*, B342:257–261, 1995.

[10] Wei-Shu Hou. Source of CP Violation for the Baryon Asymmetry of the Universe. *Chin.J.Phys.*, 47: 134, 2009. (arXiv: 0803.1234).

[11] Ricky Fok and Graham D. Kribs. Four Generations, the Electroweak Phase Transition, and Supersymmetry. *Phys.Rev.*, D78:075023, 2008. (arXiv: 0803.4207).

[12] Yoshio Kikukawa, Masaya Kohda, and Junichiro Yasuda. The Strongly coupled fourth family and a first-order electroweak phase transition. I. Quark sector. *Prog.Theor.Phys.*, 122:401–426, 2009. (arXiv: 0901.1962).

[13] A. D. Sakharov. Violation of CP Invariance, c Asymmetry, and Baryon Asymmetry of the Universe. *Pisma Zh. Eksp. Teor. Fiz.*, 5:32–35, 1967. [Usp. Fiz. Nauk161,61(1991)].

[14] Enrico Lunghi and Amarjit Soni. Hints for the scale of new CP-violating physics from B-CP anomalies. *JHEP*, 0908:051, 2009. (arXiv: 0903.5059).

[15] Soumitra Nandi and Amarjit Soni. Constraining the mixing matrix for Standard Model with four generations: time dependent and semi-leptonic CP asymmetries in B_d^0, B_s and D^0. *Phys.Rev.*, D83: 114510, 2011. (arXiv: 1011.6091).

[16] Amarjit Soni, Ashutosh Kumar Alok, Anjan Giri, Rukmani Mohanta, and Soumitra Nandi. SM with four generations: Selected implications for rare B and K decays. *Phys.Rev.*, D82:033009, 2010. (arXiv: 1002.0595).

[17] T. Aaltonen et al. First Flavor-Tagged Determination of Bounds on Mixing-Induced CP Violation in $B_s^0 \to J/\psi\phi$ Decays. *Phys.Rev.Lett.*, 100:161802, 2008. (arXiv: 0712.2397).

[18] V.M. Abazov et al. Measurement of B_s^0 mixing parameters from the flavor-tagged decay $B_s^0 \to J/\psi\phi$. *Phys.Rev.Lett.*, 101:241801, 2008. (arXiv: 0802.2255).

[19] Bernard Aubert et al. Angular Distributions in the Decays $B \to K^*\ell^+\ell^-$. *Phys.Rev.*, D79:031102, 2009. (arXiv: 0804.4412).

[20] J.-T. Wei et al. Measurement of the Differential Branching Fraction and Forward-Backword Asymmetry for $B \to K^*\ell^+\ell^-$. *Phys.Rev.Lett.*, 103:171801, 2009. (arXiv: 0904.0770).

[21] Victor Mukhamedovich Abazov et al. Evidence for an anomalous like-sign dimuon charge asymmetry. *Phys.Rev.*, D82:032001, 2010. (arXiv: 1005.2757).

[22] Ashutosh Kumar Alok, Amol Dighe, and David London. Constraints on the Four-Generation Quark Mixing Matrix from a Fit to Flavor-Physics Data. *Phys.Rev.*, D83:073008, 2011. (arXiv: 1011.2634).

[23] Diganta Das, David London, Rahul Sinha, and Abner Soffer. Measuring the Magnitude of the Fourth-Generation CKM_4 Matrix Element $V_{t'b'}$. *Phys.Rev.*, D82:093019, 2010. (arXiv: 1008.4925).

[24] Paul H. Frampton, P.Q. Hung, and Marc Sher. Quarks and leptons beyond the third generation. *Phys.Rept.*, 330:263, 2000. (arXiv: hep-ph/9903387).

[25] Eberhardt, Otto and Lenz, Alexander and Rohrwild, Jürgen. Less space for a new family of fermions. *Phys.Rev.*, D82:095006, 2010. (arXiv: 1005.3505).

[26] Wei-Shu Hou, Makiko Nagashima, and Andrea Soddu. Large time-dependent CP violation in B/s0 system and finite D^0 - $\bar{D}^0$ mass difference in four generation standard model. *Phys.Rev.*, D76:016004, 2007. (arXiv: hep-ph/0610385).

[27] Cheng-Wei Chiang, Alakabha Datta, Murugeswaran Duraisamy, David London, Makiko Nagashima, et al. New Physics in $B_s^0 \to J/\psi\phi$: A General Analysis. *JHEP*, 1004:031, 2010. (arXiv: 0910.2929).

[28] Claude Amsler et al. Review of Particle Physics. *Phys.Lett.*, B667:1–1340, 2008.

[29] Michael S. Chanowitz. Bounding CKM Mixing with a Fourth Family. *Phys.Rev.*, D79:113008, 2009. (arXiv: 0904.3570).

[30] Michael S. Chanowitz, M.A. Furman, and I. Hinchliffe. Weak Interactions of Ultraheavy Fermions. 2. *Nucl.Phys.*, B153:402, 1979.

[31] William J. Marciano, G. Valencia, and S. Willenbrock. Renormalization Group Improved Unitarity Bounds on the Higgs Boson and Top Quark Masses. *Phys.Rev.*, D40:1725, 1989.

[32] Andrzej J. Buras, Björn Duling, Thorsten Feldmann, Tillmann Heidsieck, Christoph Promberger, et al. Patterns of Flavour Violation in the Presence of a Fourth Generation of Quarks and Leptons. *JHEP*, 1009:106, 2010. (arXiv: 1002.2126).

[33] Wei-Shu Hou and Chien-Yi Ma. Flavor and CP Violation with Fourth Generations Revisited. *Phys. Rev.*, D82:036002, 2010. (arXiv: 1004.2186).

[34] Michael S. Chanowitz. Probing for ultraheavy quanta at LHC. *Phys.Lett.*, B352:376–381, 1995. (arXiv: hep-ph/9503458).

[35] Otto Eberhardt, Alexander Lenz, Andreas Menzel, Ulrich Nierste, and Martin Wiebusch. Status of the fourth fermion generation before ICHEP2012: Higgs data and electroweak precision observables. *Phys.Rev.*, D86:074014, 2012. (arXiv: 1207.0438).

[36] Tomer Yanir. Phenomenological constraints on extended quark sectors. *JHEP*, 0206:044, 2002. (arXiv: hep-ph/0205073).

[37] Bobrowski, Markus and Lenz, Alexander and Riedl, Johann and Rohrwild, Jürgen. How much space is left for a new family of fermions? *Phys.Rev.*, D79:113006, 2009. (arXiv: 0902.4883).

[38] Georges Aad et al. Comprehensive measurements of t-channel single top-quark production cross sections at $\sqrt{s} = 7$ TeV with the ATLAS detector. 2014. (arXiv: 1406.7844).

[39] Serguei Chatrchyan et al. Observation of a new boson at a mass of 125 GeV with the CMS experiment at the LHC. *Phys.Lett.*, B716:30–61, 2012. (arXiv: 1207.7235).

[40] Otto Eberhardt, Geoffrey Herbert, Heiko Lacker, Alexander Lenz, Andreas Menzel, et al. Impact of a Higgs boson at a mass of 126 GeV on the standard model with three and four fermion generations. *Phys.Rev.Lett.*, 109:241802, 2012. (arXiv: 1209.1101).

[41] W. N. Cottingham and D.A. Greenwood. *An Introduction to the Standard Model of Particle Physics*. Cambridge University Press, 2007.

[42] F. Halzen and A. D. Martin. *QUARKS AND LEPTONS: An Introductory Course in Modern Particle Physics*. John Wiley & Sons, 1984.

[43] M. E. Peskin and D. V. Schroeder. *An Introduction to Quantum Field Theory*. Westview Press, 1995.

[44] Helen Quinn. B physics and CP violation. pages 1–54, 2001. (arXiv: hep-ph/0111177).

[45] D. Ebert. *Eichtheorien*. VCH Verlagsgesellschaft mbH, 1989.

[46] J. Beringer et al. Review of Particle Physics (RPP). *Phys.Rev.*, D86:010001, 2012.

[47] Mikhail A. Shifman. Foreword to ITEP lectures in particle physics. 1995. (arXiv: hep-ph/9510397).

[48] J. Beringer et al. (Particle Data Group). Phys. Rev. D86, 010001 (2012), . URL `http://pdg.lbl.gov/2013/reviews/rpp2012-rev-qcd.pdf`.

[49] J. Beringer et al. (Particle Data Group). Phys. Rev. D86, 010001 (2012) and 2013 partial update for the 2014 edition, . URL `http://pdg.lbl.gov/2013/reviews/rpp2013-rev-neutrino-mixing.pdf`.

[50] K.A. Olive et al. Review of Particle Physics. *Chin.Phys.*, C38:090001, 2014.

[51] Gerard 't Hooft. Renormalizable Lagrangians for Massive Yang-Mills Fields. *Nucl.Phys.*, B35:167–188, 1971.

[52] Gerard 't Hooft. Renormalization of Massless Yang-Mills Fields. *Nucl.Phys.*, B33:173–199, 1971.

[53] W. Pauli and F. Villars. On the Invariant regularization in relativistic quantum theory. *Rev. Mod. Phys.*, 21:434–444, 1949.

[54] Suraj N Gupta. Quantum electrodynamics with auxiliary fields. *Proceedings of the Physical Society. Section A*, 66(2):129, 1953.

[55] S. L. Adler. Axial-vector vertex in spinor electrodynamics. *Phys. Rev.*, 177(5):2426–2438, Jan 1969.

[56] N. Cabibbo. Unitary symmetry and leptonic decays. *Phys. Rev. Lett.*, 10(12):531–533, Jun 1963.

[57] C. Jarlskog. Commutator of the Quark Mass Matrices in the Standard Electroweak Model and a Measure of Maximal CP Violation. *Phys.Rev.Lett.*, 55:1039, 1985.

[58] V. Tishchenko et al. Detailed Report of the MuLan Measurement of the Positive Muon Lifetime and Determination of the Fermi Constant. *Phys.Rev.*, D87(5):052003, 2013. (arXiv: 1211.0960).

[59] H. Lacker and A. Menzel. Simultaneous Extraction of the Fermi constant and PMNS matrix elements in the presence of a fourth generation. *JHEP*, 1007:006, 2010. (arXiv: 1003.4532).

[60] D. M. Webber et al. Measurement of the Positive Muon Lifetime and Determination of the Fermi Constant to Part-per-Million Precision. *Phys. Rev. Lett.*, 106:041803, 2011. (arXiv: 1010.0991). [Phys. Rev. Lett.106,079901(2011)].

[61] L.-L. Chau and W.-Y. Keung. Comments on the Parametrization of the Kobayashi-Maskawa Matrix. *Phys. Rev. Lett.*, 53(19):1802–1805, Nov 1984.

[62] F. J. Botella and L.-L. Chau. Anticipating the higher generations of quarks from rephasing invariance of the mixing matrix. *Physics Letters*, 168B:97–104, 1986.

[63] Wei-Shu Hou, A. Soni, and Herbert Steger. Effects of a Fourth Family on $b \to s\gamma$ and a Useful Parametrization of Quark Mixing for Rare B Decays. *Phys.Lett.*, B192:441, 1987.

[64] H. Harari and M. Leurer. Recommending a standard choice of Cabibbo angles and KM phases for any number of generations. *Physics Letters B*, 181(1-2):123 – 128, 1986. ISSN 0370-2693.

[65] E.C.G "Sudarshan and R.E." Marshak, editors. *"Proc. Padua-Venice Conf. on Mesons and Recently Discovered Particles"*, 1957.

[66] K. G. Wilson and W. Zimmermann. Operator product expansions and composite field operators in the general framework of quantum field theory. *Commun. Math. Phys.*, 24:87–106, 1972.

[67] Andrzej J. Buras. Weak Hamiltonian, CP violation and rare decays. 1998. (arXiv: hep-ph/9806471).

[68] Ikaros I.Y. Bigi and A.I. Sanda. CP violation. *Camb.Monogr.Part.Phys.Nucl.Phys.Cosmol.*, 9:1–382, 2000.

[69] M.K. Gaillard and Benjamin W. Lee. $\Delta I = 1/2$ Rule for Nonleptonic Decays in Asymptotically Free Field Theories. *Phys.Rev.Lett.*, 33:108, 1974.

[70] Guido Altarelli and L. Maiani. Octet Enhancement of Nonleptonic Weak Interactions in Asymptotically Free Gauge Theories. *Phys.Lett.*, B52:351–354, 1974.

[71] T. Inami and C.S. Lim. Effects of Superheavy Quarks and Leptons in Low-Energy Weak Processes $K_L \to \mu\overline{\mu}$, $K^+ \to \pi^+\nu\overline{\nu}$ and $K^0 \leftrightarrow \overline{K}^0$. *Prog.Theor.Phys.*, 65:297, 1981.

[72] P.F. Harrison and Helen R. Quinn. The BABAR physics book: Physics at an asymmetric B factory. 1998.

[73] R T Cox, C G McIlwraith, and B Kurrelmeyer. volume 14 of *Proceedings of the National Academy of Science*, page 544, 1928.

[74] Morris L. Swartz. PHYSICS WITH POLARIZED ELECTRON BEAMS. *Conf.Proc.*, C8708101: 83–131, 1987.

[75] T.D. Lee and Chen-Ning Yang. Question of Parity Conservation in Weak Interactions. *Phys.Rev.*, 104:254–258, 1956.

[76] C.S. Wu, E. Ambler, R.W. Hayward, D.D. Hoppes, and R.P. Hudson. Experimental Test of Parity Conservation in Beta Decay. *Phys.Rev.*, 105:1413–1414, 1957.

[77] J.H. Christenson, J.W. Cronin, V.L. Fitch, and R. Turlay. Evidence for the 2 pi Decay of the k(2)0 Meson. *Phys.Rev.Lett.*, 13:138–140, 1964.

[78] C. A. Baker et al. An Improved experimental limit on the electric dipole moment of the neutron. *Phys. Rev. Lett.*, 97:131801, 2006. (arXiv: hep-ex/0602020).

[79] Roland Waldi. Flavour Oscillation and CP Violation. In Michael Beyer, editor, *CP Violation in Particle, Nuclear and Astrophysics*, volume 591 of *Lecture Notes in Physics*, chapter 2, pages 43–195. Springer-Verlag Berlin Heidelberg New York, 2002.

[80] Gerhart Lüders. Proof of the TCP theorem. *Annals of Physics*, 2(1):1–15, 1957.

[81] O. Botner. High-energy physics. *Proceedings, International Europhysics Conference, Uppsala, Sweden, June 25 - July 1, 1987.* Vols. 1, 2. page 791, 1987.

[82] A.J. Slaughter, M.P. Schmidt, and N.S. Lockyer. Proceedings, Workshop on High Sensitivity Beauty Physics at Fermilab, November 11-14 1987, Batavia, IL. *Conf.Proc.*, C871111:pp. iii–469, 1987.

[83] C. Jarlskog. A Basis Independent Formulation of the Connection Between Quark Mass Matrices, CP Violation and Experiment. *Z.Phys.*, C29:491–497, 1985.

[84] J. Beringer et al. (Particle Data Group). Phys. Rev. D86, 010001 (2012), . URL `http://pdg.lbl.gov/2013/reviews/rpp2012-rev-ckm-matrix.pdf`.

[85] James D. Bjorken and Isard Dunietz. Rephasing Invariant Parametrizations of Generalized Kobayashi-Maskawa Matrices. *Phys.Rev.*, D36:2109, 1987.

[86] C. Jarlskog. Recursive parameterisation and invariant phases of unitary matrices. *J.Math.Phys.*, 47: 013507, 2006. (arXiv: math-ph/0510034).

[87] V. Weisskopf and E. Wigner. Over the natural line width in the radiation of the harmonius oscillator. *Z.Phys.*, 65:18–29, 1930.

[88] V. Weisskopf and Eugene P. Wigner. Calculation of the natural brightness of spectral lines on the basis of Dirac's theory. *Z.Phys.*, 63:54–73, 1930.

[89] T.T. Wu and Chen-Ning Yang. Phenomenological Analysis of Violation of CP Invariance in Decay of K^0 and anti-K^0. *Phys.Rev.Lett.*, 13:380–385, 1964.

[90] T.D. Lee and L. Wolfenstein. Analysis of CP Noninvariant Interactions and the K_1^0, K_2^0 System. *Phys.Rev.*, 138:B1490–B1496, 1965.

[91] T.D. Lee and C.S. Wu. Weak Interactions: Decays of neutral K mesons. *Ann.Rev.Nucl.Part.Sci.*, 16:511–590, 1966.

[92] J. Beringer et al. (Particle Data Group). Phys. Rev. D86, 010001 (2012) and 2013 partial update for the 2014 edition, . URL `http://pdg.lbl.gov/2013/reviews/rpp2013-rev-cp-violation.pdf`.

[93] K. Anikeev, D. Atwood, F. Azfar, S. Bailey, C.W. Bauer, et al. B physics at the Tevatron: Run II and beyond. 2001. (arXiv: hep-ph/0201071).

[94] Martin Beneke, Gerhard Buchalla, Alexander Lenz, and Ulrich Nierste. CP asymmetry in flavor specific B decays beyond leading logarithms. *Phys.Lett.*, B576:173–183, 2003. (arXiv: hep-ph/0307344).

[95] Alexander Lenz and Ulrich Nierste. Theoretical update of $B_s - \bar{B}_s$ mixing. *JHEP*, 0706:072, 2007. (arXiv: hep-ph/0612167).

[96] M. Beneke, G. Buchalla, C. Greub, A. Lenz, and U. Nierste. Next-to-leading order QCD corrections to the lifetime difference of B(s) mesons. *Phys.Lett.*, B459:631–640, 1999. (arXiv: hep-ph/9808385).

[97] M. Beneke, G. Buchalla, and I. Dunietz. Width Difference in the $B_s - \bar{B}_s$ System. *Phys. Rev.*, D54: 4419–4431, 1996. (arXiv: hep-ph/9605259). [Erratum: Phys. Rev.D83,119902(2011)].

[98] Michael E. Peskin and Tatsu Takeuchi. Estimation of oblique electroweak corrections. *Phys.Rev.*, D46:381–409, 1992.

[99] James D. Wells. TASI lecture notes: Introduction to precision electroweak analysis. pages 41–64, 2005. (arXiv: hep-ph/0512342).

[100] Otto Eberhardt. Extra doublets - Global analyses of Standard Model extensions in the fermionic or scalar sector. 2013. (arXiv: 1309.1278).

[101] Otto Eberhardt, Geoffrey Herbert, Heiko Lacker, Alexander Lenz, Andreas Menzel, et al. Joint analysis of Higgs decays and electroweak precision observables in the Standard Model with a sequential fourth generation. *Phys.Rev.*, D86:013011, 2012. (arXiv: 1204.3872).

[102] Patrick Gonzalez, Jürgen Rohrwild, and Martin Wiebusch. Electroweak Precision Observables within a Fourth Generation Model with General Flavour Structure. *Eur.Phys.J.*, C72:2007, 2012. (arXiv: 1105.3434).

[103] Arif Akhundov, Andrej Arbuzov, Sabine Riemann, and Tord Riemann. The ZFITTER project. *Phys.Part.Nucl.*, 45(3):529–549, 2014. (arXiv: 1302.1395).

[104] Henning Flacher, Martin Goebel, Johannes Haller, Andreas Höcker, Klaus Mönig, et al. Revisiting the Global Electroweak Fit of the Standard Model and Beyond with Gfitter. *Eur.Phys.J.*, C60: 543–583, 2009. (arXiv: 0811.0009).

[105] S. Schael et al. Precision electroweak measurements on the Z resonance. *Phys.Rept.*, 427:257–454, 2006. (arXiv: hep-ex/0509008).

[106] CKMfitter Group (J. Charles et al.), December 2nd 2013. URL `http://ckmfitter.in2p3.fr/www/html/ckm_main.html`.

[107] A. Höcker et al. A new approach to a global fit of the CKM matrix. *European Physics Journal C*, 21:225–259, 2001.

[108] A. Jantsch. A Mathematica based Version of the CKMfitter Package. Diploma Thesis, Institut für Kern- und Teilchenphysik, Fachrichtung Physik, TU Dresden, 2006.

[109] J. Charles. Data Analysis with Theoretical Errors, September 2015. URL `https://indico.mitp.uni-mainz.de/getFile.py/access?contribId=4&resId=0&materialId=slides&confId=28`.

[110] J. Charles et al. CP violation and the CKM matrix: Assessing the impact of the asymmetric B factories. *Eur.Phys.J.*, C41:1–131, 2005. (arXiv: hep-ph/0406184).

[111] CERN program library. URL `http://cernlib.web.cern.ch/cernlib/`.

[112] A.B. Arbuzov, M. Awramik, M. Czakon, A. Freitas, M.W. Grunewald, et al. ZFITTER: A Semi-analytical program for fermion pair production in e+ e- annihilation, from version 6.21 to version 6.42. *Comput.Phys.Commun.*, 174:728–758, 2006. (arXiv: hep-ph/0507146).

[113] Wolfram Research Inc., December 2013. URL `http://www.wolfram.com/products/mathematica/latestversion/`.

[114] David M Gay. Computing optimal locally constrained steps. *SIAM Journal on Scientific and Statistical Computing*, 2(2):186–197, 1981.

[115] OpenMP Architecture Review Board. OpenMP.org, September 2014. URL `http://openmp.org/wp`.

[116] Miguel Hermanns. *Parallel Programming in Fortran 95 using OpenMP*. Universidad Politécnica de Madrid, April 2002.

[117] J.C. Hardy. The Status of V(ud). 2007. (arXiv: hep-ph/0703165).

[118] J. C. Hardy and I. S. Towner. Superallowed + → + nuclear β decays: A new survey with precision tests of the conserved vector current hypothesis and the standard model. *Phys. Rev. C*, 79(5):055502, May 2009.

[119] Mario Antonelli et al. Precision tests of the Standard Model with leptonic and semileptonic kaon decays. 2008. (arXiv: 0801.1817).

[120] T. Kaneko et al. Chiral behavior of kaon semileptonic form factors in lattice QCD with exact chiral symmetry. *PoS*, LATTICE2012:111, 2012. (arXiv: 1211.6180).

[121] V. Lubicz, F. Mescia, S. Simula, and C. Tarantino. $K \to \pi\ell\nu$ Semileptonic Form Factors from Two-Flavor Lattice QCD. *Phys.Rev.*, D80:111502, 2009. (arXiv: 0906.4728).

[122] P.A. Boyle et al. $K \to \pi$ form factors with reduced model dependence. *Eur.Phys.J.*, C69:159–167, 2010. (arXiv: 1004.0886).

[123] Mikihiko Nakao. CP Violation and CKM Measurements. *PoS*, ICHEP2012:019, 2013.

[124] H. Abramowicz, J.G.H. de Groot, J. Knobloch, J. May, Paolo Palazzi, et al. Experimental Study of Opposite Sign Dimuons Produced in Neutrino and anti-neutrinos Interactions. *Z.Phys.*, C15:19, 1982.

[125] Francesca Romana Spada. Neutrino production of charmed particles in the CHORUS experiment. 2002. URL `http://choruswww.cern.ch/Reference/Theses/spadaThesis.pdf`.

[126] A. Kayis-Topaksu et al. Measurement of topological muonic branching ratios of charmed hadrons produced in neutrino-induced charged-current interactions. *Phys.Lett.*, B626:24–34, 2005.

[127] C. Aubin et al. Semileptonic decays of D mesons in three-flavor lattice QCD. *Phys. Rev. Lett.*, 94: 011601, 2005. (arXiv: hep-ph/0408306).

[128] Paolo Gambino and Christoph Schwanda. Inclusive semileptonic fits, heavy quark masses, and V_{cb}. *Phys.Rev.*, D89:014022, 2014. (arXiv: 1307.4551).

[129] Y. Amhis et al. Averages of B-Hadron, C-Hadron, and tau-lepton properties as of early 2012. 2012. (arXiv: 1207.1158).

[130] Jon A. Bailey, A. Bazavov, C. Bernard, C.M. Bouchard, C. DeTar, et al. Update of $|V_{cb}|$ from the $\bar{B} \to D^* \ell \bar{\nu}$ form factor at zero recoil with three-flavor lattice QCD. *Phys.Rev.*, D89:114504, 2014. (arXiv: 1403.0635).

[131] Updated results on the CKMmatrix, August 2014. URL `http://ckmfitter.in2p3.fr/www/results/plots_moriond14/num/ckmEval_results_Moriond14.pdf`.

[132] Serguei Chatrchyan et al. Observation of the associated production of a single top quark and a W boson in pp collisions at $\sqrt{s} = 8$ TeV. *Phys.Rev.Lett.*, 112:231802, 2014. (arXiv: 1401.2942).

[133] The ATLAS collaboration. Measurement of the cross-section for associated production of a top quark and a W boson at $\sqrt{s} = 8$ TeV with the ATLAS detector (ATLAS-CONF-2013-100, ATLAS-COM-CONF-2013-116). 2013.

[134] Victor Mukhamedovich Abazov et al. Evidence for s-channel single top quark production in $p\bar{p}$ collisions at $\sqrt{s} = 1.96$ TeV. 2013. (arXiv: 1307.0731).

[135] Vardan Khachatryan et al. Measurement of the t-channel single-top-quark production cross section and of the $| V_{tb} |$ CKM matrix element in pp collisions at $\sqrt{s}$= 8 TeV. *JHEP*, 1406:090, 2014. (arXiv: 1403.7366).

[136] The ATLAS collaboration. Measurement of the Inclusive and Fiducial Cross-Section of Single Top-Quark t-Channel Events in pp Collisions at $\sqrt{s} = 8$ TeV. 2014.

[137] Timo Antero Aaltonen et al. Measurement of the Single Top Quark Production Cross Section and $|V_{tb}|$ in Events with One Charged Lepton, Large Missing Transverse Energy, and Jets at CDF. 2014. (arXiv: 1407.4031).

[138] J. Alwall et al. Is $V_{tb} \simeq 1$? 2006. arXiv: hep-ph/0607.115v2.

[139] V.M. Abazov et al. Precision measurement of the ratio $\mathrm{B}(t \to Wb)/\mathrm{B}(t \to Wq)$ and Extraction of V_{tb}. *Phys.Rev.Lett.*, 107:121802, 2011. (arXiv: 1106.5436).

[140] C. Galloni. Measurement of $R = \mathcal{B}(t \to Wb)/\mathcal{B}(t \to Wq)$ in Top–quark–pair Decays using Dilepton Events and the Full CDF Run II Data set. Talk given at Young Scientist Forum-Rencontres de Moriond -EW, March 2014. URL `https://indico.in2p3.fr/getFile.py/access?contribId=196&sessionId=2&resId=0&materialId=slides&confId=9116`.

[141] H. Lacker, A. Menzel, F. Spettel, D. Hirschbühl, J. Lück, et al. Model-independent extraction of $|V_{tq}|$ matrix elements from top-quark measurements at hadron colliders. *Eur.Phys.J.*, C72:2048, 2012. (arXiv: 1202.4694).

[142] A Combination of Preliminary Electroweak Measurements and Constraints on the Standard Model, February 2007. URL `http://lepewwg.web.cern.ch/LEPEWWG/lepww/4f/Winter05/pdg05.ps`. arXiv:hep-ex/0612034v2.

[143] G. Abbiendi et al. W^+W^- production cross-section and W branching fractions in e^+e^- collisions at 189 GeV. *Phys.Lett.*, B493:249–265, 2000. (arXiv: hep-ex/0009019).

[144] G. Abbiendi et al. Measurement of the $e^+e^- \to W^+W^-$ cross section and W decay branching fractions at LEP. *Eur.Phys.J.*, C52:767–785, 2007. (arXiv: 0708.1311).

[145] Jure Zupan. The case for measuring gamma precisely. 2011. (arXiv: 1101.0134).

[146] A. Lenz, U. Nierste, J. Charles, S. Descotes-Genon, A. Jantsch, et al. Anatomy of New Physics in $B - \bar{B}$ mixing. *Phys.Rev.*, D83:036004, 2011. (arXiv: 1008.1593).

[147] Alex Bondar and Tim Gershon. On ϕ_3 measurements using $B \to D^* K^-$ decays. *Phys.Rev.*, D70: 091503, 2004. (arXiv: hep-ph/0409281).

[148] Anjan Giri, Yuval Grossman, Abner Soffer, and Jure Zupan. Determination of the angle gamma using multibody D decays in $B^\pm \to DK^\pm$. *eConf*, C0304052:WG424, 2003. (arXiv: hep-ph/0306286).

[149] Yuval Grossman, Abner Soffer, and Jure Zupan. The Effect of D - anti-D mixing on the measurement of gamma in $B \to DK$ decays. *Phys.Rev.*, D72:031501, 2005. (arXiv: hep-ph/0505270).

[150] Michael Gronau and David London. How to determine all the angles of the unitarity triangle from $B_d^0 \to DK_s$ and $B_s^0 \to D^0$. *Phys.Lett.*, B253:483–488, 1991.

[151] Michael Gronau and Daniel Wyler. On determining a weak phase from CP asymmetries in charged B decays. *Phys.Lett.*, B265:172–176, 1991.

[152] P. del Amo Sanchez et al. Measurement of CP observables in $B^{+-} - > D_{CP} K^{+-}$ decays and constraints on the CKM angle γ. *Phys.Rev.*, D82:072004, 2010. (arXiv: 1007.0504).

[153] David Atwood, Isard Dunietz, and Amarjit Soni. Enhanced CP violation with $BKD0$ (anti-D0) modes and extraction of the CKM angle gamma. *Phys.Rev.Lett.*, 78:3257–3260, 1997. (arXiv: hep-ph/9612433).

[154] Isard Dunietz. CP violation with beautiful baryons. *Z.Phys.*, C56:129–144, 1992.

[155] Anjan Giri, Yuval Grossman, Abner Soffer, and Jure Zupan. Determining gamma using $B^\pm \to DK^\pm$ with multibody D decays. *Phys.Rev.*, D68:054018, 2003. (arXiv: hep-ph/0303187).

[156] J.P. Lees et al. Observation of direct CP violation in the measurement of the Cabibbo-Kobayashi-Maskawa angle gamma with $B^\pm \to D^{(*)} K^{(*)\pm}$ decays. *Phys.Rev.*, D87:052015, 2013. (arXiv: 1301.1029).

[157] Abner Soffer. Discrete ambiguities in the measurement of the weak phase gamma. *Phys.Rev.*, D60: 054032, 1999. (arXiv: hep-ph/9902313).

[158] T. Kurimoto and A. Tomita. New physics and CP angles measurement at B factory. *Prog. Theor. Phys.*, 98:967–975, 1997. (arXiv: hep-ph/9706222).

[159] Updated results on the CKMmatrix, August 2014. URL `http://ckmfitter.in2p3.fr/www/results/plots_fpcp13/num/ckmEval_results_FPCP13.pdf`.

[160] D. Yu. Bardin, Mikhail S. Bilenky, T. Riemann, M. Sachwitz, and H. Vogt. Dizet: A Program Package for the Calculation of Electroweak One Loop Corrections for the Process $e^+e^- \to f^+f^-$ Around the Z^0 Peak. *Comput.Phys.Commun.*, 59:303–312, 1990.

[161] Dmitri Yu. Bardin, P. Christova, M. Jack, L. Kalinovskaya, A. Olchevski, et al. ZFITTER v.6.21: A Semianalytical program for fermion pair production in e+ e- annihilation. *Comput.Phys.Commun.*, 133:229–395, 2001. (arXiv: hep-ph/9908433).

[162] T. Hahn and M. Perez-Victoria. Automatized one loop calculations in four-dimensions and D-dimensions. *Comput.Phys.Commun.*, 118:153–165, 1999. (arXiv: hep-ph/9807565).

[163] Thomas Hahn. Generating Feynman diagrams and amplitudes with FeynArts 3. *Comput.Phys.Commun.*, 140:418–431, 2001. (arXiv: hep-ph/0012260).

[164] Thomas Hahn and Michael Rauch. News from FormCalc and LoopTools. *Nucl.Phys.Proc.Suppl.*, 157:236–240, 2006. (arXiv: hep-ph/0601248).

[165] Tevatron Electroweak Working Group. 2012 Update of the Combination of CDF and D0 Results for the Mass of the W Boson. 2012. (arXiv: 1204.0042).

[166] M. Awramik, M. Czakon, A. Freitas, and G. Weiglein. Precise prediction for the W boson mass in the standard model. *Phys.Rev.*, D69:053006, 2004. (arXiv: hep-ph/0311148).

[167] Tevatron Electroweak Working Group. Combination of CDF and D0 Results on the Width of the W boson. 2010. (arXiv: 1003.2826).

[168] J. Beringer et al. (Particle Data Group). Phys. Rev. D86, 010001 (2012) and 2013 partial update for the 2014 edition, . URL `http://pdg.lbl.gov/2013/listings/rpp2013-list-t-quark.pdf`.

[169] P.A. Baikov, K.G. Chetyrkin, and Johann H. Kuhn. Order α_s^4 QCD Corrections to Z and τ Decays. *Phys.Rev.Lett.*, 101:012002, 2008. (arXiv: 0801.1821).

[170] Michel Davier, Andreas Hoecker, Bogdan Malaescu, and Zhiqing Zhang. Reevaluation of the Hadronic Contributions to the Muon g-2 and to $\alpha(m_Z)$. *Eur.Phys.J.*, C71:1515, 2011. (arXiv: 1010.4180).

[171] M. Baak, M. Goebel, J. Haller, A. Hoecker, D. Kennedy, et al. The Electroweak Fit of the Standard Model after the Discovery of a New Boson at the LHC. *Eur.Phys.J.*, C72:2205, 2012. (arXiv: 1209.2716).

[172] Gerhard Buchalla, Andrzej J. Buras, and Markus E. Lautenbacher. Weak decays beyond leading logarithms. *Rev.Mod.Phys.*, 68:1125–1144, 1996. (arXiv: hep-ph/9512380).

[173] R Aaij et al. Precision measurement of the B_s^0-$\bar{B}_s^0$ oscillation frequency with the decay $B_s^0 \to D_s^-\pi^+$. *New J.Phys.*, 15:053021, 2013. (arXiv: 1304.4741).

[174] Heavy Flavour Averaging Group, May 2013. URL `http://www.slac.stanford.edu/xorg/hfag/rare/2013/radll/OUTPUT/TABLES/radll.pdf`.

[175] Alexander Lenz. Lifetimes and HQE. 2014. (arXiv: 1405.3601).

[176] M. Misiak, H.M. Asatrian, K. Bieri, M. Czakon, A. Czarnecki, et al. Estimate of $B\bar{B} \to X_s\gamma$ at $\mathcal{O}(\alpha_s^2)$. *Phys.Rev.Lett.*, 98:022002, 2007. (arXiv: hep-ph/0609232).

[177] Y. Amhis et al. Averages of b-hadron, c-hadron, and τ-lepton properties as of summer 2014. 2014. (arXiv: 1412.7515).

[178] R Aaij et al. First Evidence for the Decay $B_s^0 \to \mu^+\mu^-$. *Phys.Rev.Lett.*, 110:021801, 2013. (arXiv: 1211.2674).

[179] CMS and LHCb Collaborations. Combination of results on the rare decays $B_s^0 \to \mu^+\mu^-$ from the CMS and LHCb experiments. 2013.

[180] R. Aaij et al. Measurement of the $B_s^0 \to \mu^+\mu^-$ branching fraction and search for $B^0 \to \mu^+\mu^-$ decays at the LHCb experiment. *Phys.Rev.Lett.*, 111:101805, 2013. (arXiv: 1307.5024).

[181] Serguei Chatrchyan et al. Measurement of the $B_s \to \mu^+\mu^-$ branching fraction and search for $B^0 \to \mu^+\mu^-$ with the CMS Experiment. *Phys.Rev.Lett.*, 111:101804, 2013. (arXiv: 1307.5025).

[182] Gerhard Buchalla and Andrzej J. Buras. QCD corrections to rare K and B decays for arbitrary top quark mass. *Nucl. Phys.*, B400:225–239, 1993.

[183] Kenneth M. Watson. Some general relations between the photoproduction and scattering of π mesons. *Phys.Rev.*, 95:228–236, 1954.

[184] P. A. Boyle, N. H. Christ, N. Garron, E. J. Goode, T. Janowski, C. Lehner, Q. Liu, A. T. Lytle, C. T. Sachrajda, A. Soni, and D. Zhang. Emerging understanding of the δi=1/2 rule from lattice qcd. *Phys. Rev. Lett.*, 110:152001, Apr 2013. URL `http://link.aps.org/doi/10.1103/PhysRevLett.110.152001`.

[185] Stefan Herrlich and Ulrich Nierste. Enhancement of the K(L) - K(S) mass difference by short distance QCD corrections beyond leading logarithms. *Nucl. Phys.*, B419:292–322, 1994. (arXiv: hep-ph/9310311).

[186] Monika Blanke, Andrzej J. Buras, Stefan Recksiegel, Cecilia Tarantino, and Selma Uhlig. Correlations between epsilon-prime / epsilon and rare K decays in the littlest Higgs model with T-parity. *JHEP*, 06:082, 2007. (arXiv: 0704.3329).

[187] J.J. Hernandez et al. Review of particle properties. Particle Data Group. *Phys.Lett.*, B239:1–515, 1990.

[188] HFAG CPV & Unitarity Triangle - Results Summer 2014, 2014. URL `http://www.slac.stanford.edu/xorg/hfag/triangle/summer2014/index.shtml`.

[189] V.M. Abazov et al. Measurement of the semileptonic charge asymmetry using $B_s^0 \to D_s\mu X$ decays. *Phys.Rev.Lett.*, 110:011801, 2013. (arXiv: 1207.1769).

[190] R Aaij et al. Measurement of the flavour-specific CP-violating asymmetry a_{sl}^s in B_s^0 decays. *Phys.Lett.*, B728:607–615, 2014. (arXiv: 1308.1048).

[191] Ulrich Nierste. CP asymmetry in flavor-specific B decays. In *Proceedings, 39th Recontres de Moriond, 04 Electroweak interactions and unified theories*, pages 445–450, 2004. (arXiv: hep-ph/0406300). URL `http://lss.fnal.gov/cgi-bin/find_paper.pl?conf-04-094-T`.

[192] Victor Mukhamedovich Abazov et al. Measurement of the semileptonic charge asymmetry in B^0 meson mixing with the D0 detector. *Phys.Rev.*, D86:072009, 2012. (arXiv: 1208.5813).

[193] J.P. Lees et al. Search for CP Violation in B^0-$\bar{B}^0$ Mixing using Partial Reconstruction of $B^0 \to D^{*-}X\ell^+\nu_\ell$ and a Kaon Tag. *Phys.Rev.Lett.*, 111(10):101802, 2013. (arXiv: 1305.1575).

[194] Sven Faller, Robert Fleischer, and Thomas Mannel. Precision Physics with $B_s^0 \to J/\psi\phi$ at the LHC: The Quest for New Physics. *Phys.Rev.*, D79:014005, 2009. (arXiv: 0810.4248).

[195] Alexander Lenz. Theoretical update of B-Mixing and Lifetimes. 2012. (arXiv: 1205.1444).

[196] Andrzej J. Buras and Robert Fleischer. A General analysis of γ determinations from $B \to \pi K$ decays. *Eur.Phys.J.*, C11:93–109, 1999. (arXiv: hep-ph/9810260).

[197] Michael Gronau and David London. Isospin analysis of CP asymmetries in B decays. *Phys.Rev.Lett.*, 65:3381–3384, 1990.

[198] Harry J. Lipkin, Yosef Nir, Helen R. Quinn, and A. Snyder. Penguin trapping with isospin analysis and CP asymmetries in B decays. *Phys.Rev.*, D44:1454–1460, 1991.

[199] J.P. Lees et al. Measurement of CP-violating asymmetries in $B^0 \to (\rho\pi)^0$ decays using a time-dependent Dalitz plot analysis. *Phys.Rev.*, D88(1):012003, 2013. (arXiv: 1304.3503).

[200] Victor Mukhamedovich Abazov et al. Study of CP -violating charge asymmetries of single muons and like-sign dimuons in $p\bar{p}$ collisions. *Phys.Rev.*, D89(1):012002, 2014. (arXiv: 1310.0447).

[201] Yuval Grossman, Yosef Nir, and Guy Raz. Constraining the phase of $B_s - \bar{B}_s$ mixing. *Phys.Rev.Lett.*, 97:151801, 2006. (arXiv: hep-ph/0605028).

[202] Victor Mukhamedovich Abazov et al. Measurement of the anomalous like-sign dimuon charge asymmetry with 9 fb$^-$1 of $p\bar{p}$ collisions. *Phys.Rev.*, D84:052007, 2011. (arXiv: 1106.6308).

[203] G. Borissov and B. Hoeneisen. Understanding the like-sign dimuon charge asymmetry in $p\bar{p}$ collisions. *Phys.Rev.*, D87(7):074020, 2013. (arXiv: 1303.0175).

[204] U. Nierste. Effect of $\Delta\Gamma$ on the dimuon asymmetry in B meson decays, September 2014. URL `https://indico.cern.ch/event/253826/session/7/contribution/88/attachments/443284/614871/nierste_ckm2014.pdf`.

[205] 1286320. First combination of Tevatron and LHC measurements of the top-quark mass. 2014. (arXiv: 1403.4427).

[206] Gilberto Colangelo, Stephan Durr, Andreas Juttner, Laurent Lellouch, Heinrich Leutwyler, et al. Review of lattice results concerning low energy particle physics. *Eur.Phys.J.*, C71:1695, 2011. (arXiv: 1011.4408).

[207] Joachim Brod and Martin Gorbahn. ϵ_K at Next-to-Next-to-Leading Order: The Charm-Top-Quark Contribution. *Phys.Rev.*, D82:094026, 2010. (arXiv: 1007.0684).

[208] D. Becirevic, V. Gimenez, G. Martinelli, M. Papinutto, and J. Reyes. B parameters of the complete set of matrix elements of delta B = 2 operators from the lattice. *JHEP*, 0204:025, 2002. (arXiv: hep-lat/0110091).

[209] Samuel S Wilks. The large-sample distribution of the likelihood ratio for testing composite hypotheses. *The Annals of Mathematical Statistics*, 9(1):60–62, 1938.

[210] Martin Wiebusch. Numerical Computation of p-values with *my*Fitter. *Comput.Phys.Commun.*, 184: 2438–2445, 2013. (arXiv: 1207.1446).

[211] CP Asymmetry in semileptonic B decays , 2012. URL `http://www-cdf.fnal.gov/physics/new/bottom/070816.blessed-acp-bsemil/`.

[212] S Dittmaier, C Mariotti, G Passarino, R Tanaka, J Baglio, P Bolzoni, R Boughezal, O Brein, C Collins-Tooth, S Dawson, S Dean, A Denner, S Farrington, M Felcini, M Flechl, D de Florian, S Forte, M Grazzini, C Hackstein, T Hahn, R Harlander, T Hartonen, S Heinemeyer, J Huston, A Kalinowski, M Krämer, F Krauss, J S Lee, S Lehti, F Maltoni, K Mazumdar, S O Moch, A Mück, M Mühlleitner, P Nason, C Neu, C Oleari, J Olsen, S Palmer, F Petriello, G Piacquadio, A Pilaftsis, C T Potter, I Puljak, J Qian, D Rebuzzi, L Reina, H Rzehak, M Schumacher, P Slavich, M Spira, F Stöckli, R S Thorne, M Vazquez Acosta, T Vickey, A Vicini, D Wackeroth, M Warsinsky, M Weber, G Weiglein, C Weydert, J Yu, M Zaro, and T Zirke. *Handbook of LHC Higgs Cross Sections: 1. Inclusive Observables*. CERN, Geneva, 2011. URL `https://cds.cern.ch/record/1318996`. Comments: 153 pages, 43 figures, to be submitted to CERN Report. Working Group web page: https://twiki.cern.ch/twiki/bin/view/LHCPhysics/CrossSections.

[213] LHC Higgs Cross Section Working Group. URL `https://twiki.cern.ch/twiki/bin/view/LHCPhysics/CrossSections`. (retrieved 06.22, 2013).

[214] Julien Baglio and Abdelhak Djouadi. Predictions for Higgs production at the Tevatron and the associated uncertainties. *JHEP*, 10:064, 2010. (arXiv: 1003.4266).

[215] Abdelhak Djouadi. The Anatomy of electro-weak symmetry breaking. I: The Higgs boson in the standard model. *Phys.Rept.*, 457:1–216, 2008. (arXiv: hep-ph/0503172).

[216] Michael Spira. QCD effects in Higgs physics. *Fortsch.Phys.*, 46:203–284, 1998. (arXiv: hep-ph/9705337).

[217] A. Djouadi and P. Gambino. Leading electroweak correction to Higgs boson production at proton colliders. *Phys.Rev.Lett.*, 73:2528–2531, 1994. (arXiv: hep-ph/9406432).

[218] A. Denner, S. Dittmaier, A. Muck, G. Passarino, M. Spira, et al. Higgs Production and Decay with a Fourth Standard-Model-Like Fermion Generation. *Eur.Phys.J.*, C72:1992, 2012. (arXiv: 1111.6395).

[219] Abdelhak Djouadi and Alexander Lenz. Sealing the fate of a fourth generation of fermions. *Phys.Lett.*, B715:310–314, 2012. (arXiv: 1204.1252).

[220] Georges Aad et al. Observation of a new particle in the search for the Standard Model Higgs boson with the ATLAS detector at the LHC. *Phys.Lett.*, B716:1–29, 2012. (arXiv: 1207.7214).

[221] CMS Collaboration. Evidence for a new state decaying into two photons in the search for the standard model Higgs boson in pp collisions (CMS-PAS-HIG-12-015). 2012.

[222] Updated Combination of CDF and D0 Searches for Standard Model Higgs Boson Production with up to 10.0 fb^{-1} of Data. 2012. (arXiv: 1207.0449).

[223] Georges Aad et al. Combined search for the Standard Model Higgs boson in pp collisions at $\sqrt{s} = 7$ TeV with the ATLAS detector. *Phys.Rev.*, D86:032003, 2012. (arXiv: 1207.0319).

[224] T. Aaltonen et al. Combination of the top-quark mass measurements from the Tevatron collider. *Phys.Rev.*, D86:092003, 2012. (arXiv: 1207.1069).

[225] A. Djouadi, J. Kalinowski, and M. Spira. HDECAY: A Program for Higgs boson decays in the standard model and its supersymmetric extension. *Comput.Phys.Commun.*, 108:56–74, 1998. (arXiv: hep-ph/9704448).

[226] Lincoln Wolfenstein. Parametrization of the Kobayashi-Maskawa Matrix. *Phys.Rev.Lett.*, 51:1945, 1983.

[227] Andrzej J. Buras, Markus E. Lautenbacher, and Gaby Ostermaier. Waiting for the top quark mass, $K^+ \to \pi^+\nu\bar{\nu}, B_s^0\bar{B}_s^0$ mixing and CP asymmetries in B decays. *Phys. Rev.*, D50:3433–3446, 1994. (arXiv: hep-ph/9403384).

[228] Free Software Foundation, December 3rd 2013. URL `http://www.gnu.org/software/gawk/gawk.html`.

[229] Gerhard Buchalla and Andrzej J. Buras. The rare decays $K \to \pi\nu\bar{\nu}$, $B \to X\nu\bar{\nu}$ and $B \to \ell^+\ell^-$: An Update. *Nucl.Phys.*, B548:309–327, 1999. (arXiv: hep-ph/9901288).

[230] T. Affolder et al. First measurement of the ratio $B(t \to Wb)/B(t \to Wq)$ and associated limit on the CKM element $|V_{tb}|$. *Phys. Rev. Lett.*, 86:3233–3238, 2001. (arXiv: hep-ex/0012029).

[231] J. Beringer et al. (Particle Data Group). Phys. Rev. D86, 010001 (2012) and 2013 partial update for 2014, . URL `http://pdg.lbl.gov/2013/listings/rpp2013-list-B-zero.pdf`.

[232] Andrzej J. Buras, Björn Duling, Thorsten Feldmann, Tillmann Heidsieck, Christoph Promberger, et al. The Impact of a 4th Generation on Mixing and CP Violation in the Charm System. *JHEP*, 1007:094, 2010. (arXiv: 1004.4565).

[233] CKMfitter Group (J. Charles et al.), December 3rd 2013. URL `http://ckmfitter.in2p3.fr/wiki/index.php/Main_Page`.

[234] Measurement of Single Top Quark Production in 7.5 fb−1 of CDF Data Using Neural Networks, 2012. URL `http://www-cdf.fnal.gov/physics/new/top/confNotes/cdf10793_SingleTop_7.5_public.pdf`.

[235] E.D. Commins and P.H. Bucksbaum. Weak Interactions of Leptons and Quarks. 1983.

[236] December 2013. URL `www.gnuplot.info`.

[237] J. S. Hagelin. Mass Mixing and CP Violation in the B^0 – $\bar{B}^0$ system. *Nucl. Phys.*, B193:123–149, 1981.

[238] Heavy Flavour Averaging Group, December 2013. URL `http://www.slac.stanford.edu/xorg/hfag/triangle/summer2012/index.shtml`.

[239] Christopher T. Hill, Markus A. Luty, and Emmanuel A. Paschos. Electroweak symmetry breaking by fourth generation condensates and the neutrino spectrum. *Phys. Rev.*, D43:3011–3025, 1991.

[240] Nikolaos Kidonakis. Higher-order corrections to top-antitop pair and single top quark production. 2009. (arXiv: 0909.0037).

[241] D0 Collaboration Tevatron Electroweak Working Group, CDF Collaboration. Combination of CDF and D0 results on the mass of the top quark using up to 5.8 fb^{-1} of data. 2011. (arXiv: 1107.5255).

[242] Alexander Lenz and Ulrich Nierste. Numerical Updates of Lifetimes and Mixing Parameters of B Mesons. 2011. (arXiv: 1102.4274).

[243] S.W. Lin et al. Difference in direct charge-parity violation between charged and neutral B meson decays. *Nature*, 452:332–335, 2008.

[244] L. Lista. Top quark: Production at atlas and cms. Talk given at Rencontres de Moriond Electroweak Interactions and Unified Theories, La Thuile, March 2014. URL `https://indico.in2p3.fr/getFile.py/access?contribId=135&sessionId=6&resId=0&materialId=slides&confId=9116`.

[245] Z. Maki, M. Nakagawa, and S. and Sakata. Remarks on the unified model of elementary particles. In *High-energy physics. Proceedings, 11th International Conference, ICHEP'62, Geneva, Switzerland, Jul 4-11, 1962*, pages 663–666, 1962. URL `http://inspirehep.net/record/1341897/files/C62-07-04-p663.pdf`.

[246] A. Poluektov et al. Evidence for direct CP violation in the decay $B \to D^*K$, $D \to K_s\pi^+\pi^-$ and measurement of the CKM phase phi3. *Phys.Rev.*, D81:112002, 2010. (arXiv: 1003.3360).

[247] B. Pontecorvo. Mesonium and anti-mesonium. *Sov. Phys. JETP*, 6:429, 1957. [Zh. Eksp. Teor. Fiz.33,549(1957)].

[248] B. Pontecorvo. Neutrino Experiments and the Problem of Conservation of Leptonic Charge. *Sov. Phys. JETP*, 26:984–988, 1968. [Zh. Eksp. Teor. Fiz.53,1717(1967)].

[249] K. Shaw. Determination of the V_{tb} CKM element in single top production at Tevatron and LHC, September 2014. URL `http://vietnam.in2p3.fr/2014/flavour/MondayMorning/Shaw.pdf`.

[250] K. Trabelsi. Study of direct CP in charmed B decays and measurement of the CKM angle gamma at Belle. 2013. (arXiv: 1301.2033).

List of Figures

2.1. Examples of Feynman graph types . . . 7
2.2. Lowest order graph in the decay $\mu \to e\nu_i\bar{\nu}_j$ . . . 14
2.3. β decay in Electroweak theory and effective theory . . . 17
2.4. Unitarity Triangle of the neutral B_d meson system in the SM3 . . . 23
2.5. Lowest order Feynman graphs of meson oscillation (box graphs) . . . 31
2.6. Feynman graphs of LO contributions to B_s^0 decay . . . 31
2.7. LO Feynman graphs of gauge boson self-energy corrections . . . 32
2.8. LO Feynman graphs of $Zb\bar{b}$ vertex corrections . . . 33

4.1. Dimuon event in neutrino-nucleon deep-inelastic scattering (LO) . . . 50
4.2. Top quark production channels with subsequent decays . . . 51
4.3. $|V_{tb}|$ p-value plots obtained with ST $|V_{tb}|$ input and with EWP input . . . 54
4.4. Tree Level Feynman graphs contributing to B^- decay . . . 57
4.5. D^0 and $\overline{D}^0$ decay Feynman graphs as used in GLW method . . . 58
4.6. γ input provided by LUT, converted to p-value curve . . . 63
4.7. p-value plot of SM4 contamination δ_1 in γ extraction . . . 64
4.8. 2D LUT containing EWP constraint on SM4, converted to 2D p-value plot . . . 66
4.9. LO Feynman graph contributing to $B \to X_s\gamma$ . . . 70
4.10. Feynman graphs contributing to the decay $B_{(s)} \to \mu\bar{\mu}$ . . . 71
4.11. Feynman graphs contributing to the decay $K^0 \to \pi\pi$ . . . 82
4.12. Feynman Graphs which contribute to B^0 and $\bar{B}^0$ decays . . . 83

5.1. Structure of p-Value curve of $|V_{td}|$ in the TL set of inputs . . . 103
5.2. Illustration of discussion of $|V_{td}|$ "dip" in TL p-value plot . . . 104
5.3. P-value plots of $|V_{td}|$ in the LoopNoCPV series of fits. . . . 113
5.4. Sketch to explain the "trident" structure in Fig. 5.3 . . . 114
5.5. LoopNoCPV prediction of a_{SL}^d with LoopNoCPV input set (p-value plot) . . . 114
5.6. Correlation of δ and ϕ_3 in the LoopNoCPV input set. . . . 116
5.7. P-value plots of ϕ_3, θ_d and UT angle β with LoopNoCPV inputs . . . 117
5.8. 2D p-value plot of ϕ_2 vs. ϕ_3 with LoopCPV input . . . 120
5.9. Pulls and χ^2 shifts by individual inputs in each input set . . . 143

6.1. Main Higgs production processes at Tevatron and LHC (LO) . . . 146
6.2. Lowest-order contributions to $H \to \gamma\gamma$ . . . 147
6.3. χ^2_{min} plotted against Higgs mass in SM3 and SM4 . . . 149
6.4. Pulls of the Higgs signal strengths (SM3 and SM4 at m_H =126 GeV) . . . 150
6.5. Pulls and $\Delta\chi^2$ with all inputs in SM3 and SM4 . . . 153
6.6. Experimental values of A_{SL} . . . 155
6.7. Fit results in SM3 and SM4 and experimental inputs of a_{SL}^d and a_{SL}^s . . . 156

B.1. Ten p-value plots of $|V_{t'b'}|$ with identical settings and inputs . . . 168
B.2. Frequency of finding a given $\hat{\chi}^2$ as "minimum" . . . 171

C.1. Quark mass dependence of the Inami-Lim functions S_0 176
C.2. Quark mass dependence of the Inami-Lim function Y 176
C.3. Quark mass dependence of the eff. Wilson coefficients in $\Gamma(b \to X s\gamma)/\Gamma(b \to e\nu)$ 177

List of Tables

2.1. Fermion types in the SM . . . 5
2.2. Gauge bosons in the SM . . . 6

3.1. Quantities with negligible errors in `inputs/PDG.nb` . . . 41

4.1. $|V_{tb}|$ extractions included in the average used in the fits . . . 52
4.2. CKM factors in GLW and ADS extractions of γ. . . . 62
4.3. Inputs of EWP fits to constrain $|V_{tb'}|$ and $m_{t'}$ . . . 66
4.4. Values of effective Wilson coefficients in $\Gamma(b \to s\gamma)/\Gamma(b \to ce\bar{\nu})$ . . . 70
4.5. Tree Level results for $|V_{t's}V^*_{t'b}|$ and $|V_{us}V^*_{ub}|$ . . . 70
4.6. Parameter values from Ref. [200] to retrace the analysis performed there. . . . 92

5.1. Input values of all observables used in fits . . . 94
5.2. Input values of all parameters used in fits . . . 95
5.3. Relative magnitude of summands of the CKM matrix elements . . . 100
5.4. Constraints on moduli of CKM matrix elements with TL inputs only . . . 102
5.5. Limits on δ as obtained in the Tree Level fit . . . 102
5.6. Limits on α and β as obtained in the Tree Level fit . . . 102
5.7. Moduli of CKM matrix elements changed by addition of EWP input . . . 106
5.8. Approximate phases of the λ_u^M which occur in the observables of sec. 5.2 . . . 108
5.9. Relative Magnitudes of the contributions to the observables added in the LoopNoCPV set of inputs . . . 110
5.10. Comparison of χ^2_{min} values of different subsets of the LoopNoCPV input set . . . 110
5.11. Constraints on moduli of CKM matrix elements obtained in LoopNoCPV input set . . . 111
5.12. Constraints on SM4-related parameters obtained in the LoopNoCPV series of fits . . . 115
5.13. Constraints on moduli of CKM matrix elements with LoopCPV input set . . . 121
5.14. Constraints on SM4-related quantities with LoopCPV inputs. . . . 122
5.15. Constraints on moduli of CKM matrix elements with all inputs . . . 124
5.16. Constraints on SM4-related quantities with all inputs . . . 125
5.17. Pulls and χ^2 shifts by individual inputs in each input set . . . 142

6.1. Experimental inputs for Higgs signal strengths . . . 149
6.2. Differences between the EWP inputs in this study and in [40]. . . . 149
6.3. Pulls and $\Delta\chi^2$ with all inputs in SM3 and SM4 . . . 152
6.4. Experimental A_{SL} results . . . 155
6.5. Predictions of a^d_{SL} and a^s_{SL} in SM3 and SM4 with all inputs . . . 156

B.1. Location of $\hat{\chi}^2_0$ in the parameter space . . . 172

C.1. Constants in the expansion of the Wilson coefficient $C_7^{\text{eff},3}$ . . . 177